Inaugural dissertation

for

obtaining the doctoral degree

of the

Combined Faculty of Mathematics, Engineering and Natural Sciences

of the

Ruprecht - Karls - University

Heidelberg

Presented by

M.Sc. José Ricardo da Cruz Vieira

born in: Porto, Portugal

Oral examination: 26.05.2023

Neurovascular interactions in the spinal cord during embryonic development and pathology

Referees: Jun.-Prof. Dr. Lázaro Centanin

Prof. Dr. Carmen Ruiz de Almodóvar

Prof. Dr. Daniela Mauceri

Prof. Dr. Michael Brunner

To everyone who,
in some way or another,
made me into the scientist I am today.

“If you can't be a pine on the top of the hill
Be a scrub in the valley-but be
The best little scrub by the side of the rill;
Be a bush if you can't be a tree.

If you can't be a bush be a bit of the grass,
And some highway some happier make;
(…)
If you can't be a highway then just be a trail,
If you can't be the sun be a star;
It isn't by size that you win or you fail-
Be the best of whatever you are!”
[Be the best of whatever you are, Douglas Malloch]

Table of Contents

Summary

Formation and maintenance of such a highly specialized structure as the central nervous system (CNS) requires the concomitantly cooperation between the vascular and neural systems. Interactions between these systems are necessary to instruct each other to correctly develop and achieve homeostatic conditions. Thus, understanding neurovascular communications during embryonic development and their alterations in pathology are fundamental.

Here, I reveal a novel crosstalk occurring in the developing spinal cord between motor neurons (MNs) and endothelial cells (ECs) necessary to keep MN columns avascular for a certain period of time. From inferring and analyzing cell-to-cell communication from previously published single-cell RNA sequencing and, by using cell-specific knockout mice, I demonstrate that removal of semaphorin 3C (Sema3C) in MNs, or its receptor PlexinD1 in ECs, results in premature vascularization of MN columns. Furthermore, *in vitro* assays similarly show that removal of one of the factors in the respective cell results in increased contact between MNs and ECs. This premature vascular misspatterning leads to MN developmental defects such as impaired MN axon exiting the spinal cord at early stages. At later developmental stages, removal of PlexinD1 signaling in ECs leads to MN maturation defects. This study shows the importance of Sema3C-PlexinD1 signaling as a communication path between MNs and ECs during development. It also demonstrates that for proper spinal cord formation a timely and spatially controlled vascularization is fundamental. In the second part of my thesis, I provide additional evidence that highlights the importance of the neurovascular unit in pathology. My results suggest that ECs and their derived factors are involved in the development and/or maintenance of chronic pain. I show that persistent inflammatory pain or neuropathic pain lead to a temporal and local opening of the blood-spinal cord barrier (BSCB), even without major changes in the neurovascular structure. Furthermore, I demonstrate that leucine-rich α-2 glycoprotein 1 (Lrg1) is increased in ECs and in the bloodstream in pain conditions, and that it might be a potential regulator of BSCB permeability.

Overall, this thesis shows that interactions between neural and vascular cells are not only required to fine-tune embryonic CNS development, but that they also play a role in the regulation of pathologies, as I show for chronic pain. These results support the need of not only study such complex systems in isolation, but

that research towards better understanding their inter-relationship is also important.

Zusammenfassung

Die Bildung und Aufrechterhaltung einer so hochspezialisierten Struktur wie des Zentralnervensystems (ZNS) erfordert die gleichzeitige Zusammenarbeit zwischen dem vaskulären und dem neuronalen System. Die Interaktionen zwischen diesen Systemen sind notwendig, um sich gegenseitig zu instruieren, sich korrekt zu entwickeln und homöostatische Bedingungen zu erreichen. Daher ist das Verständnis der neurovaskulären Kommunikation während der Embryonalentwicklung und ihrer Veränderungen in der Pathologie von grundlegender Bedeutung.

Hier zeige ich eine neuartige Wechselwirkung im sich entwickelnden Rückenmark zwischen Motoneuronen (MN) und Endothelzellen (EC) auf, die notwendig ist, um die MN-Säulen für eine bestimmte Zeit avaskulär zu halten. Durch Ableitung und Analyse der Zell-zu-Zell-Kommunikation aus bereits veröffentlichten Einzelzell-RNA-Sequenzierungen und durch die Verwendung von zellspezifischen Knockout-Mäusen zeige ich, dass die Entfernung von Semaphorin 3C (Sema3C) in MNs oder seines Rezeptors PlexinD1 in EC zu einer vorzeitigen Vaskularisierung der MN-Säulen führt. Darüber hinaus zeigen In-vitro-Tests, dass die Entfernung eines der Faktoren in der jeweiligen Zelle zu einem verstärkten Kontakt zwischen MNs und EC führt. Diese vorzeitige Gefäßfehlverteilung führt zu Defekten in der MN-Entwicklung, wie z. B. einem gestörten Austritt der MN-Axone aus dem Rückenmark in frühen Stadien. In späteren Entwicklungsstadien führt die Unterbrechung der PlexinD1-Signalübertragung in den EC zu Defekten bei der MN-Reifung. Diese Studie zeigt die Bedeutung der Sema3C-PlexinD1-Signalübertragung als Kommunikationsweg zwischen MNs und EC während der Entwicklung. Sie zeigt auch, dass für die korrekte Bildung des Rückenmarks eine zeitlich und räumlich kontrollierte Vaskularisierung von grundlegender Bedeutung ist. Im zweiten Teil meiner Arbeit liefere ich zusätzliche Beweise, die die Bedeutung der neurovaskulären Einheit in der Pathologie unterstreichen. Meine Ergebnisse deuten darauf hin, dass EC und von ihnen abgeleitete Faktoren an der Entwicklung und/oder Aufrechterhaltung chronischer Schmerzen beteiligt sind. Ich zeige, dass anhaltende entzündliche Schmerzen oder neuropathische Schmerzen zu einer zeitlichen und lokalen Öffnung der Blut-Rückenmark-Schranke (BSCB) führen, auch ohne größere Veränderungen in der

neurovaskulären Struktur. Darüber hinaus zeige ich, dass das leucinreiche α-2-Glykoprotein 1 (Lrg1) bei Schmerzzuständen in EC und im Blutkreislauf erhöht ist und dass es ein potenzieller Regulator der BSCB-Permeabilität sein könnte.

Insgesamt zeigt diese Arbeit, dass Interaktionen zwischen neuronalen und vaskulären Zellen nicht nur für die Feinabstimmung der embryonalen ZNS-Entwicklung erforderlich sind, sondern dass sie auch eine Rolle bei der Regulierung von Pathologien spielen, wie ich für chronische Schmerzen zeige. Diese Ergebnisse unterstreichen die Notwendigkeit, solche komplexen Systeme nicht nur isoliert zu untersuchen, sondern auch ihre Wechselbeziehungen besser zu verstehen.

Abbreviations

Abbreviation	Full name
ATP	Adenosine Tri-Phosphate
Ang1	Angiopoetin-1
BBB	Blood-Brain Barrier
Bdnf	Brain-Derived Neurotrophic Factor
Bmp	Bone Morphogenic Proteins
BSCB	Blood-Spinal Cord Barrier
BVs	Blood Vessels
CCI	Chronic Constriction Injury
Ccl2	Chemokine Ligand 2
Ccr2	Chemokine Receptor 2
CD31	Cluster of Differentiation 31
cDNA	Complementary cDNA
CFA	Complete Freund's Adjuvant
Cgrp	Calcitonin-Gene Related Peptide
ChAT	Choline Acetyltransferase
CNS	Central Nervous System
CSF	Cerebrospinal Fluid
Cx3Cr1	Cx3C Motif Chemokine Receptor 1
Cxcl10	Chemokine Ligand 10
Cxcr3	Cxc Motif Chemokine Receptor 3
D-V	Dorso-Ventral
Da	Dalton
Dbx1	Developing Brain Homeobox Protein 1
Dbx2	Developing Brain Homeobox 2
DRG	Dorsal Root Ganglia
E	Embryonic Day
EB	Evans Blue
EC	Endothelial Cell
En-1	Engrailed-1
FBS	Fetal Bovine Serum
Fgf	Fibroblast Growth Factors
FP	Floor plate
GABA	Gamma-Aminobutyric Acid
Gap	Gtpase-Activating Protein
Gapdh	Glyceraldehyde 3-Phosphate Dehydrogenase
Gdnf	Glial Cell Derived Neurotrophic Factor
Gfap	Glial Fibrillary Acidic Protein
HBMECs	Human Brain Microvascular ECs
Hif1α	Hypoxia Inducible Factor 1
HMC	Hypaxial Motor Column

Igf-1	Insulin-Like Growth Factor-1
IgG	Immunoglobulin
Il-18	Interleukin-18
Il-1β	Interleukin-1β
Il-6	Interleukin-6
IPCs	Intermediate Progenitor Cells
IPT	Ig-Like, Plexins and Transcript Factors
Irx3	Iroquois-Class Homeodomain Protein 3
ISH	*In Situ* Hybridization
Isl1/2	Islet1/2
IsoB4	Isolectin GS-IB4
Jams	Junction Associated Molecules
kDa	Kilodalton
KO	Knockout
LMCl	Lateral Lateral Motor Column
LMCm	Medial Later Motor Column
Lrg1	Leucine-Rich A-2 Glycoprotein 1
LTP	Long-Term Potentiation
MEPs	Motor Neuron Exit Points
MMC	Medial Motor Column
MNs	Motor Neurons
mRNA	Messenger RNA
NaFlu	Sodium Fluorescein
Ngf	Require Nerve-Growth Factor
Nkx2.2	Nk2 Homeobox 2
Nkx6.1	Nk6 Homeobox 1
NO	Nitric Oxide
Nogo-A	Neurite Outgrowth Inhibition Protein
Nrp1	Neuropilin-1
NVU	Neurovascular Unit
Olig2	Oligodendrocyte Transcription Factor 2
Pax6	Paired Box Protein 6
Pax7	Paired Box Protein 7
PBS	Phosphate Buffered Saline
PCA	Principal Component Analysis
PGC	Preganglionic Autnomic Mns Column
pMN	Motor Neuron Progenitor
PNVP	Perineural Vascular Plexus
RGCs	Radial Glial Cells
rLrg1	Recombinant Lrg1
RNA	Ribonucleic Acid
RT	Room Temperature
SCI	Spinal Cord Injury

scRNAseq	Single Cell RNA Sequencing
Sema	Semaphorin
Sema3	Classe 3 Semaphorin
sFlt1	Soluble Fms-Like Tyrosine Kinase-1
Shh	Sonic Hedgehog
siLrg1	siRNAs Targeting Lrg1
siRNA	Small Interfering Rna
Slit2	Slit Guidance Ligand 2
SNI	Spared Nerve Injury
SP	Release Substance P
Tgf-β	Transforming Growth Factor Beta
TLRs	Toll-Like Receptors
Tnf-α	Tumor Necrosis Factor-α
TrkA	Tropomyosin Receptor Kinase A
Vacht	Vesicular Acetylcholine Transporter
VE	Vascular Endothelial
Vegf	Vascular Endothelial Growth Factor
Vgat	Vesicular Gaba Transporter
Wnt	Wingless-Related Integration Site
WT	Wild-Type
ZO	Zonula Occludens

List of Figures

List of Tables

1 INTRODUCTION

The generation of a single organism requires the precise construction of multiple systems, all inter-connected and functionally driven by the unique characteristics and functions developed by every single cell. And, for every cell to successfully accomplish its task, it requires to be in a constant conversation with all the neighboring cells. This is indispensable for achieving a precise development and homeostasis program. The appropriate number and size of determined cell type, the spatial-temporal window for the occurrence of an event, the presence and concentration (at the micro-scale) of a factor, are examples of how meticulously organized an organism needs to be. The vascular system, formerly seen as simple transporting 'roads', is an important player in this reciprocal communication with the other systems, which should not come as a surprise considering its physical presence in every single part of the body. With more and more research incoming, the controlling dimension exerted by and to vascular cells with its surrounding will be shown to be far beyond what was initially believed. The purpose of this Chapter 1. is to introduce the most relevant knowledge for the understanding of how the development of the central nervous system (CNS) crosstalks with the (in parallel) development of the vascular system, and how both systems in adulthood are still interacting and involved in the development of pain.

1.1. The central nervous system and its development

The vertebrated CNS is a complex organization of structures, comprised by the brain - which is subdivided in two cerebral hemispheres (or telencephalon), cerebellum, diencephalon, and brainstem -, the spinal cord and the retina. To demonstrate the complexity of such system, it was not until the twentieth century that neuroscientists acknowledged one of its fundamental cells, the neuron. Limited by the capacities of the microscopes and staining techniques available at that time, understanding the neuron, a cell type able to present so many multifaceted shapes and structures, was imaginably challenging. This was only possible by the work developed by two of the most important neuroscientists (and simultaneously Nobel prize winners) to date, Camillo Golgi, and Santiago Ramón y Cajal (Chu 2006, Lopez-Munoz, Boya et al. 2006). The CNS functions are

numerous and range from motor actions such as walking, running, and dancing, to cognitive actions such as thinking, speaking, and laughing, which in the end make individual humans unique. However, to get to such mature CNS it is required that its development, a long process that happens both pre- and postnatally, occurs precisely and correctly. From the number of each cell type to its temporal location, the entire developmental program must happen in a well-defined manner, as alterations during this period can potentially result in severe congenital disorders.

1.1.1. Early embryonic development of the CNS

Well before the appearance of the structures that will originate the CNS, embryonic development starts with a simple single cell, the zygote, that upon multiple cell divisions develops into the blastocyst. The blastocyst is composed by three distinct cell groups: an outer layer of cells, the trophectoderm, and an inner located cell mass formed by the epiblast and the primitive endoderm. From these, the epiblast gives rise to the embryo, while the other two group of cells originate the extra-embryonic structures (Rossant and Tam 2009). At embryonic day (E) 6.5 in mouse, a critical early process called gastrulation occurs, where some epiblast cells migrate and form two new cell layers, the mesoderm, and the endoderm, while the remaining steady epiblast cells form the ectoderm layer. These three germ layers are consequently responsible for the generation of all the tissues (Sadler 2005, Solnica-Krezel and Sepich 2012). Besides giving rise to the mesoderm and the endoderm, part of the migratory epiblast cells stops at the midline and form the notochord (Stemple 2005).

The ectoderm, which is the outermost layer of the three germinal layers, further develops into the neural plate, initiating the process of first neurulation (Figure 1.1). Once the neural plate is formed, the cells located at both edges start to fold - creating the neural folds –, move towards each other and, once in contact, fuse transforming the neural plate into the neural tube (Sadler 2005). During this process, a subset of neural crest cells present at the neural folds separates before neural tube formation and migrate elsewhere to form the peripheral nervous system, the pigmented cells of the skin and other peripherical cell types (Gilbert 2006). As the neural tube continues to grow and mature along an anterio-posterior axis, it compartmentalizes into the rostral and caudal vesicles, the

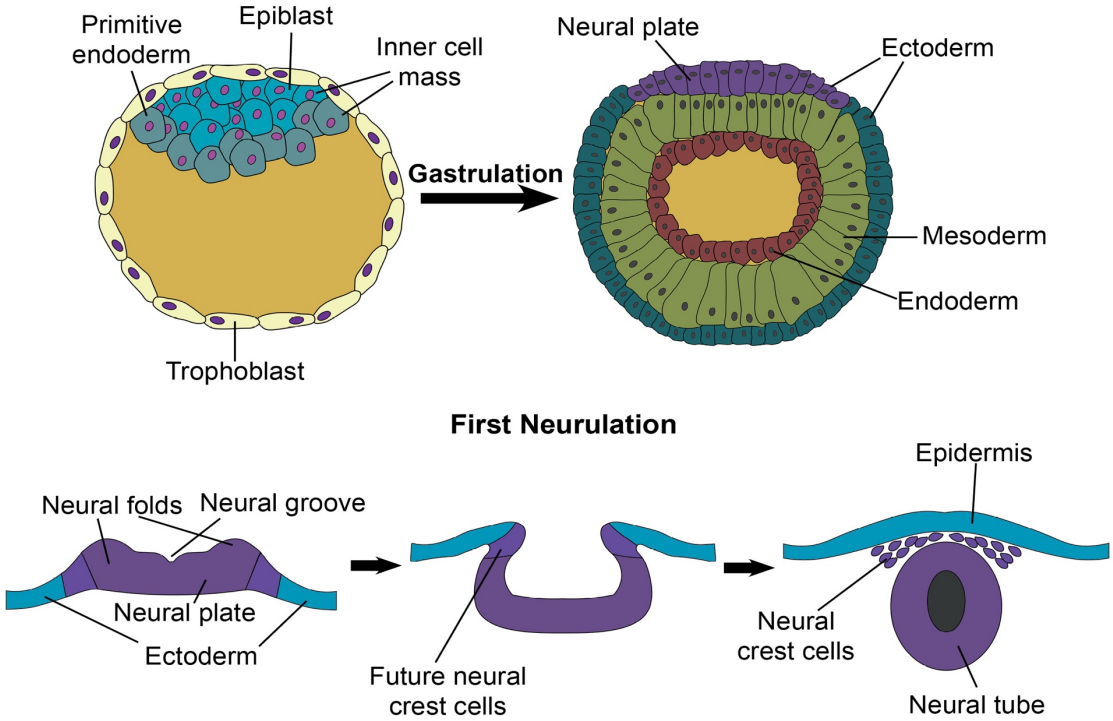

Figure 1.1. Diagram of gastrulation and first neurulation processes. Initially, the embryo (at its blastocyst developmental phase) is composed of two main tissue layers, the inner cell mass, and the trophoblast, an outer shell layer of cells. During gastrulation, the blastocyst develops into a multilayered structure called gastrula, composed by the ectoderm, mesoderm, and endoderm. A part of the ectoderm gives rise to the neural plate, which will in turn transform into the neural tube, a process called first neurulation. During neurulation, the neural plate bends dorsally resulting in the creation of the neural folds and the neural groove. These neural folds migrate towards each other and once in contact, they fuse, resulting in the newly formed neural tube. A group of cells, the neural crest cells, located at the neural folds during neural tube closure separate and migrate towards the periphery where they will differentiate into different peripheral cell types.

primitive structures that will then originate the brain (early divided into prosencephalon, mesencephalon and rhombencephalon) and spinal cord, respectively (Lumsden and Krumlauf 1996, Purves 2008).

At the end of the first neurulation (around E8 in mice), the neural tube is mainly populated by neuroepithelial cells, neural stem cells that have the capacity to originate all the different neural cell types of the CNS (figure 1.2). However, neurons are not directly generated from neuroepithelial cells, but instead through one or multiples stages of divisions with existence of middle precursors (Kriegstein and Alvarez-Buylla 2009). During neural tube growth and expansion, neuroepithelial cells divide to generate radial glial cells (RGCs), which in turn give

rise directly to neurons or intermediate progenitor cells (IPCs) (Gotz and Barde 2005, Gotz and Huttner 2005). Afterwards, IPCs divide symmetrically and generate only neurons. Neuroepithelial cell bodies are initially located in proximity to the ventricle and extend long cell processes contacting the ventricular surface (called apical process) and the pial surface (basal process). As these cells divide and differentiate, they migrate away from the ventricular zone along RGCs

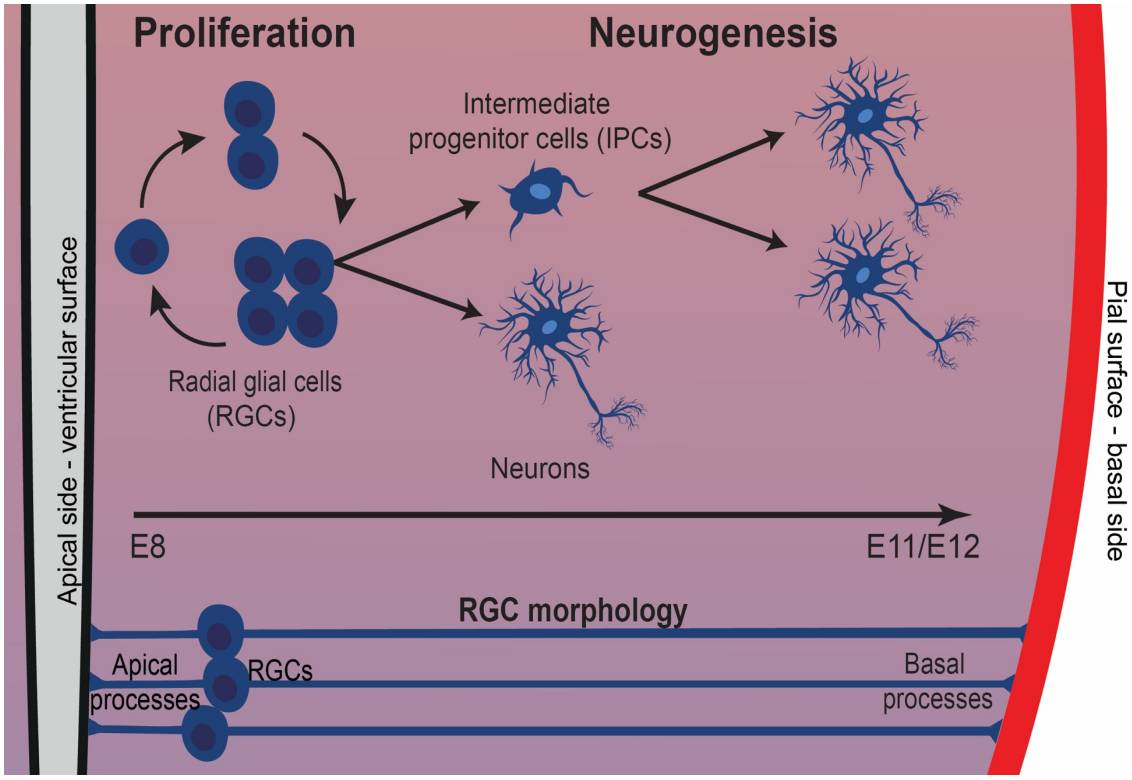

Figure 1.2. Neural tube growth and expansion during neurogenesis. Once neural tube formation is complete, the process of neurogenesis initiates. Neuroepithelial cells located in close contact with the ventricle quickly and extensively proliferate and differentiate into radial glial cells (RGCs), keeping some neuroepithelial features. These RGCs in turn divide, giving rise to either intermediate progenitors (IPCs) or directly neurons. IPCs divide symmetrically and give rise exclusively to neurons. During this process, occurring between E8 and E11/12, neurons migrate towards their final lateral position in the neural tube. Neuroepithelial cells and RGCs present long processes touching the ventricular surface and the pial surface.

processes, creating the mantle zone (Noctor, Flint et al. 2001, Noctor, Martinez-Cerdeno et al. 2008). At this point, the neural tube is divided into an undifferentiated area populated by the different progenitor cells and a differentiated area (mantle zone) occupied with newborn neurons.

In a morphological point of view, the neural progenitors in the ventricular zone look and behave in a similar manner. However, from these progenitors, postmitotic neurons that are highly unalike in their morphology, characteristics,

and function are generated. In the developing spinal cord, this is achieved by each type of postmitotic neurons being originated by a particular group of neural progenitors within the ventricular zone. These different neural progenitors are characterized by acquiring distinct identities in particular spatial positions, a process known as neural patterning (Altmann and Brivanlou 2001).

1.1.2. Dorso-ventral neural tube patterning

The developing neural tube, by the end of the first neurulation, presents a clear regionalization in a dorso-ventral (D-V) axis, achieved by the presence of factors (mainly morphogens) in a time-, location-, and concentration-controlled mode. During neural tube formation, at its upper and bottom parts, two particularly important group of cells located at the midline are specified: the floor plate (FP), located at the bottom, and the roof plate, positioned at the top of the neural tube. These two areas, together with the notochord located underneath the neural tube, are essential sources of signals that induce the D-V patterning of the neural tube (Figure 1.3). The notochord and the FP secrete and generate a gradient of Sonic Hedgehog (Shh) in the ventral part of the spinal cord, while the roof plate creates a gradient of Wingless-related integration site (Wnt) proteins and bone morphogenic proteins (Bmp) in the dorsal part. These counteracting signal gradients together are responsible for the formation of all the eleven different neural progenitor domains along the D-V axis (Briscoe, Pierani et al. 2000, Jessell 2000, Chizhikov and Millen 2005). In addition to these, other factors such as retinoic acid, transforming growth factor beta (Tgf-β) and fibroblast growth factors (Fgf) have been shown to be involved in formation of the D-V patterning (Liem, Tremml et al. 1997, Diez del Corral, Olivera-Martinez et al. 2003, Novitch, Wichterle et al. 2003, Duester 2008, Diez Del Corral and Morales 2017).

Neural progenitors in the developing spinal cord are divided into six dorsal domains (dP1-dP6, numbered from dorsal to ventral) and five ventral domains (p3, motor neuron progenitor (pMN), and p2-p0, ordered from ventral to dorsal). Each one of these domains presents a unique expression profile of transcript factors and gives rise to a specific type of neural cells (Ribes and Briscoe 2009) (figure 1.3a). Dorsal domains originate postmitotic interneurons d1-d6 and ventral domains generate postmitotic interneurons V0-V3 or motor neurons (MNs). Focusing on the ventral developing spinal cord, progenitor domains identity is

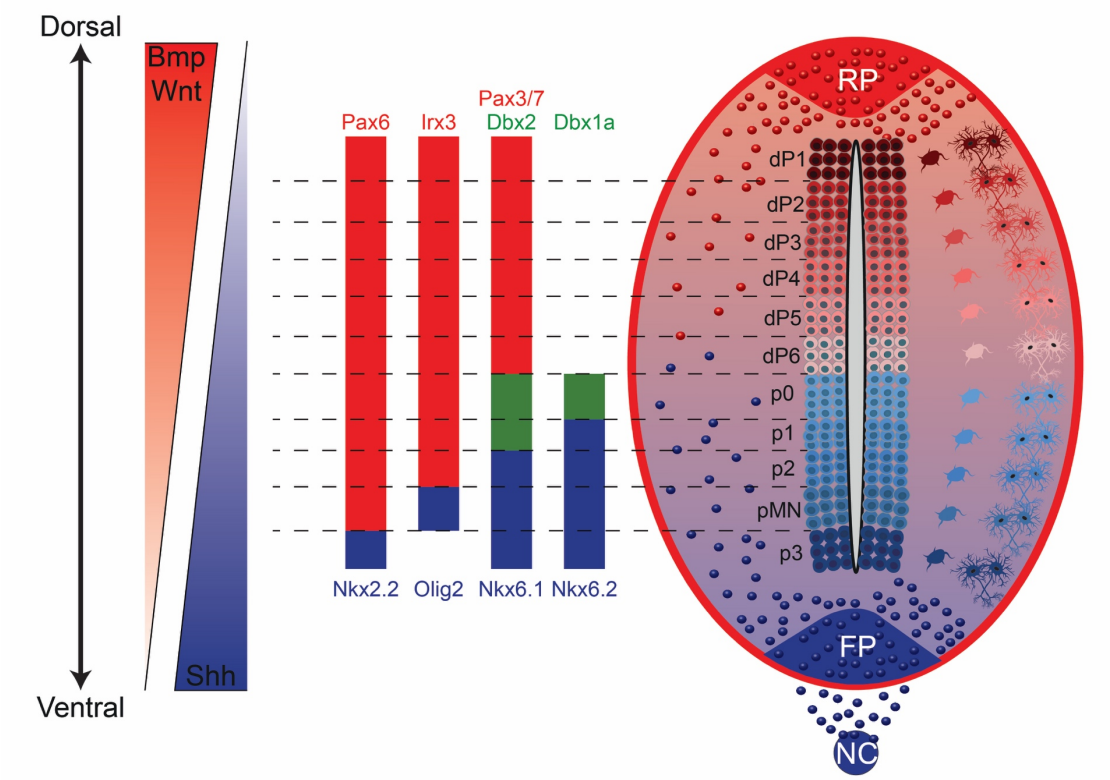

Figure 1.3. Neural tube dorsoventral patterning by Shh, Bmp and Wnt. Opposing gradients of ventral Shh and dorsal Bmp and Wnt determine the dorsoventral domains. The notochord and the floor plate (FP) are responsible for the Shh gradient, while the roof plate generates a gradient of Wnt and Bmp. These counteracting gradients together are responsible for the formation of all the different neural progenitor domains (dP1-dP6 as dorsal domains, p0-p3 and pMN as ventral domains). Each neural progenitor domain presents a unique expression profile of transcript factors (for example, pMN domain is characterized by expression of Pax6, Olig2, Nkx6.1 and Nkx6.2.), and gives rise to a specific type of neural cells.

achieved by the presence of cross-repressive interactions between transcript factors that mediate Shh-dependent signaling. These factors are divided into two subclasses: class I proteins repressed by Shh (such as paired box protein 7 (Pax7), iroquois-class homeodomain protein 3 (Irx3), developing brain homeobox protein 1 (Dbx1), Dbx2 and Pax6), and class II proteins induced by Shh (such as NK6 homeobox 1 (Nkx6.1) and Nkx2.2) (Briscoe, Pierani et al. 2000, McMahon 2000, Briscoe and Ericson 2001). The temporal and spatial expression of each of these factors is required to be precisely controlled. Loss-of-function of individual factors alters the degree of the cross-repressive interactions resulting in the deletion, expansion or contraction of progenitor domains (Dessaud, McMahon et al. 2008). During the differentiation of neural progenitors to postmitotic neurons, these cells migrate from the ventricular zone towards the

mantle zone where they populate a specific position within the spinal cord (Ribes and Briscoe 2009).

1.1.3. Motor neuron development and circuitry

MNs are a particular important neuronal cell type, differing from the remaining spinal cord (inter)neurons, whose axons project to the periphery to control the effector organs (muscles and glands). As they are responsible for all the movements of the organism, defects in their development or function can result in embryonic disorders in humans (Teoh, Carey et al. 2017), such as type I spinal muscular atrophy (Soler-Botija, Ferrer et al. 2002), and lethal arthrogryposis associated with anterior horn cell disease (Vuopala, Ignatius et al. 1995). In adulthood, impairment, and death of MNs lead to severe neurogenerative disorders, such as amyotrophic lateral sclerosis, progressive muscular atrophy, and spinal muscular atrophy.

MNs arise from the pMN domain, characterized by the expression of oligodendrocyte transcription factor 2 (Olig2), Nkx6.1 and Pax6 (Ericson, Rashbass et al. 1997, Novitch, Chen et al. 2001, Zhou and Anderson 2002). MNs are a special type of neurons, as they are one of the few neuronal cells located in the CNS that project their axons out to target the periphery, making them one of the most studied neuronal subtypes. MN development can be divided into three main phases, required for their correct function: specification of MN identity, MN clustering in functionally related groups together with MN axon projection out of the CNS into the periphery, and MN pre- and post-synaptic connectivity with other neuronal cells and muscles (figure 1.4) (Price and Briscoe 2004, Stifani 2014). Below I give more details on these processes.

MNs are one of the first neurons in the developing spinal cord to be specified, with their birth occurring around E9.5 (Jessell 2000). Initially, within the pMN domain, MNs start to acquire neuronal properties and specific characteristics of differentiating motor neurons by expressing Olig2 (Novitch, Chen et al. 2001). Afterwards, when MN progenitors are at their final cell division, Mnr2 expression is induced, acting as a determinant of MN identity (Tanabe, William et al. 1998). The induction of these two transcript factors is dependent on the activity of Nkx6.1, induced by Shh signaling (Tanabe, William et al. 1998, Novitch, Chen et al. 2001). The importance of Olig1/Olig2 transcript factors for

the specification of this domain have been further demonstrated, as deletion of either of them results in complete lack of MNs (Zhou and Anderson 2002, Wu, Wu et al. 2006). Additionally, Shh-independent mechanisms have been suggested to contribute for pMN and MN specification (Litingtung and Chiang 2000).

Following MNs specification and migration to their final ventro-lateral location in the spinal cord, MNs acquire different subtype identities and cluster into MN columns according to their innervation muscle targets (Landmesser 1980). This process starts at around E10.5 and ends at E12.5 (Francius and Clotman 2014). The first experiments demonstrating a clear segregation of MNs into columns were done by orthograde and retrograde tracing of motor neurons in chick embryos (Landmesser 1978a, Landmesser 1978b, Hollyday 1980, Gutman, Ajmera et al. 1993), where injections into different muscles resulted in tracer uptake and further labeling of specific pools of MNs. Importantly, these different MN pools express particular combinations of transcript factors, thus making them easily identifiable (Tsuchida, Ensini et al. 1994, Dasen, Liu et al. 2003, Francius and Clotman 2014). Depending on the anterior-posterior spinal cord level, MNs can be found in different pools: at brachial and lumbar levels (limb levels) MNs are segregated into medial motor column (MMC), lateral lateral motor column (LMCl) and medial later motor column (LMCm); at thoracic level MNs pool into MMC, hypaxial motor column (HMC) and preganglionic autonomic MNs column (PGC). In simultaneous, MNs from each of these columns project their axons, between E10-E12.5, to target particular muscles. MNs of the LMCm and LMCl innervate the ventral and dorsal muscles of the limbs, respectively, MNs from MMC innervate axial muscles, the PGC MNs are responsible to innervate the sympathetic chain ganglia and the HMC innervates intercostal muscles (Dasen and Jessell 2009, Francius and Clotman 2014).

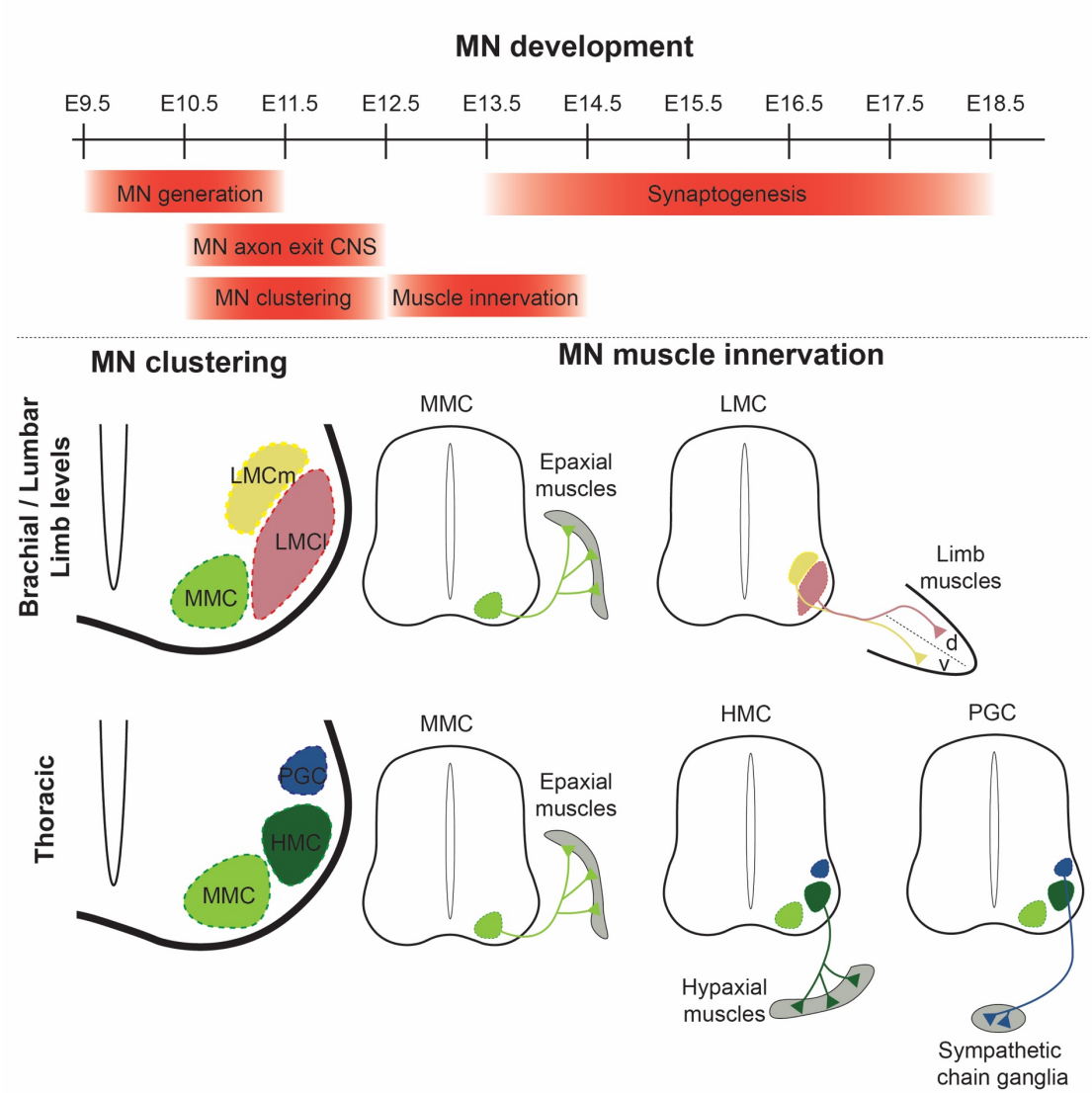

Figure 1.4. Embryonic motor neuron development. Motor neuron (MN) generation occurs early in embryonic development, at around E9.5, and its development and further maturation continues up to postnatal stages. Following MN specification, MNs start clustering into MN columns according to their innervation target. The medial motor column (MMC) is present at all the spinal cord levels, while the lateral motor column (LMC) divided into two subgroups (lateral LMC – LMCl - and medial LMC – LMCm) is found only at brachial and lumbar levels. At thoracic levels, besides the MMC, MNs cluster into the hypaxial motor column (HMC) and the preganglionic column (PGC). The MMC MNs are responsible for the innervation of epaxial muscles, the LMC columns innervate the limb muscles (the LMCl is responsible for the dorsal part of the limb, while LMCm targets the ventral part of the limb), the HMC MNs innervate the hypaxial muscles and the PGC MNs final target is the sympathetic chain ganglia. In parallel to MN clustering, MNs send their axons into the periphery in order to reach their final destination target. Afterwards, MNs start making connections with their muscle targets and start making synapsis with other neurons (interneurons and afferent neurons), creating a complex spinal cord circuit. Further synaptic refinement continues postnatally.

At around E13/E14, MNs start to make not only connections with their muscle targets in the periphery (neuromuscular junction formation and refinement

occurs up to postnatal stages) (Wu, Xiong et al. 2010), but also with other interneurons within the spinal cord, creating a complex spinal circuit (Arber 2012). MNs besides targeting the peripheral muscles, also makes synapses with V1 Renshaw interneurons (Mentis, Alvarez et al. 2005, Richards, Griffith et al. 2014). On the other hand, MNs receive and integrate inputs from multiple interneurons and sensorial neurons (Lu, Niu et al. 2015, Lai, Seal et al. 2016).

1.2. Blood vessels – formation and main aspects of the vasculature

The formation of blood vessels occurs through two main processes, angiogenesis and vasculogenesis. Vessels arising by vasculogenesis are originated by the differentiation of hemangiogenic stem cells and mesoderm-derived angioblasts into endothelial cells (ECs) and the assembly of those into primitive vascular networks, which then remodel to form the first vessels of an organism (Demir, Kayisli et al. 2006). On the other hand, angiogenesis refers to the formation of vessel branches from pre-existing vessels (Burri and Tarek 1990). Sprouting angiogenesis is the most occurring type, and its process occurs in consequently steps: in an initial phase, the basement membrane is degraded, and ECs start to proliferate and migrate; afterwards, ECs start forming 3D-shaped vessels, which get stabilized by being covered with a new basement membrane and with recruitment and attachment of mural cell types (Risau 1997, Adair and Montani 2010). During this process, vessel growth is led, at its tip, by a specialized EC termed endothelial tip cell, which extends filopodia and senses the guidance cues in the surrounding environment (Carmeliet and Tessier-Lavigne 2005, Eichmann, Makinen et al. 2005). Following the tip cell are the stalk ECs, which proliferate considerably and establish tight connections between them to ensure stability to the vessel sprout. The balance between tip and stalk phenotype is fundamental for proper sprouting angiogenesis and it has been shown to be mainly ensured by the Vegf and Notch signaling pathways (Blanco and Gerhardt 2013).

The regulation of angiogenesis is achieved by the presence and balance of anti- and pro-angiogenic factors. One of the most important inducers of angiogenesis is hypoxia, the insufficiency of adequate oxygen levels: lack of oxygen induces the stabilization of the Hypoxia-inducible factor 1 (Hif1α) which then translocate to the nucleus and, consequently, results in increased

expression of the potent pro-angiogenic factor vascular endothelial growth factor (Vegf) (Ferrara, Gerber et al. 2003). Vegf was first found to have a central role in regulating vascularization in studies using Vegf KO mice, in which mice embryos died as early as E8.5 lacking formation of several vascular structures (Carmeliet, Ferreira et al. 1996). In the CNS, removal of Vegf in a neuronal-specific manner also resulted in hipovascularization, hypoxia and subsequent neuronal death (Haigh, Morelli et al. 2003). Another main molecular mechanism shown to modulate angiogenesis in the CNS is the Wnt pathway. Wnt signaling through different complexes of receptors has been shown to promote CNS vascularization. During vessel development, canonical Wnt/β-catenin pathway is implicated in angiogenesis by influencing vessel sprout, vessel remodeling, and arterio-venous specification, while also contributing further for the maturation of vessels by inducing blood-brain barrier (BBB) properties (Dejana 2010, Reis and Liebner 2013).

1.3. CNS vascularization

The development of the embryonic vasculature starts shortly after the end of gastrulation. To meet the energetic demand of a such high consuming CNS, throughout its development a dense network of blood vessels (BVs) expands to support neural cells with oxygen and nutrients. Remarkably, as the neural compartment undergoes proliferation and differentiation, the CNS begins to be simultaneously vascularized.

1.3.1. Spinal cord vascularization

The beginning of spinal cord vascularization, similar to the brain, occurs at around E8.5 in mouse embryos with the formation of the perineural vascular plexus (PNVP), a primitive vascular network surrounding the pial surface. The assembling of the PNVP occurs via vasculogenesis, when mesoderm-derived angioblasts proliferate, migrate and differentiate giving rise to the EC lineage that forms BVs (Ambler, Nowicki et al. 2001). Experimentation in quail embryos identified VEGF and FGF-2 as key factors for the PNVP formation (Cox and Poole 2000, Hogan, Ambler et al. 2004).

Once the PNVP is assembled, the first BVs sprout from the PNVP into the spinal cord via angiogenesis. While in avians single angioblasts invade the spinal cord and generate vessels within it (Kurz, Gartner et al. 1996), in mice vessel ingression into the spinal cord only occurs via sprouting angiogenesis, with new sprouts arising from the previously formed PNVP (Nakao, Ishizawa et al. 1988, Himmels, Paredes et al. 2017). Between E9.5-E10.5 in mouse, vessel sprouts invade the neural tissue of the spinal cord in a highly stereotypical manner (figure 1.5). The first sprouts enter into the ventral part of the spinal cord in two places, between the FP and MN columns and at the opposite adjacent side of MN columns. Different factors have been involved in causing this first initial vessel ingression, such as Vegf (James, Gewolb et al. 2009, Himmels, Paredes et al. 2017), Wnt7a/b (Stenman, Rajagopal et al. 2008, Daneman, Agalliu et al. 2009) and soluble fms-like tyrosine kinase-1 (sFlt1) (Himmels, Paredes et al. 2017). Consecutively, between E10.5-E11.5, the ingressing vessels from both sides of MN columns grow towards each other, fusing, and completely surrounding these columns. In simultaneous, other sprouts from the initial vessels branch and prolong towards dorsal regions along the ventricular zone (Nakao, Ishizawa et al. 1988). Interestingly, up until this developmental time, vessels avoid entering into the ventricular zone occupied by neural progenitor somas, MN columns and the FP, despite the presence of high amounts of Vegf in these three regions (Kurz 2009, Ruiz de Almodovar, Fabre et al. 2011, Himmels, Paredes et al. 2017). At E12.5, a vast network of vessels is present within the entire spinal cord and, only at this point, sprouts invade and vascularize MN columns (however the neural progenitor and FP areas remain avascular) (Himmels, Paredes et al. 2017).

1.3.2. Neurovascular interactions controlling spinal cord vascularization

Besides its original known transporter function, vessels are actively establishing communications with neural cells (and vice-versa), which are required for a proper CNS and vascular development and function (Tata, Ruhrberg et al. 2015, Paredes, Himmels et al. 2018, Segarra, Aburto et al. 2019, Vieira, Shah et al. 2020). During spinal cord vascularization, neural cells signal to ECs in order to guide BV growth, being in part responsible for the stereotypical vessel patterning described above (figure 1.5).

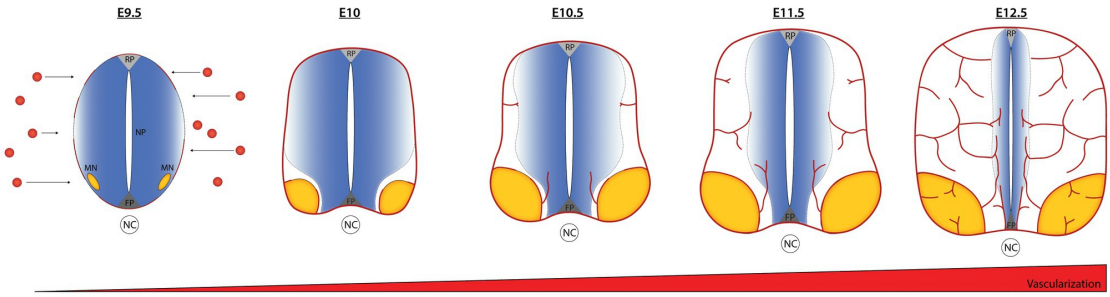

Factors involved in spinal cord vascularization

E9.5 - Development of the PNVP	E10 to E10.5 - Vessel ingression into the SC	E11.5 onwards - Stereotypical vessel patterning within the SC
FGF-2 (Cox and Poole., 2000) **VEGFA** (Hogan et al., 2004; Matsuoka et al., 2017)	**WNT7a/b** (Daneman et al., 2009; Stenman et al, 2008) **GPR124** (Kuhnert et al., 2010; Posokhova et al., 2015; Vanhollebeke et al., 2015; Zhou and Nathans, 2014) **RECK-Norrin** (Cho et al., 2017; Vanhollebeke et al., 2015) **VEGFA** (James et al., 2009) **sFLT1** (Wild et al., 2017)	**sFLT1** (Himmels et al., 2017; Matsuoka et al., 2016; Wild et al., 2017) **VEGFA** (Himmels et al., 2017; Takahashi et al., 2015)

Figure 1.5. Stereotypical spinal cord vascularization. Simultaneously to neurogenesis, spinal cord vascularization is also occurring. The spinal cord starts to be vascularized at E8.5-E9.5 by the formation of the peri-neural vascular plexus (PNVP) that surrounds the entire CNS. At around E10, the first blood vessels ingress into the spinal cord from the PNVP and follow a highly specific invading patterning: the first sprouts ingress in between the floor plate (FP) and motor neuron (MN) columns (in yellow); afterwards, vessels completely surround the MN columns and continue to grow towards the dorsal part of the spinal cord, but constantly avoid entering into the MNs columns, FP, and part of the neural progenitors (NP) area for a particular time window. At E12.5, vessels start to finally vascularize MN columns and a dense network of vessels is present within the spinal cord to support its growth and development. The known factors involved in the different steps of spinal cord vascularization are indicated in the table. Reprinted with author permission from Frontiers in physiology (Vieira et al 2020).

Coincident to the first initial vessel ingression into the spinal cord, Wnt7a and Wnt7b, as other Wnt family members, are expressed in dorsal and ventral neural progenitors of the spinal cord (Parr, Shea et al. 1993, Stenman, Rajagopal et al. 2008, Daneman, Agalliu et al. 2009). While removal of either ligand does not result in any abnormal phenotype, Wnt7a/b double null mutants show a ventral spinal cord completely devoid of vessels, with only a few sprouts in the dorsal part. (Stenman, Rajagopal et al. 2008, Daneman, Agalliu et al. 2009). Additionally, this neural-derived signaling was not only shown to contribute for spinal cord vascularization, but also to promote BBB formation (Stenman, Rajagopal et al. 2008, Daneman, Agalliu et al. 2009).

Interestingly, despite of Vegf being present in MN columns, BVs avoid entering into them for a specific developmental time window (E10.5-E12.5). This is accomplished by MNs maintaining a balance of simultaneously secreted Vegf, in a hypoxia inducible factor 1 (Hif1α) dependent manner, and the Vegf decoy

receptor sFlt1 in a neuropilin-1 (Nrp1) dependent manner (Himmels, Paredes et al. 2017). This tight balance is indispensable, as overexpression of Vegf or reduction of either sFlt1 or Nrp1 in MNs result in premature BV ingression into MN columns (Himmels, Paredes et al. 2017). The importance of neural cells in creating a Vegf-sFlt1 balance for controlling spinal cord vascularization has also been demonstrated in zebrafish (Matsuoka, Rossi et al. 2017, Wild, Klems et al. 2017). While Vegf-sFlt1 equilibrium can be created by a neural cell type secreting both factors, it can also be achieved by neural cells secreting VEGF and ECs responding by secreting sFLT1 (Takahashi, Takase et al. 2015). Within the spinal cord, BVs grow from the ventral region towards dorsal areas along and in close contact with the undifferentiated neural progenitors in mice. Comparably, in avian, vessels extend from ventral to dorsal areas by growing in between the neural progenitor zone (undifferentiated region) and the differentiated mantle zone, but constantly avoiding to enter into the neural progenitor zone (Takahashi, Takase et al. 2015). This vessel patterning is obtained by neural progenitors secreting VEGF, attracting vessels to grow in their vicinity but, simultaneously, ECs respond by secreting sFLT1 to counter Vegf attraction (Takahashi, Takase et al. 2015).

Besides the above described neural-exerted signals used to control developing spinal cord vascularization, other mechanisms and molecular cues have been shown to guide vessels during development of the other two structures of the CNS, the brain and retina (Paredes, Himmels et al. 2018, Segarra, Aburto et al. 2019). Some examples are Wnt7a/b (as demonstrated in the spinal cord, mentioned above) (Cho, Smallwood et al. 2017), Tgf-β1 (Siqueira, Francis et al. 2018), neurite outgrowth inhibition protein (Nogo-A) (Walchli, Pernet et al. 2013, Walchli, Ulmann-Schuler et al. 2017), slit guidance ligand 2 (Slit2) (Rama, Dubrac et al. 2015), semaphorin (Sema) family members (Kim, Oh et al. 2011) and others (Paredes, Himmels et al. 2018). Interestingly, despite of most of these signaling molecules being also expressed by neural cells in the developing spinal cord, their role in controlling vascularization has not been described.

Among all these possible modulators of vascularization, several Sema members are substantially expressed by the spinal cord neural compartment during early spinal cord vascularization. However, little is known whether a possible effect of Sema proteins in ingressing ECs exists.

1.3.3. The semaphorin family and its plexin/neuropilin receptors

The first Sema member to be discovered, initially called Fasciclin IV, was described to be involved in axon guidance in the grasshopper embryo (Kolodkin, Matthes et al. 1992). Nowadays, Semas are a large family of more than twenty transmembrane or secreted proteins, subdivided into eight different classes (figure 1.6). Classes 1 and 2 are present in invertebrates, classes 3 to 7 are found in vertebrates (Sema5c is an exception as it is also found in invertebrates) and class 8 is viral-encoded (Alto and Terman 2017). Structurally, Semas are composed of a highly conserved Sema domain and a plexin-semaphorin-integrin (PSI) domain, with other additional domains differentiating Semas (Feiner, Koppel et al. 1997, Zhou, Gunput et al. 2008). From the 8 subclasses, Semas can be membrane-associated (classes 1 and 4-7) or secreted (classes 2, 3 and 8).

The primary receptors for Semas are plexins and Nrps (Tamagnone and Comoglio 2000). Plexins are arranged into four classes (A-D), with each class composed of multiple individual plexins (figure 1.6). Plexins structure includes a Sema domain, three PSI domains and three Ig-like, plexins and transcript factors (IPT) domains in their extracellular region, and a divided GTPase-activating protein (GAP) intracellular domain. Most of the bindings between Semas and plexins occurs through the Sema domains present in both proteins. However, class 3 semaphorin (Sema3) members additionally require the association of plexins to Nrps to form a receptor complex (He and Tessier-Lavigne 1997, Kolodkin, Levengood et al. 1997), with exception of Sema3E binding to PlexinD1, which occurs without Nrps (Gu, Yoshida et al. 2005). There are two different Nrps, Nrp1 and Nrp2. Nrps are transmembrane glycoproteins and, besides binding to Sema3, also act as receptors for Vegf (Pellet-Many, Frankel et al. 2008, Schwarz and Ruhrberg 2010). As Nrps cytoplasmic domain is considerably small, lacking catalytic activity, they require the formation of a complex with other cell surface receptors for signal transduction (Larrivee, Freitas et al. 2009, Schwarz and Ruhrberg 2010). Besides signaling through Sema-receptor binding, Sema3 members, once produced, can have their function regulated by furin or furin-like endoproteinases, which recognize consensus RXK/RR motifs in the Sema's PSI domain and C-terminus, cleaving them and altering the degree of their effect (Adams, Lohrum et al. 1997). From the different subclasses of Semas, Sema3-

PlexinD1/Nrp interactions have been demonstrated to play key roles in the embryonic development of the cardiovascular system and to control local angiogenesis.

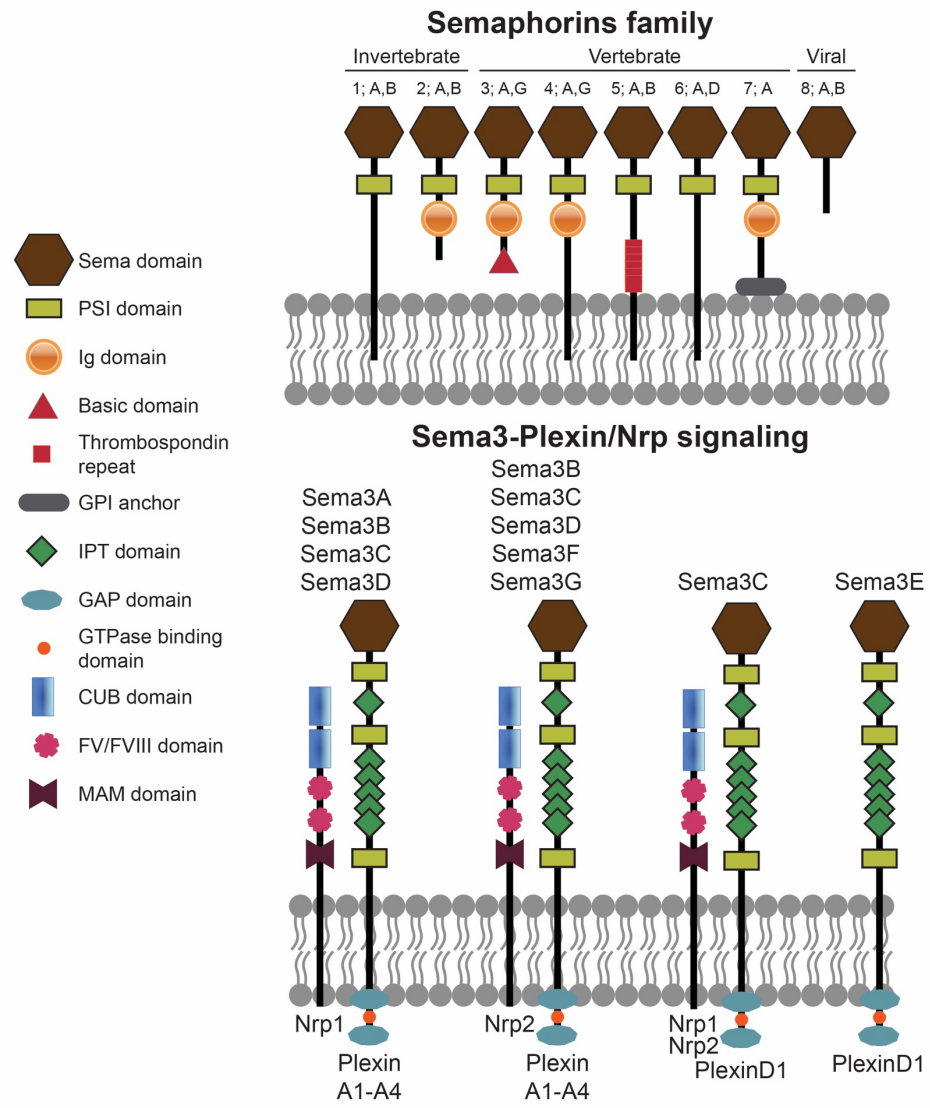

Figure 1.6. Structure of semaphorins and Sema3 interactions with Plexins and Neuropilins. Semaphorin family is divided into eight classes: class 1 and 2 being present in invertebrates (together with Sema5C), class 3 to 7 representing vertebrate semaphorins and class 8 being viral semaphorins. All semaphorins (excluding class 8) have a Sema domain and a PSI domain, and based on their class, can contain other domains, such as Ig and basic domains. Classes 2, 3 and 8 are secreted proteins. Sema3 members signal through different receptor complexes. Sema3A, 3B, 3C and 3D signal to PlexinA1-A4 in combination with neuropilin 1 (Nrp1), Sema3B-3G signal through PlexinA1-A4/Nrp2, Sema3C can in addition signal to PlexinD1/Nrp1(2) and Sema3E is the only Sema3E member that can signal directly to PlexinD1 without Nrps as co-receptors.

1.3.4. Sema3-PlexinD1/Nrp signaling for vascular development

The role of Nrps in cardiovascular development was initially discovered by analysis of Nrp1 overexpression or null transgenic mice, which presented excessive leaky BVs or a considerably underdeveloped vascularization, respectively (Kitsukawa, Shimono et al. 1995, Kawasaki, Kitsukawa et al. 1999). In contrast, Nrp2 appears to play mainly a compensatory role for the lack of Nrp1 (Takashima, Kitakaze et al. 2002, Gu, Rodriguez et al. 2003, Plein, Calmont et al. 2015), with Nrp2-null mice not presenting obvious developmental angiogenesis defects (Shen, Samul et al. 2004). Nrp1 and Nrp2 are expressed in ECs and neurons during embryonic development, with Nrp2 being later restricted to veins and lymphatic vessels (Herzog, Kalcheim et al. 2001, Yuan, Moyon et al. 2002, Fantin, Schwarz et al. 2011, Himmels, Paredes et al. 2017). Despite of Nrp1 being present in both tip and stalk ECs, it was found to be particularly important for tip cell function (Fantin, Vieira et al. 2013, Fantin, Lampropoulou et al. 2015). Similar to Nrps, PlexinD1 is mainly expressed by ECs (van der Zwaag, Hellemons et al. 2002) and plays a central role in cardiac development, with both PlexinD1-null and EC-specific PlexinD1 knockout (KO) mice presenting cardiovascular abnormalities, vascular patterning defects and embryonic lethality at birth (Gitler, Lu et al. 2004, Zhang, Singh et al. 2009).

Sema3E-PlexinD1 signaling, without Nrps as co-receptors, is one of the most well-known pathways regulating developmental vascularization. In the trunk, somites secrete Sema3E that binds to PlexinD1 in ECs, in order to repel and avoid that ECs enter into the somites area (Gitler, Lu et al. 2004, Gu, Yoshida et al. 2005). When either Sema3E or PlexinD1 are genetically knocked out, the vascular network disorganizes, and vessels penetrate into the somites. Sema3A has also been shown to contribute for preventing intersegmental vessels from entering into somites (Torres-Vazquez, Gitler et al. 2004). Mechanistically, in the developing mouse retina and in zebrafish, Sema3E-PlexinD1 pathway was shown to crosstalk with Vegf signaling (Fukushima, Okada et al. 2011, Kim, Oh et al. 2011). In zebrafish, Sema3E-PlexinD1 activation in ECs results in increased expression of sFlt1 that subsequently antagonizes proangiogenic Vegf signaling. When PlexinD1 is removed, the sFlt1-specific Vegf inhibition is reduced and increased vessel sprouting occurs (Zygmunt, Gay et al. 2011). In a slightly different way, in the developing retina, Sema3E-PlexinD1 signaling regulates

Vegf pathway by negatively modulating the activity of Vegf-induced Delta-like 4 (Dll4)-Notch signaling (Kim, Oh et al. 2011). Additionally, Sema3A has been demonstrated to induce anti-angiogenic responses in ECs (Acevedo, Barillas et al. 2008, Maione, Molla et al. 2009). In pathological conditions, Sema3C signals through the PlexinD1/Nrp1 receptor complex in ECs, causing disruption of EC junctions, suppression of EC focal adhesion and decreased EC migration and survival, which in turn results in inhibition of pathological angiogenesis (Yang, Hu et al. 2015).

1.4. Beyond embryonic development: chronic pain as a CNS pathology

The CNS development, including its vascularization, is meticulously controlled to ensure that its function is not compromised. However, even when development goes flawless, environmental factors, physical injuries or aging related degeneration can originate disorders of the CNS. Abnormal neurovascular interactions have been associated to numerous CNS pathologies. However, for many others, including chronic pain, much is still waiting to be unraveled. In these next sections, I introduce key concepts for the understanding of the somatosensory system, the development of acute pain and its transition to chronic pain, and the contribution of neurovascular interactions to chronic pain.

1.4.1. The somatosensory system

The ability to transduce, encode, perceive, and transmit the information of continuous stimuli coming from the surrounding environment is possible due to the existence of the somatic sensory system. However, the different types of stimuli are not processed in the same way, having the somatic sensory system two main subsystems: a subsystem dedicated to detect and to process mechanical stimuli (such as vibration and pressure), and another for the detection of painful stimuli (called nociception) and temperature. The nociception is a fundamental protective mechanism: it alerts for damage or injury that should be avoided or treated, otherwise an unnoticed harmful event might provoke permanent damage. However, occasionally, persistent pain (or chronic pain) with no apparent useful purpose occurs.

1.4.2. The sensory transductors of nociceptive stimuli: nociceptors

Harmful stimuli to a region of the body – creating the pain sensation - are detected by free nerve endings called nociceptors (Basbaum, Bautista et al. 2009). These nociceptors, like other sensorial receptors, are part of primary afferent neurons that have their cell body located in dorsal root ganglias (DRGs), projecting one axon branch into the dorsal horn of the spinal cord and another branch to innervate peripheral organs. Depending on their diameter, degree of myelination and conduction velocity, sensory receptors can be categorized in Aβ-fibers, Aδ-fibers and C-fibers (figure 1.7) (Willis 2004). Aβ-fibers, responsible for the detection of innocuous mechanical stimuli, have a large diameter (>10 μm), present thick myelination and have fast conduction velocity (30-100 m/s). Nociceptors are divided into medium diameter Aδ-fibers (2-6 μm), with thin myelination and moderate conduction velocities (12-30 m/s), and C-fibers, small unmyelinated fibers (0,4-1,2 μm) with low conduction velocity (<2 m/s) (Woolf and Ma 2007, Basbaum, Bautista et al. 2009). Due to their different conductivity differences, when a peripherical nociceptive stimulus is triggered, Aδ-fibers are responsible for the acute, strong localized pain sensation felt immediately after stimulus (referred as first pain), while the following diffused and longer-lasting pain sensation (called second pain) is carried by C-fibers (Basbaum, Bautista et al. 2009).

Considering their neurochemistry (figure 1.7), all the nociceptors release glutamate, the most abundant neurotransmitter of the nervous system. However, C-fiber nociceptors can be further separated in peptidergic C-fibers and non-peptidergic C-fibers (Basbaum, Bautista et al. 2009). Peptidergic C-fibers, characterized by expressing tropomyosin receptor kinase A (trkA), release substance P (SP) or calcitonin-gene related peptide (Cgrp) and require nerve-growth factor (Ngf) for their development and survival (Urban, Thompson et al. 1995, Mizumura and Murase 2015). On the other hand, as the name indicates, non-peptidergic C-fibers do not use peptides as neurotransmitters and depend on brain-derived neurotrophic factor (Bdnf) for their development (Abraira and Ginty 2013). These non-peptidergic C-fibers can be recognized by the presence of particular isolectins and purinergic receptors. Aδ-fibers only use glutamate as neurotransmitter and can be identified by antibodies against RT97 (Basbaum,

Bautista et al. 2009). Besides these neurotransmitters, nociceptors can additionally transmit nociceptive information by releasing prostaglandins, adenosine tri-phosphate (ATP) and nitric oxide (NO) into the dorsal horn of the spinal cord (Dickenson, Besson et al. 1997).

Different groups of nociceptors can detect and transduce different types of nociceptive stimuli depending on their trigger (figure 1.7). Thus, nociceptors can also be classified according to their sensitivity to three types of nociceptive stimulus: mechanical, thermal, or chemical. Most of the C-fibers are designated as polymodal, since they are sensible to thermal, mechanical and chemical stimuli (Perl 2007). However, there are subgroups of C-fibers that can transduce either only thermal, only chemical or both thermal and chemical (all being mechano-insensible). A fourth group of C-fibers is classified as silent nociceptors, as they are insensitive to noxious mechanical stimuli under normal conditions, but become responsive to mechanical stimulation only during inflammation or tissue injury (Schmidt, Schmelz et al. 1995). These group of nociceptors has been particularly studied in the articulations and are thought to be involved in the chronification of pain.

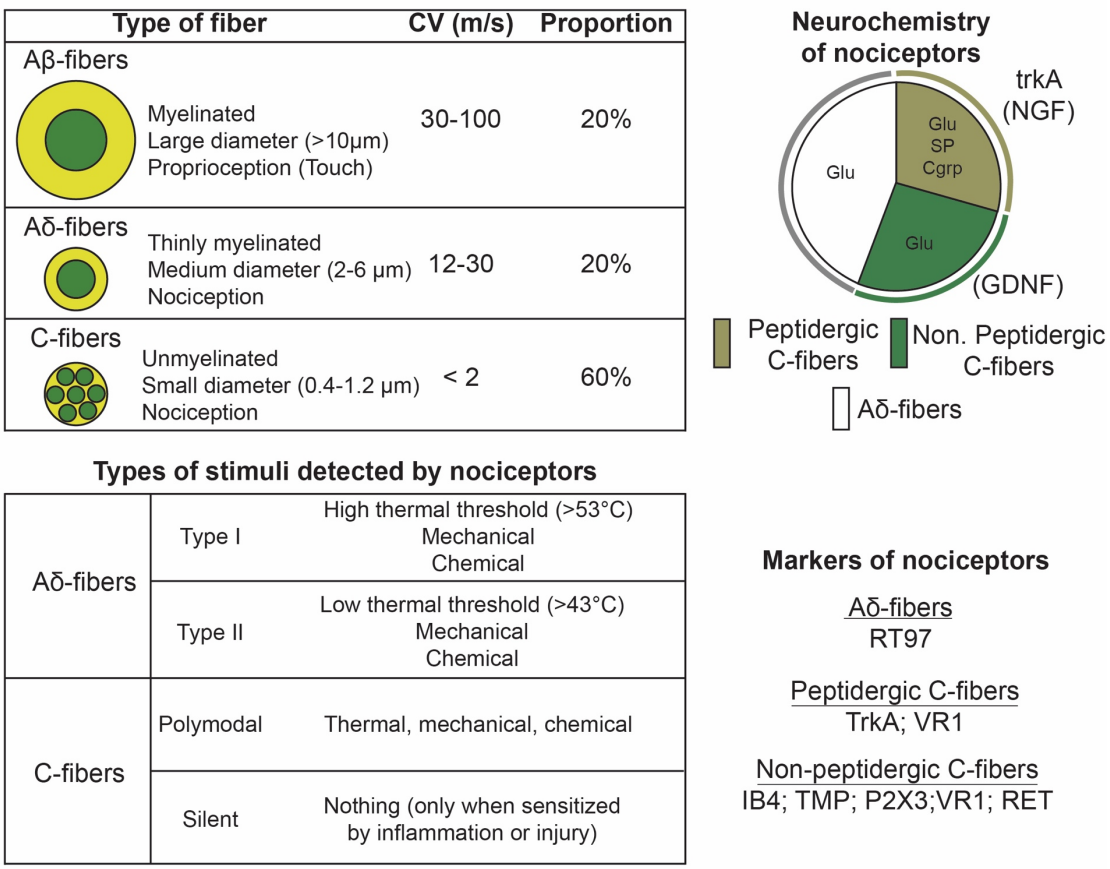

Figure 1.7. Somatosensory neurons and types of nociceptors. Somatosensory neurons can be divided into three categories according to their degree of myelination, diameter, and signal conduction velocity: Aβ-fibers, Aδ-fibers and C-fibers. Aβ-fibers are large, heavily myelinated and have fast conduction velocities. Aδ-fibers are of medium size, have a thin layer of myelin and have intermediate velocity of signal conduction. C-fibers are the most abundant type, they are small unmyelinated fibers, and conduct signals at a slow velocity. While Aβ respond to innocuous mechanical stimuli, Aδ-fibers and C-fibers transduce nociceptive stimuli. Nociceptors can also be subdivided based on their neurochemistry. Aδ-fibers release mainly glutamate as neurotransmitter. C-fibers are subdivided into peptidergic and non-peptidergic and, while peptidergic C-fibers secrete glutamate, substance P and CGRP, non-peptidergic fibers secrete mainly glutamate. Peptidergic C-fibers also express TrkA and respond to nerve growth factor (NGF), whereas non-peptidergic C fibers respond to glial-derived neurotrophic factor (GDNF). Additionally, nociceptors can be categorized according to the type of stimuli that they detect, and different markers have been found to identify the different subtypes of nociceptors.

1.4.3. From detecting to feeling it: the complex pain pathways

Pain, as described by the International Association for the Study of Pain (IASP) is 'An unpleasant sensory and emotional experience associated with, or resembling that associated with, actual or potential tissue damage' (Merskey, Bogduk et al. 1994). In a mechanistically point of view, these two elements of a

painful experience, the sensory discriminative component - where it is processed the information of the location, intensity, and type of stimuli – and the affective-motivational component, are processed by two distinct pathways. The sensory discriminative component is thought to depend mainly in the transmission of information to the somatosensory cortex areas, while the affective-emotional part depends on additional cortex areas and brainstem pathways (Purves 2018). Due to my work presented in this thesis, I will be focusing on the discriminative component of pain, specifically in the spinal cord.

1.4.4. Dorsal horn of the spinal cord as a key intermediary processing center

The action potentials generated by nociceptive stimuli, detected by the nociceptors, are required to be transmitted to the brain for further processing. After detection, afferent sensory neurons axons along the peripheral nerves conduct the nociceptive information to the spinal cord (Basbaum, Bautista et al. 2009). As they initiate the sensorial processing, DRG sensorial neurons can also be called as first-order neurons. When the axons of these neurons reach the dorsal horn of the spinal cord, they typically branch – forming the dorsolateral tract of Lissauer –, and climb or dive a few spinal cord segments before ingressing into the gray matter (Purves 2018). Afterwards, sensorial axons contact and transmit action potentials to second-order neurons located in different Rexed's laminae (system of gray matters layers described by neuroanatomist Bror Rexed, who defined them according to the structural features of neurons in different regions of cat's spinal cord) (figure 1.8) (Rexed 1952, Rexed 1954), which in turn send their axons to cross the spinal cord midline, and project them into the brainstem and thalamus – forming the anterolateral system (Willis and Westlund 1997). Of note, somatic sensory information is conveyed through a different pathway, the dorsal column-medial lemniscus pathway, one of the reasons why nociception (and temperature) and innocuous stimuli are treated separately (Patestas and Gartner 2016). In the spinal cord, most of C-fibers project into laminae I and II, with peptidergic C-fibers projecting into the superficial laminae I and outer laminae II and nonpeptidergic C-fibers into the inner part of laminae II (figure 1.8). On the other hand, Aδ-fibers

terminate in laminae I, II and V. Aβ-fibers project into lamina III, IV and V (Julius and Basbaum 2001, Abraira, Kuehn et al. 2017). The incoming information from the different fibers is further transmitted to inhibitory and excitatory interneurons and/or projection neurons. While interneurons act as intermediary neurons that synapse with other interneurons or with projection neurons within the dorsal horn, the latter are responsible for carrying information to the brain (more specifically the brainstem and thalamus) (Willis and Westlund 1997).

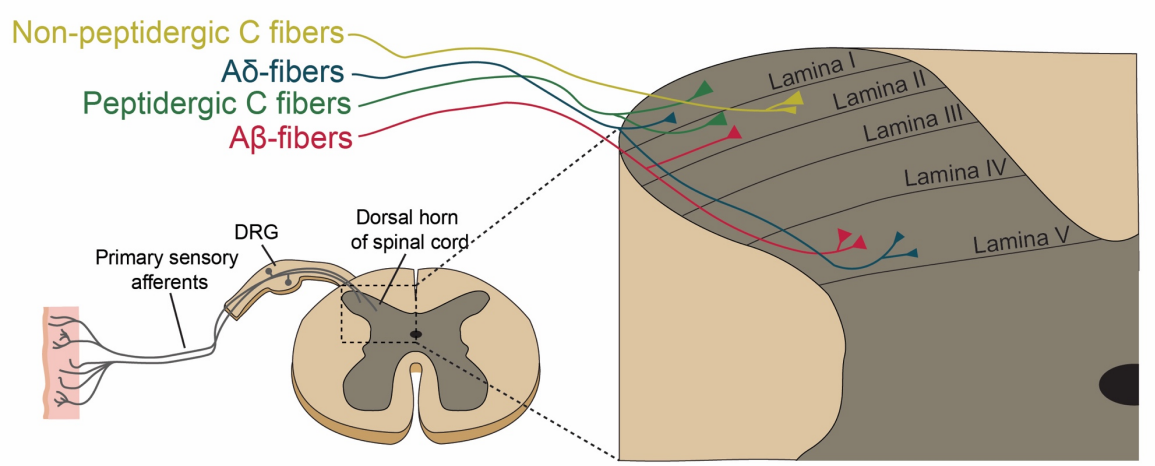

Figure 1.8. Primary sensory afferents projections into dorsal horn laminae. The cell bodies of primary sensory neurons are located in dorsal root ganglia (DRGs) and project into the periphery and the dorsal horn of the spinal cord. Different types of primary afferent neurons project into the dorsal horn of the spinal cord in a specific termination pattern: peptidergic C-fibers (green) and Aδ-fibers (blue) project into the most superficially lamina I. Additionally, these fibers project into lamina II and lamina V, respectively. Non-peptidergic C-fibers (yellow) terminate in the lamina II, while the large Aβ-fibers (red) project into the laminae II and V. These primary afferents once in the spinal cord synapse either with interneurons or projection neurons.

1.4.5. Mechanisms of central sensitization

Following high, long levels of nociceptive afferents stimulation, as a result of inflammation, nerve injury or tissue damage, pain can transit from acute to chronic. There are two main mechanisms responsible for the chronification of pain: peripheral sensitization (increased sensitivity in the peripheral nervous system, including nociceptors) and central sensitization, this latter caused by structural and functional plasticity in neurons of the spinal cord dorsal horn, which amplify signals arriving from the periphery (Julius and Basbaum 2001, Latremoliere and Woolf 2009). Chronic pain can be manifested as long abnormal pain sensations, including greater sensitivity to painful stimuli (hyperalgesia), pain sensation in response to stimuli that would be innocuous in normal conditions

(allodynia), and spontaneous pain (Sandkuhler 2009). These central sensitization-related phenomena can occur by a conjunction of multiple changes in the sensorial afferents and in the spinal cord, including a change in the GABAergic and/or glycinergic inhibition neurotransmission (disinhibition) and long-term potentiation (LTP) (Latremoliere and Woolf 2009).

While most of the current knowledge in the pain field has been acquired in a neuronal-centered view, current treatments for pain focusing on blocking neurotransmission and neuronal activity have so far resulted in very limited success. However, there is increasing evidence for the involvement of non-neuronal cells and its factors in the development and maintenance of chronic pain (Scholz and Woolf 2007), explored in sections 1.4.7-1.4.8, which suggest that additional targeting of these cells might improve the management of pain.

1.4.6. The neurovascular unit

For a proper CNS function, the CNS demands large amounts of oxygen, metabolites, and factors. This is being accomplished by the presence of a vast network of vessels. However, at the same time, the CNS needs to be protected from molecules and toxins circulating in the bloodstream that otherwise could provoke damage. Thus, the microvasculature of the CNS developed special barriers called BBB and blood-spinal cord barrier (BSCB). (Daneman and Prat 2015) The demonstration of such barriers was achieved more than 100 hundred years ago when an intravenously injected dye (trypan blue) failed to stain the brain and the spinal cord, and an injection into the cerebrospinal fluid (CSF) filled area (more specifically the subarachnoid space) resulted in dye extravasation into the brain but not the into the blood (Goldmann 1909, Goldmann 1913). Thus, suggesting indeed the existence of a separation between the blood and the CNS.

In close proximity to the ECs that make the BBB and the BSCB, it is possible to find additional cells that are involved in the development and maintenance of the barriers. Altogether, these tightly connected cells form the neurovascular unit (NVU), constituted by cellular and non-cellular players, such as ECs, basement membrane, pericytes and/or vascular smooth muscle cells, astrocytes, microglia and neurons (figure 1.9) (Schaeffer and Iadecola 2021). Since the role of neurons in pain is considerably well described, in the next

subsections I introduce the importance of non-neuronal cell types and their significance for chronic pain.

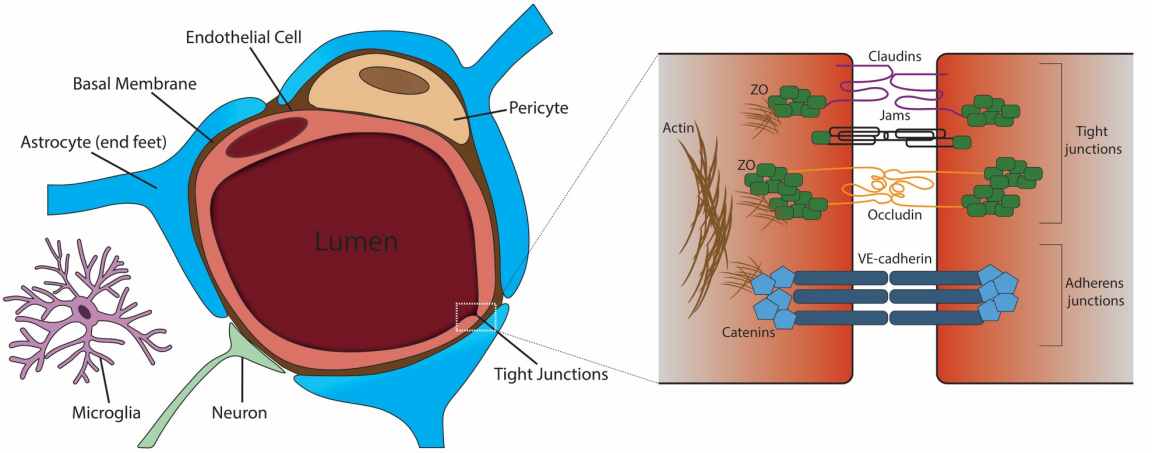

Figure 1.9. The neurovascular unit and the composition of the blood spinal cord barrier. The neurovascular unit (NVU) is characterized by the association of different cell types and extracellular matrix. Endothelial cells (ECs) form the sphere-shaped blood vessels and are surrounded by pericytes and basal membrane. Astrocytes send their endfeet to ensheath these cells and matrix, and nearby microglia and neuronal terminations communicate with the remaining cells. Interactions between all these NVU constituents is essential for the development and maintenance of a proper blood spinal cord barrier (BSCB). This barrier is mainly achieved by the presence of tight junctions, such as claudins, jams and occludin, which highly restrict the paracellular passage of molecules, cells, and factors. Additionally, adherens junctions also support the tightness achieved between ECs. These tight junctions and adherens junctions in turn form a structural association with zonula occludens (ZO) or catenins, which are linked to the actin cytoskeleton.

1.4.6.1. Endothelial cells

The BBB and the BSCB exist primarily as a barrier constituted by a thin layer of ECs with special features when compared to those in the periphery (Bartanusz, Jezova et al. 2011, Daneman and Prat 2015). More recently, taking advantage of next-generation sequencing, studies have shown a clear distinct transcriptomic profile between CNS ECs and peripheral ECs (Munji, Soung et al. 2019, Jambusaria, Hong et al. 2020, Kalucka, de Rooij et al. 2020). ECs of the CNS are characterized by the absence of cell membrane fenestrations (Fenstermacher, Gross et al. 1988), a high number of mitochondria (Oldendorf, Cornford et al. 1977) and absence of pinocytic vacuoles (Sedlakova, Shivers et al. 1999), giving the endothelium the capacity for high metabolic activity - to be

able to fuel all the active transport mechanisms constantly ongoing - and, simultaneously, restrict free transcellular passage of molecules from the blood to the parenchyma (Hawkins and Davis 2005). This reduced paracellular diffusion is achieved by the presence of numerous interendothelial junctions: the tight junctions, adherens junctions, and gap junctions (figure 1.9) (Bernacki, Dobrowolska et al. 2008, Abbott, Patabendige et al. 2010). However, while the presence of both barriers is essential, it simultaneously creates an obstacle for possible drug administration targeting the CNS. To overcome it, it is important to develop strategies for creating a transitory increase of permeability for drug passage (Bellettato and Scarpa 2018, Boye, Geraldo et al. 2022).

1.4.6.2. Junctional complexes for barrier integrity

The presence of transmembrane tight junction proteins, such as occludin, claudins and junction associated molecules (Jams) are essential for the development of the EC barrier properties. In the cytoplasm, additional proteins such as zonula occludens (ZOs) associate with the tight junctions and connect them to the cellular actin cytoskeleton, ensuring the stability of these protein complexes (Wolburg and Lippoldt 2002).

Within the different tight junctions, the first to be identified was occludin, a 65 kilodalton (kDa) protein initially found in chicken (Furuse, Hirase et al. 1993) and afterwards found to be also in mammals (Ando-Akatsuka, Saitou et al. 1996). It was shown to be regulated postnatally, with its expression increasing from postnatal day 8 to postnatal day 70 (Hirase, Staddon et al. 1997). The role of occludin is still controversial. In *occludin* null mice, tight junctions present a similar morphology to the ones in wild-type (WT) mice, suggesting that occludin is not essential for tight junctions' formation (Saitou, Furuse et al. 2000). However, the opposite has been suggested, with multiple studies showing that occludin is an important protein controlling paracellular permeability (Balda, Whitney et al. 1996, Wong and Gumbiner 1997).

Claudins are a large family of tight junction proteins that are differently present in different tissues. Within this family, claudin-5 was shown to be particular important for the formation and maintenance of endothelial barriers. In *claudin-5* deficient mice, molecules that would normally not cross the barrier were able to, even if the morphology of BVs was not altered (Nitta, Hata et al. 2003).

Additionally, Vegf signaling was shown to promote BBB breakdown by disrupting claudin-5 (Argaw, Gurfein et al. 2009)

Besides occludin and claudins, Jams also contribute for the EC barrier integrity. The Jam family is composed of Jam-1, Jam-2, and Jam-3, and can be found in ECs, epithelial cells and other cell types (Mandell and Parkos 2005). In these cells, Jam was shown to regulate tight junctions assembly in epithelial cells (Liu, Nusrat et al. 2000) and to be involved in the control of angiogenesis by enhancing EC migration (Naik, Mousa et al. 2003) and regulating bFGF-induced angiogenesis (Naik, Mousa et al. 2003a).

In addition to tight junctions, adherens junctions also contribute for the barrier integrity. Adherens junctions are mainly comprised by cadherin and catenin family members, such as vascular endothelial (VE)-cadherin and α-/β-/p-120-catenin proteins, respectively. Similar to tight junctions, adherens junctions are also connected to the actin cytoskeleton (Hartsock and Nelson 2008). The protein complexes, in special VE-cadherin, are described to be important for BBB integrity (Corada, Mariotti et al. 1999) and angiogenesis (Wallez, Vilgrain et al. 2006).

1.4.6.3. Pericytes

Pericytes, previously known as Rouget cells after being discovered by Charles Rouget, are mural cells found alongside microvessels, being surrounded by the basal membrane together with ECs (Bergers and Song 2005). They actively influence the endothelial function by secreting multiple factors such as Tgf-β, angiopoetin-1 (Ang1) and Vegf (Wilhelm and Krizbai 2014). Pericytes have been demonstrated to play an important role in EC barrier formation and vessel stability. Pericyte loss was shown to lead to increased BBB permeability (Lindahl, Johansson et al. 1997, Armulik, Genove et al. 2010) and, while vessel density, length and branching was not altered in a pericyte loss mouse model, ECs presented hyperplasia and abnormal EC shape and structure (Hellstrom, Gerhardt et al. 2001). Another well described role for pericytes is in controlling blood flow (Peppiatt, Howarth et al. 2006, Hall, Reynell et al. 2014). Furthermore, pericytes are able to induce occludin expression in ECs by secreting Ang1(Hori, Ohtsuki et al. 2004) and contribute for the formation of EC tight junctions (Daneman, Zhou et al. 2010, Sagare, Bell et al. 2013).

1.4.6.4. Astrocytes

Astrocytes are specialized glial cells, and one of the most abundant cells in the CNS. To communicate with the other cells of the NVU, particularly pericytes, neurons and ECs, these star-shaped cells use their several foot processes for contacts (Abbott, Patabendige et al. 2010). Astrocytes have a key role in inducing and maintaining barrier integrity (Janzer and Raff 1987), as shown in *in vitro* studies where co-cultures of ECs with astrocytes resulted in enhanced (in terms of length, width and complexity) tight junctions (Tao-Cheng, Nagy et al. 1987). Several factors are synthesized by astrocytes that may influence ECs, such as Tgf-β, glial cell derived neurotrophic factor (Gdnf) and basal Fgf (Wilhelm and Krizbai 2014). Communication between astrocytes and endothelial cells is not only done by secretion of factors, but also occurs through calcium signals, influencing permeability and BBB functioning (Braet, Paemeleire et al. 2001). Additionally, astrocytes play an important intermediary role between neurons and ECs, as they respond to neuronal activity and consequently modulate cerebral blood flow (Attwell, Buchan et al. 2010, Gordon, Howarth et al. 2011).

1.4.6.5. Basement membrane

As a non-cellular member of the NVU, the basement membrane is constituted by collagens, laminins, and other extracellular matrix proteins. It is mainly produced by NVU cells and surrounds ECs and pericytes (Kalluri 2003, LeBleu, Macdonald et al. 2007, Stratman and Davis 2012). Despite not being as well studied as the cellular members of the NVU, the basement membrane contributes for the regulation of the BBB regulation (Berzin, Zipser et al. 2000, Gautam, Zhang et al. 2016), as it was shown that BBB breakdown occurs in part due to changes in the basement membrane composition (Rascher, Fischmann et al. 2002). In line with that, collagen IV, one of the most abundant proteins of the basement membrane, can regulate occludin expression and location in ECs (Savettieri, Di Liegro et al. 2000), and was shown to be able to regulate angiogenesis (Bonanno, Iurlaro et al. 2000, Mundel and Kalluri 2007, Bahramsoltani, Slosarek et al. 2014).

1.4.6.6. Microglia

Due to its sensitivity and importance, the CNS is constantly immune surveyed by two main CNS-resident immune cells, the microglia, and macrophages, to be able to quickly respond to possible insults (Nimmerjahn, Kirchhoff et al. 2005). Microglia are the primary immune cell type in the CNS and are present in the first steps of embryogenesis, as early as E10.5, when glial cells (astrocytes and oligodendrocytes) are still absent (Ginhoux, Greter et al. 2010). Already at this stage, microglia play a role in supporting and controlling CNS vascularization (Fantin, Vieira et al. 2010, Rymo, Gerhardt et al. 2011). While it is still debatable and further evidence is required, it is suggested that microglia shape the nervous system circuitry by eliminating synapses at embryonic and postnatal stages (Stevens, Allen et al. 2007, Perry and O'Connor 2010, Paolicelli, Bolasco et al. 2011, Schafer, Lehrman et al. 2012). Additionally, microglia also influence the survival of layer V neurons in the somatosensory cortex via insulin-like growth factor-1 (IGF-1) secretion (Ueno, Fujita et al. 2013). Microglia phenotype is highly controlled by interactions with neurons and astrocytes, whose factors down-regulate the active state of microglia and contribute for the dampening of inflammation in the CNS (Neumann, Misgeld et al. 1998, Hoek, Ruuls et al. 2000, Lee, Schwab et al. 2011). Finally, microglia can be found associated with vessels, regulating their structure, and modulating blood flow during neurovascular coupling (Luo, Gao et al. 2014, Bisht, Okojie et al. 2021, Csaszar, Lenart et al. 2022)

Overall, these previous sections show that not only during embryonic development but also in adulthood, different cells (and in particularly the ones from the NVU) require constant communications with each other's for achieving their proper function.

1.4.7. Contribution of the spinal cord NVU to chronic pain

In parallel to neuronal-linked mechanisms, non-neuronal NVU cells are increasingly getting recognized as initiators and modulators of chronic pain (Scholz and Woolf 2007, McMahon and Malcangio 2009, Milligan and Watkins 2009, Ren and Dubner 2010). This section is not intended to be a complete description of all the NVU-linked factors and NVU alterations in pain, but instead

its goal is demonstrating the importance of NVU cells in chronic pain by giving some main examples. Great reviews about the topic are available for further reading (Willis, Brooks et al. 2008, Ji, Berta et al. 2013, Radu, Bramanti et al. 2013, Xu, Li et al. 2023).

The association between pain and glia activation was first described in the spinal cord after nerve injury, where an increase of glial fibrillary acidic protein (Gfap) immunoreactivity was observed (Garrison, Dougherty et al. 1991). To date, Gfap, which is a major constituent of astrocyte intermediate filaments, is recurrently used as a marker of astrocytes and reactive astrocytes (Eng, Vanderhaeghen et al. 1971), however by itself it is not an absolute marker of reactivity (even if often correlates with injury severity) as astrocytes can present different levels of Gfap expression due to physiological adaptive plasticity (Escartin, Galea et al. 2021). In neuropathic pain models, proliferation of astrocytes in the spinal cord contributes for the development of pain (Liu, Rudin et al. 2000, Tsuda, Kohro et al. 2011), with its inhibition resulting in reduced pain sensitivity (Tsuda, Kohro et al. 2011). Generally, astrocyte reactivity is present in multiple pain models (either by assessing Gfap levels or astrocyte morphological changes) such as spinal cord injury (Garrison, Dougherty et al. 1994, Nesic, Lee et al. 2005, Zhuang, Wen et al. 2006) and complete Freund's Adjuvant (CFA) administration (Raghavendra, Tanga et al. 2004, Sun, Cao et al. 2007, Gao, Xu et al. 2010). In a temporal view, astrocyte reactivity seems to be more persistent compared to microglial reactivity, with Gfap upregulation being present up to 150 days after nerve injury and 9 months after spinal cord injury (Nesic, Lee et al. 2005, Zhuang, Gerner et al. 2005, Zhang and De Koninck 2006, Gwak, Kang et al. 2012).

Similar to astrocytes, microglia reactivity is also visible in the spinal cord of nerve injury and inflammation pain models and, its neutralization via antibodies or *CX3C motif chemokine receptor 1* (Cx3cr1) genetic KO, results in inhibition of inflammatory and neuropathic pain (Verge, Milligan et al. 2004, Zhuang, Kawasaki et al. 2007). Chemokine ligand 2 (Ccl2) is a well-known chemokine playing a role in neuropathic pain and linked to microglia reactivity. Ccl2 promotes microgliosis in the spinal cord (Zhang, Shi et al. 2007, Thacker, Clark et al. 2009) and its signaling blockage by antagonizing or knocking-out its receptor chemokine receptor 2 (Ccr2) results in reduced microgliosis and neuropathic pain

(Zhang, Shi et al. 2007) (Abbadie, Lindia et al. 2003). Similarly, interferon-γ upregulation after nerve injury strongly activates microglia, which is abrogated together with mechanical allodynia in *interferon-γ* KO mice (Tsuda, Masuda et al. 2009). ATP-mediated activation of P2X ion channels and toll-like receptors (TLRs) are also well characterized mechanisms that activate microglia in pain models (Tanga, Nutile-McMenemy et al. 2005, Kim, Kim et al. 2007, Trang, Beggs et al. 2012, Tozaki-Saitoh, Takeda et al. 2022). Several other pro-inflammatory factors and cytokines have been described to promote and maintain inflammatory and neuropathic pain, such as tumor necrosis factor-α (TNF-α) (Zhang, Berta et al. 2011), interleukin-1β (IL-1β) (Clark, Staniland et al. 2010), IL-6 (Zhou, Liu et al. 2016), IL-18 (Miyoshi, Obata et al. 2008) and others.

1.4.8. BSCB permeability in pain

While it is not as well studied as astrocytes and microglia, the vasculature can also contribute for the development and maintenance of pain. In particular, BSCB permeability and integrity has been found to be compromised in several inflammatory and nerve injury pain models. After peripheral nerve injury, the BSCB permeability was found to be increased (assessed by accumulation of Evans Blue (EB) and horseradish peroxidase, used as tracers), with its peak at 24h-48h, returning to normal levels after 7 days (Beggs, Liu et al. 2010). Stimulation itself of C-fibers, but not A-fibers, either by electrical stimulation or capsaicin application, is able to increase BSCB permeability at 24h, suggesting that neuronal activity might modulate it (Beggs, Liu et al. 2010). Moreover, BSCB is also more permeable in rats with chronic constriction injury (CCI) between 1- and 7-days using the sodium fluorescein (NaFlu) tracer (Sauer, Kirchner et al. 2017, Li, Huang et al. 2020). In rats with contusive-compressive spinal cord injury (SCI), increased EB extravasation into spinal cord parenchyma is equally observed, happening as early as 1h after injury and being maintained up to 5 days post injury (Figley, Khosravi et al. 2014). In partial sciatic nerve ligation, in rats, increase of BSCB permeability was found at 3, 7 and 28 days at lumbar levels using EB and NaFlu (Echeverry, Shi et al. 2011). Additional plasma proteins (immunoglobulin (IgG) and fibronectin) were found to extravasate from the blood into the plasma. This barrier opening can be in part explained by the

downregulation of junctions (ZO-1, occludin and caveolin-1) in microvessels after 3 days of injury (Echeverry, Shi et al. 2011). On the other hand, microglia seemed to not be involved as administration of a microglial inhibitor (minocycline) did not prevent EB extravasation (Echeverry, Shi et al. 2011).

One of the ways that BSCB increased permeability might contribute for pain sensitivity is by allowing the infiltration of T-lymphocytes. Indeed, T-lymphocyte-deficient mice (*Rag1 null* mice) display significantly less pain sensitivity after spared nerve injury (SNI), particularly at later timepoints (7 to 21 days) and not at early timepoints (3 days) (Costigan, Moss et al. 2009). This result is corroborated by the reduction in hypersensitivity in T-lymphocyte-deficient nude mice after SNI (Costigan, Moss et al. 2009) or L5 spinal nerve transaction (Cao and DeLeo 2008). Mechanistically, in rats with CCI, injecting intrathecally neutralizing C-X-C motif chemokine ligand 10 (Cxcl10) antibody reversed the increase of BSCB permeability and T-lymphocyte infiltration, and alleviated hyperalgesia, suggesting a role for Cxcl10 signaling in neuropathic pain (Li, Huang et al. 2020).

Overall, an opening of the BSCB has been described in pain conditions. However, reports using different animal models of pain or even within the same model, present different outcomes, such as the degree of permeability, the temporal window of such opening and the spatial information of the BSCB disruption. Additionally, multiple studies focus on individual analysis, missing a possible link between BSCB permeability, NVU activation and pain.

2. AIMS OF THE THESIS

The CNS and the vascular system maintain constant communications to achieve proper CNS function. Yet, how they interact during development, adulthood and pathology are still largely unknown. The aim of the present thesis is to further investigate the association of both systems in the spinal cord during embryonic development and in pain pathology. For this I established the following aims:

1. To characterize the correlation between neural development and spinal cord vascularization.

2. To unravel the cellular and molecular mechanisms used by neural cells to control vascular patterning in the developing spinal cord.

3. To elucidate the consequences of altered vascular patterning in the development of the neural compartment.

4. To investigate the contribution of the NVU for the development of chronic pain.

3. RESULTS

Note: The results presented in the section 3.1 have been partially published and can be found in Vieira et al., 2022 (Vieira, Shah et al. 2022), where I am the first author of the study. Results or experimental procedures performed by colleagues and collaborators are described in the respective figure legends and in the methods section.

3.1. Neurovascular interactions during spinal cord development

3.1.1. Neural-vascular proximity occurs during early spinal cord vascularization

As previously described, from the PNVP, BVs ingress into the ventral part of the developing spinal cord at very specific locations and, already within the spinal cord, follow highly stereotypical patterns (Himmels, Paredes et al. 2017, Vieira, Shah et al. 2020). This raised the hypothesizes that this patterning could be resulting from the involvement of the different neural cell populations in directing vessel growth. To address that, the positioning of growing BVs and the neural cells at E11.5, when BVs already invaded the spinal cord and further branched and elongated, was characterized. In agreement with previous work (Himmels et al., 2017), BVs ingress in between the FP (Figure 3.1A, blue arrowhead) and MN columns (Figure 3.1A), while avoiding to ingress into these areas, and extend through the V3 postmitotic interneuron cluster (Figure 3.1B). In addition, BVs also entered the spinal cord laterally to the MN columns through the V1 postmitotic interneuron cluster (Figure 3.1C,D). Already within the spinal cord, interestingly, vessels extended and surrounded the V2 and V0 postmitotic interneurons cluster (Figure 3.1E,F). Similar to what happens in the developing mouse brain, vessels grow along the central canal next to the RGCs (Takahashi, Takase et al. 2015, Himmels, Paredes et al. 2017). These results demonstrate that vessels are in very close proximity with the different neural cells and prefer to ingress into the spinal cord through specific interneuron populations while surrounding and avoiding to invade other populations.

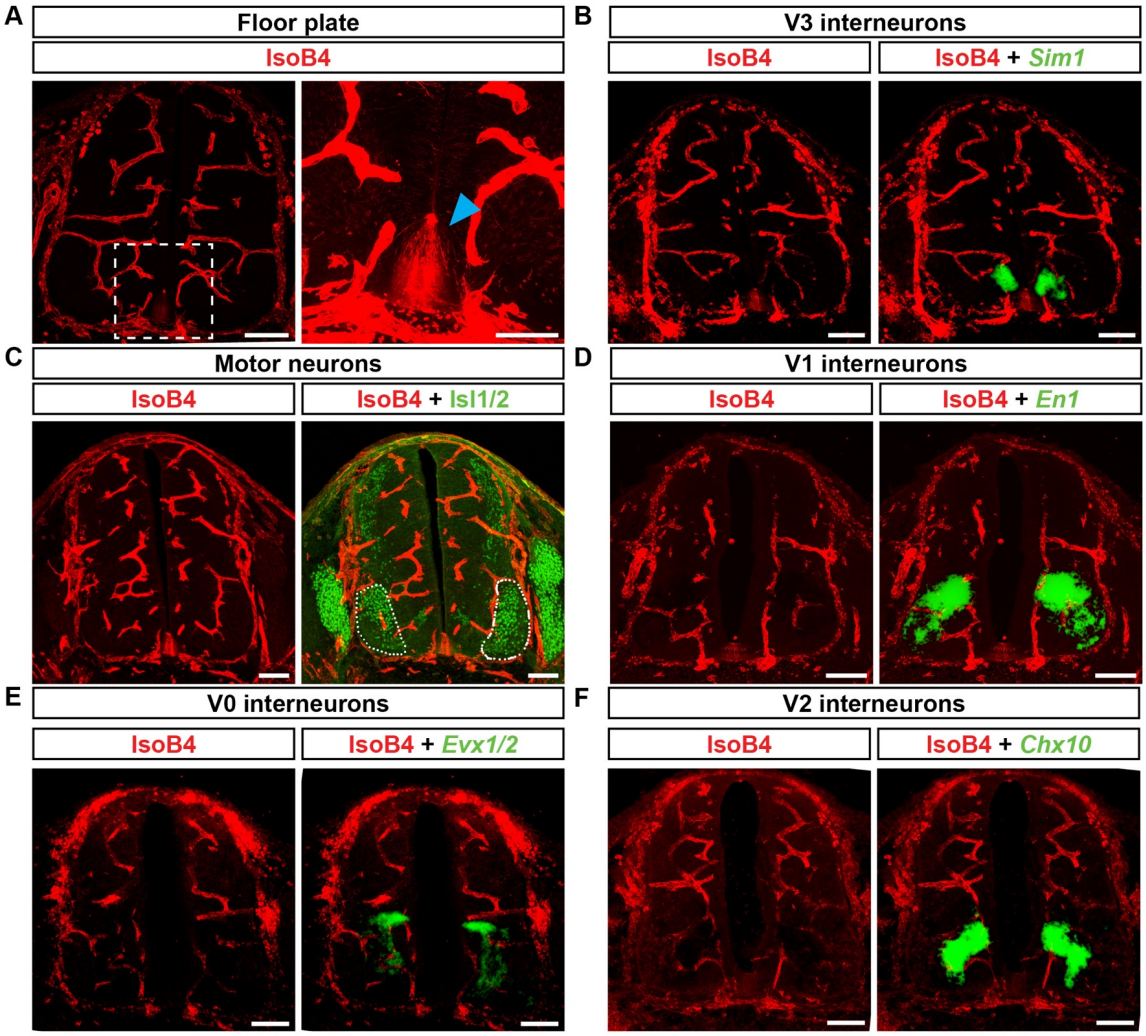

Figure 3.1. Vessel growth patterning within the spinal cord correlates with neural cell positioning. Representative images of spinal cord sections stained for blood vessels (IsoB4$^+$) and their spatial location within neural cells: floor plate (IsoB4$^+$, blue arrow in higher magnification inset) (A), V3 interneurons (*Sim1*$^+$) (B), Motor neurons (Isl1/2$^+$, white dashed circle) (C), V1 interneurons (*En1*$^+$) (D), V0 interneurons (*Evx1/2*$^+$) (E) and V2 interneurons (*Chx10*$^+$) (F). Scale bars 100 µm for all images.

3.1.2. The predicted developing ventral spinal cord interactome reveals extensive crosstalk between neural cells and ECs

Considering that neural and vascular cells are physically intermingled, it is plausible that ventral postmitotic neurons, FP and ECs communicate with each other. To understand the molecular mechanisms that might be controlling vessel patterning within the SC, *in silico* analyses to identify those potential interactions were performed. For that, taking advantage of a previously published single cell RNA sequencing (scRNAseq) of the developing spinal cord (Delile, Rayon et al. 2019), the sequencing data of the following ventral neural spinal cord-located

cells was extracted: FP; V0, V1, V2 and V3 interneurons; all motor neurons; and the blood cell cluster containing ECs (Figure 3.2A). To identify the ECs within the blood cell cluster, the cluster was filtered in order to select only the cells expressing the canonical EC markers *Kdr*, *Cdh5* and *Pecam1* (Figure 3.2A) (Khan, Taverna et al. 2019, Kalucka, de Rooij et al. 2020, Rohlenova, Goveia et al. 2020). As the focus was on early spinal cord vascularization – when the process is highly stereotypical - only cells derived from embryos younger than E11.5 (inclusive) were further considered. To identify potential cell-cell communication pathways between the selected cells, the tool CellChat (Jin, Guerrero-Juarez et al. 2021), which analyses scRNA-seq data based on a curated database of experimentally identified ligand-receptor interactions, was used (Figure 3.2A). Reflecting how intermingled and proximal the neural cells are to ECs, the predicted interactome showed that all the different cell types were theoretically able to communicate to each other (Appendix Fig. 1A). Furthermore,

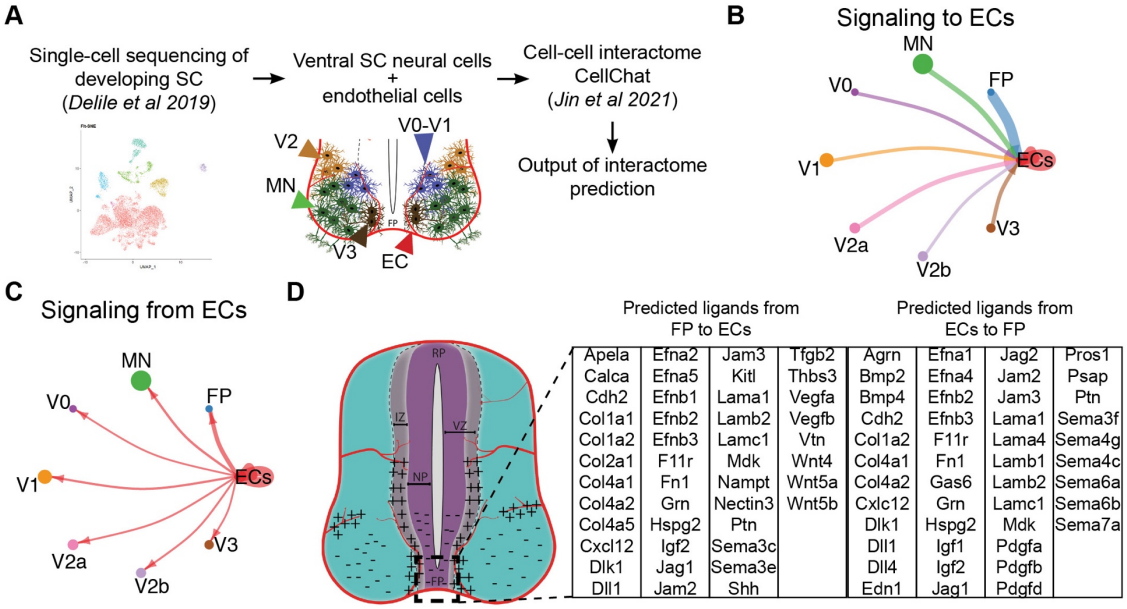

Figure 3.2. Predicted bidirectional interactions between ECs and neural cells. (A) Scheme representing the bioinformatic pipeline used to obtain the cell-cell interactome prediction. (B-C) Graphs showing the predicted signaling from ventral neural cells to endothelial cells (ECs) (B) and from ECs to ventral neural cells (C). (D) Predicted ligands used as communication from floor plate (FP) to ECs and from ECs to FP.

the communication was bidirectional, as all neural cells could signal to ECs (Figure 3.2B), and ECs could also potentially signal to all neural cells (Figure 3.2C). This interactome approach has the advantage that filters and returns only ligands that can indeed signal to ECs since their receptor is present in ECs,

excluding any ligand that might be expressed by neural cells, but ECs cannot sense (the same for EC signaling to neural cells) – as exemplified between FP and ECs (Figure 3.2D).

Through the immunohistochemistry characterization presented above (see Figure 3.1), together with the interactome results, I then built an angiogenic/anti-angiogenic gene expression map to identify the angiogenic and anti-angiogenic regulators expressed in neural-occupied regions that are permissive or not for vessel growth. To exemplify, considering the immunohistochemistry characterization, the FP is a region avoided by vessels, suggesting it might express and secret anti-angiogenic factors. Thus, by filtering the predicted signaling from the FP to ECs for described repulsive molecules, it would be possible to find the top candidates for the FP-mediated EC repulsion. For example, the predicted Sema3E and Wnt5 could be potential repellents for ECs, as both have been described to inhibit angiogenesis (Shi, Zhu et al. 2017). Additionally, while not explored in this work, this approach also allows to understand how the growing vasculature influences developing neural cells during spinal cord formation, by determining the factors expressed by ECs that are able to signal to the different neural cells.

3.1.3. Semaphorin class 3 signaling is predicted as a MN-EC communication

When looking at the possible signals involved in the predicted developing ventral spinal cord interactome, five signaling pathways were predominant: the Notch, Epha, Laminin, Jam and Sema3 (Figure 3.3A). Interestingly, while the first four pathways were equally involved in the potential communication between ECs and all the neural cell types (Appendix Fig. 1B-E), the Sema3 pathway was predominantly used as communication between MNs and ECs (Figure 3.3B). Closer analysis to the MN-EC Sema3 communication revealed that the strongest predicted interaction was between MN-derived Sema3C and EC-PlexinD1 (with or without Nrp1 as co-receptor) (Figure 3.3C).

Considering that Sema3C-PlexinD1-Nrp1 signaling was described to be involved in the repulsion of ECs during pathological angiogenesis (Yang, Hu et al. 2015), I hypothesized that the predicted Sema3C-PlexinD1 signaling could play a role in maintaining MN columns avascular for the precise development

time window between E9.5-E12.5 (Figure 3.1C). First, to confirm the *in-silico* analysis, *PlexinD1*, *Nrp1* and *Sema3C* temporal and spatial expression were characterized in the developing spinal cord. *PlexinD1* mRNA was exclusively found in ECs (Figure 3.3D and 3.3G) at all spinal cord levels (Appendix Fig. 1H) and its peak expression occurred at E11.5 (Appendix Fig. 1F-G). *Nrp1* was found primarily in ECs and MNs in the developing spinal cord, result in agreement with a previous study (Himmels, Paredes et al. 2017), with its peak expression occurring between E10.5-E11.5 (Appendix Fig. 1I-L). The expression of *Sema3C* in the ventral spinal cord was found to be mainly in MNs (Figure 3.3E-F and Appendix Fig. 2A) and, as seen for *PlexinD1* and *Nrp1*, its peak of expression occurred at E11.5 (Appendix Fig. 2B-C). When looking in more detail to the MN-specific expression of *Sema3C*, its expression was detected in all MN columns, but with higher levels in the MMC, found at brachial and lumbar levels (Appendix Fig. 2D-G).

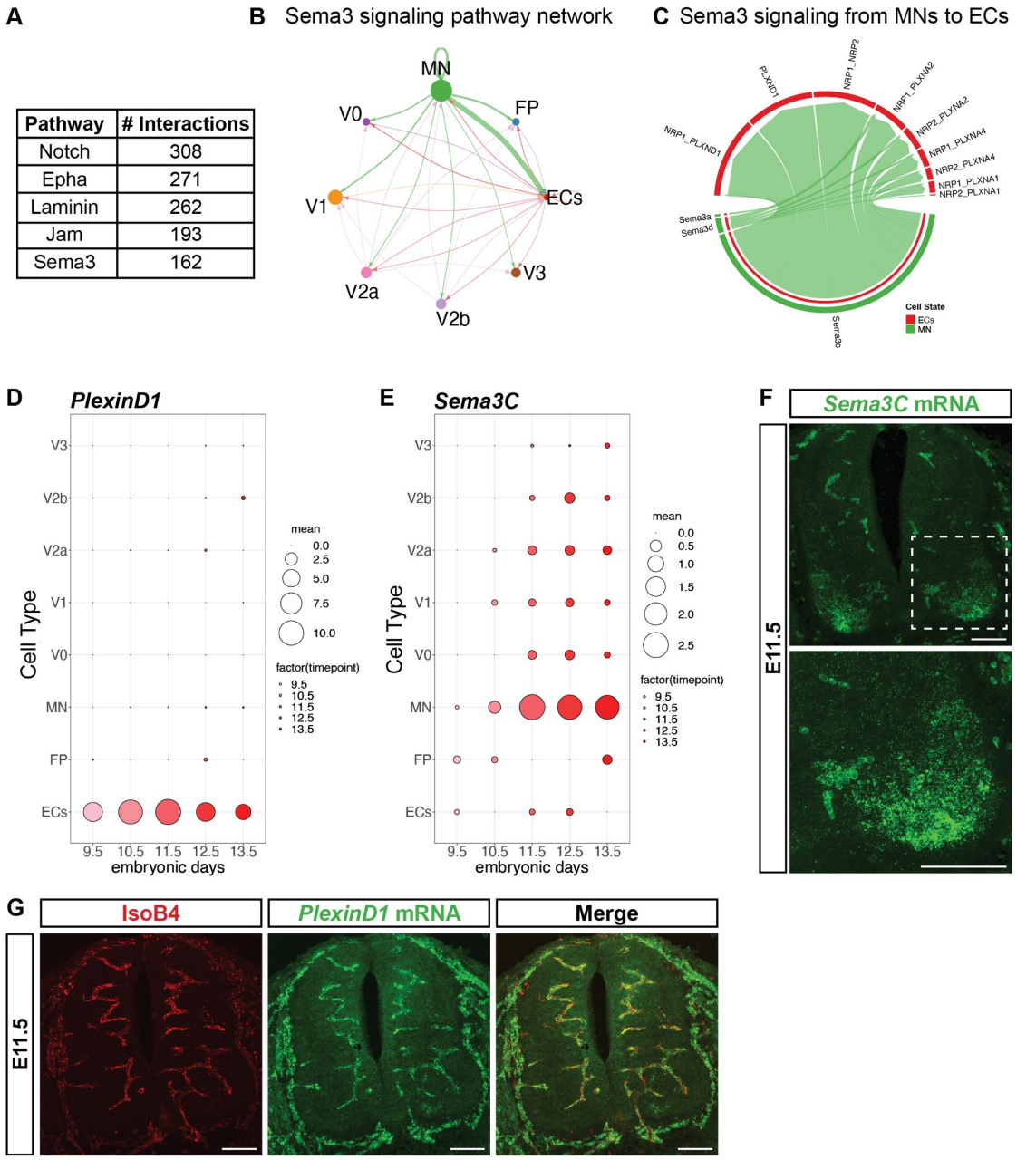

Pathway	# Interactions
Notch	308
Epha	271
Laminin	262
Jam	193
Sema3	162

Figure 3.3. MN-derived Sema3C is predicted to interact with EC-specific PlexinD1 in the embryonic developing spinal cord. (A) List of the top five signaling pathways (ordered by the total number of interactions) used between cell types. (B) Representation of the interactions predicted between the different cell types using the Sema3 signaling pathway network. (C) Representation of the Sema3 signaling from MNs to ECs, showing the MNs-expressed Sema3 family ligands and their respective EC-expressed receptors (D-E) Plot of the predicted expression of *PlexinD1* (D) and *Sema3C* (E) in the different cell types between E9.5 to E13.5, using previously published single-cell RNAseq data (Delile, Rayon et al. 2019). (F-G) Representative images of RNAscope Multiplex Fluorescent Assay using *Sema3C* (F) and *PlexinD1* (G) probes combined with staining for blood vessels (IsoB4^{+}) at E11.5. Inset shows higher magnification of MN columns. Scale bars 100 µm.

3.1.4. Global and EC-specific PlexinD1 loss results in premature MN column vascularization

Confirmed the expression of both ligands and receptors, the requirement for PlexinD1 and Nrp1 in ECs in preventing ingression of BVs into MN columns in mouse embryos was initially evaluated by performing an *in vitro* assay previously named by my research group as 'tube-touching assay' (Figure 3.4A) (Himmels, Paredes et al. 2017). In this assay MN explants from E11.5 embryonic spinal cords are co-cultured together with ECs on a matrigel layer, where ECs assemble into 3D tubes and can either touch the explant (attractive response) or not contact and be repelled (repulsive response) (Figure 3.4A) (Himmels, Paredes et al. 2017). MN explants from E11.5 BL6 WT mice were microdissected via open-book preparation and co-cultured in matrigel with human brain microvascular ECs (HBMECs) previously transfected with a non-targeting control small interfering RNA (siRNA), to exclude non-specific effects related to the transfection, or with siRNA to knockdown *PlexinD1* or *Nrp1* expression (Appendix Fig. 3A-B). Quantification of the number of HBMEC tubes contacting the MN explants 16h after starting the co-cultures demonstrated that knocking down either receptor (HBMECs-PlexinD1-KD or HBMECs-Nrp1-KD) resulted in a higher number of HBMEC-KD tubes touching the MN explants compared to the control (HBMECs-Control-KD) (Figure 3.4B-C and Appendix Fig. 3C-D). These differences were independent on the explant size (Appendix Fig. 3E-F). Together with the expression pattern *in vivo*, these results suggest that the receptor complex PlexinD1-Nrp1 in ECs is involved in the repulsive response of ECs towards MNs during spinal cord development. To confirm whether the repulsive response of ECs via PlexinD1 signaling prevents premature ingression of BVs into MN columns *in vivo*, characterization of MN columns vascularization in WT and *PlexinD1* full KO embryos (lacking PlexinD1 expression in all cells) was performed (Appendix Fig. 4A). With the assumption that PlexinD1 signaling could result into EC repulsion and thus prevent premature ingression of BVs into MN columns, analysis were focused at E11.5 when MN columns remain avascular (Figure 3.1C). *PlexinD1* KO embryos presented a strikingly increased vascularization and vessel length in MN columns, at all spinal cord levels, compared to *PlexinD1* WT embryos (Figure 3.4D-F), and an overall increase of total spinal cord vascularization (Appendix Fig. 4B).

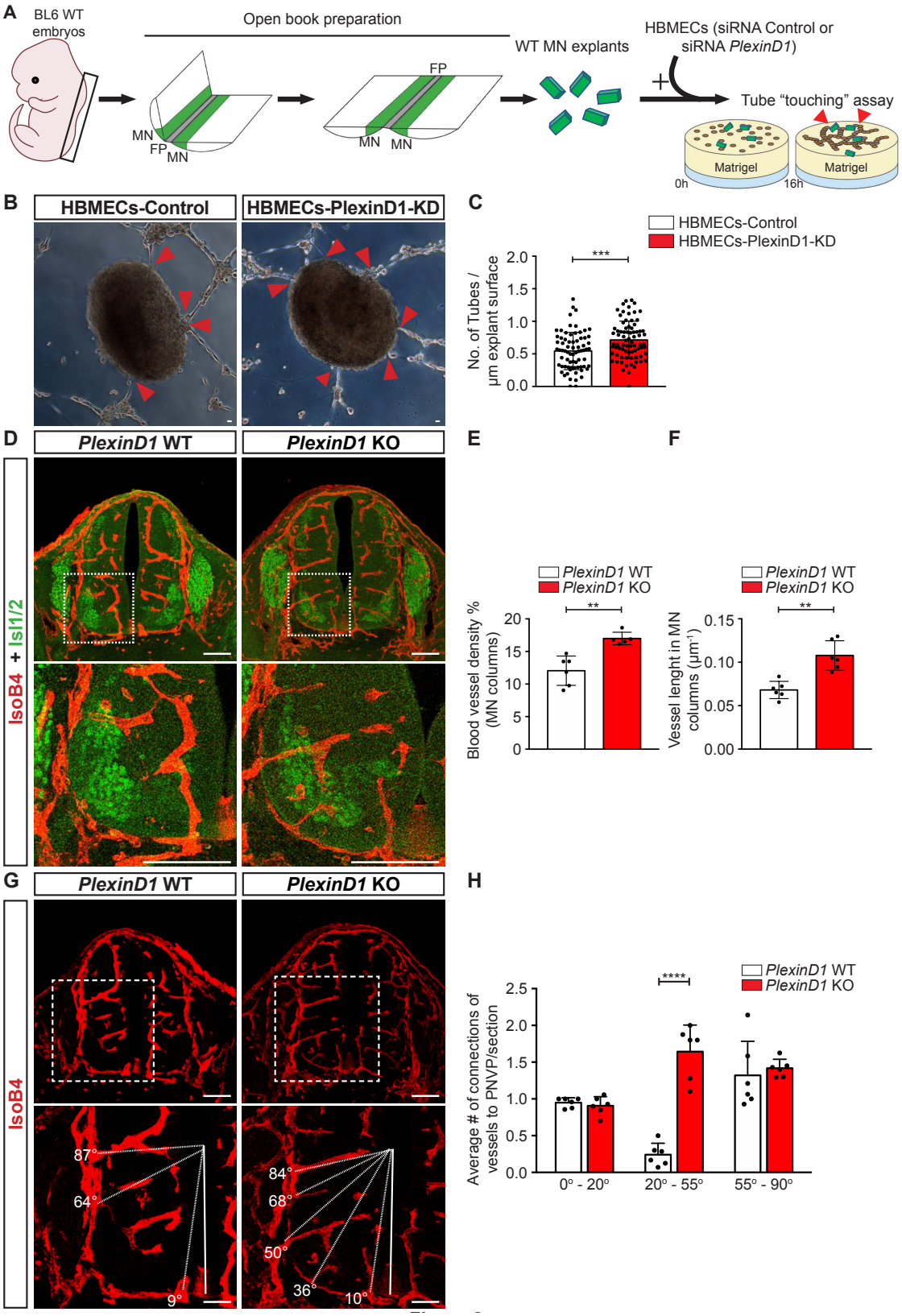

Figure 3.4. PlexinD1 regulates vessel ingression into motor neuron (MN) columns. (A) Scheme of the steps followed to perform the *in vitro* "tube-touching" assay. BL6 wild-type (WT) mouse embryos were dissected at E11.5, and the isolated spinal cords were flattened via open book preparation. MN explants were then microdissected. WT MN explants were co-cultured in matrigel with HBMECs transfected with either siRNA Ctrl (HBMECs-Control) or siRNA *PlexinD1* (HBMECs-PlexinD1-KD).

(B) Representative images of the “tube-touching” assay showing HBMEC tubes touching MN explants. Red arrowheads in (A) and (B) indicate contacts between HBMEC tubes and explants.(C) Quantification of the number of either HBMECs-Control or HBMECs-PlexinD1-KD tubes touching MN explants, normalized to the explant perimeter (n=72 explants siRNA Ctrl, n=77 explants siRNA PlexinD1, from 2 independent experiments (each experiment consisting of 2 independent litters). (D) Representative images of spinal cord sections at thoracic level stained for vessels ($IsoB4^+$) and MNs ($Isl1/2^+$) showing increased vessel ingression into the MNs columns of *PlexinD1* KO embryos compared with WT littermates (E11.5). Insets showing higher magnifications of MN columns. (E-F) Quantification of blood vessel density (E) and length (F) in MN columns of WT and *PlexinD1* KO embryos at E11.5. n=6 WT, n=5 *PlexinD1* KO for vessel density; n=6 WT, n=6 *PlexinD1* KO for vessel length, from two independent litters. (G) Representative images of vessel ($IsoB4^+$) ingression analysis in the ventral part of the spinal cord in WT and *PlexinD1* KO embryos (E11.5) at thoracic level. Dashed lines indicate the angle of ingression into the spinal cord of the PNVP-derived sprouts. Insets showing higher magnifications of MN columns. (H) Quantification of the angles of vessel ingression into the ventral half of the spinal cord (0° to 90°). n=6 WT and n=6 *PlexinD1* KO at E11.5, from two independent litters; two-way ANOVA with Sidak’s multiple comparisons test. Parametric distribution, two tailed unpaired Student’s t-test for (C), (E) and (F). All data shown as mean ± SD. All scale bars 100 μm.

To better understand the increase in BVs in MN columns, their patterning was also investigated by studying the ingression angle of BVs from the PNVP into the ventral spinal cord (from 0° to 90°, with the FP being the reference for 0°) (James, Gewolb et al. 2009, Himmels, Paredes et al. 2017). While in WT embryos BVs avoid entering into the spinal cord through the MN columns (located between 20° to 55°), in *PlexinD1* KO embryos BVs ingressed regularly through the MN columns (Figure 3.4G-H), reinforcing the hypothesis that PlexinD1 signaling in ECs is necessary to keep vessels outside the MN columns.

It was previously described that, at later stages (E15.5 onward), *PlexinD1* is expressed in DRG sensory neurons in order to control sensory-MN connections (Pecho-Vrieseling, Sigrist et al. 2009, Fukuhara, Imai et al. 2013). While the presence of PlexinD1 in any other cell type of the spinal cord except in ECs could not be detected - at the developmental time points studied – (Figure 3.3G and Appendix Fig. 1H), to completely rule out the contribution of PlexinD1 signaling from other cell types (perhaps express at low undetectable levels) I decided to confirm the cell autonomous role of PlexinD1 in ECs. For this, transgenic *PlexinD1 fl/fl*$^{Tie2:Cre}$ embryos, where PlexinD1 is specifically KO in ECs under the EC-specific promotor Tie2, were generated and analyzed. *PlexinD1*

fl/fl$^{Tie2:Cre}$ mice were generated by crossing *PlexinD1* floxed mice (*PlexinD1* fl/fl, further used as control littermates) (Zhang, Singh et al. 2009) with the Tie2:Cre mouse driver line (Kisanuki, Hammer et al. 2001) (Figure 3.5A and Appendix Fig. 4C). Similar to the *PlexinD1* KO phenotype, *PlexinD1 fl/fl*$^{Tie2:Cre}$ embryos presented a significant increase of BVs ingressing into the MN columns at E11.5 (Figure 3.5B-D), as well as total spinal cord vascularization (Appendix Fig. 4D), indicating that specific deletion of PlexinD1 in ECs is sufficient to cause the premature ingression of BVs into MN columns. Also, this premature vascularization resulted from the ingression of vessels from the PNVP through the MN columns (Figure 3.5E-F). Altogether, these results demonstrate a role for PlexinD1 in ECs during MN column vascularization and suggest that activation of PlexinD1 in ECs governs EC patterning.

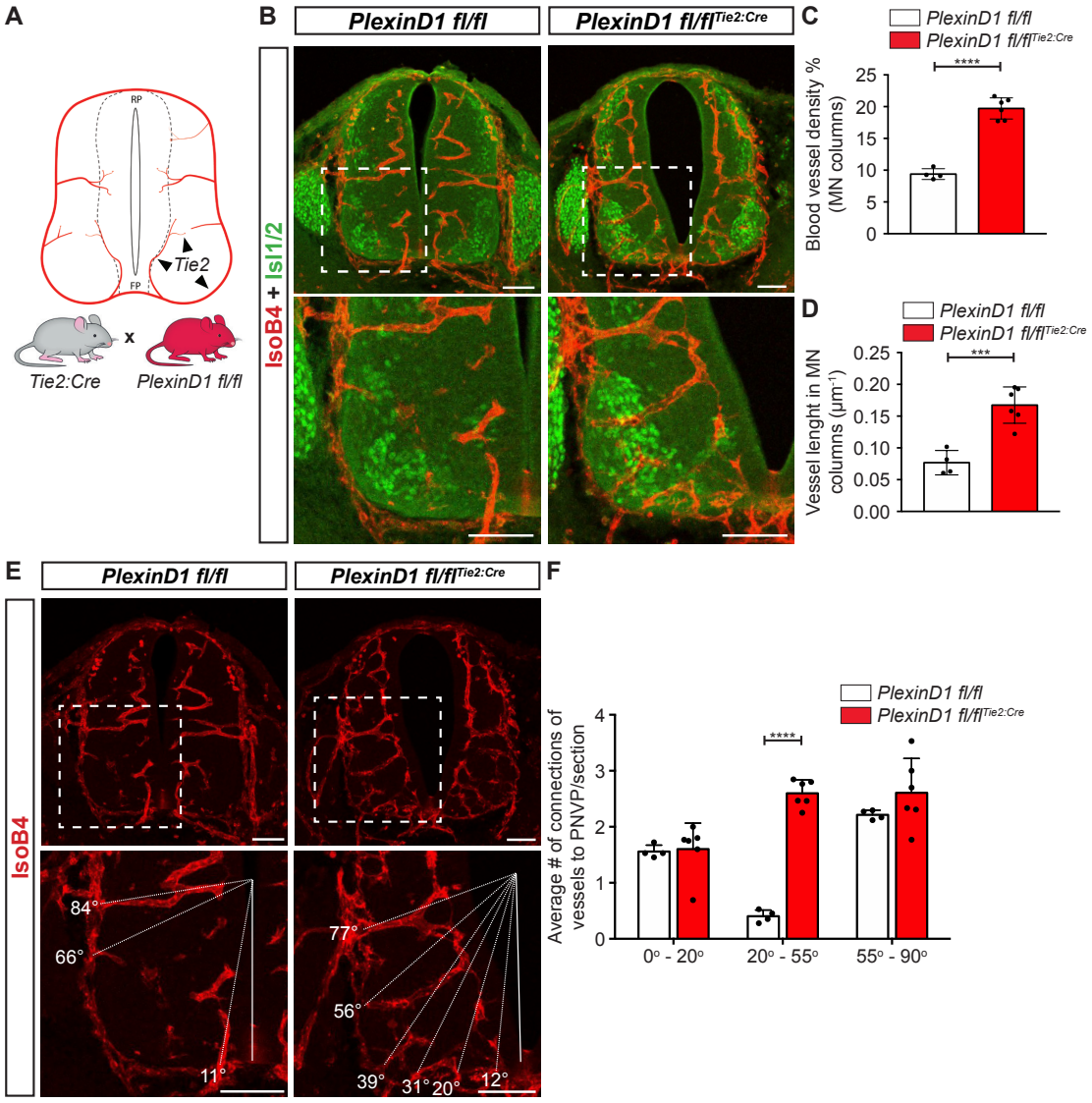

Figure 3.5. EC-specific loss of PlexinD1 causes premature MN column vascularization. (A) Scheme showing Tie2 expression in ECs of blood vessels to illustrate the use of *Tie2-Cre* to generate EC-specific *PlexinD1* knockout mice (*PlexinD1 fl/fl*$^{Tie2:Cre}$) by crossing *Tie2:Cre* mice with *PlexinD1 fl/fl* mice. (B) Representative images of spinal cord sections at thoracic level stained for vessels (IsoB4^{+}) and MNs (Isl1/2^{+}) showing increased vessel ingression into the MNs columns of *PlexinD1 fl/fl*$^{Tie2:Cre}$ embryos compared with control littermates at E11.5. Insets showing higher magnifications of MN columns. (C-D) Quantification of blood vessel density (C) and length (D) in MN columns of *PlexinD1 fl/fl* and *PlexinD1 fl/fl*$^{Tie2:Cre}$ embryos at E11.5. n=4 *PlexinD1 fl/fl*, n=6 *PlexinD1 fl/fl*$^{Tie2:Cre}$, from two independent litters. (E) Representative images of vessel (IsoB4^{+}) ingression analysis in the ventral half of the spinal cord at thoracic level in *PlexinD1 fl/fl* and *PlexinD1 fl/fl*$^{Tie2:Cre}$ embryos at E11.5. Dashed lines indicate the ingression angle of the PNVP-derived sprouts into the spinal cord. Insets showing higher magnifications of MN columns. (F) Quantification of vessel ingression angles into the ventral half of the spinal cord (0° to 90°). n=4 *PlexinD1 fl/fl*, n=6 *PlexinD1 fl/fl*$^{Tie2:Cre}$ at E11.5, from two independent litters; two-way ANOVA with Sidak's multiple comparisons test. Parametric distribution, two tailed unpaired Student's t-test for (C) and (D). All data shown as mean ± SD. All scale bars 100 µm.

3.1.5. Motor neuron-specific Sema3C loss causes premature MN vascularization

The analysis of predicted interactions between MNs and ECs (Figure 3.3C) indicated MN-derived Sema3C as the potential ligand for PlexinD1 in ECs. Considering the validation of *Sema3C* expression in MNs using *in silico*, ISH and RNAscope analysis (Figure 3.3E-F and Appendix Fig. 2A-G), and to explore the role of MNs-derived Sema3C for vessel repulsion, the MN-specific Sema3C conditional KO mouse line *Sema3C fl/fl*$^{Olig2:Cre}$ was generated by crossing Sema3C floxed mice (*Sema3C* fl/fl, further used as control littermates) (Plein, Calmont et al. 2015) with the Olig2:Cre mouse driver line (Dessaud, McMahon et al. 2008), which allows targeting of the neural progenitor domain pMN and its consequent cell lineage (which includes MNs). Successful Cre activity driven by Olig2 was observed by the deletion of *Sema3C* in MNs but not in the roof plate (Appendix Fig. 4E). Using this mouse line, I then perform *in vitro* assays and *in vivo* analysis. To study whether MN-Sema3C is able to repel EC tubes, HBMECs were co-cultured with MN explants from *Sema3C* fl/fl or *Sema3C fl/fl*$^{Olig2:Cre}$ embryos to perform the tube-touching assay (Figure 3.6A). Interestingly, the number of HBMEC tubes contacting *Sema3C* fl/fl$^{Olig2:Cre}$-derived MN explants was significantly higher compared to *Sema3C* fl/fl-MN explants (Figure 3.6B-C and Appendix Fig. 4F), indicating that removal of *Sema3C* from MNs is sufficient to reduce the repulsive action towards ECs. To determine whether repulsive Sema3C signaling is also present *in vivo*, MN vascularization of *Sema3C* fl/fl and *Sema3C fl/fl*$^{Olig2:Cre}$ at brachial and thoracic levels was evaluated. Quantification of BV density and vessel length in MN columns revealed a premature vascularization of MN columns in *Sema3C fl/fl*$^{Olig2:Cre}$ embryos (Figure 3.6D-F). Analysis of vessel ingression into the ventral spinal cord showed that while in *Sema3C* fl/fl embryos vessels ingress laterally to MN columns (~13° and >70°), in *Sema3C fl/fl*$^{Olig2:Cre}$ prematurely ingressing vessels entered the SC through the MN columns (Figure 3.6G-H). Vessel density in the total spinal cord was similar between control and KO embryos (Appendix Fig. 4G). These results suggest that MN-derived Sema3C is required for controlling vessel ingression into MN columns by signaling via PlexinD1.

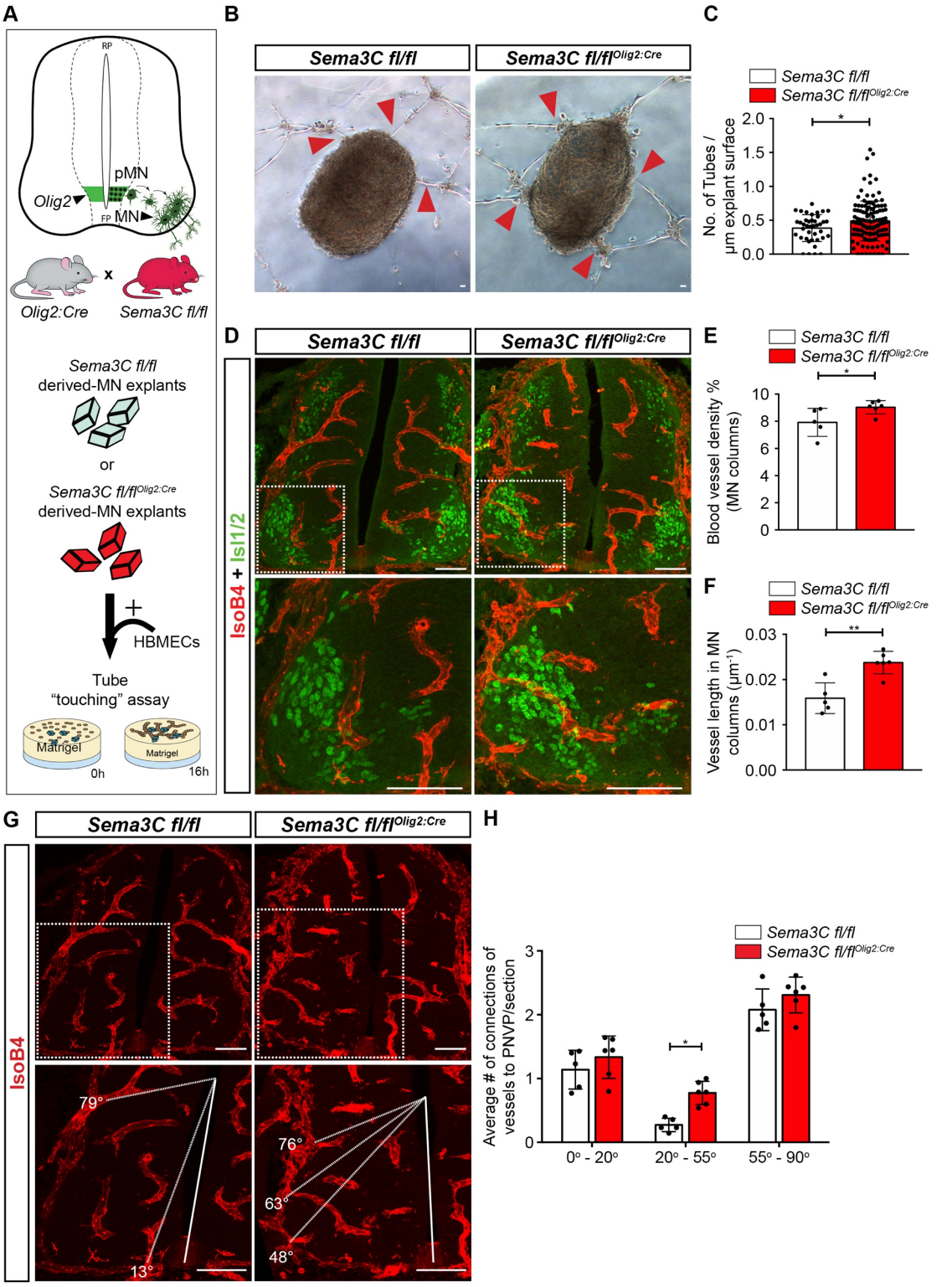

Figure 3.6. Absence of Sema3C in MNs leads to premature MN column vascularization. (A) Top: Scheme showing *Olig2* expression in the motor neuron progenitor domain (pMN) to illustrate the use of *Olig2-Cre* to delete Sema3C in MNs (*Sema3C fl/fl*$^{Olig2:Cre}$) by crossing *Olig2:Cre* with *Sema3C fl/fl* mice. Bottom: Schematic representation of the *in vitro* "tube-touching" assay co-culturing MN explants from

Sema3C fl/fl and *Sema3C fl/fl*$^{Olig2:Cre}$ embryos (E11.5) in matrigel with HBMECs. (B) Representative images of the "tube-touching" assay showing HBMEC tubes touching MN explants. Red arrowheads pointing at connections between HBMEC tubes and explants. (C) Quantification of the number of HBMEC tubes touching MN explants from *Sema3C fl/fl* or *Sema3C fl/fl*$^{Olig2:Cre}$ embryos, normalized to the explant perimeter (n=40 explants *Sema3C fl/fl*, n=125 explants *Sema3C fl/fl*$^{Olig2:Cre}$, from two independent litters). (D) Representative images of spinal cord sections at brachial level stained for blood vessels (IsoB4^{+}) and MNs (Isl1/2^{+}) demonstrating increased vessel ingression into the MNs columns of *Sema3C fl/fl*$^{Olig2:Cre}$ embryos compared with control littermates at E11.5. Insets showing higher magnifications of MN columns. (E-F) Quantification of vessel density (E) and length (F) in MN columns of *Sema3C fl/fl* or *Sema3C fl/fl*$^{Olig2:Cre}$ at E11.5. n=5 *Sema3C fl/fl*, n=6 *Sema3C fl/fl*$^{Olig2:Cre}$ from two independent litters. (G) Representative images of vessel (IsoB4^{+}) ingression analysis in the ventral half of the spinal cord at brachial level in *Sema3C fl/fl* or *Sema3C fl/fl*$^{Olig2:Cre}$ embryos at E11.5. Dashed lines indicate the angle of ingression into the spinal cord of the PNVP-derived sprouts. Insets showing higher magnifications of MN columns. (H) Quantification of vessel ingression angles into the ventral half of the spinal cord (E11.5) (0° to 90°). n=5 *Sema3C fl/fl*, n=6 *Sema3C fl/fl*$^{Olig2:Cre}$, from two independent litters; two-way ANOVA with Sidak's multiple comparisons test. Parametric distribution, two tailed unpaired Student's t-test for (C), (E) and (F). All data shown as mean ± SD. All scale bars 100 µm.

3.1.6. Sema3E is expressed in brachial MNs but not required to prevent premature MN vascularization

Besides Sema3C, Sema3-PlexinD1 signaling can also occur through the binding of Sema3E to PlexinD1 (Zhang, Singh et al. 2009, Gay, Zygmunt et al. 2011). The Sema3E-PlexinD1 signaling is known to control BV patterning during the development of the mouse retina, spinal cord, and heart by repulsing ECs (Torres-Vazquez, Gitler et al. 2004, Gu, Yoshida et al. 2005, Kim, Oh et al. 2011, Zygmunt, Gay et al. 2011). Despite of Sema3E not showing as a potential MN-expressed ligand signaling to EC-PlexinD1 (the reason why Sema3E did not appear in the *in silico* analysis as a candidate is discussed below in the section 4.3. of the discussion), previous work had identified the presence of *Sema3E* in the LMC MNs at E12.5 and E13.5 (Cohen, Funkelstein et al. 2005), thus raising the question whether Sema3E could be expressed at earlier stages and play a role, at least at brachial level, in keeping MN columns avascular. Using the developing spinal cord scRNAseq dataset mentioned above (Figure 3.2) and *in situ* hybridization, *Sema3E* expression was found in MNs at brachial levels (also expressed in the FP throughout the entire spinal cord) at E11.5 and E12.5, but

not at thoracic levels (Appendix Fig. 5A-B), corroborating the previous described findings.

To address whether Sema3E prevents premature ingression of BVs into MN columns, MN columns vascularization in WT and *Sema3E* full KO embryos (lacking Sema3E expression in all cells) at E11.5 was investigated (Appendix Fig. 5C). Considering the expression pattern of *Sema3E*, analyses were done only the brachial level or brachial and thoracic levels together. In either analysis, quantification of MN vascularization did not reveal any significant difference between *Sema3E* WT and *Sema3E* KO embryos (Appendix Fig. 5D-F). The same was observed for total spinal cord vascularization (Appendix Fig. 5G). Altogether, these results suggest that Sema3E (at least by itself alone) is not involved in maintaining MN columns avascular, even at brachial levels where it is expressed.

3.1.7. Premature vascularization of MN columns impairs early MN axon exiting patterning

The above-described findings so far demonstrate that MNs tightly control their column vascularization. But why do MNs require to remain avascular for a particular time window? During the period between E9 to E12.5, when columns are avascular, different fundamental MN development processes are occurring, including MN migration, MN clustering and MN axon exiting from the spinal cord to the periphery to reach their final muscle targets (described in section 1.1.3) (Huber, Kania et al. 2005, Lieberam, Agalliu et al. 2005, Dessaud, McMahon et al. 2008, Bonanomi and Pfaff 2010). Thus, it is conceivable that premature vascularization could interfere with any of these processes and, as such, MNs developed mechanisms to control prevent vessel ingression. To address this hypothesis, different MN development steps were assessed in the different transgenic mouse lines *PlexinD1* KO, *PlexinD1 fl/fl*$^{Tie2:Cre}$ and *Sema3C* fl/fl$^{Olig2:Cre}$. First, the MN area was evaluated. While MN area was not altered in *PlexinD1* KO and *PlexinD1 fl/fl*$^{Tie2:Cre}$ embryos (Appendix Fig. 6A-B), *Sema3C fl/fl*$^{Olig2:Cre}$ had a slightly decreased MN area compared with *Sema3C* fl/fl control littermates (Appendix Fig. 6C). Next, MN clustering was examined in *PlexinD1 fl/fl*$^{Tie2:Cre}$ embryos by analyzing the positioning of MNs in columns (LMCm, LMCl, and MMC) at

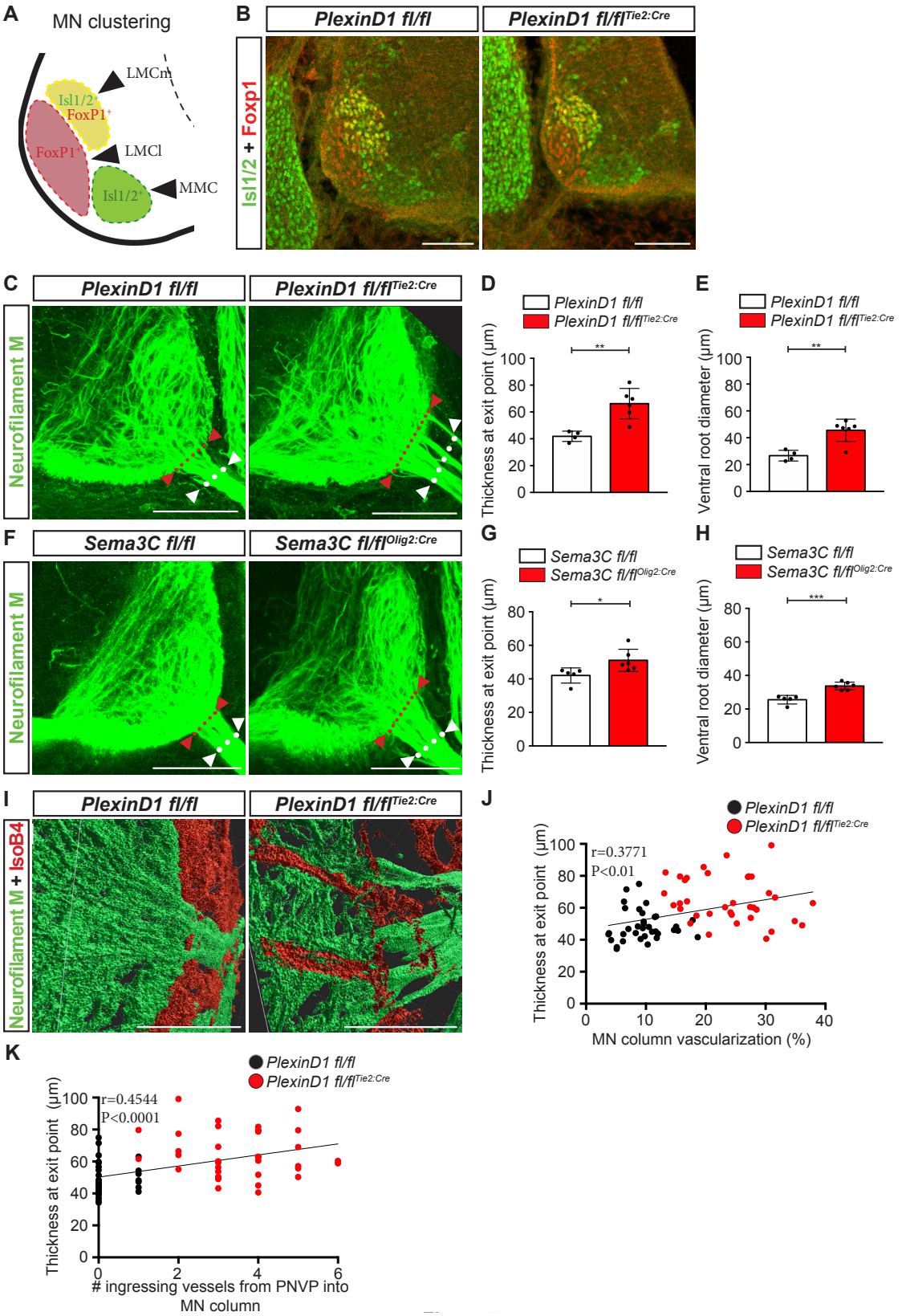

Figure 3.7. Premature ingression of blood vessels impairs MN axons patterning. (A) Schematic representation of MN clustering and positioning at brachial level of the spinal cord at E11.5 embryos. (B) Immunostaining showing the different MN columns at brachial level in *PlexinD1 fl/fl* and *PlexinD1 fl/fl*$^{Tie2:Cre}$ embryos at E11.5. MN clustering into the medial division of the lateral motor column (LMCm, Isl1/2^{+} and FoxP1^{+}), lateral

division of the lateral motor column (LMCl, FoxP1^{+}) and the medial motor column (MMC, Isl1/2^{+}) is not affected in *PlexinD1 fl/fl*$^{Tie2:Cre}$ embryos. (C) Representative images of 300 µm thick sections stained for neurofilament M showing MN axons exiting the spinal cord at brachial level (red arrowheads and red dotted line indicate MN axon fascicle thickness at the motor neuron exit points (MEP); white arrowheads and dotted line indicate the ventral root diameter) in *PlexinD1 fl/fl* and *PlexinD1 fl/fl*$^{Tie2:Cre}$ embryos at E11.5. (D) Quantification of the MN axon fascicle thickness at the MEP in *PlexinD1 fl/fl* and *PlexinD1 fl/fl*$^{Tie2:Cre}$ embryos at E11.5. n=4 *PlexinD1 fl/fl*, n=6 *PlexinD1 fl/fl*$^{Tie2:Cre}$, from two independent litters. (E) Quantification of ventral root diameter at E11.5 in *PlexinD1 fl/fl* and *PlexinD1 fl/fl*$^{Tie2:Cre}$ embryos. n=4 *PlexinD1 fl/fl*, n=6 *PlexinD1 fl/fl*$^{Tie2:Cre}$, from two independent litters. (F) Representative images of 300 µm thick sections stained for neurofilament M showing MN axons exiting the spinal cord at brachial level (red arrowheads and red dotted line indicate the MN axon fascicle thickness at the MEP, and white dotted line indicates the ventral root diameter) in *Sema3C fl/fl* and *Sema3C fl/fl*$^{Olig2:Cre}$ embryos at E11.5. (G) Quantification of the MN axon fascicle thickness at the MEP in *Sema3C fl/fl* and *Sema3C fl/fl*$^{Olig2:Cre}$ embryos at E11.5. n=5 *Sema3C fl/fl*, n=6 *Sema3C fl/fl*$^{Olig2:Cre}$, from two independent litters. (H) Quantification of ventral root diameter *Sema3C fl/fl* and *Sema3C fl/fl*$^{Olig2:Cre}$ embryos at E11.5. n=5 *Sema3C fl/fl*, n=6 *Sema3C fl/fl*$^{Olig2:Cre}$, from two independent litters. (I) Three-dimensional representation of the MN axons (neurofilament M) and ingressing vessels (IsoB4) in MN columns of *PlexinD1 fl/fl* and *PlexinD1 fl/fl*$^{Tie2:Cre}$ embryos at E11.5. (J-K) Correlation between MN axon thickness at exit point at E11.5 with MN column vascularization (J) and with the number of ingressing vessels (K). n=35 MN columns/MEPs from 3 embryos *PlexinD1 fl/fl*, n=36 MN columns/MEPs from 3 embryos *PlexinD1 fl/fl*$^{Tie2:Cre}$. Parametric distribution, two tailed unpaired Student's t-test for (D), (E), (G) and (H). All data shown as mean ± SD. All scale bars 100 µm, except for (I) scale bar 50 µm.

brachial level (Figure 3.7A). Here, no alterations in MN cell body positioning were found (Figure 3.7B and Appendix Fig. 6D). Last, MN axon exiting from the spinal cord at the MN exit points (MEPs) into the periphery was evaluated. MNs are able to find correctly the laterally located MEP, as the distance between the midline (determined by the positioning of the FP) and the MEPs was not altered in neither *PlexinD1 fl/fl*$^{Tie2:Cre}$ nor *Sema3C fl/fl*$^{Olig2:Cre}$ embryos (Appendix Fig. 6E-I). However, despite of MN axons leaving the spinal cord at the correct place, they do it in a defasciculated manner, as they take up a wider region as they leave the spinal cord (Figure 3.7C-D and 3.7F-G). This MN axon exit widening is kept even after leaving the spinal cord as quantification of the ventral root diameter in *PlexinD1 fl/fl*$^{Tie2:Cre}$ and *Sema3C fl/fl*$^{Olig2:Cre}$ reveals that ventral roots are enlarged (Figure 3.7E and 3.7H). As BVs ingress prematurely into the MN columns through the PNVP, it could be possible that there would be a correlation between the ectopic vessel presence in MN columns and the defasciculating exiting MN

axons. Indeed, aberrant MN exit increased proportionally with the presence of ectopic vessels within MNs (Figure 3.7J-K). Interestingly, detailed co-imaging of axons and vessels and its 3D reconstruction showed that vessels ingressed into the MN columns in-between exiting MN axons (Figure 3.7I and Appendix Fig. 6J), physically obstructing the axonal projections and resulting in axon defasciculation by forcing them to circumvent vessels.

3.1.8. EC-PlexinD1 removal results in impaired late MN maturation

At earlier stages, MN-Sema3C signaling to EC-PlexinD1 was demonstrated to be important for keeping MN columns avascular and consequently MN development. However, whether this signaling is also important for late MN maturation is elusive. Focusing on the *PlexinD1 fl/fl*$^{Tie2:Cre}$ mouse line, spinal cords from E18.5 embryos were used, as embryos die at birth from cardiovascular defects (Zhang, Singh et al. 2009), making it impossible to analyze postnatal stages. At this developmental stage, *PlexinD1 fl/fl*$^{Tie2:Cre}$ embryos still presented increased ventral spinal cord vascularization when compared to *PlexinD1* fl/fl littermates (Figure 3.8A-B). In line to what was observed at E11.5, no differences were observed in MN numbers, MN column area and average MN soma size between *PlexinD1 fl/fl*$^{Tie2:Cre}$ and *PlexinD1* fl/fl embryos (Appendix Fig. 7A-H). Next, MN maturation and MN terminal differentiation were studied by quantifying the gene expression levels of previously published sets of genes involved in MN terminal differentiation (*Nrg1*, *Sema5a*, *Mcam*, *Pappa* and *Glra2*) (Catela, Chen et al. 2022, Patel, Hammelman et al. 2022), cholinergic pathway – as MNs are cholinergic neurons – (*Slc18a3*, *Slc5a7, ChAT* and *Slc10a4*) (Halder and Lal 2021) and neuronal activity (*Fos*). Gene expression was performed by quantifying RNAscope signals of the mentioned genes in MN nuclei on tissue sections. Results show that the transcript levels of *Mcam*, *Glra2*, *Nrg1*, *Slc18a3* and *ChAT* were altered in *PlexinD1 fl/fl*$^{Tie2:Cre}$ compared to control littermates (Figure 3.8C-D, Appendix Fig. 8A-F and Appendix Fig. 9A-E). The choline acetyltransferase (ChAT) protein levels, the critical rate-limiting enzyme for the production of the MN neurotransmitter acetylcholine (Blusztajn and Wurtman 1983), were also quantified. In line with the *ChAT* gene expression changes, MNs from *PlexinD1 fl/fl*$^{Tie2:Cre}$ embryos also presented a reduction of ChAT protein levels compared to *PlexinD1* fl/fl

littermates (Figure 3.8E-F), suggesting defective cholinergic maturation of MNs in EC-specific KO embryos.

Besides MN maturation, other MN developmental processes occur between E11.5 (the early time pointed analyzed) and E18.5; MNs start receiving input connections from sensorial neurons and other interneurons (excitatory, inhibitory, or cholinergic subtypes) and the MN axons, which projected into the periphery, make local synapses with the targeted muscles, forming neuromuscular junctions. To see whether sensorial input was affected, sensory axons arising from DRG-located neurons were traced via DiI staining, showing no alterations in their general arborization pattern, in the pattern of ingression of the most prominent fibers (from a dorsal to ventral direction), and in their targeting of MNs (Appendix Fig. 7I-L). Similarly, the density of both afferent inhibitory inputs (identified by immunostaining for vesicular GABA transporter (Vgat)) and afferent cholinergic inputs (identified by immunostaining for vesicular acetylcholine transporter (VACht)) to MNs showed no differences between *PlexinD1 fl/fl*$^{Tie2:Cre}$ and *PlexinD1* fl/fl embryos (Appendix Fig. 7M-Q). These findings suggest that removal of PlexinD1 in ECs does not alter the signaling to MNs, but rather interferes with MNs neurotransmission capacity. Finally, to assess the MN targeting of muscles, the MN axon patterning and neuromuscular junctions were analyzed in the intercostal and diaphragm muscles. Muscle targeting was not affected, as both muscles were correctly innervated (Figure 3.8G-H and Appendix Fig. 8G), but a closer look at the nerve structure revealed increased (and disorganized) branching of the phrenic nerve in *PlexinD1 fl/fl*$^{Tie2:Cre}$ embryos (Figure 3.8H-K). However, the number of postsynaptic acetylcholine receptors (AchR^{+}) on the muscles was not altered (Appendix Fig. 8H), indicating that the additional branches might be non-functional or immature.

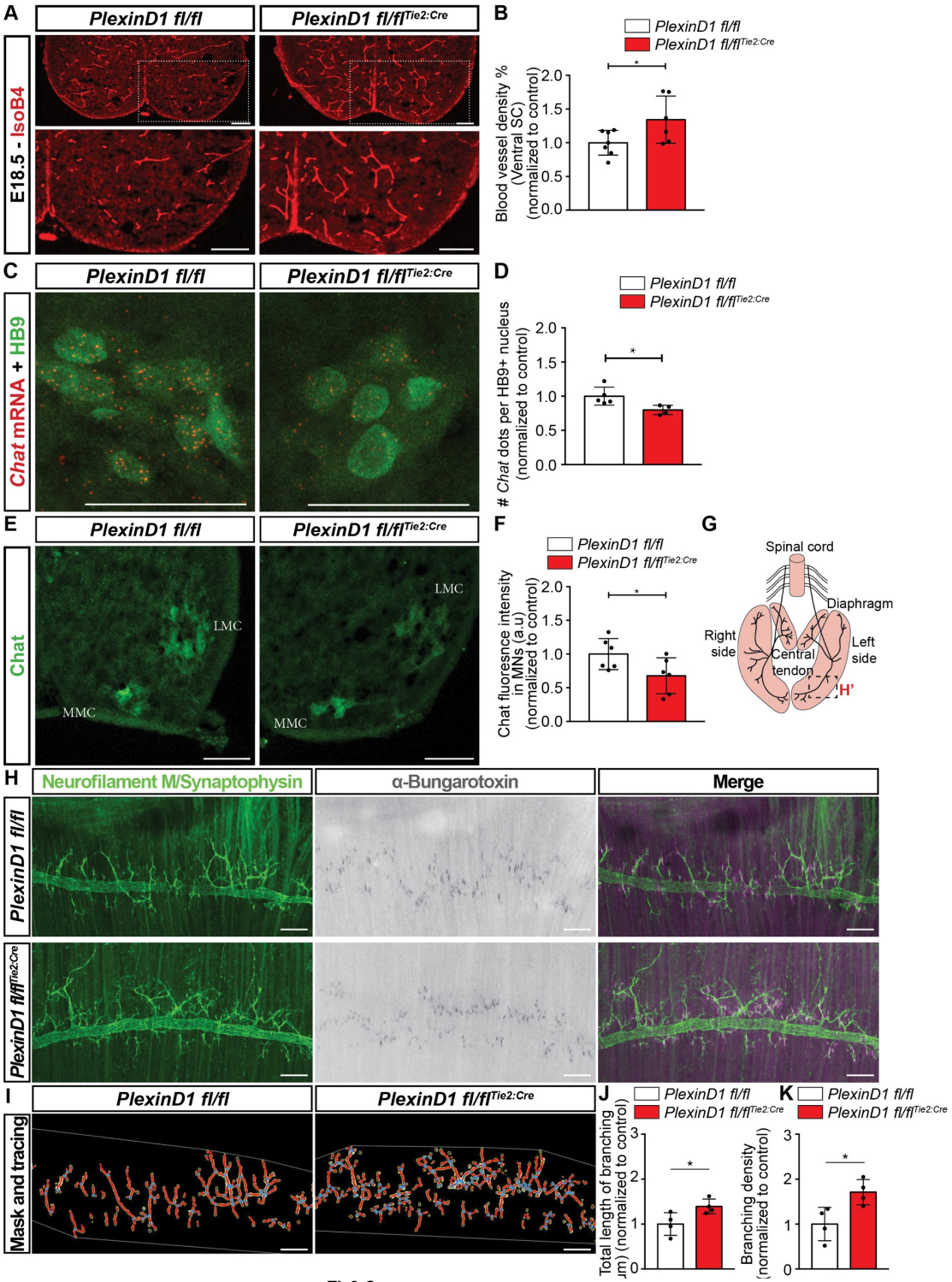

Figure 3.8. *PlexinD1 fl/fl*$^{Tie2:Cre}$ embryos present increased spinal cord vascularization and altered MN maturation defects at E18.5. (A) Immunostaining for vessels (IsoB4^{+}) in E18.5 spinal cords from *PlexinD1 fl/fl* and *PlexinD1 fl/fl*$^{Tie2:Cre}$ embryos. Insets show higher magnification of one side of the ventral spinal cord. (B) Quantification of vessel density in the ventral spinal cord of *PlexinD1 fl/fl* and *PlexinD1 fl/fl*$^{Tie2:Cre}$ embryos, normalized to control littermates at E18.5. n=7 *PlexinD1 fl/fl*, n=6 *PlexinD1 fl/fl*$^{Tie2:Cre}$, from two independent litters. (C-D) Representative images of RNAscope for *ChAT* co-stained with HB9 and (D) respective quantification of the number of *ChAT* dots per HB9^{+} nucleus (normalized to control littermates). Scale bars 25 μm.

n=5 *PlexinD1 fl/fl*, n=4 *PlexinD1 fl/fl*$^{Tie2:Cre}$, from two independent litters. (E) Representative image of ChAT immunostaining in MNs from the medial motor column (MMC) and lateral motor column (LMC) of *PlexinD1 fl/fl* and *PlexinD1 fl/fl*$^{Tie2:Cre}$ embryos at E18.5. (F) Quantification of ChAT fluorescence intensity in *PlexinD1 fl/fl* and *PlexinD1 fl/fl*$^{Tie2:Cre}$ embryos at E18.5. Data normalized to the control. n=6 PlexinD1 fl/fl, n=6 PlexinD1 fl/fl$^{Tie2:Cre}$, from two independent litters. (G) Scheme representing the innervation of diaphragm by the phrenic nerve. Inset represents the location where pictures shown in H were taken. (H-I) Representative images of the diaphragm of *PlexinD1 fl/fl* and *PlexinD1 fl/fl*$^{Tie2:Cre}$ embryos at E18.5 stained to show the phrenic nerve and its branching (Neurofilament M + Synapthophysin), AchR^{+} clusters (α-bungarotoxin) and (I) representation of the output result of branching points and length (using the neurofilament + Synapthophysin staining) image analysis. (J) Quantification of the total length of phrenic nerve branching in the diaphragm muscle at E18.5. Data normalized to the control. n=4 *PlexinD1 fl/fl*, n=4 *PlexinD1 fl/fl*$^{Tie2:Cre}$, from two independent litters. (K) Quantification of the branching density of phrenic nerve at E18.5 in *PlexinD1 fl/fl* and *PlexinD1 fl/fl*$^{Tie2:Cre}$ embryos. Data normalized to control littermates. n=4 *PlexinD1 fl/fl*, n=4 *PlexinD1 fl/fl*$^{Tie2:Cre}$, from two independent litters. Parametric distribution, two tailed unpaired Student's t-test for all the analyses. All data shown as mean ± SD. Unless mentioned, scale bars 100 μm.

3.2. Neurovascular unit interactions in the spinal cord in chronic pain

Precise interactions between distinct cell types are essential for the different stages of life, from embryonic development, as shown in section 3.1., to adulthood and pathology. In chronic pain, while the research has been mainly neuronal-driven for a long time, recent cumulative research demonstrated an important role for non-neural cells and their expressed/secreted factors in the development and maintenance of pain. However, the neurovascular unit remains insufficient studied in the context of pain. In this next section, the interplay between all the cell types is further explored.

3.2.1. Neurovascular unit transcriptome is altered in inflammatory and traumatic chronic pain

The neurovascular unit has been described to be dysfunctional resulting into BSCB disruption, immune cell infiltration and secretion of inflammatory factors in several pathologies. In an attempt to understand whether there are molecular changes occurring in the NVU of the spinal cord in pain, previously published bulk-RNAseq of mice injected with saline of CFA (persistent inflammatory CFA model) (Litke, Hagenston et al. 2022), and a scRNAseq dataset from spinal cord of mice after SCI (Matson, Russ et al. 2022) were

studied. As bulk-RNAseq measures the transcriptomic levels of genes from pooled cell populations, a published single cell sequencing of the adult spinal cord (Sathyamurthy, Johnson et al. 2018) was used to identify which are the cellular sources of the significantly altered genes identified in the CFA model (Litke, Hagenston et al. 2022). Interestingly, most of these altered genes were identified to be expressed mainly in non-neuronal cells, especially in vascular cells, meninges/Schwann cells and microglia (Figure 3.9A), supporting an important role of multiple cells in inflammatory pain. To verify if the same applies in the SCI model, the different cell populations from the scRNAseq were pseudobulked per animal and were unsupervised clustered using the Principal Component Analysis (PCA) method, allowing to explore the similarity or difference between cells according to the treatment, from non-injured and injured tissues. Plotting of the first two principal components revealed that besides neurons (Figure 3.9B), all the analyzed non-neuron cell types – astrocytes, microglia, and ECs – clustered accordingly to the treatment (non-injured vs injured) (Figure 3.9C-E), suggesting that also in SCI non-neuronal cells respond to injury and present altered transcriptomic profile.

Altogether, these results suggest that the cells comprising the NVU present gene expression alteration in inflammatory pain and traumatic SCI and might play a role in pain sensitivity. Thus, it is of interest studying them in the different pain models.

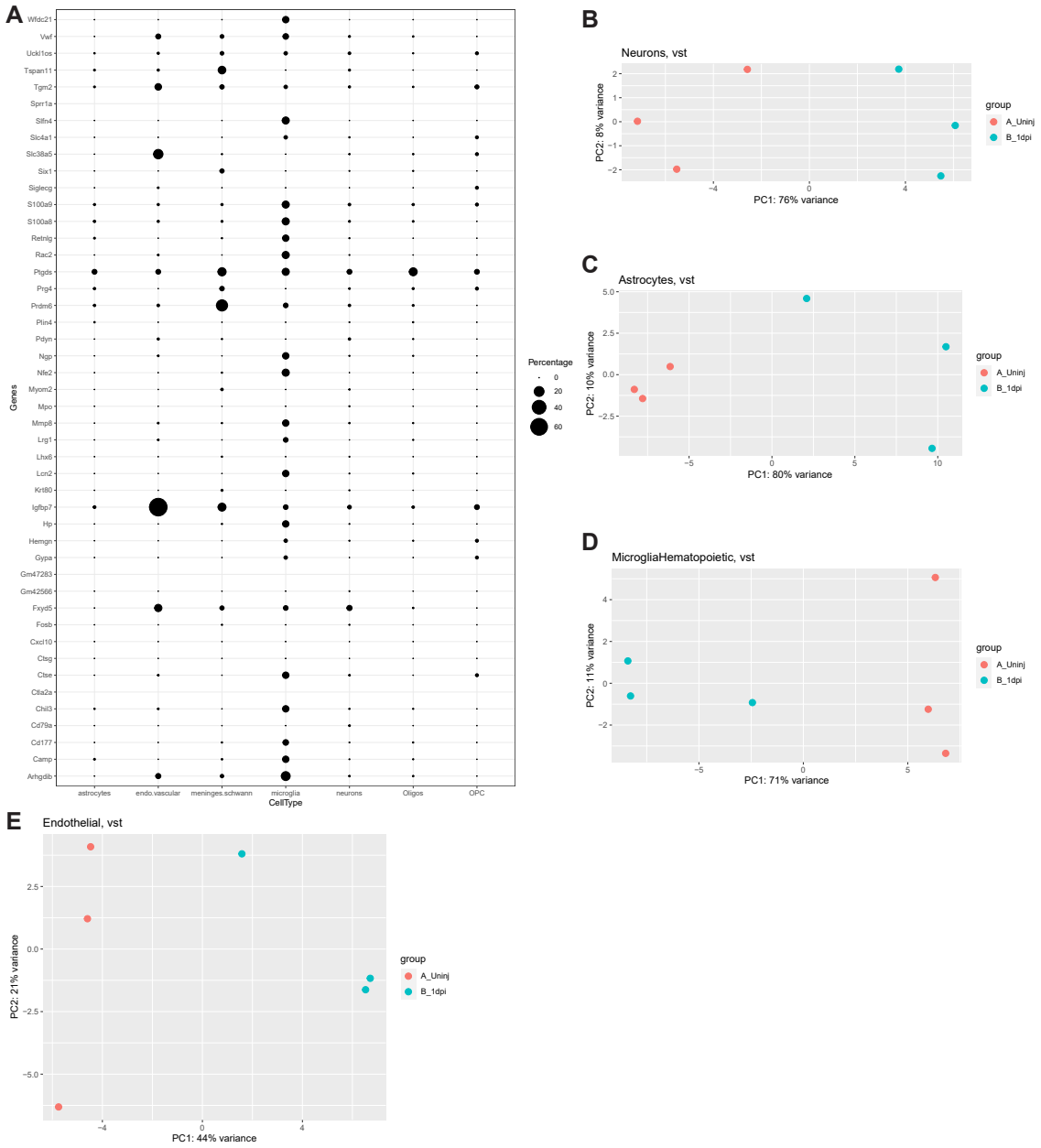

Figure 3.9. Non-neuronal cells present transcriptomic alterations in inflammatory pain and spinal cord injury. (A) Plot of the percentage of cells expressing the significant altered genes found in CFA-induced inflammatory (Litke, Hagenston et al. 2022) pain using a previously published scRNA-sequencing to obtain the cell type-specific transcriptome (Sathyamurthy, Johnson et al. 2018). (B-E) PCA plot of scRNA-sequencing dataset of sham and SCI samples after 24 h, pseudo-bulked by cell type, showing that the treatment (sham or SCI) is responsible for the separation observed in the PCA for neurons (B), astrocytes (C), microglia/hematopoietic cells (D) and endothelial cells (E). These plots indicate that there are substantial changes in the transcriptome of the different cell types after SCI compared to Sham.

3.2.2. The neurovascular unit structure is not altered upon CFA, but the spinal cord presents a pro-inflammatory environment

Considering that NVU seems to be, at least, affected at the gene expression level upon pain, it would be possible that this is a reflex of greater NVU structural changes. Thus, in a first step, to determine whether the NVU in the spinal cord is remodeled upon a pain stimulus, its cellular components were characterized at the structural level in Saline or CFA-treated mice at 24h, 48h, 4d and 7d. The choice of these timepoints allowed to investigate the early, intermediate, and longer effects of CFA. Quantification of BV density, pericyte coverage, collagen IV density and claudin-5 density (and astrocyte density, data not shown) at the spinal cord segments L3-L5 revealed no changes between saline and CFA-treated mice at any of the timepoints analyzed (Figure 3.10A-G), suggesting that there are no major alterations of the NVU structure in the CFA model. Consistent with previous reports, I found an increase of microglial cells at 7 days timepoint in the spinal cord of CFA-injected mice (Appendix Fig. 10A-B). Additionally, a decrease of anti-inflammatory M2-type macrophages was observed at the same time (Appendix Fig. 10C-E), indicating that the dorsal horn of the spinal cord presents a pro-inflammatory environment 7 days after CFA treatment.

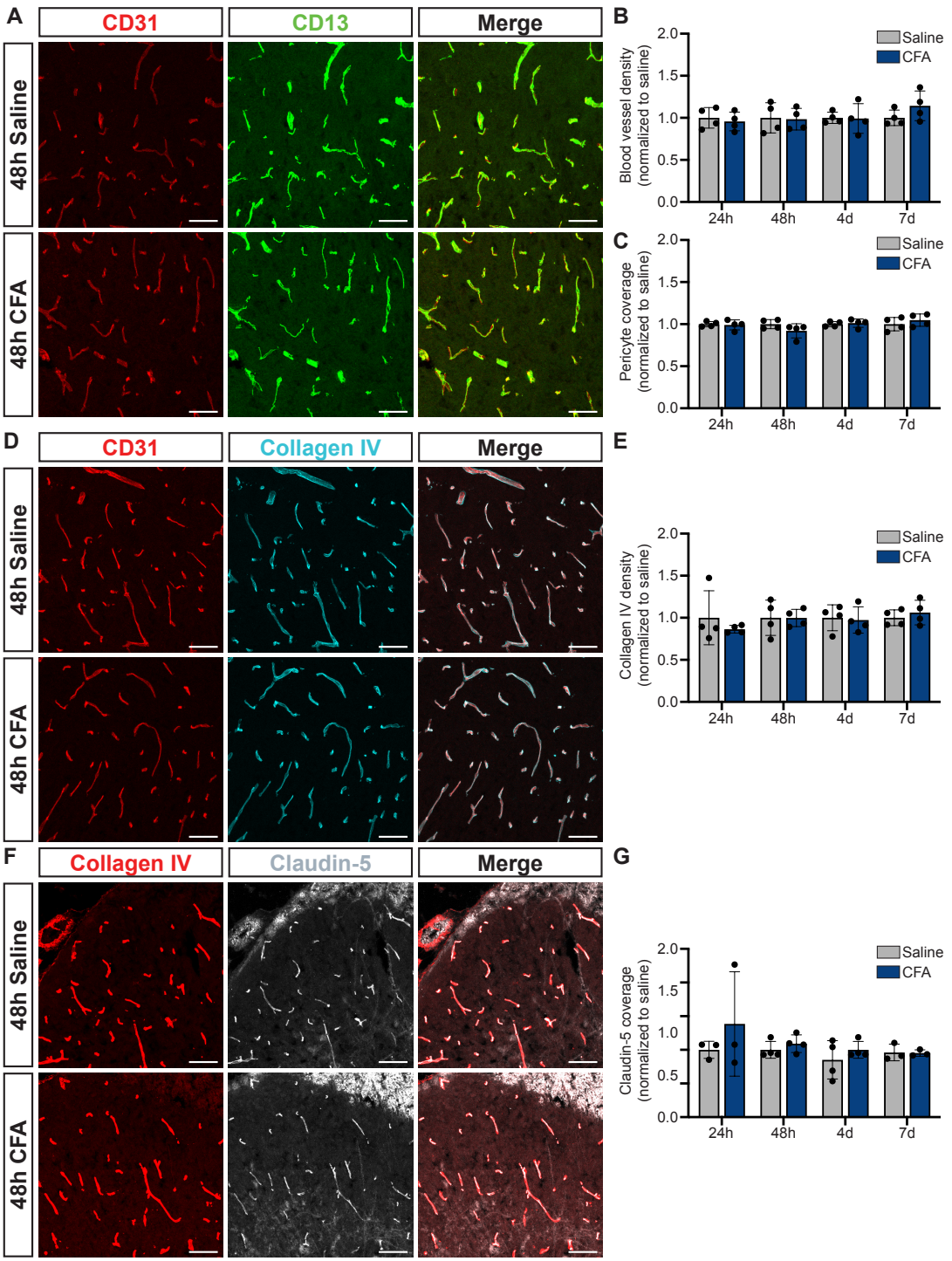

Figure 3.10. Neurovascular unit is not structurally altered upon CFA administration. (A) Representative images of immunostaining for blood vessels ($CD31^+$) together with pericytes ($CD13^+$) after 48h injection of saline or CFA. (B-C) Quantification of vessel density (B) and pericyte coverage (C) after 24h, 48h, 4 days and 7 days following saline (control) or CFA intraplantar injection. Data normalized to the control. n=4 saline, n=4 CFA. (D) Representative images of immunostaining for blood vessels ($CD31^+$) together with collagen IV ($Col\ IV^+$) 48h following injection of saline or CFA. (E) Quantification of collagen IV after 24h, 48h, 4 days and 7 days following saline (control) or CFA intraplantar injection. Data normalized to the control. n=4 saline, n=4 CFA. (F) Representative images of immunostaining for collagen IV

(ColIV$^+$) together with tight junction protein claudin-5 48h following injection of saline or CFA. (G) Quantification of claudin-5 after 24h, 48h, 4 days and 7 days following saline or CFA injection. The imaging and analysis for claudin-5 were partially done by Lea Gartner, who did her MSc thesis under my supervision. Data normalized to the control. n=4 saline, n=4 CFA. Statistical analyses were done for all comparisons using parametric distribution, two tailed unpaired Student's t-test. All scale bars 50 μm.

3.2.3. Local and transient opening of the BSCB occurs in CFA and SNI pain models

The NVU is involved in the development and maintenance of the BSCB, an important barrier required to protect the spinal cord from unwanted toxic substances that might circulate in the blood. In pathological situations, this barrier is disrupted exposing the spinal cord to toxins, excessive ions, and inflammatory factors. To see whether the BSCB is altered in pain situations, the functional integrity of the BSCB in Saline and CFA-injected mice was analyzed for the same time frames of the structural characterization described above. For that, after the CFA/Saline injection, NaFlu – a fluorescent tracer of 376.27 Da – was injected intravenously into the mouse tail and allowed to circulate for 30 min (Figure 3.11A). At the respective timepoint, the spinal cord was dissected and tracer extravasation from blood to parenchyma was quantified by fluorescence reading (Figure 3.11A). To determine if any changes are local to the spinal cord levels where hindpaw sensorial afferents project to (dorsal horn of L3-L5 levels) or propagate to other rostral or caudal regions, the L1-L3 segments and L3-L5 ventral part of the spinal cord were separately analyzed. Also, as an additional control the L3-L5 ventral region was also microdissected and analyzed. Interesting, the permeability readout revealed that the BSCB opens at 48h after CFA intraplantar injection, being closed both before at 24h and after 4 days (Figure 3.11B-E). Remarkably, this transient opening of the BSCB occurred specifically at the dorsal spinal cord at L3-L5 levels (Figure 3.11B-M), suggesting that the sensorial afferents into the dorsal horn are involved in the BSCB permeability observed. To check if this increased permeability is also present in neuropathic pain, BSCB permeability was assessed in Sham- or SNI-operated mice. Here, a similar opening of the barrier was observed, however greater in time: at 48h no opening was present (Appendix Fig. 11A,B,E,H), but at 7d (Appendix Fig. 11C,F,I) and 28d (Appendix Fig. 11D,G,J) there was an

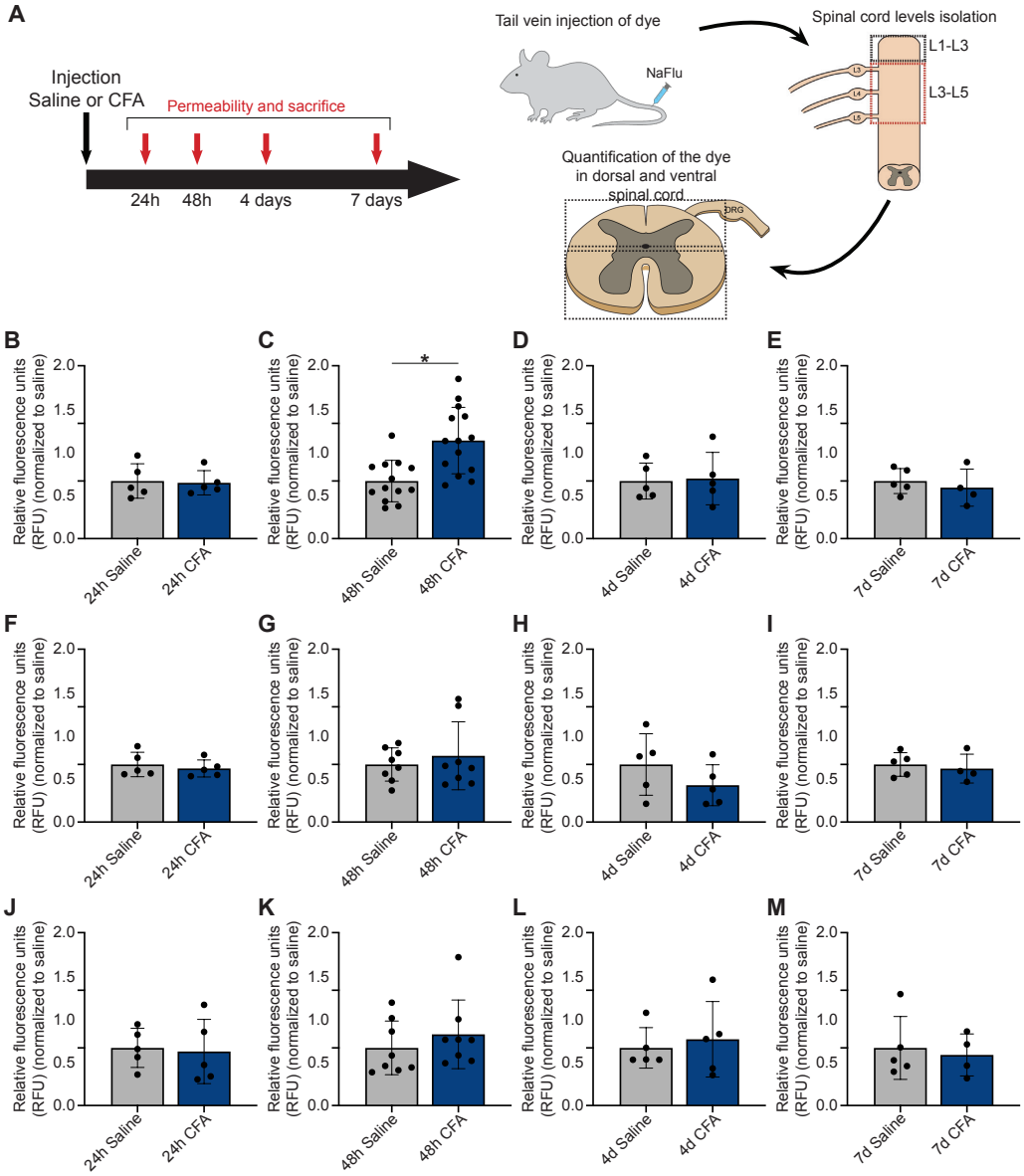

Figure 3.11. CFA injection induces a temporal and local transient opening of the blood-spinal cord barrier. (A) Schematic illustration of the experimental protocol used to measure BSCB permeability upon saline or CFA injection. Mice were injected either with saline or CFA and, at the respective timepoint, injected with sodium fluorescein (NaFlu), which was allowed to circulate for 30 min. Afterwards, mice were perfused with PBS, the spinal cord levels and regions dissected, and the extravasation of NaFlu was quantified. (B-E) Quantification of tracer extravasation into the dorsal region of L3-L5 spinal cord levels upon saline or CFA injection at the respective timepoints. N=5 saline and n=5 CFA for 24 h; N=13 saline and n=14 CFA for 48 h; N=5 saline and n=5 CFA for 4 d and 7 d. (F-I) Quantification of tracer extravasation into the ventral region of L3-L5 spinal cord levels upon saline or CFA injection. N=5 saline and n=5 CFA for 24 h; N=8 saline and n=8 CFA for 48 h; N=5 saline and n=5 CFA for 4 d and 7 d. (J-M) Quantification of tracer extravasation into the dorsal region of L1-L3 spinal cord levels upon saline or CFA injection. N=5 saline and n=5 CFA for 24 h; N=8 saline and n=8 CFA for 48 h; N=5 saline and n=5 CFA for 4 d and 7 d. Statistical analyses were done for all comparisons using parametric distribution, two tailed unpaired Student's t-test.

increased opening of the BSCB. This increase was also specifically found at dorsal L3-L5 levels (Appendix Fig. 11C-D). Overall, these results demonstrate that the BSCB is compromised, but more importantly this barrier opening is transient and occurs in a very localized area (dorsal L3-L5) where afferent neurons project into. This BSCB opening might then further exacerbate pain sensitization by the infiltration of immune cells or entrance of toxic substances.

3.2.4. Lrg1 leads to opening of the BSCB

I next aimed to understand the factors that could be responsible for the transient opening of the BSCB, the list of significantly altered genes in the bulk-RNAseq of saline or CFA injected mice (Litke, Hagenston et al. 2022) was screened to identify previously described modulators of permeability. Within the

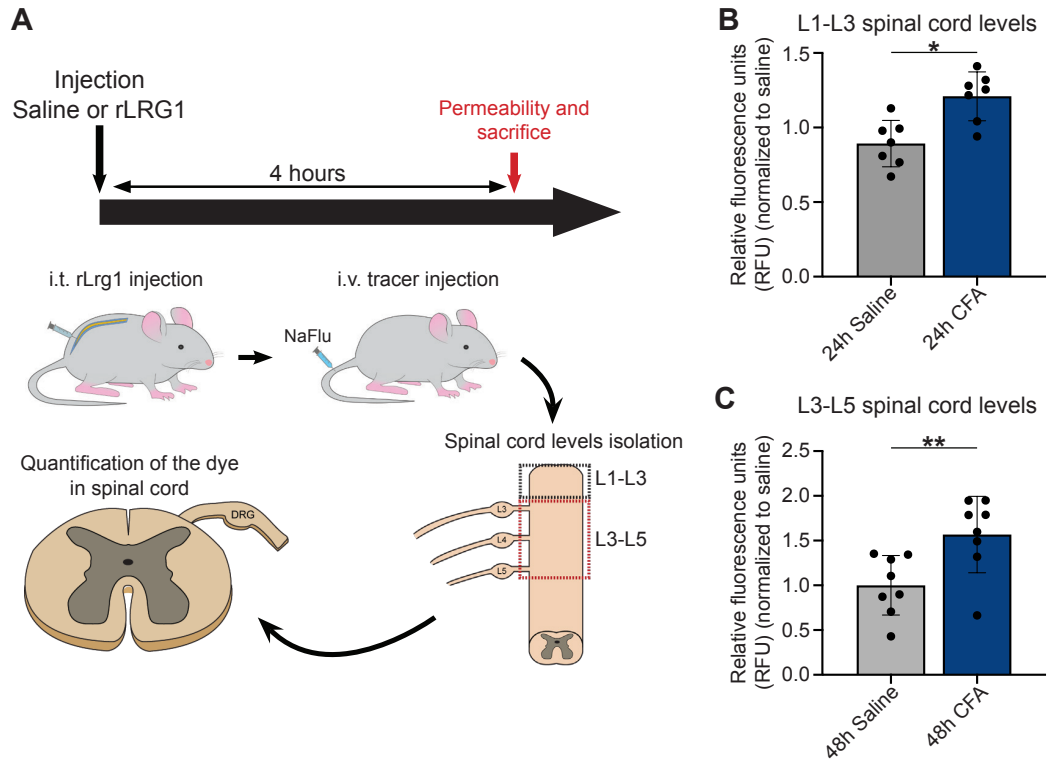

Figure 3.12. rLRG1 intrathecal administration results in blood-spinal cord barrier opening. (A) Schematic illustration of the experimental protocol used to measure blood-spinal cord barrier permeability upon saline or rLRG1 injection at 4 h. Mice were injected either with saline or rLrg1 and, after 4 h, injected with sodium fluorescein (NaFlu), which was allowed to circulate for 30 min. Afterwards, mice were perfused with PBS, the spinal cord levels and regions dissected, and the extravasation of NaFlu into parenchyma was quantified. (B-C) Quantification of tracer extravasation into L1-L3 spinal cord levels (B) and into L3-L5 spinal cord levels (C) upon saline (control) or rLRG1 intrathecal injection. Data normalized to the control. N=8 saline and n=8 rLrg1, parametric distribution, two tailed unpaired Student's t-test.

top of most upregulated genes upon CFA was the Leucine-rich α-2 glycoprotein 1 (Lrg1) (data shown in Litke et al. 2022). Lrg1 is a multifunctional molecule described to be involved in pathological situations (Camilli, Hoeh et al. 2022) and, additionally, it has been shown that genetic removal of Lrg1 reduced permeability in laser injured retina (Wang, Abraham et al. 2013). To assess whether Lrg1 could modulate BSCB permeability, recombinant human LRG1 was injected intrathecally in mice and after 4 hours the tracer extravasation experiment was performed (Figure 3.12A). Remarkably, intrathecal injection of rLRG1 by itself was able to increase BSCB permeability similar to the one observed upon CFA injection. As expected, permeability was also observed at the L1-L3 levels, since intrathecal injection introduces rLRG1 into the subarachnoid spatial and can therefore reach the entire SC (Figure 3.12B-C). Altogether indicating that Lrg1, which is upregulated in CFA after 24h, might be one of the factors contributing for the barrier opening at 48h.

3.2.5. Lrg1 is expressed mainly by ECs and is increased in CFA and SNI models

The previous data indicate that Lrg1 is upregulated upon CFA treatment and is able to modulate BSCB permeability. However, as the entire dorsal spinal cord was used in the RNA-bulk sequencing, the cellular source of Lrg1 was still undetermined. To address it, mice were injected with either Saline or CFA and the different cell populations from the dorsal spinal cord were obtained by magnetic-activated cell sorting (Figure 3.13A), resulting in three main cell fractions: $CD45^+$ labelled fraction consisting of immune cells, $CD45^-CD31^+$ fraction containing ECs and the $CD45^-CD31^-$ fraction with the remaining cells (mainly neurons and to some extent glia cells) (Figure 3.13A). *Lrg1* gene expression levels were drastically upregulated in the ECs fraction of CFA-injected mice compared to the saline control (Figure 3.13B). An upregulation of *Lrg1*, however milder, was also observed in the immune cells fraction (Figure 3.13B). On the other hand, *Lrg1* was not detected in neurons and other glia cells (Figure 3.13B, data not shown). Previous research has demonstrated that Lrg1 levels, in pathological situations, besides being increased in activated ECs of different organs, can also be upregulated in the liver and in the bloodstream (via liver-Lrg1 secretion) (Camilli, Hoeh et al. 2022) and act as a systemic factor. To understand

if that also occurs upon CFA administration, *Lrg1* gene expression was assessed in the brain (hippocampus and cortex regions) and liver, and LRG1 protein level was determined in the plasma. In agreement with previous work, at 24h, *Lrg1* levels were increased in all the analyzed tissues (Figure 3.13C-E) and plasma (Figure 3.13F) upon CFA treatment. Additionally, in agreement with the idea that Lrg1 is involved in acute phases of pathologies (Camilli, Hoeh et al. 2022), the 24h *Lrg1* upregulation observed in the spinal cord upon CFA quickly decreased after 48h (Figure 3.13G), with no differences observed after 3 days (Figure 3.13H). Importantly, the results observed are not exclusive for the CFA model. *Lrg1* mRNA levels in the spinal cord are also upregulated in SNI-operated mice compared to Sham mice (Figure 3.13I), and bioinformatic analysis indicate that the same holds truth in SCI mice (Figure 3.13J).

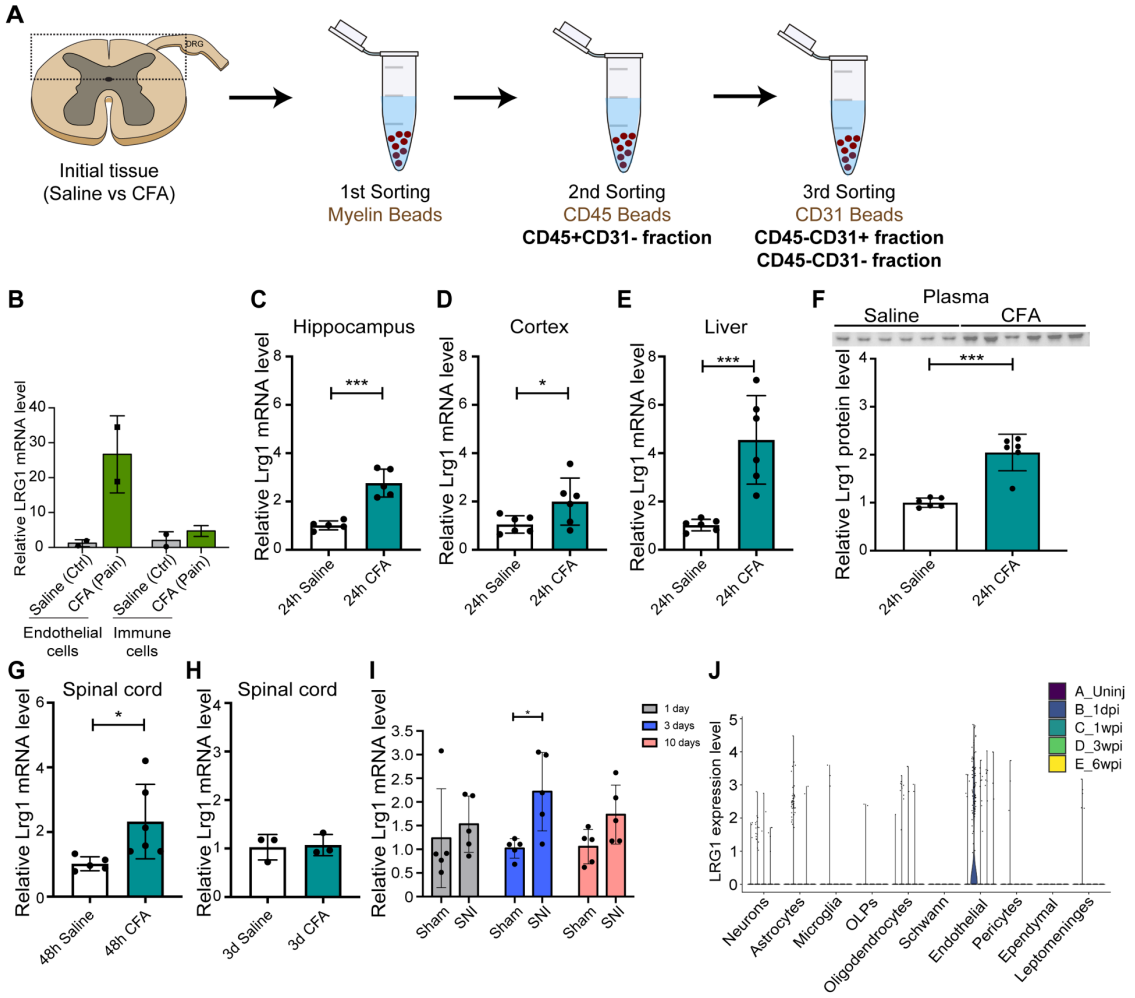

Figure 3.13. Lrg1 expression is upregulated in endothelial cells in inflammatory pain, neuropathic pain, and traumatic chronic pain. (A) Schematic illustration of the magnetic-activated cell sorting of tissue from saline or CFA-treated mice after 24h. Cell fractions were obtained from spinal cord tissue by sequential sorting using myelin beads (to remove myelin), CD45 beads (resulting in the immune cell fraction $CD45^{-}CD31^{+}$) and CD31 beads (generating $CD45^{-}CD31^{+}$ endothelial cell fraction and $CD45^{-}CD31^{-}$ neuronal and glial fraction). (B) Quantification of fraction-specific expression of *Lrg1* following 24 h saline or CFA injections. N=2 saline (control) and n=2 CFA (each dot results from the pooling of two animals). (C-E) Quantification of *Lrg1* gene expression in hippocampus (C), cortex (D) and liver (E) following 24h saline or CFA injection. n=5 saline (control), n=5 CFA for hippocampus, n=6 saline, n=6 CFA for cortex and liver. (F) Quantification of immunoblots (above the graph) for LRG1 from plasma of saline or CFA injected mice. n=6 saline (control), n=6 CFA. (G-H) Quantification of *Lrg1* gene expression in the dorsal part of spinal cord following 48 h (G) and 3 d (H). n=5 for saline 48 h, n=5 for CFA 48 h; n=3 for saline 3 d, n=3 for CFA 3 d. (I) Quantification of *Lrg1* gene expression in the dorsal part of spinal cord following sham or SNI surgeries at 1 d, 3 d and 7 d. These SNI samples were provided by Dr. Anna Hertle. For all timepoints n=5 for sham, n=5 for SNI. (J) *In silico* analysis of *Lrg1* expression in different cell types and timepoints using a published single-cell sequencing SCI dataset. *Lrg1* is particularly increased in endothelial cells at 1 day post injury (dpi). All data were normalized to control. For statistical comparisons between two groups: parametric distribution, two tailed unpaired Student's t-test. For (I) 2-way ANOVA with Sidak's multiple comparisons.

3.2.6. Lrg1 plays a role in pain sensitization

As cells require interactions with other cells for proper functionality, to achieve perfect results, I also interacted and collaborated with other researchers for the successful development of this 3.2. section. In pain research, behavioral testing in mice is necessary to quantify the degree of 'pain-like' behaviors or nociception in different experimental setups. Thus, considering all the results that here demonstrate the involvement of Lrg1 in persistent inflammatory pain, it is logical to assess whether modulating Lrg1 levels would have an impact in pain sensitivity. As I did not directly do the behavior experiments (the Lrg1 behavior experiments were generated by Ann-Kristin Kenkel), the results are not included in my thesis. However, with the permission of Prof. Dr. Daniela Mauceri, the head of the group where the behavior experiments were performed, I summarize the main behavior findings linking Lrg1 and pain sensitivity.

In a first experiment, siRNAs targeting *Lrg1* (siLrg1) to achieve KO of Lrg1 were delivered intrathecally. Here, mice that received siLrg1 presented significantly reduced CFA-triggered mechanical hypersensitivity compared to siCtrl up to 24h after CFA treatment. In an opposite setup, increase of LRG1 protein levels by intrathecal administration of recombinant LRG1 (rLRG1) resulted in increased mechanical sensitivity. Last, intrathecal injection of rLRG1 together with intraplantar administration of CFA led to an exacerbation of CFA-triggered mechanical hypersensitivity. Overall, the results in section 3.2. and these behavioral experiments suggest that Lrg1 is a key factor for spinal sensitization.

3.2.7. *Ctnnb1 fl/fl*$^{Cdh5:CreERT2}$ transgenic mice as a tool to understand the impact of increased permeability in CFA

The opening of the BSCB can result in the passage of unwanted substances or cells from the bloodstream to the spinal cord parenchyma that might contribute for the progression and maintenance of pain. Thus, restoring of the barrier by preventing the increased permeability observed at 48h upon CFA (Figure 3.11C), could perhaps have an impact in reducing pain sensitivity maintenance at a later stage. With that goal, I explored the possibility of preventing the opening of the BSCB to then determine whether chronic pain is ameliorated under those conditions. For this, I used a transgenic mouse line that present a tighter BBB barrier and tested whether inflammatory pain would then not induce SBSCB opening. For this I used *Ctnnb1 Ex3 fl/+*$^{Cdh5:CreERT}$ mice, where the Wnt/β-catenin pathway is constitutively activated in ECs (gain-of-function model), and which has been shown to have increased barrier tightness and thus reduce its permeability upon Cre recombination (Liebner, Corada et al. 2008, Benz, Wichitnaowarat et al. 2019). To induce Cre recombination, 8 weeks mice were injected with tamoxifen (500 μg/day) for 5 consecutive days (Figure 3.14A). Activation of Wnt/β-catenin was allowed to occur for 21 days, timepoint shown to

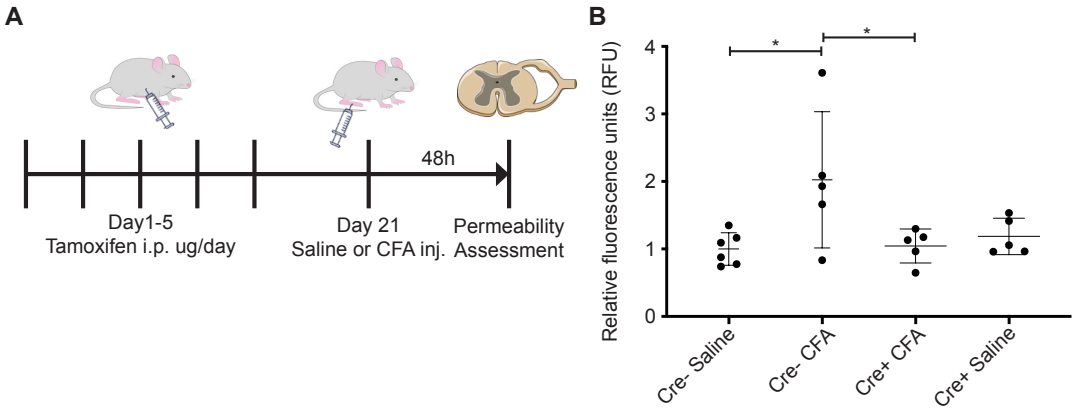

Figure 3.14. Conditional activation of endothelial Ctnnb1 in *Ctnnb1 Ex3 fl/+*$^{Cdh5:CreERT2}$ prevents CFA-mediated BSCB opening. (A) Schematic representation of the protocol used to induce endothelial-specific Ctnnb1 gain of function by tamoxifen administration. Mice were injected (via i.p.) with 500 μg/day of tamoxifen for five consecutive days. 21 days after the first injection, mice were injected either with saline or CFA and BSCB permeability was assessed at 48 h. (B) Quantification of tracer extravasation into dorsal L3-L5 spinal cord levels upon saline or CFA injections. Data normalized to the Cre- Saline. N=6 Cre- saline and n=5 for remaining experimental groups. Comparison in ordinary one-way ANOVA.

be optimal for maximal activation (Benz, Wichitnaowarat et al. 2019), and then Cre- and Cre+ mice were injected with either saline or CFA (Figure 3.14A). Activation of Wnt/β-catenin in ECs was able to prevent the increased permeability induced by CFA at 48h (Figure 3.14B). Behavior analysis using this transgenic mouse line are currently on going.

4. DISCUSSION

The work presented in this thesis reveals the importance of having an accurately intermingled nervous and vascular system during development and pathology. First, I demonstrate a new mechanism used by MNs to control their own column vascularization during embryonic development. Through the expression of Sema3C, MNs signal to ECs via PlexinD1/Nrp1 to repel and prevent vessel ingressing into MN columns, a requirement for them to achieve proper development and maturation. Second, I show that the NVU, and in particular ECs, are involved in the development of chronic pain. I identified the glycoprotein Lrg1 that is derived from ECs and is a likely candidate contributing for chronic pain, and that the BSCB is transiently and locally permeable, which might further contribute for central sensitization.

Overall, this project does not only provide new molecular pathways regulating vascular-CNS communication in physiology and pathology, but the findings also supporting the relevance of neurovascular interactions for proper CNS development and function.

4.1. Bidirectional neurovascular interactions during spinal cord vascularization

Spinal cord vascularization does not occur randomly. Instead, BVs ingress, sprout and extend at very precise locations. Within the spinal cord, at E11.5, vessels ingress into the spinal cord by crossing areas occupied by interneurons, and surround other interneuron populations in honeycomb-type structures (see section 3.1). Notably, sprouting vessels clearly avoid regions occupied by some neural cells (FP, MNs and undifferentiated neural progenitors). But how is this vessel patterning controlled? Are these different neural cells responsible for guiding vessels?

My *in silico* results, using a published scRNAseq from embryonic mouse spinal cord (Delile, Rayon et al. 2019), demonstrate that in the ventral spinal cord all neural cell types are predicted to signal to ECs, supporting the idea of a neural-exerted control of spinal cord vascularization. To the moment, most of the known factors involved in spinal cord vascularization belong to the Vegf or Wnt signaling

pathways. Additionally to those, the *in silico* analysis identified further potential unknown signaling pathways occurring between neural and endothelial cells.

While the work developed in my thesis focused on a neural-to-EC communication, it is important to highlight that the *in silico* interactome predicted signaling from ECs to all the ventral neural cells. Remarkably, within the top pathways occurring during spinal cord development is laminin signaling, particularly predicted to occur from EC-to-all neural cells (Appendix Fig. 1D). Laminins (and other extracellular matrix proteins), besides providing structural support, have been shown *in vitro* to enhance proliferation of neuroepithelial cells, increase the proliferation and survival of neural stem cells and promote neural stem cell differentiation (Drago, Nurcombe et al. 1991, Flanagan, Rebaza et al. 2006, Ma, Tavakoli et al. 2008). Furthermore, laminin modulates neuronal cell development, for example by stimulating neurite outgrowth (Lander, Fujii et al. 1985, Myers, Santiago-Medina et al. 2011). Thus, it is possible that ECs, while they grow through the neural tissue, influence, and shape the neighbor neural cells via laminin-mediated interactions.

It is important to mention that my interactome analysis using a scRNAseq present the downside of not being able to spatially localize the different ECs from this scRNAseq, thus the analysis consider that the different spatially localized spinal cord ECs are relatively similar at the transcriptomic level, which needs to be tested. Nevertheless, such limitation can and was surpassed by confirming any candidate of interest by immunohistochemistry or *in situ* hybridization.

4.2. Sema3C-PlexinD1 signaling as a regulator of MN vascularization

Among the top signaling pathways identified was Sema3 signaling. Interestingly, Sema3 signaling was predicted to occur predominantly between MNs and ECs (Figure 3.3B). This specificity can in part be explained by the numerous Sema3 members particularly expressed by MNs compared to the remaining neural cells (Cohen, Funkelstein et al. 2005, Huber, Kania et al. 2005).

In this work, I validated one of the predicted ligand-receptor interactions within the Sema3 pathway, Sema3C-PlexinD1, by demonstrating that MN-secreted Sema3C signals to EC-PlexinD1 and that cell-specific removal of either of them results in premature BV ingression into MN columns (Figure 4.1) Interestingly, both Sema3C and PlexinD1 expression peaks at E11.5 and is

reduced at E12.5, when avascular MN columns become firstly invaded by vessels. Sema3C-PlexinD1 ability to repulse/inhibit angiogenesis was only demonstrated previously in pathological conditions (Yang, Hu et al. 2015). I show here, for the first time, that this signaling is also important in a physiological development process.

Besides the results of my work, it was shown that MNs additionally control their vascularization by creating a tight balance of Vegf-sFlt1 (Himmels, Paredes et al. 2017). This raises the question of whether Sema3C-PlexinD1 signaling could interact with Vegf signaling to fine-tune MN vascularization, as in

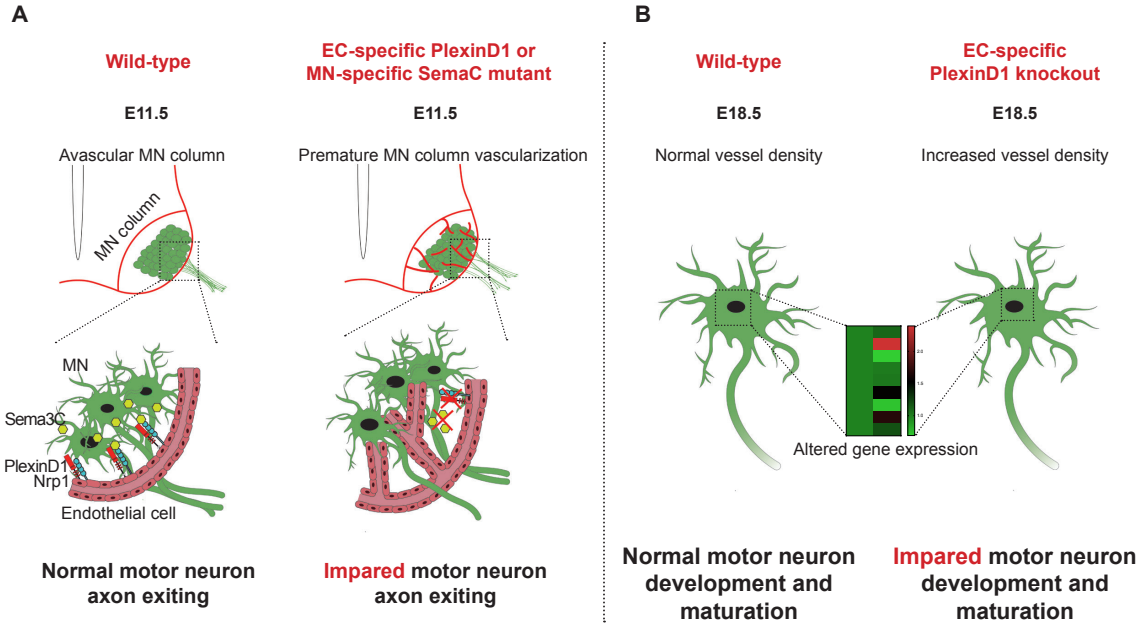

Figure 4.1. Proposed model for MN-EC communication required for proper spinal cord vascularization and MN development. (A) MN columns of WT embryos are avascular at E11.5. This is achieved by MN-secreted Sema3C signaling to PlexinD1/NRP1 in ECs, thereby controlling their ingression into MN columns, and allowing proper MN development and maturation. However, in EC- specific *PlexinD1* or MN-specific *Sema3C* transgenic mice, this signaling is interrupted and blood vessels ingress into MN columns prematurely. Furthermore, MN development is impaired (B) showing defects in axon organization at their exit into to the periphery at E11.5, and dysregulated expression of terminal differentiation markers and functional factors for MNs at E18.5.

pathological conditions, Sema3C-PlexinD1 pathway in ECs was described to crosstalk with the Vegf signaling in order to inhibit pathological retinal angiogenesis (Yang, Hu et al. 2015). However, whether this occurs also in this physiological developmental process requires further investigation.

4.3. Sema3E is not involved in keeping MNs avascular

Sema3E has been previously shown to be involved in BV development, particularly in inducing vessel repulsion, by signaling through PlexinD1 (Gu, Yoshida et al. 2005, Meadows, Fletcher et al. 2012). However, the *in silico* interactome did not predict Sema3E as a possible MN-expressed ligand for PlexinD1 in ECs. As my bioinformatic analysis group all MN pools from all the different spinal cord levels together, candidates that might be expressed only at a certain spinal cord level or only by few MN subtypes would probably not be predicted. And, indeed, Sema3E falls into this group of genes, thus not being an output candidate of my analysis. I showed that Sema3E expression at E11.5 is restricted to MNs only at brachial levels, similarly to what was previously shown at later developmental timepoints (Cohen, Funkelstein et al. 2005). Nevertheless, being aware of the literature, I analyzed *Sema3E* KO mouse embryos, finding that that Sema3E is not influencing MN columns vascularization or embryonic spinal cord vascularization, at least itself alone.

4.4. MN vascularization phenotype is greater in *PlexinD1 fl/fl*$^{Tie2:Cre}$ mice compared to Sema3C fl/fl$^{Tie2:Cre}$

Removal of PlexinD1 from ECs (*PlexinD1* fl/fl$^{Tie2:Cre}$) resulted in a stronger MN vascularization when compared to the removal of Sema3C from MNs (*Sema3C* fl/fl$^{Tie2:Cre}$). I hypothesize that this can be explained by three different, non-exclusive, mechanisms. First, as mentioned before, other Sema3 family members able to bind PlexinD1 are expressed by MNs (Cohen, Funkelstein et al. 2005). Thus, upon Sema3C removal, it is possible that other Sema3 proteins, such as Sema3A and Sema3E, takeover and compensate in part for the repulsive action of Sema3C. For example, while Sema3E by itself does not have an effect in MN vascularization, it might act in synergy with Sema3C, or replace Sema3C when this one is absent. Second, it was demonstrated that PlexinD1 in ECs can act as a mechanosensory (Mehta, Pang et al. 2020), independent of its ligands, being activated by mechanical forces and leading to cytoskeleton rearrangement of ECs and control vessel growth. Thus, a similar action of PlexinD1 in ECs of developing spinal cord vessels is possible. Last, as discussed in section 4.2., Sema3C-PlexinD1 signaling in ECs can crosstalk with the Vegf signaling and regulate vessel growth (Yang, Hu et al. 2015). Whether any of these three

mechanisms occurs upon Sema3C removal at this developmental stage needs to be further explored.

4.5. Importance of avascular MN columns for a particular developmental time window

Vessels ingress into the spinal cord laterally to the MN columns and further completely surround them at E11.5. But why would MNs prevent vessel ingression for such particular time window?

The data presented in this thesis suggests that this timely vessel ingression into MN columns is required for proper MN development. Indeed, premature vascularization of MN columns resulted in MN axon exit defects (Figure 4.1). While MN axons normally exit the spinal cord in a single organized bundle, MN axons in both *PlexinD1 fl/fl*$^{Tie2:Cre}$ and Sema3C fl/fl$^{Tie2:Cre}$ transgenic mouse embryos exit into the periphery in disorganized, segregated fascicles. In between these segregated fascicles, I identified vessels that had prematurely invaded into the MN columns, suggesting that vessels create a physical barrier to growing MN axons, which in turn have to circumvent those vessels. Moreover, it is possible that MN axons have a tropism for vessels so that upon premature vascularization, MN axons associate with those vessels and grow/migrate along their surface. MN axon guidance from the spinal cord to the periphery was described to be regulated by repulsive signals within the spinal cord and attractive signals from the MEP and peripheral targets (Bonanomi, Valenza et al. 2019, Suter and Jaworski 2019). Here, I reveal another possible layer of regulation, where MN-secreted Sema3C acts as a repulsive signal to keep vessels outside MN columns until axons have projected out of the spinal cord in an organized manner. Supporting this idea, a similar premature vascularization, though achieved by interfering with Vegf levels, resulted in similar MN axon defasciculation (Himmels, Paredes et al. 2017).

4.6. MN defects at late embryonic development

At the end of embryonic development, E18.5, MNs in *PlexinD1 fl/fl*$^{Tie2:Cre}$ embryos show alteration in the expression patterning of genes associated with axon terminal differentiation and functionality, in particular ChAT. ChAT is a key

enzyme in acetylcholine production, the neurotransmitter released by MNs, suggesting that MN neurotransmission potential is reduced. As this reduction does not seem to be caused by loss of afferent inputs, these MN transcriptomic profile changes might be a consequence of the premature vessel ingression observed at E11.5 or alterations in the EC-secretome of *PlexinD1 fl/fl*$^{Tie2:Cre}$ embryos, requiring further investigation. Additionally, while this worked focused mainly in MNs and their development, it remains to be understood whether the transcriptomic profile of other neighbor interneurons might be similarly affected. Besides maturation defects, the axon terminal of the phrenic nerve was found to be hyperbranched. Remarkably, this abnormal increased nerve branching in *PlexinD1 fl/fl*$^{Tie2:Cre}$ embryos might be explained by the reduction in ChAT and Nrg1 expression in MNs, as KO mice for either gene were shown to present abnormal increase of axon branching (Wolpowitz, Mason et al. 2000, Brandon, Lin et al. 2003). Additionally, it needs to be further investigated if the changes in the transcriptomic profile and abnormal branching of MNs result in indeed in neurotransmission defects or not – for example by doing electrophysiology experiments. The defects observed at this late embryonic development might be in part explained by compromised MN axon patterning in the CNS periphery. In fact, in parallel to my groups study, PlexinD1 removal in ECs has been shown to provoke ectopic vessel agglomeration, which acts as a barrier and obstructs the MN axons to growth in direction to their muscle targets (Martins, Brambilla et al. 2022). Furthermore, bulk-RNAseq of MNs derived from WT or EC-specific *PlexinD1* KO embryos demonstrated that transcriptional changes within MNs are present at E12, including an increase of *Slc18a3* at E12 (as I found at E18.5) (Martins, Brambilla et al. 2022).

While it would be of interest to know the impact of the MN phenotypes observed at postnatal or adult stages, *PlexinD1 fl/fl*$^{Tie2:Cre}$ embryos die at birth due to cardiovascular defects (Zhang, Singh et al. 2009), making it impossible to be done. Nevertheless, as it is possible that EC-specific removal of PlexinD1 leads to a different EC-secretome, it would be interesting to do such deletion in postnatal embryos and investigate whether there are any particular MN alterations.

4.7. Involvement of neurovascular cells in pain

The results presented in this thesis show that at early stages of CFA-induced inflammatory pain and SCI (both at 24h), non-neuronal cells express most of the significantly altered genes and present well-defined clustering dependent on the treatment. In particular, microglia and ECs seem to be the most affected. Considering these changes, I hypothesized that besides transcriptomic alterations, also additional structural changes in the non-neuronal cells could additionally be present.

In this work I show that microglia density is increased 7 days after CFA injection. However, as both microglia and macrophages share many cell markers (Jurga, Paleczna et al. 2020), including Iba1, it would be of relevance to use additional markers to understand the contribution of the distinct immune cell types for the increase observed (for example, to distinguish microglia from macrophages). Nevertheless, when comparing to the literature, the microglia phenotype in inflammatory pain is not consensual. While morphological changes and activation in microglia have been suggested to occur after CFA injection from 3 to 14 days post-injection (Raghavendra, Tanga et al. 2004, Xu, Jiang et al. 2019), other studies have not seen significant alterations (Clark, Gentry et al. 2007, Lin, Li et al. 2007, Ikeda, Kiritoshi et al. 2012). My result suggests that though mild, there is an increase in microglia density upon CFA injection. Similarly, activation of astrocytes is debatable. My observation that no changes are observed after CFA treatment go in line with a previous report (authors investigated Gfap levels at 4 days) (Xu, Jiang et al. 2019). However, there are other studies suggesting that astrocytic activation, by measuring Gfap intensity (at 7 days) (Ikeda, Kiritoshi et al. 2012), Gfap gene and protein levels (at 4 and 14 days) (Raghavendra, Tanga et al. 2004) and astrocyte morphology (after 3 and 10 days) (Cao and Zhang 2008), is present after 3 days and is present as long as 14 days post-injection. Due to the discrepancies between results, further detailed studies need to be performed in order to clearly untangle these differences. The solely use of Gfap and Iba1 as markers of reactivity/activation has been controversial, as both can variate even in physiological situations. Thus, besides other already published activation markers (such as CD68, a phagocytosis marker expressed by microglia) (Candlish and Hefendehl 2021, Escartin, Galea et al. 2021), newly generated scRNAseq will provide new

indicators of microglia activation or astrocyte reactivity, which will help in the future to clarify whether both are present in chronic pain.

Here I show that there are no significant changes in vessel density after CFA. While this informs that no considerable angiogenesis or vessel regression occur, it does not allow to perceive the impact on EC activation. An important message that my thesis carries is that ECs are not merely forming vessels for transporting oxygen and nutrients, but are much more than that. Thus, it is reasonable that EC activation is present without alteration in their density. EC activation is usually induced by inflammatory cues, which are present in the pain models here used, and can be observed by the expression of cell-surface adhesion molecules and leukocyte adhesion molecules, such as VCAM-1, ICAM-1, E-selectin, P-selectin and von Willebrand factor (Vwf) (Liao 2013). Thus, potential EC activation should be taken in consideration and further investigated.

4.8. BSCB breakdown as one of the multi-temporal events ocurring in chronic pain

Dysregulation of the BSCB has been observed in different pain models (Beggs, Liu et al. 2010, Echeverry, Shi et al. 2011, Figley, Khosravi et al. 2014).

In this work I show that the BSCB is transiently open at 48h after CFA injection, while in SNI mice the opening of the BSCB is maintained from 7 days (at least) up to 28 days, correlating with the severity of the model. It is important to highlight that this opening was found to be local to the L3-L5 levels of the SC (this is further discussed below). To the best of my knowledge, only one study investigated the BSCB status in CFA model, where no extravasation of EB (69 kDa when bound to albumin) into the SC was observed at 24h (Lu, Gonzales et al. 2009). In an acute model of inflammatory pain, single time points have been investigated by different groups: BSCB permeability (using EB) was not affected 24h after carrageenan injection (Lu, Gonzales et al. 2009), it was increase 48h post-carrageenan injection (Gillardon, Vogel et al. 1997), and at 3 days no EB or NaFlu extravasation was observed in spinal cords of carrageenan-injected mice (Xanthos, Pungel et al. 2012). Interestingly, the timepoint of the transient opening matches in both models, despite of carrageenan being a much shorter duration model than CFA-induced inflammatory model (Ren and Dubner 1999).

BSCB breakdown seems to be a clear feature in animal pain models, however its contribution for the CFA-induced pain sensitization remains elusive. The onset of the nociception in this model does not directly correlate with the changes in BSCB permeability, which are transient, suggesting that BSCB disruption is neither a trigger nor a contributor for the initial pain nociception. In line with this idea, a dynamic contrast-enhanced magnetic resonance imaging study has shown that genetically different strains of mice present variable SNI-induced pain hypersensitivity, and that BSCB permeability did not correlated with the differences in mechanical sensitivity of the diverse mouse strains (Cahill, Laliberte et al. 2014).

While not acting as an initiator, BSCB increased permeability might contribute indirectly to the development of hypersensitivity and further maintenance of spinal sensitization. Essentially, chronic pain is a multi-temporal sequence of events where BSCB plays an intermediary role (Figure 4.2). I hypothesize that BSCB permeability would be inserted in chronic pain development as follows: shortly after pain induction, an initial burst of signals are generated causing the acute pain (either neuronal- or non-neural-triggered, often by the 'inflammatory soup' (Basbaum, Bautista et al. 2009)). Within these signals, there are factors that can in parallel induce BSCB permeability, one of them being Lrg1 as suggested in this work. Once the barrier is more permeable, non-desired cells or factors invade the spinal cord parenchyma and, at this timepoint, the 'system' reacts by activating compensatory mechanisms to close the BSCB, explaining why the barrier opening is transitory. A similar mechanism was suggested for the multiple sclerosis mouse model experimental autoimmune encephalomyelitis (Lengfeld, Lutz et al. 2017). These cell/factors infiltration, together with the mechanisms of central sensitization (section 1.3.5.), promote the development and maintenance of chronic pain until other mechanisms emerge for pain resolution (Figure 4.2). To understand whether this is true, assessment of pain behavior in *Ctnnb1 Ex3 fl/+*$^{Cdh5:CreERT2}$ (the model I present here that prevents BSCB opening) injected with CFA will be performed at timepoints later than the BSCB increased permeability, to investigate whether pain sensitivity is reduced after the 48h timepoint by restoring the BSCB.

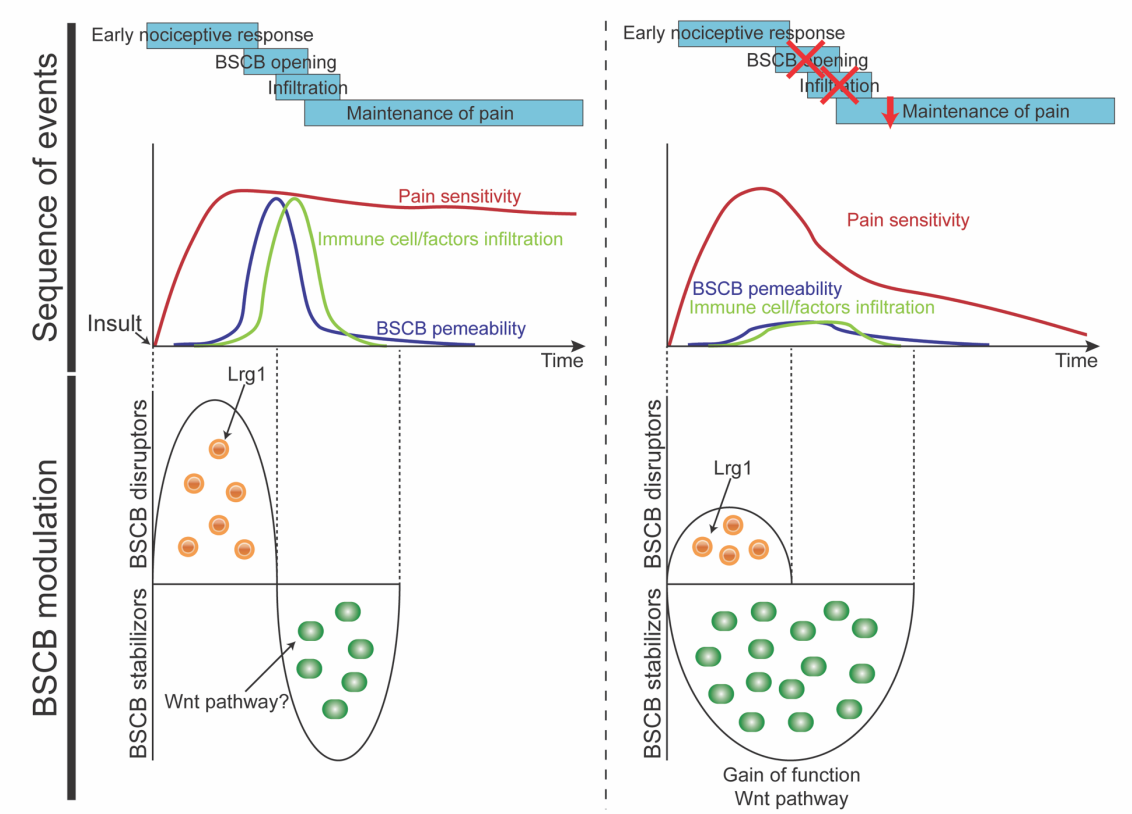

Figure 4.2 Proposed model for the involvement of the NVU-related BSCB in persistent inflammatory pain. (A) Injection of CFA causes an initial early nociceptive response. During this early period, BSCB disruptors are highly upregulated, including Lrg1 shown in this work, which lead to a time window where BSCB permeability is increased. This opening in turn allows for the easier immune cell or factors infiltration from the bloodstream to the spinal cord parenchyma. This is a key event that further exacerbates and permits the maintenance of pain. However, as this opening is not desired, the biological response is the upregulation of BSCB stabilizers to counter it, to which Wnt pathway might contribute, as shown for other pathological situations. (B) Thus, early BSCB repair by Wnt pathway gain-of-function, which would create an imbalance towards higher levels of stabilizers than disruptors, would prevent cell/factors infiltration into the spinal cord and reduce the maintenance of pain. Overall, BSCB increased permeability might be seen as a key intermediary step in the development of persistent inflammatory pain, and its prevention might induce an earlier resolving of pain sensitivity.

The increase of permeability I observed was restricted to the dorsal part of the spinal cord at L3-L5 levels, while at the adjacent L3-L5 ventral side and dorsal L1-L3 levels no differences in BSCB opening were observed. The specificity for the region, which coincides to be the target area of afferent neurons innervating the hindpaw of mice, suggests a role for this sensorial neurons in the selective local opening. Purely hypothetically, it is possible that intensified release of neurotransmitters from afferent neurons and interneurons within the dorsal horn upon nociceptive stimuli provokes directly BSCB loss of integrity. ECs are

described to express the receptors for common neurotransmitters, such as N-methyl-D-aspartate (NMDA) receptor (Sharp, Hines et al. 2003, LeMaistre, Sanders et al. 2012, Lu, Hogan-Cann et al. 2019, Sailem and Al Haj Zen 2020) and GABA receptors (Li, Kumar et al. 2018, Choi and Vasudevan 2019, Agrud, Subburaju et al. 2022), hence being able to respond to them. Supporting this hypothesis, it was shown *in vitro* that glutamate is actually able to induce EC monolayer breakdown (Sharp, Hines et al. 2003).

4.9. Cell invasion during the increased BSCB permeability time window

One hypothesis is that breakdown of the BSCB allows the infiltration of myeloid cells from the blood into the spinal cord, as shown previously (Zhang, Shi et al. 2007, Costigan, Moss et al. 2009, Isami, Haraguchi et al. 2013, Kalin, Miller et al. 2018), which will further exacerbate and maintain nociception that further develops into chronic pain. However, the invasion of blood-derived cells is still questioned, with few studies reporting no myeloid cell infiltration following SNI (unexpectedly as authors used the exact same conditions as in Costigan et al 2009 (Costigan, Moss et al. 2009)) (Gattlen, Clarke et al. 2016), partial ligation of the sciatic nerve (PSNL) (Kim and Moalem-Taylor 2011), CCI (Austin, Kim et al. 2012), spinal nerve transection (SNT) (Gu, Peng et al. 2016) or L4 spinal nerve injury (Kobayashi, Konishi et al. 2016). One of the reasons of such variability is the experimental approaches used to detect immune cell infiltration. To clarify it, one study employing different techniques demonstrated that SNI surgeries done in C57Bl/6 chimeric mice, which after irradiation-depletion receive bone marrow transfusion from mice expressing GFP in hematopoietic cells, result in increase of GFP^+ cells in the spinal cord. However, when they used instead a simple reporter line, no infiltration of immune cells was observed (Guimaraes, Davoli-Ferreira et al. 2019). As leukocyte invasion also occurred substantially in non-injured mice in the first approach, it suggests that the infiltration observed was independent of SNI induction, and probably caused by the irradiation itself, as suggested before (Yuan, Gaber et al. 2003, Mildner, Schlevogt et al. 2011, Kierdorf, Katzmarski et al. 2013).

Additionally, it is important to consider that perhaps immune cell infiltration is not a direct consequence of BSCB disruption and that both are independent

events, although in cases where both are observed, the former may be a direct consequence of the latter.

Besides the view of a physical opening of the barrier, potential alterations in the expression of immune cell trafficking molecules in ECs should be taken in consideration as a possible contributor for immune invasion. It is possible that immune infiltration is enhanced by increased expression of chemokine receptors, selectin proteins and immune cell adhesion molecules in ECs, which facilitate and augment not only the paracellular but also transcellular immune cell infiltration (independently of tight junctions remodeling) (Lopes Pinheiro, Kooij et al. 2016, Lutz, Smith et al. 2017, Amersfoort, Eelen et al. 2022).

Essentially, one of the take-home messages of sections 4.7-4.9 is that the discrepancy of results between studies reflects the different experimental approaches, timepoints analyzed and the fact that most of the studies focus in short single experiments instead of performing a more global, complete panel of different analysis (i.e. perform simultaneously pain behavior evaluations, permeability experiments, assessment of immune cell invasion, neurovascular cell levels and their activation) to get a clear full picture of the connection between processes that might lead to pain chronification.

4.10. Lrg1 as key player in pain

Lrg1 was found to be a top upregulated gene upon 24h CFA in a published RNAseq (Litke, Hagenston et al. 2022). Interestingly, the temporal increased expression of *Lrg1* in spinal cord ECs peaks and overlaps with the opening of the BSCB, and its reduction coincides with the closing of the barrier, making it an obvious candidate as a BSCB disruption initiator. Indeed, I show here that administration of rLRG1 leads to an increase in BSCB permeability after 4h. However, it remains to explain why a hypothetical Lrg1-induced BSCB opening would occur locally at dorsal L3-L5 and not in other regions, as the increase of *Lrg1* expression and LRG1 protein circulation could potentially target all the CNS vasculature. One possibility is that Lrg1 action in ECs would occur indirectly through other cells. A second option is that for an unknown reason, perhaps due to exacerbated neuronal activity, the ECs at that region are ‘primed’ and sense Lrg1 signaling at higher levels. To directly confirm whether Lrg1 is a main

contributor for the barrier opening in CFA, further permeability experiments using EC-specific *Lrg1* KO or *Lrg1*-global KO mice must be done.

Interestingly, *Lrg1* increase after CFA was observed in completely different organs (while I demonstrated that in the SC this increase occurs in ECs, the remaining organs were used as a whole, therefore further experiments to determine whether the increase is also in ECs are required), suggesting that its upregulation is caused by a systemic factor (e.g., from the bloodstream) instead of a local stimulator in the spinal cord. However, the importance of a local regulation of Lrg1 expression should not be discard. One of the key inducers of *Lrg1* transcription in ECs is Il-6, which curiously has been described to be acutely (<12h) increased after neuropathic and inflammatory pain (Nakamura, Houghtling et al. 2003, Gattlen, Clarke et al. 2016, Zhou, Liu et al. 2016). Hypothetically, it would be possible that neurons within the dorsal horn of the spinal cord (or sensorial neurons), upon injury, secrete Il-6 that would signal to ECs, leading to increased Lrg1. Additionally, other inflammatory interleukins, TNF-α and Tgf-β can regulate Lrg1 expression, making them possible candidates (Camilli, Hoeh et al. 2022). Lrg1 levels were previously shown to be considerably increased in the liver as early as 6h upon LPS injection (Shirai, Hirano et al. 2009), and I show that after 24h CFA LRG1 protein levels are increased. Theoretically, it might also be possible that early circulating LRG1, mainly secreted by the liver, somehow contributes for the BSCB destabilization as shown in other pathological situations (Camilli, Hoeh et al. 2022). To investigate the role of different cellular sources and locations for Lrg1 for pain sensitivity, further experiments using *Lrg1 fl/fl*$^{Cdh5:CreERT2}$ (EC-specific removal of Lrg1) or global *Lrg1* KO mice are further planned. Moreover, the use of available Lrg1 neutralizing antibodies (Moss, Kallenberg et al. 2018, Kallenberg, Tripathi et al. 2021) could be a promising therapeutic approach for treating chronic pain.

5. CONCLUSION

In summary, the work developed in this thesis shows that from embryonic development to adulthood to pathology, the CNS requires a continuous commitment with the vascular system, exposing the importance of neurovascular biology. During physiological embryonic development, the novelty in the presented findings relies on the newly described mechanism that MNs use to signal to ECs, and the importance of temporal control of neurovascular processes for achieving proper CNS development. In particular, I show that MNs express Sema3C in order to prevent premature ingression of vessels into their columns, a signal received by ECs through the receptor complex PlexinD1/Nrp1. MNs require the maintenance of this avascular period as to be able to develop and mature correctly. The results related to the embryonic work here shown provide a better understanding on how impaired crosstalk between neural and vascular systems might contribute to neurodevelopment disorders and neurodegenerative diseases, particularly when timely regeneration and vascularization needs to occur.

In pathological conditions, the presented findings in this thesis demonstrate that non-neuronal NVU cells play a significant part in inflammatory pain. While not presenting considerable structural alterations, most of the transcriptomic changes happening upon CFA are occurring in NVU cells. One of them, Lrg1, is greatly increased in ECs and in plasma, and leads to increased mechanical hypersensitivity (the latter not shown in this work, part of an ongoing collaboration). Additionally, persistent inflammatory pain induces a transient and local opening of the BSCB, which can be recapitulated by intrathecal delivery of rLrg1. These results not only provide new knowledge about the impact of non-neuronal cells in pain, but also new targets for potential therapeutic approaches.

6. MATERIALS AND METHODS

6.1. Materials

6.1.1. Chemicals and reagents

Table 6.1: Chemicals and reagents used in this thesis.

Chemical/Reagent	Reference	Supplier
2-methylbutane	M32631	Sigma-Aldrich
20x Saline-sodium citrate (SSC) Buffer	15557-044	Life Technologies
Agarose	A9539	Sigma-Aldrich
Albumin Fraction V	8076.2	Roth
Bio-Rad protein assay dye reagent concentrate	5000006	Bio-Rad
Blocking Reagent	11096176001	Roche
CD31 Microbeads	130-097-418	MACS Milteny Biotec
CD45 Microbeads	130-052-301	MACS Milteny Biotec
Citric acid monohydrate	A1414	AppliChem
Clarity™ Western ECL Substrate	170-5061	Bio-Rad
Complete Freund's Adjuvant (CFA)	F5881	Sigma-Aldrich
Complete™ cocktail protease inhibitors	4693159001	Roche
Corn oil	C8267	Sigma-Aldrich
Corning Matrigel Matrix	356234	Corning
D-(+)-Glucose	G5767	Sigma-Aldrich
DAPI	D1306	Invitrogen
Deoxynucleotides (dNTPs)	N0447S	NEB
Diethylpyrocarbonate (DEPC)	40718	Sigma-Aldrich
Dimethyl sulfoxide (DMSO)	10282	Gruessing
DNA ladder 100 bp	N3231S	Thermo Scientific
DNA loading dye (6x)	R0611	Thermo Scientific
DNA stain	39803.01	Serva
Dulbecco's phosphate buffered saline	D8537	Sigma-Aldrich
EDTA	A3553	AppliChem
Endopan-3 Basal Medium	P04-0010B	PAN Biotech
Ethanol	32205	Sigma-Aldrich
Fetal bovine serum (FBS)	F7524	Sigma
Fluoromount-G	0100-01	Linaris
Formamide	47670	Sigma-Aldrich
Gelatin from porcine skin	G1890	Sigma-Aldrich
Glutamine	25030-024	Life Technologies
HBMECs	ACBRI376	Cell Systems
HEPES	9105.2	Roth
Horse serum	26050-88	Life Technologies
Hydrochloric acid	35328	Sigma-Aldrich
LB-Medium (Bacto™Agar)	214010	BD
LB-Medium (Bacto™Tryptone)	211705	BD
LB-Medium (Bacto™Yeast Extract)	212750	BD

Magnesium chloride	A3618	AppliChem
Maleic Acid	M03575	Sigma-Aldrich
Methanol	32213	Sigma-Aldrich
Methyl-cellulose	M0512	Sigma-Aldrich
Midori Green Advance	MG04	Nippon Genetics
Myelin removal II Microbeads	130-096-733	MACS Milteny Biotec
NBT/BCIP	S3771	Thermo Scientific
NEG-50	6502	Thermo Scientific
Neuro-DiI	60016	Biotium
Normal donkey Serum	017-00-121	Dianova
Oligofectamine	12252011	Invitrogen
PageRuler™ Prestained protein ladder, 10 to 180 kDa	26616	Thermo Scientific
Para-formaldehyde	P6148	Sigma-Aldrich
Penicillin-Streptomycin	15140-122	Gibco
Ponceau S Solution for Eletrophoresis	33427.01	SERVA
Potassium chloride	A3582	AppliChem
Potassium dihydrogenphosphate	A3620	AppliChem
Proteinase K	7528.1	Roth
Q5 HighFidelity DNA polymerase	M0491	NEB
Recombinant LRG1	13371-HCCH	Sino Biologicals
RNAse-Free DNA set	79256	Qiagen
RNAseOUT Recombinant Ribonuclease Inhibitor	10777019	Thermo Scientific
ROTI®Histofix 4%	P087.3	Carl Roth
Sodium bicarbonate	31437	Sigma-Aldrich
Sodium chloride	31434	Sigma-Aldrich
Sodium dodecyl sulfate (SDS)	CN30.3	Roth
Sodium fluorescein	F6377	Sigma-Aldrich
Sodium hydroxide	30620	Sigma-Aldrich
Sodium phosphate dibasic dihydrate	4272	Sigma-Aldrich
Sodium phosphate monobasic monohydrate	72504	Sigma-Aldrich
Sodium pyruvate solution	S8636	Sigma
Tamoxifen	13258	Cayman Chemical
Tri-sodium citrate dehydrate	A2403	AppliChem
Tris(hydroxymethyl)aminomethane (TRIS)	4855.2	Roth
Triton X-100	108603	Merck
Trypsin-EDTA	25300-054	Gibco
Tween®20	9127.1	Roth

6.1.2. Consumables

Table 6.2.: List of consumables used in this thesis.

Consumables	Type/Reference	Supplier
21G Butterfly	4056504-01	Venofix Safety
27G Butterfly	4056501-01	Venofix Safety
75 cm^2 culture flasks	CLS430641	Sigma-Aldrich
96 well qRT-PCR plate	710874	Biozym
Amersham™ Protran™ 0.45 mm	10600002	Merck
Cell Scraper	541070	Greiner
Covers for PCR plates	4311971	Applied Biosystems
Coverslips 24 x 60 mm	BB024060A1	Menzel Gläser
Cryotubes	123263	Greiner Bio-one
EasyStrainer 40 mm	542040	Greiner
EasyStrainer 70 mm	542070	Greiner
Eppendorf tubes	1.5 ml, 2 ml	Eppendorf
Falcon tubes	15 ml, 50 ml	Cell Star
Filter for Syringes	0.2 mm, 0.45 mm pore size	GE Healthcare
GentleMACS C-tubes	130-093-237	MACS Milteny Biotec
Liquid blocker Super Pap Pen	Z377821-1EA	Sigma-Aldrich
LS Columns	130-042-401	MACS Milteny Biotec
µ–Slide 15 wells	81506	Ibidi
MicroAmp™ Fast Optical 96-Well reaction plate	4346907	Thermo Scientific
MicroAmp™ Optical Adhesive Film	4311971	Thermo Scientific
Microplate 96 wells	655209	Greiner Bio-one
Microscopy slides, Superfrost® Plus slides	J1800AMNZ	Thermo Scientific
MS columns	130-042-201	MACS Milteny Biotec
Multiwell cell culture plates	6-, 12-, 24-, 48-, 96-well	Greiner Bio-one
Needles	21G, 27G, 30G	BD Microlance™
Nitrile gloves, powder-free	Size L	Microflex®XCEED
Pasteur pipettes, flass	7095B9	Corning
Pasteur pipettes, plastic	LW4000	Alpha Laboratories
PCR tubes	A1402-3700	STARLAB
Pipette tips	10 ml, 100 ml, 200 ml, 1000 ml	Greiner Bio-one
Pipette tips (with filter)	10 ml, 100 ml, 200 ml, 1000 ml	STARLAB
Sterile filters	150 ml, 500 ml	Faust
Syringe filter 0.2 mm	10462200	Whatmann
Syringes	1 ml, 2 ml, 5 ml, 10 ml	BD

6.1.3. Equipment

Table 6.3.: List of equipment used in this thesis.

Equipment	Model	Supplier
Centrifuge	MEGAFUGE 16R	Heraus
Centrifuge	5424R	Eppendorf
Chemidoc™ Imaging System	17001402	Bio-Rad
CLARIOstar Plus		BMG LABTECH
CO_2 incubator	HERA CELL 150i	Thermo Scientific
Confocal microscope	LSM510 and LSM800 with Airyscan	Zeiss
Confocal microscope	A1r	Nikon
Cryostat	CM3050	Leica
Cryostat	CM1950	Leica
Dumont #5 Forceps - Standard / Dumoxel	11251-30	Fine Science Tools
Epifluorescence microscope	Axiovert 200	Zeiss
Fine Scissors - ToughCut	14058-09	Fine Science Tools
gentleMACS™ Dissociator	130-093-235	Milteny Biotec
Graefe Forceps - Angled / Serrated	11049-10	Fine Science Tools
Graefe Forceps - Straight / Serrated	11050-10	Fine Science Tools
HybEZ™ Oven	241000 ACD-2	Advanced Cell Diagnostics
Laminar flow hood	SAFE 2020	Thermo Scientific
MACS Multistand	130-042-303	Milteny Biotec
MACSmix™ Tube Rotator	130-090-753	Milteny Biotec
Microplate reader	Rosys Anthos 2001	Anthos Mikrosysteme Gmbh
Midi MACS separator	130-042-302	Milteny Biotec
OctoMACS™ Separator	130-042-108	Milteny Biotec
PCR Machine	ProFlex PCR System	Applied Biosystems
Pipettes	P-2, P-10, P-20, P-100, P-200, P-1000	Eppendorf
qRT-PCR machine	StepOne	Applied Biosystems
qRT-PCR machine	StepOne Plus	Applied Biosystems
Scissors - Straight / Sharp / Blunt	14001-13	Fine Science Tools
Spectrophotometer	Nanodrop1000	Peqlab
Spectrophotometer	DS-11 Series	DeNovix
Spring Scissors - Angled	15006-09	Fine Science Tools
Stereomicroscope	M210F	Leica
Vibratome	VT1200S	Leica

6.1.4. Kits

Table 6.4.: List of kits used in this thesis.

Kits	Reference	Supplier
Arcurtus™ PicoPure RNA Isolation	12204-01	Applied Bioscience
cDNA synthesis Superscipt® Vilo™	11754-050	Invitrogen
Collagenase/Dispase	10269638001	Sigma-Aldrich
Digoxigenin (DIG) RNA labeling kit	11175025910	Roche
DNAse I	LS002139	Worthington Biochemical
DNAse I, RNAse-free	EN0521	Thermo Scientific
Endopan 3 complete medium	P04-0010K	PAN-Biotech
Fast SYBR Green Master Mix	43-856-12	Thermo Scientific
High-Capacity cDNA Reverse Transcription	4368814	Thermo Scientific
Maxima Reverse Transcriptase	EP0742	Thermo Scientific
NEB T4 DNA Ligase	M0202	NEB
Neural tissue dissociation	130-092-628	Milteny Biotec
NucleoSpin®Gel and PCR Clean-Up	740609.25	Machery-Nagel
PCR-CleanUp	A9281	Promega
Plasmid Plus MAXI Kit	12963	Qiagen
Rnaeasy® Mini kit	74104	Qiagen
RNAscope®Multiplex Fluorescent assay	320850	Advanced Cell Diagnostics
TaqMan Master-Mix	4369510	Thermo Scientific

6.1.5. Softwares

Table 6.5.: List of softwares used in this thesis.

Software	Source	Website
Fiji	NIH	https://fiji.sc/
Graphpad Pris 7.0 and 9.0	GraphPad Software, Inc	https://www.graphpad.com
iLastik 1.4.0rc8	Anna Kreshuk's lab (at EMBL)	https://www.ilastik.org
Illustrator	Adobe Systems Inc	https://www.adobe.com
Imaris	Oxford Instruments	https://imaris.oxinst.com
InDesign	Adobe Systems Inc	https://www.adobe.com
Photoshop	Adobe Systems Inc	https://www.adobe.com
R		https://www.r-project.org
StepOne™ and StepOnePlus™ Software v2.3	Thermo Scientific	https://www.thermofisher.com
StepOneTM Software v2.1	Applied Biosystems	www.thermofisher.com

ZEN blue	Zeiss	www.zeiss.com

6.1.6. Oligonucleotides

6.1.6.1. *ISH* Primers

Table 6.6.: List of primers for making ISH probes used in this thesis.

ISH primers	Forward 5' → 3'	Reverse 5' → 3'
Mouse *Chx10*	CGGTGTGGCGAGTTCTCT	AAGCTCTGGGTGAGGGCT
Mouse *En1*	ACACAACCCTGCGATCCTACT	CCAGCAAATAGAGATCGCTACAC
Mouse *Evx1/2*	TGTCACCTCTCTTCTCAGATGC	CTGGGTTAAGGGAGAAGAGGTT
Mouse *PlexinD1*	GTACCAACTGTCGAGTGCCA	TTCTCGAAGCGGTGGTCTTC
Mouse *Sema3C*	AGGTCAGAGGACCAGGTATTCA	GAGTGTTGTCCTTGGATTGTCA
Mouse *Sema3E*	CCACACGATCTACACCCGAG	CACAGCAGAGGCTGATCCAA
Mouse *Sim1*	TATACTGCCTTTGGGGAGAG	CTACCCGTACAACCTTTGTG

6.1.6.2. qRT-PCR Primers and TaqMan probes

Table 6.7.: List of primers and TaqMan probes for qRT-PCR used in this thesis.

qRT-PCR primers	Forward 5' → 3'	Reverse 5' → 3'
Human *Gapdh*	TGCCGTCTAGAAAAACCTGC	ACCCTGTTGCTGTAGCCAAA
Human *Nrp1*	CGCTCCCGCCTGAACTACCCT	TGAGGTGCGGGTGGAAGTGCC
Human *PlexinD1*	AACATCTCCAGCCAGAGCAG	CCAGGAAGACCGCTGTGTAG
Mouse *Gapdh*	GGTCCTCAGTGTAGCCCAAG	AATGTGTCCGTCGTGGATCT
Mouse *Lrg1*	CCATGTCAGTGTGCAGATTC	AAGAGTGAGAGGTGGAAGAG
TaqMan probes	**Gene name**	**Assay ID**
Mouse *Gapdh*	glyceraldehyde-3-phosphate dehydrogenase	Mm99999915_g1
Mouse *Lrg1*	leucine-rich alpha-2-glycoprotein 1	Mm01278767_m1

6.1.6.3. siRNAs

Table 6.8.: List of siRNAs used in this thesis.

siRNA	siRNA ID	Supplier
siRNA Universal control	SIC001	Merck/Sigma
siRNA against human *PlexinD1*	SASI_Hs01_00194034	Merck/Sigma
siRNA against human *Nrp1*	SASI_Hs02_00307190	Merck/Sigma

6.1.6.4. RNAscope probes

Table 6.9.: List of RNAscope probes used in this thesis.

RNAscope probes	Reference	Supplier
Mouse *Chat*	408731	ACD Bio-Techne
Mouse *Fos*	316921	ACD Bio-Techne
Mouse *Glra2*	510301	ACD Bio-Techne
Mouse *Mcam*	406321	ACD Bio-Techne
Mouse *Nrg1*	418181	ACD Bio-Techne
Mouse *Nrp1*	471621	ACD Bio-Techne
Mouse *Pappa*	443921	ACD Bio-Techne
Mouse *PlexinD1*	405931	ACD Bio-Techne
Mouse *Sema3C*	441441	ACD Bio-Techne
Mouse *Sema5a*	508091	ACD Bio-Techne
Mouse *Slc10a4*	544771	ACD Bio-Techne
Mouse *Slc18a3*	448771	ACD Bio-Techne
Mouse *Slc5a7*	439941	ACD Bio-Techne

6.1.7. Antibodies

6.1.7.1. Primary antibodies

Table 6.10.: List of primary antibodies used in this thesis.

Primary antibodies	Catalogue number	Supplier	Dilution	Method
Goat α-CD31	AF3628	R&D	1:250	IHC
Goat α-ChAT	Ab144P	Sigma	1:200	IHC
Guinea-pig α-VACht	139105	Synaptic Systems	1:200	IHC
Mouse α-Claudin-5	35-2500	Invitrogen	1:100	IHC
Mouse α-Isl1/2	39.4D5	DSHB	1:100	IHC
Mouse α-Neurofilament M (RMO 270)	13-0700	Thermo Scientific	1:300	IHC
Mouse α-Synaptophysin	SAB4200544	Sigma	1:200	IHC
Mouse α-VGAT	131011	Synaptic Systems	1:100	IHC
Rabbit α-Collagen IV	CO20451	Biozol	1:300	IHC

Rabbit α-FoxP1	Ab16645	Abcam	1:300	IHC
Rabbit α-HB9	N/A	(Thaler, Harrison et al. 1999)	1:8000	IHC
Rabbit α-Iba1	019-19741	Wako	1:300	IHC
Rabbit α-Lrg1	NBP1-82823	Novus	1:500	WB
Rabbit α-Neurofilament M	841001	Biolegend	1:300	IHC
Rabbit α-VACht	139103	Synaptic Systems	1:200	IHC
Rat α-CD13	Ab33489	Abcam	1:250	IHC

6.1.7.2. Secondary antibodies

Table 6.11.: List of secondary antibodies used in this thesis.

Secondary Antibodies	Catalogue number	Supplier	Dilution	Method
a-Bungarotoxin Alexa 594 Conjugated	B13423	Thermofisher	1:100	IHC
Alkaline phosphatase-coupled anti-DIG	11093274910	Roche Diagnostics	1:500 or 1:1500	ISH
Donkey a-goat Alexa 647	705-605-147	Jackson ImmunoResearch	1:500	IHC
Donkey a-guinea pig Alexa 488	706-546-148	Jackson ImmunoResearch	1:500	IHC
Donkey a-guinea pig Alexa 594	706-586-148	Jackson ImmunoResearch	1:500	IHC
Donkey a-mouse Alexa 488	715-545-150	Jackson ImmunoResearch	1:500	IHC
Donkey a-rabbit Alexa 488	A21206	Invitrogen	1:500	IHC
Donkey a-rabbit Alexa 568	A10042	Invitrogen	1:500	IHC
Isolectin GS-IB4 Alexa Fluor 568	I21412	Invitrogen	1:250	IHC
Isolectin GS-IB4 Alexa Fluor 647	I32450	Invitrogen	1:250	IHC
Peroxidase AffiniPure goat a-rabbit IgG (H+L)	111-035-144	Jackson Immuno Research	1:5000	WB

6.2. Methods

6.2.1. Animals

All experimental protocols, handling and care of mice were conducted in accordance with the local authorities and animal welfare officers (Germany, Baden-Württemberg, Regierungspräsidium Karlsruhe: animal projects approved under the licenses T38/19, I19/13, I21/02 and G3/19. UK: a project license to Prof. Christiana Ruhrberg was attributed by the United Kingdom Home Office and reviewed by the University College London Institute of Ophthalmology Animal Welfare and Review Body).

The following transgenic mouse lines were previously described and were used in this thesis: *PlexinD1* full KO (Gitler, Lu et al. 2004), *Tie2:Cre* (Kisanuki, Hammer et al. 2001), *PlexinD1 fl/fl* (Zhang, Singh et al. 2009), *Sema3E* full KO (Gu, Yoshida et al. 2005), *Olig2:Cre* (Dessaud, Yang et al. 2007), *Sema3C fl/fl* ((Plein, Calmont et al. 2015), *Cdh5:Cre* (Wang, Nakayama et al. 2010) and *Ctnnb1^{Ex3} fl/fl* (Harada, Tamai et al. 1999). The deletion of PlexinD1 from ECs was achieved by crossing *PlexinD1 fl/fl* mice with *PlexinD1 fl/+$^{Tie2:Cre}$* mice, resulting in the generation of the mouse line *PlexinD1 fl/fl$^{Tie2:Cre}$*. Deletion of Sema3C in MNs was accomplished by crossing *Sema3C fl/fl* mice with the *Olig2:Cre* line to generate *Sema3C fl/fl$^{Olig2:Cre}$* mice. To determine the embryonic stages, the morning of vaginal plug formation after mating was considered as E0.5. *PlexinD1* full KO, *PlexinD1 fl/fl$^{Tie2:Cre}$* and *Sema3E* full KO embryos were kindly provided by Prof. Dr. Christiana Ruhrberg, a collaborator of the study.

To remove Ctnnb1 from ECs in adult mice, *Ctnnb1^{Ex3} fl/fl* mice were crossed with *Cdh5:CreERT2* mice to generate *Ctnnb1 Ex3 fl/fl$^{Cdh5:CreERT2}$* (these mice were kindly provided by Prof. Dr. Stefan Liebner, Frankfurt). To induce deletion of the exon 3 of Ctnnb1 by CreERT2, intraperitoneal injections of tamoxifen (500 µg/mouse/day; Cayman #13258) prepared using corn oil (Sigma-Aldrich #C8267) were administered for 5 consecutive days starting at 8 weeks of age. Experiments involving this mouse line were performed after 3 weeks of the first tamoxifen injection. Animals were genotyped by conventional PCR.

Adult male or pregnant female C57BL/6N WT mice were purchased from Charles River Laboratories and Janvier Labs, respectively. Adult males were aged between 8 to 12 weeks old during all experiments. All animals were housed

under controlled humidity and on a 12h light-dark cycle, and had free access to food and water.

6.2.2. Complete Freund's Adjuvant (CFA) pain model

CFA injections were mainly administered by Dr. Christian Litke or Ann-Kristin (a former PhD student and a current master student in Prof. Dr. Daniela Mauceri's group, respectively) in a project collaboration. A smaller group of CFA injections were administered by me. The induction of the CFA inflammatory pain model was done by injecting subcutaneously 20 µl of CFA (Sigma Aldrich #F5881) into the plantar surface of both hind paws (Stosser, Agarwal et al. 2010). Control mice were similarly injected with 20 µl of 0.9% saline. During the intraplantar injections, animals were kept under isoflurane anesthesia.

6.2.3. Spared nerve injury (SNI) model

All the surgeries were performed by Dr. Manuela Simonetti, a collaborator of the project. Nerve or sham injuries were done as previously described (Simonetti, Hagenston et al. 2013). Mice were kept anesthetized under 1.5-2.5% isoflurane during procedure. After no reflexes were observed, an incision was made in the skin on the lateral surface of the thigh to expose the sciatic nerve and its branches. The common peroneal and tibial branches were ligated and a 1-2 mm distal portion of the nerve was cut, while the sural nerve branch was left intact. Sham animal underwent the same surgical procedure, but without the final nerve injury steps.

6.2.4. Intrathecal injections

Intrathecal injections were performed by a project collaborator, Dr. Manuela Simonetti, and were performed following previously published protocols (Njoo, Heinl et al. 2014). Anesthesia was initially induced by placing the mice under 3 % isoflurane (in O_2) until the mice presented no reflexes after pinching the tail or paw. Mice were then kept under continuous 1.5% isoflurane (in O_2) throughout the injection procedure. First, to visualize the spinal column, the lower back of the animals was shaved and wiped with 70 % EtOH. Then, the L6 vertebra was identified, and a previously prepared and loaded 0.3 ml insulin

syringe with a 30 G needle was gently inserted between the vertebrae L5 and L6, followed by slow injection of the solution. In most of the injections, a tail flick would be observed, indicating successful entry of the needle into the intradural space. Mice were then placed back in their cages and monitored until the end of the experiment. Intrathecal injections were used to deliver 0.8 µg of rLRG1 (13371-H02H) in 10 µl of 0.9% saline solution. As control, mice were injected with 10 µl of 0.9% saline solution.

6.2.5. Endothelial cell culture

Primary human brain microvascular endothelial cells (HBMECs) (ACBRI 376, Cell Systems) were cultured in 75 cm^3 flasks or 6-well plates (previously coated with 0.1% gelatin) in Endopan 3 complete medium for ECs (P04-0010K, PAN-Biotech) complemented with 10% FBS, 100 U ml^{-1} of penicillin and 100 µg ml^{-1} of streptomycin (15140122, ThermoFisher) in a 5% CO_2 humidified incubator at 37°C. For the experiments, HBMECs from passages 6 to 10 were used.

6.2.6. Histology

At the respective development stage (E11.5, E12.5, and E18.5), embryos were collected and fixed in 4% paraformaldehyde (PFA)/PBS (for the embryos used for ISH or RNAscope, PBS was DEPC-treated) at 4°C overnight. Afterwards, embryos were cryopreserved in 30% sucrose in PBS at 4°C until sinking, and then embedded in optimal cutting temperature (OCT) compound and stored at -20°C or -80°C until the day of sectioning. For experiments, 20- and 40 µm thick sections were made using a cryostate (MICROM HM560) and collected on SuperFrost Plus slides (Menzel-Glaeser, Braunschweig, Germany).

For the visualization of MN axons exiting the spinal cord, embryos were fixed in 4% PFA at 4°C overnight, and then kept in PBS until sectioning (no cryopreservation with 30% sucrose). Embryos were embedded in 3-5% low-melting agarose on the day of sectioning, and blocks were cut on a vibratome (VT1200S, Leica) to obtain 300 µm thick slices.

For immunohistochemistry experiments using adult mice, at the respective experimental timepoints, mice were euthanized with an overdose of Narcoren (300mg/kg, intraperitoneal injection). After loss of reflexes, mice were

transcardiac perfused with PBS and subsequently 4% PFA. Spinal cord lumbar L3-L5 levels were isolated and post-fixed in 4% PFA at 4° overnight. Afterwards, tissues were cryoprotected in 30% sucrose in PBS (DEPC-treated) at 4°C until sinking and embedded as mentioned for mouse embryos. Spinal cords were cut at 20 µm thickness using a cryostat (MICROM HM560 or C1950 from Leica) and collected on SuperFrost Plus slides (Menzel-Glaeser, Braunschweig, Germany).

6.2.7. Immunohistochemistry

Frozen sections were allowed to thaw at room temperature (RT) for 20 min before staining. Sections were washed with PBS, and blocked in 5% normal donkey serum in 0.3% Triton X-100/PBS (being permeabilized in simultaneously) for 1h. Afterwards, sections were incubated with primary antibodies in blocking buffer at 4°C overnight. The primary antibodies used can be found in table 6.1.7.1. The next day, sections were washed three times with PBS and further incubated with secondary antibodies (listed in table 6.1.7.2.) at RT for 2 h. Labeling of blood vessels using Isolectin GS-IB4 (I21412 and I32450, 1:250, Invitrogen) was done with secondary antibodies incubation. A similar protocol was used for the immunostaining of 300 µm thick sections, but with two alterations: sections were incubated with primary antibodies at 4°C for 72 h, and with secondary antibodies at 4°C for 24 h. For all sections, after secondary antibody incubations, sections were washed three times with PBS and mounted with fluoromount G (00-4958-02, Invitrogen). Images were acquired on a confocal microscope on a Nikon AR1 confocal microscope with x20/0.75 Plan-Fluor Objective and Zeiss LSM800 confocal microscope with x20/0.8 Plan-APOCHROMAT. For the 3D reconstructions, image processing was performed using IMARIS software (version 9.5.1).

6.2.8. *In situ* hybridization

The mRNA expression and localization of the target genes was performed by ISH using the following protocol: after thawing, sections were incubated with hybridization buffer at 68°C for 1h. Then, the hybridization step with digoxigenin (DIG)-labeled antisense riboprobes (sequence information of the primers used to generate the probes is available in Table 6.1.6.1.) was performed at 68°C

overnight. Digoxigenin (DIG) riboprobes were detected using an alkaline phosphatase-coupled anti-DIG antibody (1:500 for 2 h or 1:1500 overnight, Roche Diagnostics, Mannheim, Germany). The alkaline phosphatase reaction was performed with nitroblue tetrazolium/5-bromo-3-chloro-3-indolyl phosphate (NBT-BCIP, Promega) as a chromogenic substrate, resulting in a violet precipitate after some hours. Total incubation times varied between 14 h and 18 h, depending on the specific probe used. As a negative control, sections were incubated in parallel with sense probes that generate no specific signal. For the combination of ISH and immunofluorescence, the immunohistochemistry experimental protocol described in 6.2.7. for frozen sections was done after completion of the ISH protocol. Regular ISH or combined ISH and immunofluorescence were imaged using a Zeiss Axiovert 200 fluorescence microscope or a confocal microscope Zeiss LSM800.

6.2.9. RNAscope multiplex fluorescent assay

Detection of mRNA specific targets in embryonic spinal cord frozen sections was done using the RNAscope probes listed in table 6.1.6.4., which were all acquired from Advanced Cell Diagnostics. RNAscope without co-staining was performed following the manufacturer's instructions (Advanced Cell Diagnostics). For the RNAscope with co-staining for MN markers HB9, Isl1/2 and Foxp1, sections were initially blocked and stained with primary antibodies as mentioned in section 6.2.7, and post-fixed in 4% PFA. Afterwards, the RNAscope was proceeded with Protease III treatment, probe binding and signal amplification following the manufacturer's instructions (Advanced Cell Diagnostics). After the last RNAscope step, sections were washed, incubated with secondary antibodies (including blood vessel staining with Isolectin GS-IB4 Alexa Fluor 568 or 647 conjugate) at RT for 2 h and mounted with fluoromount-G (00-4958-02, Invitrogen). As negative control a RNAscope probe detecting *dapb* (bacterial gene) was used, and as positive control I used the 3-Plex-positive control RNAscope probe targeting *Polr2a*, *Ppib* and *Ubc* (both provided by the manufacturer). Image acquisition was done using a Zeiss LSM800 confocal microscope with x20/0.8 Plan-APOCHROMAT and 40x/1.30 C Plan-APOCHROMAT objectives. The number of mRNA transcripts detected in $HB9^{+}$ nuclei were counted manually.

6.2.10. Immunoblot analysis

Lrg1 expression at the protein level was analyzed by Western Blot. Adult mice were initially anesthetized using Narcoren (300mg/kg, intraperitoneal injection) until the loss of any tail or paw reflexes. Afterwards, the lower part of the abdomen was cleaned with 70 % EtOH and the abdomen was opened by a longitudinal incision. The inferior vena cava was exposed and punctured to collect blood into eppendorfs filled with 40 µl of EDTA to obtain plasma. Blood samples were centrifuged at 3000 rpm at 4°C for 15 min, and the supernatant was transferred into a new tube and frozen at -80°C until further use. The concentration of the protein samples was determined using a colorimetric assay based on the Braford method (5000006, Bio-Rad), with BSA used as standard. 30 µg of plasma were mixed with 4x Laemmli sample buffer (160 mM Tris HCl pH 6.8, 4% SDS, 30% glycerol, 0.02% bromophenol blue) and 1% dithiothreitol, and heated at 95°C for 10. For SDS-PAGE, samples were loaded on 3.75% acrylamide stacking gel and a 10% acrylamide resolving gel. Gel electrophoresis was performed at constant amperage (35 mA per running gel) in running buffer (10 mM glycine, 2.5 mM Tris, 0.01% SDS). Proteins were then transferred onto a nitrocellulose membrane (Amersham™ 0.45 µm, GE Healthcare) at constant voltage of 18V for 2 h in transfer buffer (15 mM glycine, 2mM Tris, 0.01 % SDS, 20 % methanol). Membrane was stained with Ponceau S solution (33427.01, SERVA) to verify successful transfer, and blocked in 5% milk powder in PBST (0.1 % Tween 20 in 1x PBS) at RT for 1 h. Primary antibody incubation (listed in section 6.1.7.2.) was performed at 4°C overnight. The next day, membranes were washed with three 10 min washes with PBST, and incubated with HRP-conjugated secondary antibody at RT for 1 h. Then, membranes were washed again three times with PBST and blots were developed using Clarity™ Western ECL substrate (#170-5061, Bio-Rad). Detection was done using the Chemidoc™ Imaging System (Bio-Rad). Quantification of relative protein band density was done using ImageJ.

6.2.11. siRNA transfection

To knockdown specific targets, HBMECs were transfected with siRNA Universal control (SIC001, Sigma), siRNA against human *PlexinD1* (siRNA ID: SASI_Hs01_00194034, Sigma) or siRNA against human *Nrp1* (siRNA ID:

SASI_Hs02_00307190, Sigma). Transfection of HBMECs (12×10^4 cells) in 6-well plates (657-160, Greiner Cell Star) with siRNA (with a final concentration of 200 nM) was performed with Oligofectamine according to the manufacturer's transfection protocol (12252011, ThermoFisher). First, HBMECs were transfected with siRNAs Opti-MEM reduced serum medium (51985034, ThermoFisher) for 4 h. Then, cells were washed with PBS and cultured in Endopan 3 complete medium for 24 h. At this point, cells were used either in the tube-touching assay experiments or collected using RLT buffer (74104, Qiagen) for total RNA extraction to confirm successful knockdown of *PlexinD1* or *Nrp1.* siRNA Universal control was used to exclude non-specific effects related to the transfection.

6.2.12. Spinal cord MN explant dissection

MN explants from embryonic spinal cords were generated as previously described (Himmels, Paredes et al. 2017). Spinal cords from E11.5 embryos were dissected via open-book preparation (Langlois, Morin et al. 2010) on L15 medium (L5520, Sigma) supplemented with 5% horse serum, 50 U ml^{-1} of penicillin and 50 µg ml^{-1} of streptomycin. Spinal cords were flattened and the visible MN columns were isolated and cut in approximately 1 cm explants under a stereomicroscope. As the explants generated might contain also neural progenitors, due to the experimental procedure followed to dissect and prepare these explants, in the experiments using explants from BL6 WT embryos (co-cultured with HBMECs-PlexinD1-KD or HBMECs-Nrp1-KD and respective controls), explants originating from the same embryo and dissection were used in both the KD and Ctrl conditions.

6.2.13. Muscle innervation immunohistochemistry

Mouse embryos were collected at E18.5 and fixed in 4% PFA at 4°C overnight. Then, muscles were dissected, washed in PBS for 30 min and blocked in 10% normal donkey serum at 4°C overnight. Afterwards, muscles were incubated with primary antibodies (listed in section 6.1.7.1.) diluted in blocking buffer at 4°C for 72h. Tissue was washed three times for 30 mins, and incubated with secondary antibodies (listed in section 6.1.7.2.), including blood vessel

staining using Isolectin GS-IB4 Alexa Fluor 647 conjugate at 4°C overnight. Tissues were then washed three times for 30 mins, mounted with fluoromount G (00-4958-02, Invitrogen), and imaged using a confocal Zeiss LSM800 with x20/0.8 Plan-APOCHROMAT and 40x/1.30C Plan-APOCHROMAT objectives.

6.2.14. DiI tracing

E18.5 mouse embryos were dissected, fixed in 4% PFA at 4°C overnight, and the spinal cord dissected and washed in PBS. Afterwards, I handled the spinal cords to Dr. Sebástian Dupraz, a senior scientist in my lab, who did the DiI tracing experiments. 100 μl drops of Neuro-DiI (60016, Biotium)-ethanol solutions were added on a slide grass and allowed to evaporate in order to form a thin layer of DiI crystals. These crystals were then scratch-collected using tungsten needles (10130-20, FST) and inserted into DRGs to be incorporated by sensorial neurons and label the afferent projections into the spinal cord. In simultaneous, ventral roots were cut to avoid leakage of DiI labeling into ventral MN columns. Tissue was then incubated in 4% PFA at 37°C for seven days. Afterwards, spinal cords were cryopreserved in 30% sucrose in PBS at 4°C overnight, and 50 μm cryosections were made. Images were acquired using a CellDiscoverer 7 (combined with Zeiss LSM900) with x20/095 Plan-APOCHROMAT objective.

6.2.15. Tube-touching assay

Tube-touching assays were performed in μ-Slide Angiogenesis wells (81506, ibidi GmbH). 10 μl of Corning Matrigel matrix (356234, Corning) were added per well and allowed to polymerize at 37°C for 30-45 min. 50 μl of HBMECs suspension (in HBMECs starving medium (HBMECs culture medium without VEGF, FGF-2 and FBS) containing $1x10^4$ cells and MN explants was added to each well (each suspension contained approximately 3–4 explants). Cells together with the explants were incubated in a humidified chamber at 37°C, 5% CO2 for 16-18 h. Acquisition of images was done using a microscope Zeiss Axiovert 200 M with 5x/0,16 EC Plan-NEOFLUAR Objective. The tubes touching the explant were counted manually and I was blinded to the experimental conditions during quantification.

6.2.16. Gene expression analysis – qRT-PCR

RNA from HBMECs (ACBRI 376, Cell Systems) was extracted using the RNeasy Mini Kit (74104, Qiagen). RNA was treated with DNase I (EN0521, Thermo Scientific) and afterwards reverse transcribed into cDNA using SuperScript IV Vilo (11756-050, Thermo Scientific) following the manufacturer's protocol. mRNA expression levels were assessed by qRT-PCR using Fast SYBR Green Master Mix (00408995, Thermo Scientific), relative to the expression level of the housekeeping gene *Gapdh.*

Liver, hippocampus, cortex, and dorsal part of L3-L5 spinal cord levels were harvested, frozen in liquid nitrogen and stored at -80°C until further use. Total RNA from these mouse tissues was extracted using the RNeasy Mini Kit including the optional DNAse in-column step (#79254, Quiagen) accordingly to manufacturer's instructions. Extracted RNA was then reverse transcribed into cDNA using the High-Capacity cDNA Reverse Transcription Kit (#4368814, Applied Biosystems). Quantitative reverse transcriptase PCR was performed on a StepOne plus real-time PCR system using TaqMan® gene expression assays (#4369016, Applied Biosystems). Expression of target genes was normalized to the endogenous control gene *Gapdh*.

Due to the low amount of cells obtained, the extraction of RNA from the different cell fractions obtained by MACS was done using the Arcturus™ PicoPure RNA isolation kit (12204-01, Applied Bioscience), following the manufacturers' protocol. The extracted RNA was then processed and converted to cDNA as mentioned for HBMECs-derived RNA.

The list of qRT-PCR primers and probes used in this work are described in Table 6.1.6.2.

6.2.17. Magnetic cell separation (MACS) and cell isolation

Freshly collected L3-L5 dorsal spinal cord tissues were collected from mice injected either with saline of CFA. Tissue was chopped in smaller pieces, dissociated, and digested following the neural tissue dissociation kit protocol (130-092-628, Milteny Biotec). Digestion of tissue was done using Collagenase/Dispase (10269638001, Sigma-Aldrich) and DNase I (LS002139, Worthington Biochemical) with final concentrations of 3 mg/ml and 0.25 mg/ml, respectively. The homogenate solution was passed through a 70 μm cell strainer

and washed several times with 2% FBS in 1x PBS. After dissociation, a myelin removal step was performed using the myelin removal beads II (130-096-733, Milteny Biotec) following the manufacturers' protocol. Isolation of the different cell fractions was performed following the step 'Isolation of endothelial cells' of the protocol 'Isolation and cultivation of endothelial cells from adult mouse brain' available from Milteny Biotec. $CD45^+$ immune cells were isolated by incubating the single cell solution with CD45 Microbeads (130-052-301, Milteny Biotec) in 2% FBS/PBS at 4°C for 15min and then applied on separation columns. The CD45 positive cell fraction was collected and frozen (this cell fraction contains only immune cells), while the flowthrough containing $CD45^-$ cells was collected, incubated with $CD31^+$ Microbeads (130-097-418. Milteny Biotec) in 2% FBS/PBS at 4°C for 15min, and then applied on separation columns. Here, the positive fraction containing only ECs ($CD31^+CD45^-$ fraction) and the flowthrough containing mainly neuronal/glia unlabeled cells ($CD31^-CD45^-$ fraction) were collected and frozen until the day of RNA extraction.

6.2.18. In vivo tracer permeability

At the respective timepoint of interest, 120 μl of 10 mg/ml solution of sodium fluorescein (F6377, Sigma-Aldrich) were injected intravenously into the tail vein and allowed to circulate for 30 min. Afterwards, animals were injected with an overdose of Narcoren (300mg/kg, intraperitoneal injection). After loss of reflexes, 300 μl of blood were collected into an eppendorf tube containing 40 μl of EDTA and thereafter, mice were perfused for 2 min (at 5 ml/min) with PBS. The different regions of the spinal cord were then isolated, weighted, and homogenized in 100 μl PBS. In parallel, blood was centrifuged at 15000 *g* at 4°C for 5 min, and supernatant (plasma) was collected. Homogenized spinal cord samples were then centrifuged at 10000 *g* at 4°C for 15 min. Spinal cord supernatants and plasma (at a dilution of 1:100 or 1:1000) were then loaded on a 96-well plate (655209, Greiner Bio-one) and fluorescence emissions (relative fluorescence units (RFU)) were measured in a microplate reader (Rosys Anthos 2001, Anthos Mikrosysteme Gmbh; CLARIOstar Plus, BMG LABTECH) at excitation/emission of 460/515 nm. Non-injected sham animals were used in

parallel to subtract tissue and plasma auto-fluorescence values. Permeability index was calculated as (Tissue RFU/Tissue weight)/(Plasma RFUs).

6.2.19. Quantification of blood vessel density and ingression angles

For the quantification of spinal cord vascularization, sections from brachial and thoracic levels were used for all lines except for Sema3E WT and KO embryos, where only the brachial level was considered as Sema3E is only expressed at this spinal cord level. Total spinal cord vascularization was calculated as the covered IsoB4 staining area per spinal cord area (excluding the FP, which is also labeled by IsoB4, and the central ventricle). Similarly, MN column vascularization was calculated as the percentage of MN column (labeled by Isl1/2^{+} staining) area covered by IsoB4 staining. All above quantifications were performed using the NIH ImageJ software. Blood vessel ingression into the ventral spinal cord was analyzed as previously described (James, Gewolb et al. 2009), considering the FP as the reference 0°. The angle of blood vessels ingressing was measured using the *Angle Tool* of NIH ImageJ software. Quantification of vessel length in MN columns was done using the software "Angiotool" (Zudaire, Gambardella et al. 2011)

6.2.20. Analysis of MEP position, quantification of thickness of MN axon bundle at MEP and measure of ventral root diameter

MEPs positioning in the ventral spinal cord was determined by quantifying the distance from the ventral midline (at the FP position) to the most ventral axon bundle (labeled with neurofilament M) at MEPs. Similarly, the average position of MEP was calculated by measuring the distance from the ventral midline to the average middle position of the motor neuron axon bundle. To exclude variations in the embryos size, the distances were divided by the respective embryo height (calculated as the distance between dorsal and ventral midlines) (Kim, Fontelonga et al. 2017). MN axon bundles thickness was quantified at MEP by measuring the distance between the most ventral and most dorsal axon bundle leaving the spinal cord in 300 µm vibratome sections. Similarly, ventral root diameter was measured at a distance of 30 µm from the MEP in 300 µm vibratome sections. Quantifications were done using NIH ImageJ software.

Maximum intensity projections were created only from confocal z-stacks containing the entire ventral root.

6.2.21. Analysis of MN number, soma size, synaptic input density and synaptic input puncta

At E18.5, MNs were identified by staining for the MN-specific transcript factor HB9. The total number of MNs ($HB9^+$ cells) located in the ventral spinal cord were manually. MN soma size was quantified by measuring the area of $HB9^+/ChAT^+$ cells. Total area occupied by input synapses (synaptic density) was quantified by measuring the $VAChT^+$ or $VGAT^+$ staining area overlapping with $HB9^+/ChAT^+$ MNs. Synaptic density was then normalized for the respective MN soma area. All quantifications were performed using NIH ImageJ software.

6.2.22. *In Silico* analysis

These bioinformatic analysis were done with the support of Dr. Géza Schermann, a bioinformatician in the lab, who introduced me to the bioinformatic field and was always available to check my R code workflows in case I needed during my analysis.

For the embryonic *in silico* analysis, publicly available scRNAseq data from the embryonic spinal cord (Delile, Rayon et al. 2019) were downloaded from ArrayExpress (accession number E-MTAB-7320) and analyzed using R (version 4.0.2; http://www.R-project.org/). The bioinformatic analysis were done as follows: first, the selection of ECs was performed by extracting the cluster classified as ‘Blood’ and identify the cells within this cluster expressing the commonly accepted EC markers *Cdh5, Kdr* and *Pecam1*. Ventral neural cells were already identified in the dataset and thus directly extracted. The prediction of cell-cell interactions occurring between ventral neural cells and ECs was performed using the R toolkit CellChat (Jin, Guerrero-Juarez et al. 2021). The interactome prediction was performed using the original pipeline published by the CellChat authors (Jin, Guerrero-Juarez et al. 2021) (github.com/sqjin/CellChat) with minor changes: computation of the communication probability was done using the method type “truncatedMean” with “trim = 0.07”, as the previously described Vegf-Kdr interaction in developing motor neurons was not predicted

using the original default method (Himmels, Paredes et al. 2017). Plots for *Sema3C*, *PlexinD1* and *Nrp1* expression were done using the original pipeline described in Delile et al. (Delile, Rayon et al. 2019), with the minor change that no threshold was applied to the minimum number of cells needed to express the genes.

For the adult *in silico* analysis, publicly available bulk-RNAseq data from spinal cords derived from mice injected with saline or CFA (with additional intraspinal delivery of expressing construct for LacZ) (Litke, Hagenston et al. 2022) were downloaded from Gene Expression Omnibus (GEO) (accession number GSE159895) and analyzed using R. To see which cells expressed the significant genes obtained in the comparison saline vs CFA, previously published scRNAseq data from the adult spinal cord (Sathyamurthy, Johnson et al. 2018) were downloaded from GEO (GSE103892) and used to plot the expression of significant altered genes in each cell type in baseline conditions. For the pseudobulk comparisons for the different cell types derived from non-injured or SCI mice (Matson, Russ et al. 2022), the available scRNAseq dataset was download from GEO (GSE172167). Then, cells from the same cell type were pseudobulked and differential gene expression analysis between treatments was performed using the R package DESeq2 (Love, Huber et al. 2014). PCA plots were done using transformed data (using the variance stabilizing transformation).

6.2.23. Statistical analysis

All results in this thesis were plotted as the mean for each group, and respective error bars represent means ± standard deviation. For each embryonic experiment at least two independent experiments (or independent litters) were analyzed. Sample sizes for each experiment are provided in the respective figure legends. Statistical significances between two groups were calculated using parametric two tailed unpaired Student's t-test, while multiple comparisons between three or more groups were performed using One-way analysis of variance (ANOVA) followed by Sidak's multiple comparisons test correction. Outliers were detected using the Outlier calculator (GraphPad Prism, version 7.0 and version 9.0) with an Alpha=0.05 significance level. Statistically significant results are indicated in the figures using *P < 0.05, **P < 0.01 ***P < 0.001 and ****P < 0.0001 and respective figure legends. Analyses were performed blinded

to the experimental conditions for all the experiments. The statistical analysis were performed using GraphPad Prism (version 7.0 and version 9.0).

7. REFERENCES

Abbadie, C., J. A. Lindia, A. M. Cumiskey, L. B. Peterson, J. S. Mudgett, E. K. Bayne, J. A. DeMartino, D. E. MacIntyre and M. J. Forrest (2003). "Impaired neuropathic pain responses in mice lacking the chemokine receptor CCR2." Proc Natl Acad Sci U S A **100**(13): 7947-7952.

Abbott, N. J., A. A. Patabendige, D. E. Dolman, S. R. Yusof and D. J. Begley (2010). "Structure and function of the blood-brain barrier." Neurobiol Dis **37**(1): 13-25.

Abraira, V. E. and D. D. Ginty (2013). "The sensory neurons of touch." Neuron **79**(4): 618-639.

Abraira, V. E., E. D. Kuehn, A. M. Chirila, M. W. Springel, A. A. Toliver, A. L. Zimmerman, L. L. Orefice, K. A. Boyle, L. Bai, B. J. Song, K. A. Bashista, T. G. O'Neill, J. Zhuo, C. Tsan, J. Hoynoski, M. Rutlin, L. Kus, V. Niederkofler, M. Watanabe, S. M. Dymecki, S. B. Nelson, N. Heintz, D. I. Hughes and D. D. Ginty (2017). "The Cellular and Synaptic Architecture of the Mechanosensory Dorsal Horn." Cell **168**(1-2): 295-310 e219.

Acevedo, L. M., S. Barillas, S. M. Weis, J. R. Gothert and D. A. Cheresh (2008). "Semaphorin 3A suppresses VEGF-mediated angiogenesis yet acts as a vascular permeability factor." Blood **111**(5): 2674-2680.

Adair, T. H. and J. P. Montani (2010). Angiogenesis. San Rafael (CA).

Adams, R. H., M. Lohrum, A. Klostermann, H. Betz and A. W. Puschel (1997). "The chemorepulsive activity of secreted semaphorins is regulated by furin-dependent proteolytic processing." EMBO J **16**(20): 6077-6086.

Agrud, A., S. Subburaju, P. Goel, J. Ren, A. S. Kumar, B. J. Caldarone, W. Dai, J. Chavez, D. Fukumura, R. K. Jain, R. A. Kloner and A. Vasudevan (2022). "Gabrb3 endothelial cell-specific knockout mice display abnormal blood flow, hypertension, and behavioral dysfunction." Sci Rep **12**(1): 4922.

Altmann, C. R. and A. H. Brivanlou (2001). "Neural patterning in the vertebrate embryo." Int Rev Cytol **203**: 447-482.

Alto, L. T. and J. R. Terman (2017). "Semaphorins and their Signaling Mechanisms." Methods Mol Biol **1493**: 1-25.

Ambler, C. A., J. L. Nowicki, A. C. Burke and V. L. Bautch (2001). "Assembly of trunk and limb blood vessels involves extensive migration and vasculogenesis of somite-derived angioblasts." Dev Biol **234**(2): 352-364.

Amersfoort, J., G. Eelen and P. Carmeliet (2022). "Immunomodulation by endothelial cells - partnering up with the immune system?" Nat Rev Immunol **22**(9): 576-588.

Ando-Akatsuka, Y., M. Saitou, T. Hirase, M. Kishi, A. Sakakibara, M. Itoh, S. Yonemura, M. Furuse and S. Tsukita (1996). "Interspecies diversity of the occludin sequence: cDNA cloning of human, mouse, dog, and rat-kangaroo homologues." J Cell Biol **133**(1): 43-47.

Arber, S. (2012). "Motor circuits in action: specification, connectivity, and function." Neuron **74**(6): 975-989.

Argaw, A. T., B. T. Gurfein, Y. Zhang, A. Zameer and G. R. John (2009). "VEGF-mediated disruption of endothelial CLN-5 promotes blood-brain barrier breakdown." Proc Natl Acad Sci U S A **106**(6): 1977-1982.

Armulik, A., G. Genove, M. Mae, M. H. Nisancioglu, E. Wallgard, C. Niaudet, L. He, J. Norlin, P. Lindblom, K. Strittmatter, B. R. Johansson and C. Betsholtz (2010). "Pericytes regulate the blood-brain barrier." Nature **468**(7323): 557-561.

Attwell, D., A. M. Buchan, S. Charpak, M. Lauritzen, B. A. Macvicar and E. A. Newman (2010). "Glial and neuronal control of brain blood flow." Nature **468**(7321): 232-243.

Austin, P. J., C. F. Kim, C. J. Perera and G. Moalem-Taylor (2012). "Regulatory T cells attenuate neuropathic pain following peripheral nerve injury and experimental autoimmune neuritis." Pain **153**(9): 1916-1931.

Bahramsoltani, M., I. Slosarek, W. De Spiegelaere and J. Plendl (2014). "Angiogenesis and collagen type IV expression in different endothelial cell culture systems." Anat Histol Embryol **43**(2): 103-115.

Balda, M. S., J. A. Whitney, C. Flores, S. Gonzalez, M. Cereijido and K. Matter (1996). "Functional dissociation of paracellular permeability and transepithelial electrical resistance and disruption of the apical-basolateral intramembrane diffusion barrier by expression of a mutant tight junction membrane protein." J Cell Biol **134**(4): 1031-1049.

Bartanusz, V., D. Jezova, B. Alajajian and M. Digicaylioglu (2011). "The blood-spinal cord barrier: morphology and clinical implications." Ann Neurol **70**(2): 194-206.

Basbaum, A. I., D. M. Bautista, G. Scherrer and D. Julius (2009). "Cellular and molecular mechanisms of pain." Cell **139**(2): 267-284.

Beggs, S., X. J. Liu, C. Kwan and M. W. Salter (2010). "Peripheral nerve injury and TRPV1-expressing primary afferent C-fibers cause opening of the blood-brain barrier." Mol Pain **6**: 74.

Bellettato, C. M. and M. Scarpa (2018). "Possible strategies to cross the blood-brain barrier." Ital J Pediatr **44**(Suppl 2): 131.

Benz, F., V. Wichitnaowarat, M. Lehmann, R. F. Germano, D. Mihova, J. Macas, R. H. Adams, M. M. Taketo, K. H. Plate, S. Guerit, B. Vanhollebeke and S. Liebner (2019). "Low wnt/beta-catenin signaling determines leaky vessels in the subfornical organ and affects water homeostasis in mice." Elife **8**.

Bergers, G. and S. Song (2005). "The role of pericytes in blood-vessel formation and maintenance." Neuro Oncol **7**(4): 452-464.

Bernacki, J., A. Dobrowolska, K. Nierwinska and A. Malecki (2008). "Physiology and pharmacological role of the blood-brain barrier." Pharmacol Rep **60**(5): 600-622.

Berzin, T. M., B. D. Zipser, M. S. Rafii, V. Kuo-Leblanc, G. D. Yancopoulos, D. J. Glass, J. R. Fallon and E. G. Stopa (2000). "Agrin and microvascular damage in Alzheimer's disease." Neurobiol Aging **21**(2): 349-355.

Bisht, K., K. A. Okojie, K. Sharma, D. H. Lentferink, Y. Y. Sun, H. R. Chen, J. O. Uweru, S. Amancherla, Z. Calcuttawala, A. B. Campos-Salazar, B. Corliss, L. Jabbour, J. Benderoth, B. Friestad, W. A. Mills, 3rd, B. E. Isakson, M. E. Tremblay, C. Y. Kuan and U. B. Eyo (2021). "Capillary-associated microglia regulate vascular structure and function through PANX1-P2RY12 coupling in mice." Nat Commun **12**(1): 5289.

Blanco, R. and H. Gerhardt (2013). "VEGF and Notch in tip and stalk cell selection." Cold Spring Harb Perspect Med **3**(1): a006569.

Blusztajn, J. K. and R. J. Wurtman (1983). "Choline and cholinergic neurons." Science **221**(4611): 614-620.

Bonanno, E., M. Iurlaro, J. A. Madri and R. F. Nicosia (2000). "Type IV collagen modulates angiogenesis and neovessel survival in the rat aorta model." In Vitro Cell Dev Biol Anim **36**(5): 336-340.

Bonanomi, D. and S. L. Pfaff (2010). "Motor axon pathfinding." Cold Spring Harb Perspect Biol **2**(3): a001735.

Bonanomi, D., F. Valenza, O. Chivatakarn, M. J. Sternfeld, S. P. Driscoll, A. Aslanian, K. Lettieri, M. Gullo, A. Badaloni, J. W. Lewcock, T. Hunter and S. L. Pfaff (2019). "p190RhoGAP Filters Competing Signals to Resolve Axon Guidance Conflicts." Neuron **102**(3): 602-620 e609.

Boye, K., L. H. Geraldo, J. Furtado, L. Pibouin-Fragner, M. Poulet, D. Kim, B. Nelson, Y. Xu, L. Jacob, N. Maissa, D. Agalliu, L. Claesson-Welsh, S. L. Ackerman and A. Eichmann (2022). "Endothelial Unc5B controls blood-brain barrier integrity." Nat Commun **13**(1): 1169.

Braet, K., K. Paemeleire, K. D'Herde, M. J. Sanderson and L. Leybaert (2001). "Astrocyte-endothelial cell calcium signals conveyed by two signalling pathways." Eur J Neurosci **13**(1): 79-91.

Brandon, E. P., W. Lin, K. A. D'Amour, D. P. Pizzo, B. Dominguez, Y. Sugiura, S. Thode, C. P. Ko, L. J. Thal, F. H. Gage and K. F. Lee (2003). "Aberrant patterning of neuromuscular synapses in choline acetyltransferase-deficient mice." J Neurosci **23**(2): 539-549.

Briscoe, J. and J. Ericson (2001). "Specification of neuronal fates in the ventral neural tube." Curr Opin Neurobiol **11**(1): 43-49.

Briscoe, J., A. Pierani, T. M. Jessell and J. Ericson (2000). "A homeodomain protein code specifies progenitor cell identity and neuronal fate in the ventral neural tube." Cell **101**(4): 435-445.

Burri, P. H. and M. R. Tarek (1990). "A novel mechanism of capillary growth in the rat pulmonary microcirculation." Anat Rec **228**(1): 35-45.

Cahill, L. S., C. L. Laliberte, X. J. Liu, J. Bishop, B. J. Nieman, J. S. Mogil, R. E. Sorge, C. D. Jones, M. W. Salter and R. M. Henkelman (2014). "Quantifying blood-spinal cord barrier permeability after peripheral nerve injury in the living mouse." Mol Pain **10**: 60.

Camilli, C., A. E. Hoeh, G. De Rossi, S. E. Moss and J. Greenwood (2022). "LRG1: an emerging player in disease pathogenesis." J Biomed Sci **29**(1): 6.

Candlish, M. and J. K. Hefendehl (2021). "Microglia Phenotypes Converge in Aging and Neurodegenerative Disease." Front Neurol **12**: 660720.

Cao, H. and Y. Q. Zhang (2008). "Spinal glial activation contributes to pathological pain states." Neurosci Biobehav Rev **32**(5): 972-983.

Cao, L. and J. A. DeLeo (2008). "CNS-infiltrating CD4+ T lymphocytes contribute to murine spinal nerve transection-induced neuropathic pain." Eur J Immunol **38**(2): 448-458.

Carmeliet, P., V. Ferreira, G. Breier, S. Pollefeyt, L. Kieckens, M. Gertsenstein, M. Fahrig, A. Vandenhoeck, K. Harpal, C. Eberhardt, C. Declercq, J. Pawling, L. Moons, D. Collen, W. Risau and A. Nagy (1996). "Abnormal blood vessel development and lethality in embryos lacking a single VEGF allele." Nature **380**(6573): 435-439.

Carmeliet, P. and M. Tessier-Lavigne (2005). "Common mechanisms of nerve and blood vessel wiring." Nature **436**(7048): 193-200.

Catela, C., Y. Chen, Y. Weng, K. Wen and P. Kratsios (2022). "Control of spinal motor neuron terminal differentiation through sustained Hoxc8 gene activity." Elife **11**.

Chizhikov, V. V. and K. J. Millen (2005). "Roof plate-dependent patterning of the vertebrate dorsal central nervous system." Dev Biol **277**(2): 287-295.

Cho, C., P. M. Smallwood and J. Nathans (2017). "Reck and Gpr124 Are Essential Receptor Cofactors for Wnt7a/Wnt7b-Specific Signaling in Mammalian CNS Angiogenesis and Blood-Brain Barrier Regulation." Neuron **95**(5): 1221-1225.

Choi, Y. K. and A. Vasudevan (2019). "Mechanistic insights into autocrine and paracrine roles of endothelial GABA signaling in the embryonic forebrain." Sci Rep **9**(1): 16256.

Chu, N. S. (2006). "[Centennial of the nobel prize for Golgi and Cajal--founding of modern neuroscience and irony of discovery]." Acta Neurol Taiwan **15**(3): 217-222.

Clark, A. K., C. Gentry, E. J. Bradbury, S. B. McMahon and M. Malcangio (2007). "Role of spinal microglia in rat models of peripheral nerve injury and inflammation." Eur J Pain **11**(2): 223-230.

Clark, A. K., A. A. Staniland, F. Marchand, T. K. Kaan, S. B. McMahon and M. Malcangio (2010). "P2X7-dependent release of interleukin-1beta and nociception in the spinal cord following lipopolysaccharide." J Neurosci **30**(2): 573-582.

Cohen, S., L. Funkelstein, J. Livet, G. Rougon, C. E. Henderson, V. Castellani and F. Mann (2005). "A semaphorin code defines subpopulations of spinal motor neurons during mouse development." Eur J Neurosci **21**(7): 1767-1776.

Corada, M., M. Mariotti, G. Thurston, K. Smith, R. Kunkel, M. Brockhaus, M. G. Lampugnani, I. Martin-Padura, A. Stoppacciaro, L. Ruco, D. M. McDonald, P. A. Ward and E. Dejana (1999). "Vascular endothelial-cadherin is an important determinant of microvascular integrity in vivo." Proc Natl Acad Sci U S A **96**(17): 9815-9820.

Costigan, M., A. Moss, A. Latremoliere, C. Johnston, M. Verma-Gandhu, T. A. Herbert, L. Barrett, G. J. Brenner, D. Vardeh, C. J. Woolf and M. Fitzgerald (2009). "T-cell infiltration and signaling in the adult dorsal spinal cord is a major contributor to neuropathic pain-like hypersensitivity." J Neurosci **29**(46): 14415-14422.

Cox, C. M. and T. J. Poole (2000). "Angioblast differentiation is influenced by the local environment: FGF-2 induces angioblasts and patterns vessel formation in the quail embryo." Dev Dyn **218**(2): 371-382.

Csaszar, E., N. Lenart, C. Cserep, Z. Kornyei, R. Fekete, B. Posfai, D. Balazsfi, B. Hangya, A. D. Schwarcz, E. Szabadits, D. Szollosi, K. Szigeti, D. Mathe, B. L. West, K. Sviatko, A. R. Bras, J. C. Mariani, A. Kliewer, Z. Lenkei, L. Hricisak, Z. Benyo, M. Baranyi, B. Sperlagh, A. Menyhart, E. Farkas and A. Denes (2022). "Microglia modulate blood flow, neurovascular coupling, and hypoperfusion via purinergic actions." J Exp Med **219**(3).

Daneman, R., D. Agalliu, L. Zhou, F. Kuhnert, C. J. Kuo and B. A. Barres (2009). "Wnt/beta-catenin signaling is required for CNS, but not non-CNS, angiogenesis." Proc Natl Acad Sci U S A **106**(2): 641-646.

Daneman, R. and A. Prat (2015). "The blood-brain barrier." Cold Spring Harb Perspect Biol **7**(1): a020412.

Daneman, R., L. Zhou, A. A. Kebede and B. A. Barres (2010). "Pericytes are required for blood-brain barrier integrity during embryogenesis." Nature **468**(7323): 562-566.

Dasen, J. S. and T. M. Jessell (2009). "Hox networks and the origins of motor neuron diversity." Curr Top Dev Biol **88**: 169-200.

Dasen, J. S., J. P. Liu and T. M. Jessell (2003). "Motor neuron columnar fate imposed by sequential phases of Hox-c activity." Nature **425**(6961): 926-933.

Dejana, E. (2010). "The role of wnt signaling in physiological and pathological angiogenesis." Circ Res **107**(8): 943-952.

Delile, J., T. Rayon, M. Melchionda, A. Edwards, J. Briscoe and A. Sagner (2019). "Single cell transcriptomics reveals spatial and temporal dynamics of gene expression in the developing mouse spinal cord." Development **146**(12).

Demir, R., U. A. Kayisli, S. Cayli and B. Huppertz (2006). "Sequential steps during vasculogenesis and angiogenesis in the very early human placenta." Placenta **27**(6-7): 535-539.

Dessaud, E., A. P. McMahon and J. Briscoe (2008). "Pattern formation in the vertebrate neural tube: a sonic hedgehog morphogen-regulated transcriptional network." Development **135**(15): 2489-2503.

Dessaud, E., L. L. Yang, K. Hill, B. Cox, F. Ulloa, A. Ribeiro, A. Mynett, B. G. Novitch and J. Briscoe (2007). "Interpretation of the sonic hedgehog morphogen gradient by a temporal adaptation mechanism." Nature **450**(7170): 717-720.

Dickenson, A. H., J.-M. R. Besson and I. Appleton (1997). The pharmacology of pain. Berlin ; New York, Springer.

Diez Del Corral, R. and A. V. Morales (2017). "The Multiple Roles of FGF Signaling in the Developing Spinal Cord." Front Cell Dev Biol **5**: 58.

Diez del Corral, R., I. Olivera-Martinez, A. Goriely, E. Gale, M. Maden and K. Storey (2003). "Opposing FGF and retinoid pathways control ventral neural pattern, neuronal differentiation, and segmentation during body axis extension." Neuron **40**(1): 65-79.

Drago, J., V. Nurcombe and P. F. Bartlett (1991). "Laminin through its long arm E8 fragment promotes the proliferation and differentiation of murine neuroepithelial cells in vitro." Exp Cell Res **192**(1): 256-265.

Duester, G. (2008). "Retinoic acid synthesis and signaling during early organogenesis." Cell **134**(6): 921-931.

Echeverry, S., X. Q. Shi, S. Rivest and J. Zhang (2011). "Peripheral nerve injury alters blood-spinal cord barrier functional and molecular integrity through a selective inflammatory pathway." J Neurosci **31**(30): 10819-10828.

Eichmann, A., T. Makinen and K. Alitalo (2005). "Neural guidance molecules regulate vascular remodeling and vessel navigation." Genes Dev **19**(9): 1013-1021.

Eng, L. F., J. J. Vanderhaeghen, A. Bignami and B. Gerstl (1971). "An acidic protein isolated from fibrous astrocytes." Brain Res **28**(2): 351-354.

Ericson, J., P. Rashbass, A. Schedl, S. Brenner-Morton, A. Kawakami, V. van Heyningen, T. M. Jessell and J. Briscoe (1997). "Pax6 controls progenitor cell identity and neuronal fate in response to graded Shh signaling." Cell **90**(1): 169-180.

Escartin, C., E. Galea, A. Lakatos, J. P. O'Callaghan, G. C. Petzold, A. Serrano-Pozo, C. Steinhauser, A. Volterra, G. Carmignoto, A. Agarwal, N. J. Allen, A. Araque, L. Barbeito, A. Barzilai, D. E. Bergles, G. Bonvento, A. M. Butt, W. T. Chen, M. Cohen-Salmon, C. Cunningham, B. Deneen, B. De Strooper, B. Diaz-Castro, C. Farina, M. Freeman, V. Gallo, J. E. Goldman, S. A. Goldman, M. Gotz, A. Gutierrez, P. G. Haydon, D. H. Heiland, E. M. Hol, M. G. Holt, M. Iino, K. V. Kastanenka, H. Kettenmann, B. S. Khakh, S. Koizumi, C. J. Lee, S. A. Liddelow, B. A. MacVicar, P. Magistretti, A. Messing, A. Mishra, A. V. Molofsky, K. K. Murai, C. M. Norris, S. Okada, S. H. R. Oliet, J. F. Oliveira, A. Panatier, V. Parpura, M. Pekna, M. Pekny, L. Pellerin, G. Perea, B. G. Perez-Nievas, F. W. Pfrieger, K. E. Poskanzer, F. J. Quintana, R. M. Ransohoff, M. Riquelme-Perez, S. Robel, C. R. Rose, J. D. Rothstein, N. Rouach, D. H. Rowitch, A. Semyanov, S. Sirko, H. Sontheimer, R. A. Swanson, J. Vitorica, I. B. Wanner, L. B. Wood, J. Wu, B. Zheng, E. R. Zimmer, R. Zorec, M. V. Sofroniew and A. Verkhratsky (2021). "Reactive astrocyte nomenclature, definitions, and future directions." Nat Neurosci **24**(3): 312-325.

Fantin, A., A. Lampropoulou, G. Gestri, C. Raimondi, V. Senatore, I. Zachary and C. Ruhrberg (2015). "NRP1 Regulates CDC42 Activation to Promote Filopodia Formation in Endothelial Tip Cells." Cell Rep **11**(10): 1577-1590.

Fantin, A., Q. Schwarz, K. Davidson, E. M. Normando, L. Denti and C. Ruhrberg (2011). "The cytoplasmic domain of neuropilin 1 is dispensable for angiogenesis, but promotes the spatial separation of retinal arteries and veins." Development **138**(19): 4185-4191.

Fantin, A., J. M. Vieira, G. Gestri, L. Denti, Q. Schwarz, S. Prykhozhij, F. Peri, S. W. Wilson and C. Ruhrberg (2010). "Tissue macrophages act as cellular chaperones for vascular anastomosis downstream of VEGF-mediated endothelial tip cell induction." Blood **116**(5): 829-840.

Fantin, A., J. M. Vieira, A. Plein, L. Denti, M. Fruttiger, J. W. Pollard and C. Ruhrberg (2013). "NRP1 acts cell autonomously in endothelium to promote tip cell function during sprouting angiogenesis." Blood **121**(12): 2352-2362.

Feiner, L., A. M. Koppel, H. Kobayashi and J. A. Raper (1997). "Secreted chick semaphorins bind recombinant neuropilin with similar affinities but bind different subsets of neurons in situ." Neuron **19**(3): 539-545.

Fenstermacher, J., P. Gross, N. Sposito, V. Acuff, S. Pettersen and K. Gruber (1988). "Structural and functional variations in capillary systems within the brain." Ann N Y Acad Sci **529**: 21-30.

Ferrara, N., H. P. Gerber and J. LeCouter (2003). "The biology of VEGF and its receptors." Nat Med **9**(6): 669-676.

Figley, S. A., R. Khosravi, J. M. Legasto, Y. F. Tseng and M. G. Fehlings (2014). "Characterization of vascular disruption and blood-spinal cord barrier permeability following traumatic spinal cord injury." J Neurotrauma **31**(6): 541-552.

Flanagan, L. A., L. M. Rebaza, S. Derzic, P. H. Schwartz and E. S. Monuki (2006). "Regulation of human neural precursor cells by laminin and integrins." J Neurosci Res **83**(5): 845-856.

Francius, C. and F. Clotman (2014). "Generating spinal motor neuron diversity: a long quest for neuronal identity." Cell Mol Life Sci **71**(5): 813-829.

Fukuhara, K., F. Imai, D. R. Ladle, K. Katayama, J. R. Leslie, S. Arber, T. M. Jessell and Y. Yoshida (2013). "Specificity of monosynaptic sensory-motor connections imposed by repellent Sema3E-PlexinD1 signaling." Cell Rep **5**(3): 748-758.

Fukushima, Y., M. Okada, H. Kataoka, M. Hirashima, Y. Yoshida, F. Mann, F. Gomi, K. Nishida, S. Nishikawa and A. Uemura (2011). "Sema3E-PlexinD1 signaling selectively suppresses disoriented angiogenesis in ischemic retinopathy in mice." J Clin Invest **121**(5): 1974-1985.

Furuse, M., T. Hirase, M. Itoh, A. Nagafuchi, S. Yonemura, S. Tsukita and S. Tsukita (1993). "Occludin: a novel integral membrane protein localizing at tight junctions." J Cell Biol **123**(6 Pt 2): 1777-1788.

Gao, Y. J., Z. Z. Xu, Y. C. Liu, Y. R. Wen, I. Decosterd and R. R. Ji (2010). "The c-Jun N-terminal kinase 1 (JNK1) in spinal astrocytes is required for the maintenance of bilateral mechanical allodynia under a persistent inflammatory pain condition." Pain **148**(2): 309-319.

Garrison, C. J., P. M. Dougherty and S. M. Carlton (1994). "GFAP expression in lumbar spinal cord of naive and neuropathic rats treated with MK-801." Exp Neurol **129**(2): 237-243.

Garrison, C. J., P. M. Dougherty, K. C. Kajander and S. M. Carlton (1991). "Staining of glial fibrillary acidic protein (GFAP) in lumbar spinal cord increases following a sciatic nerve constriction injury." Brain Res **565**(1): 1-7.

Gattlen, C., C. B. Clarke, N. Piller, G. Kirschmann, M. Pertin, I. Decosterd, R. D. Gosselin and M. R. Suter (2016). "Spinal Cord T-Cell Infiltration in the Rat Spared Nerve Injury Model: A Time Course Study." Int J Mol Sci **17**(3): 352.

Gautam, J., X. Zhang and Y. Yao (2016). "The role of pericytic laminin in blood brain barrier integrity maintenance." Sci Rep **6**: 36450.

Gay, C. M., T. Zygmunt and J. Torres-Vazquez (2011). "Diverse functions for the semaphorin receptor PlexinD1 in development and disease." Dev Biol **349**(1): 1-19.

Gilbert, S. F. (2006). Developmental biology. Sunderland, Mass., Sinauer Associates, Inc. Publishers.

Gillardon, F., J. Vogel, S. Hein, M. Zimmermann and E. Uhlmann (1997). "Inhibition of carrageenan-induced spinal c-Fos activation by systemically administered c-fos antisense oligodeoxynucleotides may be facilitated by local opening of the blood-spinal cord barrier." J Neurosci Res **47**(6): 582-589.

Ginhoux, F., M. Greter, M. Leboeuf, S. Nandi, P. See, S. Gokhan, M. F. Mehler, S. J. Conway, L. G. Ng, E. R. Stanley, I. M. Samokhvalov and M. Merad (2010). "Fate mapping analysis reveals that adult microglia derive from primitive macrophages." Science **330**(6005): 841-845.

Gitler, A. D., M. M. Lu and J. A. Epstein (2004). "PlexinD1 and semaphorin signaling are required in endothelial cells for cardiovascular development." Dev Cell **7**(1): 107-116.

Goldmann, E. E. (1909). Die äussere und innere Sekretion des gesunden und kranken Organismus im Lichte der "vitalen Färbung": Teil 1, H. Laupp.

Goldmann, E. E. (1913). Vitalfärbung am Zentralnervensystem: Beitrag zur Physio-Pathologie des Plexus chorioideus und der Hirnhäute, Königl. Akademie der Wissenschaften.

Gordon, G. R., C. Howarth and B. A. MacVicar (2011). "Bidirectional control of arteriole diameter by astrocytes." Exp Physiol **96**(4): 393-399.

Gotz, M. and Y. A. Barde (2005). "Radial glial cells defined and major intermediates between embryonic stem cells and CNS neurons." Neuron **46**(3): 369-372.

Gotz, M. and W. B. Huttner (2005). "The cell biology of neurogenesis." Nat Rev Mol Cell Biol **6**(10): 777-788.

Gu, C., E. R. Rodriguez, D. V. Reimert, T. Shu, B. Fritzsch, L. J. Richards, A. L. Kolodkin and D. D. Ginty (2003). "Neuropilin-1 conveys semaphorin and VEGF signaling during neural and cardiovascular development." Dev Cell **5**(1): 45-57.

Gu, C., Y. Yoshida, J. Livet, D. V. Reimert, F. Mann, J. Merte, C. E. Henderson, T. M. Jessell, A. L. Kolodkin and D. D. Ginty (2005). "Semaphorin 3E and plexin-D1 control vascular pattern independently of neuropilins." Science **307**(5707): 265-268.

Gu, N., J. Peng, M. Murugan, X. Wang, U. B. Eyo, D. Sun, Y. Ren, E. DiCicco-Bloom, W. Young, H. Dong and L. J. Wu (2016). "Spinal Microgliosis Due to Resident Microglial Proliferation Is Required for Pain Hypersensitivity after Peripheral Nerve Injury." Cell Rep **16**(3): 605-614.

Guimaraes, R. M., M. Davoli-Ferreira, M. M. Fonseca, L. E. A. Damasceno, F. V. Santa-Cecilia, R. Kusuda, G. B. Menezes, F. Q. Cunha, J. C. Alves-Filho and T. M. Cunha (2019). "Frontline Science: Blood-circulating leukocytes fail to infiltrate the spinal cord parenchyma after spared nerve injury." J Leukoc Biol **106**(3): 541-551.

Gutman, C. R., M. K. Ajmera and M. Hollyday (1993). "Organization of motor pools supplying axial muscles in the chicken." Brain Res **609**(1-2): 129-136.

Gwak, Y. S., J. Kang, G. C. Unabia and C. E. Hulsebosch (2012). "Spatial and temporal activation of spinal glial cells: role of gliopathy in central neuropathic pain following spinal cord injury in rats." Exp Neurol **234**(2): 362-372.

Haigh, J. J., P. I. Morelli, H. Gerhardt, K. Haigh, J. Tsien, A. Damert, L. Miquerol, U. Muhlner, R. Klein, N. Ferrara, E. F. Wagner, C. Betsholtz and A. Nagy (2003). "Cortical and retinal defects caused by dosage-dependent reductions in VEGF-A paracrine signaling." Dev Biol **262**(2): 225-241.

Halder, N. and G. Lal (2021). "Cholinergic System and Its Therapeutic Importance in Inflammation and Autoimmunity." Front Immunol **12**: 660342.

Hall, C. N., C. Reynell, B. Gesslein, N. B. Hamilton, A. Mishra, B. A. Sutherland, F. M. O'Farrell, A. M. Buchan, M. Lauritzen and D. Attwell (2014). "Capillary pericytes regulate cerebral blood flow in health and disease." Nature **508**(7494): 55-60.

Harada, N., Y. Tamai, T. Ishikawa, B. Sauer, K. Takaku, M. Oshima and M. M. Taketo (1999). "Intestinal polyposis in mice with a dominant stable mutation of the beta-catenin gene." EMBO J **18**(21): 5931-5942.

Hartsock, A. and W. J. Nelson (2008). "Adherens and tight junctions: structure, function and connections to the actin cytoskeleton." Biochim Biophys Acta **1778**(3): 660-669.

Hawkins, B. T. and T. P. Davis (2005). "The blood-brain barrier/neurovascular unit in health and disease." Pharmacol Rev **57**(2): 173-185.

He, Z. and M. Tessier-Lavigne (1997). "Neuropilin is a receptor for the axonal chemorepellent Semaphorin III." Cell **90**(4): 739-751.

Hellstrom, M., H. Gerhardt, M. Kalen, X. Li, U. Eriksson, H. Wolburg and C. Betsholtz (2001). "Lack of pericytes leads to endothelial hyperplasia and abnormal vascular morphogenesis." J Cell Biol **153**(3): 543-553.

Herzog, Y., C. Kalcheim, N. Kahane, R. Reshef and G. Neufeld (2001). "Differential expression of neuropilin-1 and neuropilin-2 in arteries and veins." Mech Dev **109**(1): 115-119.

Himmels, P., I. Paredes, H. Adler, A. Karakatsani, R. Luck, H. H. Marti, O. Ermakova, E. Rempel, E. T. Stoeckli and C. Ruiz de Almodovar (2017). "Motor neurons control blood vessel patterning in the developing spinal cord." Nat Commun **8**: 14583.

Hirase, T., J. M. Staddon, M. Saitou, Y. Ando-Akatsuka, M. Itoh, M. Furuse, K. Fujimoto, S. Tsukita and L. L. Rubin (1997). "Occludin as a possible determinant of tight junction permeability in endothelial cells." J Cell Sci **110 (Pt 14)**: 1603-1613.

Hoek, R. M., S. R. Ruuls, C. A. Murphy, G. J. Wright, R. Goddard, S. M. Zurawski, B. Blom, M. E. Homola, W. J. Streit, M. H. Brown, A. N. Barclay and J. D. Sedgwick (2000). "Down-regulation of the macrophage lineage through interaction with OX2 (CD200)." Science **290**(5497): 1768-1771.

Hogan, K. A., C. A. Ambler, D. L. Chapman and V. L. Bautch (2004). "The neural tube patterns vessels developmentally using the VEGF signaling pathway." Development **131**(7): 1503-1513.

Hollyday, M. (1980). "Organization of motor pools in the chick lumbar lateral motor column." J Comp Neurol **194**(1): 143-170.

Hori, S., S. Ohtsuki, K. Hosoya, E. Nakashima and T. Terasaki (2004). "A pericyte-derived angiopoietin-1 multimeric complex induces occludin gene expression in brain capillary endothelial cells through Tie-2 activation in vitro." J Neurochem **89**(2): 503-513.

Huber, A. B., A. Kania, T. S. Tran, C. Gu, N. De Marco Garcia, I. Lieberam, D. Johnson, T. M. Jessell, D. D. Ginty and A. L. Kolodkin (2005). "Distinct roles for secreted semaphorin signaling in spinal motor axon guidance." Neuron **48**(6): 949-964.

Ikeda, H., T. Kiritoshi and K. Murase (2012). "Contribution of microglia and astrocytes to the central sensitization, inflammatory and neuropathic pain in the juvenile rat." Mol Pain **8**: 43.

Isami, K., K. Haraguchi, K. So, K. Asakura, H. Shirakawa, Y. Mori, T. Nakagawa and S. Kaneko (2013). "Involvement of TRPM2 in peripheral nerve injury-induced infiltration of peripheral immune cells into the spinal cord in mouse neuropathic pain model." PLoS One **8**(7): e66410.

Jambusaria, A., Z. Hong, L. Zhang, S. Srivastava, A. Jana, P. T. Toth, Y. Dai, A. B. Malik and J. Rehman (2020). "Endothelial heterogeneity across distinct vascular beds during homeostasis and inflammation." Elife **9**.

James, J. M., C. Gewolb and V. L. Bautch (2009). "Neurovascular development uses VEGF-A signaling to regulate blood vessel ingression into the neural tube." Development **136**(5): 833-841.

Janzer, R. C. and M. C. Raff (1987). "Astrocytes induce blood-brain barrier properties in endothelial cells." Nature **325**(6101): 253-257.

Jessell, T. M. (2000). "Neuronal specification in the spinal cord: inductive signals and transcriptional codes." Nat Rev Genet **1**(1): 20-29.

Ji, R. R., T. Berta and M. Nedergaard (2013). "Glia and pain: is chronic pain a gliopathy?" Pain **154 Suppl 1**(0 1): S10-S28.

Jin, S., C. F. Guerrero-Juarez, L. Zhang, I. Chang, R. Ramos, C. H. Kuan, P. Myung, M. V. Plikus and Q. Nie (2021). "Inference and analysis of cell-cell communication using CellChat." Nat Commun **12**(1): 1088.

Julius, D. and A. I. Basbaum (2001). "Molecular mechanisms of nociception." Nature **413**(6852): 203-210.

Jurga, A. M., M. Paleczna and K. Z. Kuter (2020). "Overview of General and Discriminating Markers of Differential Microglia Phenotypes." Front Cell Neurosci **14**: 198.

Kalin, S., K. R. Miller, R. E. Kalin, M. Jendrach, C. Witzel and F. L. Heppner (2018). "CNS myeloid cells critically regulate heat hyperalgesia." J Clin Invest **128**(7): 2774-2786.

Kallenberg, D., V. Tripathi, F. Javaid, C. Pilotti, J. George, S. Davis, J. W. Blackburn, M. O'Connor, L. Dowsett, C. E. Bowers, S. Liyanage, M. Gourlaouen, A. Hoeh, F. Mota, D. Selwood, J. Bainbridge, A. Tufail, V. Chudasama, J. Greenwood and S. E. Moss (2021). "A Humanized Antibody against LRG1 that Inhibits Angiogenesis and Reduces Retinal Vascular Leakage." bioRxiv: 2020.2007.2025.218149.

Kalluri, R. (2003). "Basement membranes: structure, assembly and role in tumour angiogenesis." Nat Rev Cancer **3**(6): 422-433.

Kalucka, J., L. de Rooij, J. Goveia, K. Rohlenova, S. J. Dumas, E. Meta, N. V. Conchinha, F. Taverna, L. A. Teuwen, K. Veys, M. Garcia-Caballero, S. Khan, V. Geldhof, L. Sokol, R. Chen, L. Treps, M. Borri, P. de Zeeuw, C. Dubois, T. K. Karakach, K. D. Falkenberg, M. Parys, X. Yin, S. Vinckier, Y. Du, R. A. Fenton, L. Schoonjans, M. Dewerchin, G. Eelen, B. Thienpont, L. Lin, L. Bolund, X. Li, Y. Luo and P. Carmeliet (2020). "Single-Cell Transcriptome Atlas of Murine Endothelial Cells." Cell **180**(4): 764-779 e720.

Kawasaki, T., T. Kitsukawa, Y. Bekku, Y. Matsuda, M. Sanbo, T. Yagi and H. Fujisawa (1999). "A requirement for neuropilin-1 in embryonic vessel formation." Development **126**(21): 4895-4902.

Khan, S., F. Taverna, K. Rohlenova, L. Treps, V. Geldhof, L. de Rooij, L. Sokol, A. Pircher, L. C. Conradi, J. Kalucka, L. Schoonjans, G. Eelen, M. Dewerchin, T. Karakach, X. Li, J. Goveia and P. Carmeliet (2019). "EndoDB: a database of endothelial cell transcriptomics data." Nucleic Acids Res **47**(D1): D736-D744.

Kierdorf, K., N. Katzmarski, C. A. Haas and M. Prinz (2013). "Bone marrow cell recruitment to the brain in the absence of irradiation or parabiosis bias." PLoS One **8**(3): e58544.

Kim, C. F. and G. Moalem-Taylor (2011). "Detailed characterization of neuro-immune responses following neuropathic injury in mice." Brain Res **1405**: 95-108.

Kim, D., M. A. Kim, I. H. Cho, M. S. Kim, S. Lee, E. K. Jo, S. Y. Choi, K. Park, J. S. Kim, S. Akira, H. S. Na, S. B. Oh and S. J. Lee (2007). "A critical role of toll-like receptor 2 in nerve injury-induced spinal cord glial cell activation and pain hypersensitivity." J Biol Chem **282**(20): 14975-14983.

Kim, J., W. J. Oh, N. Gaiano, Y. Yoshida and C. Gu (2011). "Semaphorin 3E-Plexin-D1 signaling regulates VEGF function in developmental angiogenesis via a feedback mechanism." Genes Dev **25**(13): 1399-1411.

Kim, M., T. M. Fontelonga, C. H. Lee, S. J. Barnum and G. S. Mastick (2017). "Motor axons are guided to exit points in the spinal cord by Slit and Netrin signals." Dev Biol **432**(1): 178-191.

Kisanuki, Y. Y., R. E. Hammer, J. Miyazaki, S. C. Williams, J. A. Richardson and M. Yanagisawa (2001). "Tie2-Cre transgenic mice: a new model for endothelial cell-lineage analysis in vivo." Dev Biol **230**(2): 230-242.

Kitsukawa, T., A. Shimono, A. Kawakami, H. Kondoh and H. Fujisawa (1995). "Overexpression of a membrane protein, neuropilin, in chimeric mice causes anomalies in the cardiovascular system, nervous system and limbs." Development **121**(12): 4309-4318.

Kobayashi, M., H. Konishi, A. Sayo, T. Takai and H. Kiyama (2016). "TREM2/DAP12 Signal Elicits Proinflammatory Response in Microglia and Exacerbates Neuropathic Pain." J Neurosci **36**(43): 11138-11150.

Kolodkin, A. L., D. V. Levengood, E. G. Rowe, Y. T. Tai, R. J. Giger and D. D. Ginty (1997). "Neuropilin is a semaphorin III receptor." Cell **90**(4): 753-762.

Kolodkin, A. L., D. J. Matthes, T. P. O'Connor, N. H. Patel, A. Admon, D. Bentley and C. S. Goodman (1992). "Fasciclin IV: sequence, expression, and function during growth cone guidance in the grasshopper embryo." Neuron **9**(5): 831-845.

Kriegstein, A. and A. Alvarez-Buylla (2009). "The glial nature of embryonic and adult neural stem cells." Annu Rev Neurosci **32**: 149-184.

Kurz, H. (2009). "Cell lineages and early patterns of embryonic CNS vascularization." Cell Adh Migr **3**(2): 205-210.

Kurz, H., T. Gartner, P. S. Eggli and B. Christ (1996). "First blood vessels in the avian neural tube are formed by a combination of dorsal angioblast immigration and ventral sprouting of endothelial cells." Dev Biol **173**(1): 133-147.

Lai, H. C., R. P. Seal and J. E. Johnson (2016). "Making sense out of spinal cord somatosensory development." Development **143**(19): 3434-3448.

Lander, A. D., D. K. Fujii and L. F. Reichardt (1985). "Purification of a factor that promotes neurite outgrowth: isolation of laminin and associated molecules." J Cell Biol **101**(3): 898-913.

Landmesser, L. (1978). "The development of motor projection patterns in the chick hind limb." J Physiol **284**: 391-414.

Landmesser, L. (1978). "The distribution of motoneurones supplying chick hind limb muscles." J Physiol **284**: 371-389.

Landmesser, L. T. (1980). "The generation of neuromuscular specificity." Annu Rev Neurosci **3**: 279-302.

Langlois, S. D., S. Morin, P. T. Yam and F. Charron (2010). "Dissection and culture of commissural neurons from embryonic spinal cord." J Vis Exp(39).

Larrivee, B., C. Freitas, S. Suchting, I. Brunet and A. Eichmann (2009). "Guidance of vascular development: lessons from the nervous system." Circ Res **104**(4): 428-441.

Latremoliere, A. and C. J. Woolf (2009). "Central sensitization: a generator of pain hypersensitivity by central neural plasticity." J Pain **10**(9): 895-926.

LeBleu, V. S., B. Macdonald and R. Kalluri (2007). "Structure and function of basement membranes." Exp Biol Med (Maywood) **232**(9): 1121-1129.

Lee, M., C. Schwab and P. L. McGeer (2011). "Astrocytes are GABAergic cells that modulate microglial activity." Glia **59**(1): 152-165.

LeMaistre, J. L., S. A. Sanders, M. J. Stobart, L. Lu, J. D. Knox, H. D. Anderson and C. M. Anderson (2012). "Coactivation of NMDA receptors by glutamate and D-serine induces dilation of isolated middle cerebral arteries." J Cereb Blood Flow Metab **32**(3): 537-547.

Lengfeld, J. E., S. E. Lutz, J. R. Smith, C. Diaconu, C. Scott, S. B. Kofman, C. Choi, C. M. Walsh, C. S. Raine, I. Agalliu and D. Agalliu (2017). "Endothelial Wnt/beta-catenin signaling reduces immune cell infiltration in multiple sclerosis." Proc Natl Acad Sci U S A **114**(7): E1168-E1177.

Li, H. L., Y. Huang, Y. L. Zhou, R. H. Teng, S. Z. Zhou, J. P. Lin, Y. Yang, S. M. Zhu, H. Xu and Y. X. Yao (2020). "C-X-C Motif Chemokine 10 Contributes to the Development of Neuropathic Pain by Increasing the Permeability of the Blood-Spinal Cord Barrier." Front Immunol **11**: 477.

Li, S., T. P. Kumar, S. Joshee, T. Kirschstein, S. Subburaju, J. S. Khalili, J. Kloepper, C. Du, A. Elkhal, G. Szabo, R. K. Jain, R. Kohling and A. Vasudevan (2018). "Endothelial cell-derived GABA signaling modulates neuronal migration and postnatal behavior." Cell Res **28**(2): 221-248.

Liao, J. K. (2013). "Linking endothelial dysfunction with endothelial cell activation." J Clin Invest **123**(2): 540-541.

Lieberam, I., D. Agalliu, T. Nagasawa, J. Ericson and T. M. Jessell (2005). "A Cxcl12-CXCR4 chemokine signaling pathway defines the initial trajectory of mammalian motor axons." Neuron **47**(5): 667-679.

Liebner, S., M. Corada, T. Bangsow, J. Babbage, A. Taddei, C. J. Czupalla, M. Reis, A. Felici, H. Wolburg, M. Fruttiger, M. M. Taketo, H. von Melchner, K. H. Plate, H. Gerhardt and E. Dejana (2008). "Wnt/beta-catenin signaling controls development of the blood-brain barrier." J Cell Biol **183**(3): 409-417.

Liem, K. F., Jr., G. Tremml and T. M. Jessell (1997). "A role for the roof plate and its resident TGFbeta-related proteins in neuronal patterning in the dorsal spinal cord." Cell **91**(1): 127-138.

Lin, T., K. Li, F. Y. Zhang, Z. K. Zhang, A. R. Light and K. Y. Fu (2007). "Dissociation of spinal microglia morphological activation and peripheral inflammation in inflammatory pain models." J Neuroimmunol **192**(1-2): 40-48.

Lindahl, P., B. R. Johansson, P. Leveen and C. Betsholtz (1997). "Pericyte loss and microaneurysm formation in PDGF-B-deficient mice." Science **277**(5323): 242-245.

Litingtung, Y. and C. Chiang (2000). "Specification of ventral neuron types is mediated by an antagonistic interaction between Shh and Gli3." Nat Neurosci **3**(10): 979-985.

Litke, C., A. M. Hagenston, A. K. Kenkel, E. Paldy, J. Lu, R. Kuner and D. Mauceri (2022). "Organic anion transporter 1 is an HDAC4-regulated mediator of nociceptive hypersensitivity in mice." Nat Commun **13**(1): 875.

Liu, L., M. Rudin and E. N. Kozlova (2000). "Glial cell proliferation in the spinal cord after dorsal rhizotomy or sciatic nerve transection in the adult rat." Exp Brain Res **131**(1): 64-73.

Liu, Y., A. Nusrat, F. J. Schnell, T. A. Reaves, S. Walsh, M. Pochet and C. A. Parkos (2000). "Human junction adhesion molecule regulates tight junction resealing in epithelia." J Cell Sci **113 (Pt 13)**: 2363-2374.

Lopes Pinheiro, M. A., G. Kooij, M. R. Mizee, A. Kamermans, G. Enzmann, R. Lyck, M. Schwaninger, B. Engelhardt and H. E. de Vries (2016). "Immune cell trafficking across the barriers of the central nervous system in multiple sclerosis and stroke." Biochim Biophys Acta **1862**(3): 461-471.

Lopez-Munoz, F., J. Boya and C. Alamo (2006). "Neuron theory, the cornerstone of neuroscience, on the centenary of the Nobel Prize award to Santiago Ramon y Cajal." Brain Res Bull **70**(4-6): 391-405.

Love, M. I., W. Huber and S. Anders (2014). "Moderated estimation of fold change and dispersion for RNA-seq data with DESeq2." Genome Biol **15**(12): 550.

Lu, D. C., T. Niu and W. A. Alaynick (2015). "Molecular and cellular development of spinal cord locomotor circuitry." Front Mol Neurosci **8**: 25.

Lu, L., A. D. Hogan-Cann, A. K. Globa, P. Lu, J. I. Nagy, S. X. Bamji and C. M. Anderson (2019). "Astrocytes drive cortical vasodilatory signaling by activating endothelial NMDA receptors." J Cereb Blood Flow Metab **39**(3): 481-496.

Lu, P., C. Gonzales, Y. Chen, A. Adedoyin, M. Hummel, J. D. Kennedy and G. T. Whiteside (2009). "CNS penetration of small molecules following local inflammation, widespread systemic inflammation or direct injury to the nervous system." Life Sci **85**(11-12): 450-456.

Lumsden, A. and R. Krumlauf (1996). "Patterning the vertebrate neuraxis." Science **274**(5290): 1109-1115.

Luo, Z. Z., Y. Gao, N. Sun, Y. Zhao, J. Wang, B. Tian and J. Shi (2014). "Enhancing the interaction between annexin-1 and formyl peptide receptors regulates microglial activation to protect neurons from ischemia-like injury." J Neuroimmunol **276**(1-2): 24-36.

Lutz, S. E., J. R. Smith, D. H. Kim, C. V. L. Olson, K. Ellefsen, J. M. Bates, S. P. Gandhi and D. Agalliu (2017). "Caveolin1 Is Required for Th1 Cell Infiltration, but Not Tight Junction Remodeling, at the Blood-Brain Barrier in Autoimmune Neuroinflammation." Cell Rep **21**(8): 2104-2117.

Ma, W., T. Tavakoli, E. Derby, Y. Serebryakova, M. S. Rao and M. P. Mattson (2008). "Cell-extracellular matrix interactions regulate neural differentiation of human embryonic stem cells." BMC Dev Biol **8**: 90.

Maione, F., F. Molla, C. Meda, R. Latini, L. Zentilin, M. Giacca, G. Seano, G. Serini, F. Bussolino and E. Giraudo (2009). "Semaphorin 3A is an endogenous angiogenesis inhibitor that blocks tumor growth and normalizes tumor vasculature in transgenic mouse models." J Clin Invest **119**(11): 3356-3372.

Mandell, K. J. and C. A. Parkos (2005). "The JAM family of proteins." Adv Drug Deliv Rev **57**(6): 857-867.

Martins, L. F., I. Brambilla, A. Motta, S. de Pretis, G. P. Bhat, A. Badaloni, C. Malpighi, N. D. Amin, F. Imai, R. D. Almeida, Y. Yoshida, S. L. Pfaff and D. Bonanomi (2022). "Motor neurons use push-pull signals to direct vascular remodeling critical for their connectivity." Neuron **110**(24): 4090-4107 e4011.

Matson, K. J. E., D. E. Russ, C. Kathe, I. Hua, D. Maric, Y. Ding, J. Krynitsky, R. Pursley, A. Sathyamurthy, J. W. Squair, B. P. Levi, G. Courtine and A. J. Levine (2022). "Single cell atlas of spinal cord injury in mice reveals a pro-regenerative signature in spinocerebellar neurons." Nat Commun **13**(1): 5628.

Matsuoka, R. L., A. Rossi, O. A. Stone and D. Y. R. Stainier (2017). "CNS-resident progenitors direct the vascularization of neighboring tissues." Proc Natl Acad Sci U S A **114**(38): 10137-10142.

McMahon, A. P. (2000). "Neural patterning: the role of Nkx genes in the ventral spinal cord." Genes Dev **14**(18): 2261-2264.

McMahon, S. B. and M. Malcangio (2009). "Current challenges in glia-pain biology." Neuron **64**(1): 46-54.

Meadows, S. M., P. J. Fletcher, C. Moran, K. Xu, G. Neufeld, S. Chauvet, F. Mann, P. A. Krieg and O. Cleaver (2012). "Integration of repulsive guidance cues generates avascular zones that shape mammalian blood vessels." Circ Res **110**(1): 34-46.

Mehta, V., K. L. Pang, D. Rozbesky, K. Nather, A. Keen, D. Lachowski, Y. Kong, D. Karia, M. Ameismeier, J. Huang, Y. Fang, A. Del Rio Hernandez, J. S. Reader,

E. Y. Jones and E. Tzima (2020). "The guidance receptor plexin D1 is a mechanosensor in endothelial cells." Nature **578**(7794): 290-295.

Mentis, G. Z., F. J. Alvarez, A. Bonnot, D. S. Richards, D. Gonzalez-Forero, R. Zerda and M. J. O'Donovan (2005). "Noncholinergic excitatory actions of motoneurons in the neonatal mammalian spinal cord." Proc Natl Acad Sci U S A **102**(20): 7344-7349.

Merskey, H., N. Bogduk and International Association for the Study of Pain. Task Force on Taxonomy. (1994). Classification of chronic pain : descriptions of chronic pain syndromes and definitions of pain terms. Seattle, IASP Press.

Mildner, A., B. Schlevogt, K. Kierdorf, C. Bottcher, D. Erny, M. P. Kummer, M. Quinn, W. Bruck, I. Bechmann, M. T. Heneka, J. Priller and M. Prinz (2011). "Distinct and non-redundant roles of microglia and myeloid subsets in mouse models of Alzheimer's disease." J Neurosci **31**(31): 11159-11171.

Milligan, E. D. and L. R. Watkins (2009). "Pathological and protective roles of glia in chronic pain." Nat Rev Neurosci **10**(1): 23-36.

Miyoshi, K., K. Obata, T. Kondo, H. Okamura and K. Noguchi (2008). "Interleukin-18-mediated microglia/astrocyte interaction in the spinal cord enhances neuropathic pain processing after nerve injury." J Neurosci **28**(48): 12775-12787.

Mizumura, K. and S. Murase (2015). "Role of nerve growth factor in pain." Handb Exp Pharmacol **227**: 57-77.

Moss, S., D. Kallenberg, V. Tripathi, S. Davis, J. George, M. O'Connor, L. Dowsett and J. Greenwood (2018). "Preclinical development and testing of a therapeutic antibody against LRG1." Cancer Research **78**(13_Supplement): 5757-5757.

Mundel, T. M. and R. Kalluri (2007). "Type IV collagen-derived angiogenesis inhibitors." Microvasc Res **74**(2-3): 85-89.

Munji, R. N., A. L. Soung, G. A. Weiner, F. Sohet, B. D. Semple, A. Trivedi, K. Gimlin, M. Kotoda, M. Korai, S. Aydin, A. Batugal, A. C. Cabangcala, P. G. Schupp, M. C. Oldham, T. Hashimoto, L. J. Noble-Haeusslein and R. Daneman (2019). "Profiling the mouse brain endothelial transcriptome in health and disease models reveals a core blood-brain barrier dysfunction module." Nat Neurosci **22**(11): 1892-1902.

Myers, J. P., M. Santiago-Medina and T. M. Gomez (2011). "Regulation of axonal outgrowth and pathfinding by integrin-ECM interactions." Dev Neurobiol **71**(11): 901-923.

Naik, M. U., S. A. Mousa, C. A. Parkos and U. P. Naik (2003). "Signaling through JAM-1 and alphavbeta3 is required for the angiogenic action of bFGF: dissociation of the JAM-1 and alphavbeta3 complex." Blood **102**(6): 2108-2114.

Nakamura, M., R. A. Houghtling, L. MacArthur, B. M. Bayer and B. S. Bregman (2003). "Differences in cytokine gene expression profile between acute and secondary injury in adult rat spinal cord." Exp Neurol **184**(1): 313-325.

Nakao, T., A. Ishizawa and R. Ogawa (1988). "Observations of vascularization in the spinal cord of mouse embryos, with special reference to development of boundary membranes and perivascular spaces." Anat Rec **221**(2): 663-677.

Nesic, O., J. Lee, K. M. Johnson, Z. Ye, G. Y. Xu, G. C. Unabia, T. G. Wood, D. J. McAdoo, K. N. Westlund, C. E. Hulsebosch and J. Regino Perez-Polo (2005). "Transcriptional profiling of spinal cord injury-induced central neuropathic pain." J Neurochem **95**(4): 998-1014.

Neumann, H., T. Misgeld, K. Matsumuro and H. Wekerle (1998). "Neurotrophins inhibit major histocompatibility class II inducibility of microglia: involvement of the p75 neurotrophin receptor." Proc Natl Acad Sci U S A **95**(10): 5779-5784.

Nimmerjahn, A., F. Kirchhoff and F. Helmchen (2005). "Resting microglial cells are highly dynamic surveillants of brain parenchyma in vivo." Science **308**(5726): 1314-1318.

Nitta, T., M. Hata, S. Gotoh, Y. Seo, H. Sasaki, N. Hashimoto, M. Furuse and S. Tsukita (2003). "Size-selective loosening of the blood-brain barrier in claudin-5-deficient mice." J Cell Biol **161**(3): 653-660.

Njoo, C., C. Heinl and R. Kuner (2014). "In vivo SiRNA transfection and gene knockdown in spinal cord via rapid noninvasive lumbar intrathecal injections in mice." J Vis Exp(85).

Noctor, S. C., A. C. Flint, T. A. Weissman, R. S. Dammerman and A. R. Kriegstein (2001). "Neurons derived from radial glial cells establish radial units in neocortex." Nature **409**(6821): 714-720.

Noctor, S. C., V. Martinez-Cerdeno and A. R. Kriegstein (2008). "Distinct behaviors of neural stem and progenitor cells underlie cortical neurogenesis." J Comp Neurol **508**(1): 28-44.

Novitch, B. G., A. I. Chen and T. M. Jessell (2001). "Coordinate regulation of motor neuron subtype identity and pan-neuronal properties by the bHLH repressor Olig2." Neuron **31**(5): 773-789.

Novitch, B. G., H. Wichterle, T. M. Jessell and S. Sockanathan (2003). "A requirement for retinoic acid-mediated transcriptional activation in ventral neural patterning and motor neuron specification." Neuron **40**(1): 81-95.

Oldendorf, W. H., M. E. Cornford and W. J. Brown (1977). "The large apparent work capability of the blood-brain barrier: a study of the mitochondrial content of capillary endothelial cells in brain and other tissues of the rat." Ann Neurol **1**(5): 409-417.

Paolicelli, R. C., G. Bolasco, F. Pagani, L. Maggi, M. Scianni, P. Panzanelli, M. Giustetto, T. A. Ferreira, E. Guiducci, L. Dumas, D. Ragozzino and C. T. Gross

(2011). "Synaptic pruning by microglia is necessary for normal brain development." Science **333**(6048): 1456-1458.

Paredes, I., P. Himmels and C. Ruiz de Almodovar (2018). "Neurovascular Communication during CNS Development." Dev Cell **45**(1): 10-32.

Parr, B. A., M. J. Shea, G. Vassileva and A. P. McMahon (1993). "Mouse Wnt genes exhibit discrete domains of expression in the early embryonic CNS and limb buds." Development **119**(1): 247-261.

Patel, T., J. Hammelman, S. Aziz, S. Jang, M. Closser, T. L. Michaels, J. A. Blum, D. K. Gifford and H. Wichterle (2022). "Transcriptional dynamics of murine motor neuron maturation in vivo and in vitro." Nat Commun **13**(1): 5427.

Patestas, M. A. and L. P. Gartner (2016). A textbook of neuroanatomy. Hoboken, New Jersey, Wiley Blackwell.

Pecho-Vrieseling, E., M. Sigrist, Y. Yoshida, T. M. Jessell and S. Arber (2009). "Specificity of sensory-motor connections encoded by Sema3e-Plxnd1 recognition." Nature **459**(7248): 842-846.

Pellet-Many, C., P. Frankel, H. Jia and I. Zachary (2008). "Neuropilins: structure, function and role in disease." Biochem J **411**(2): 211-226.

Peppiatt, C. M., C. Howarth, P. Mobbs and D. Attwell (2006). "Bidirectional control of CNS capillary diameter by pericytes." Nature **443**(7112): 700-704.

Perl, E. R. (2007). "Ideas about pain, a historical view." Nat Rev Neurosci **8**(1): 71-80.

Perry, V. H. and V. O'Connor (2010). "The role of microglia in synaptic stripping and synaptic degeneration: a revised perspective." ASN Neuro **2**(5): e00047.

Plein, A., A. Calmont, A. Fantin, L. Denti, N. A. Anderson, P. J. Scambler and C. Ruhrberg (2015). "Neural crest-derived SEMA3C activates endothelial NRP1 for cardiac outflow tract septation." J Clin Invest **125**(7): 2661-2676.

Price, S. R. and J. Briscoe (2004). "The generation and diversification of spinal motor neurons: signals and responses." Mech Dev **121**(9): 1103-1115.

Purves, D. (2008). Neuroscience. Sunderland, Mass., Sinauer.

Purves, D. (2018). Neuroscience. New York, Oxford University Press.

Radu, B. M., P. Bramanti, F. Osculati, M. L. Flonta, M. Radu, G. Bertini and P. F. Fabene (2013). "Neurovascular unit in chronic pain." Mediators Inflamm **2013**: 648268.

Raghavendra, V., F. Y. Tanga and J. A. DeLeo (2004). "Complete Freunds adjuvant-induced peripheral inflammation evokes glial activation and proinflammatory cytokine expression in the CNS." Eur J Neurosci **20**(2): 467-473.

Rama, N., A. Dubrac, T. Mathivet, R. A. Ni Charthaigh, G. Genet, B. Cristofaro, L. Pibouin-Fragner, L. Ma, A. Eichmann and A. Chedotal (2015). "Slit2 signaling through Robo1 and Robo2 is required for retinal neovascularization." Nat Med **21**(5): 483-491.

Rascher, G., A. Fischmann, S. Kroger, F. Duffner, E. H. Grote and H. Wolburg (2002). "Extracellular matrix and the blood-brain barrier in glioblastoma multiforme: spatial segregation of tenascin and agrin." Acta Neuropathol **104**(1): 85-91.

Reis, M. and S. Liebner (2013). "Wnt signaling in the vasculature." Exp Cell Res **319**(9): 1317-1323.

Ren, K. and R. Dubner (1999). "Inflammatory Models of Pain and Hyperalgesia." ILAR J **40**(3): 111-118.

Ren, K. and R. Dubner (2010). "Interactions between the immune and nervous systems in pain." Nat Med **16**(11): 1267-1276.

Rexed, B. (1952). "The cytoarchitectonic organization of the spinal cord in the cat." J Comp Neurol **96**(3): 414-495.

Rexed, B. (1954). "A cytoarchitectonic atlas of the spinal cord in the cat." J Comp Neurol **100**(2): 297-379.

Ribes, V. and J. Briscoe (2009). "Establishing and interpreting graded Sonic Hedgehog signaling during vertebrate neural tube patterning: the role of negative feedback." Cold Spring Harb Perspect Biol **1**(2): a002014.

Richards, D. S., R. W. Griffith, S. H. Romer and F. J. Alvarez (2014). "Motor axon synapses on renshaw cells contain higher levels of aspartate than glutamate." PLoS One **9**(5): e97240.

Risau, W. (1997). "Mechanisms of angiogenesis." Nature **386**(6626): 671-674.

Rohlenova, K., J. Goveia, M. Garcia-Caballero, A. Subramanian, J. Kalucka, L. Treps, K. D. Falkenberg, L. de Rooij, Y. Zheng, L. Lin, L. Sokol, L. A. Teuwen, V. Geldhof, F. Taverna, A. Pircher, L. C. Conradi, S. Khan, S. Stegen, D. Panovska, F. De Smet, F. J. T. Staal, R. J. McLaughlin, S. Vinckier, T. Van Bergen, N. Ectors, P. De Haes, J. Wang, L. Bolund, L. Schoonjans, T. K. Karakach, H. Yang, G. Carmeliet, Y. Liu, B. Thienpont, M. Dewerchin, G. Eelen, X. Li, Y. Luo and P. Carmeliet (2020). "Single-Cell RNA Sequencing Maps Endothelial Metabolic Plasticity in Pathological Angiogenesis." Cell Metab **31**(4): 862-877 e814.

Rossant, J. and P. P. Tam (2009). "Blastocyst lineage formation, early embryonic asymmetries and axis patterning in the mouse." Development **136**(5): 701-713.

Ruiz de Almodovar, C., P. J. Fabre, E. Knevels, C. Coulon, I. Segura, P. C. Haddick, L. Aerts, N. Delattin, G. Strasser, W. J. Oh, C. Lange, S. Vinckier, J. Haigh, C. Fouquet, C. Gu, K. Alitalo, V. Castellani, M. Tessier-Lavigne, A. Chedotal, F. Charron and P. Carmeliet (2011). "VEGF mediates commissural axon chemoattraction through its receptor Flk1." Neuron **70**(5): 966-978.

Rymo, S. F., H. Gerhardt, F. Wolfhagen Sand, R. Lang, A. Uv and C. Betsholtz (2011). "A two-way communication between microglial cells and angiogenic sprouts regulates angiogenesis in aortic ring cultures." PLoS One **6**(1): e15846.

Sadler, T. W. (2005). "Embryology of neural tube development." Am J Med Genet C Semin Med Genet **135C**(1): 2-8.

Sagare, A. P., R. D. Bell, Z. Zhao, Q. Ma, E. A. Winkler, A. Ramanathan and B. V. Zlokovic (2013). "Pericyte loss influences Alzheimer-like neurodegeneration in mice." Nat Commun **4**: 2932.

Sailem, H. Z. and A. Al Haj Zen (2020). "Morphological landscape of endothelial cell networks reveals a functional role of glutamate receptors in angiogenesis." Sci Rep **10**(1): 13829.

Saitou, M., M. Furuse, H. Sasaki, J. D. Schulzke, M. Fromm, H. Takano, T. Noda and S. Tsukita (2000). "Complex phenotype of mice lacking occludin, a component of tight junction strands." Mol Biol Cell **11**(12): 4131-4142.

Sandkuhler, J. (2009). "Models and mechanisms of hyperalgesia and allodynia." Physiol Rev **89**(2): 707-758.

Sathyamurthy, A., K. R. Johnson, K. J. E. Matson, C. I. Dobrott, L. Li, A. R. Ryba, T. B. Bergman, M. C. Kelly, M. W. Kelley and A. J. Levine (2018). "Massively Parallel Single Nucleus Transcriptional Profiling Defines Spinal Cord Neurons and Their Activity during Behavior." Cell Rep **22**(8): 2216-2225.

Sauer, R. S., J. Kirchner, S. Yang, L. Hu, M. Leinders, C. Sommer, A. Brack and H. L. Rittner (2017). "Blood-spinal cord barrier breakdown and pericyte deficiency in peripheral neuropathy." Ann N Y Acad Sci **1405**(1): 71-88.

Savettieri, G., I. Di Liegro, C. Catania, L. Licata, G. L. Pitarresi, S. D'Agostino, G. Schiera, V. De Caro, G. Giandalia, L. I. Giannola and A. Cestelli (2000). "Neurons and ECM regulate occludin localization in brain endothelial cells." Neuroreport **11**(5): 1081-1084.

Schaeffer, S. and C. Iadecola (2021). "Revisiting the neurovascular unit." Nat Neurosci **24**(9): 1198-1209.

Schafer, D. P., E. K. Lehrman, A. G. Kautzman, R. Koyama, A. R. Mardinly, R. Yamasaki, R. M. Ransohoff, M. E. Greenberg, B. A. Barres and B. Stevens (2012). "Microglia sculpt postnatal neural circuits in an activity and complement-dependent manner." Neuron **74**(4): 691-705.

Schmidt, R., M. Schmelz, C. Forster, M. Ringkamp, E. Torebjork and H. Handwerker (1995). "Novel classes of responsive and unresponsive C nociceptors in human skin." J Neurosci **15**(1 Pt 1): 333-341.

Scholz, J. and C. J. Woolf (2007). "The neuropathic pain triad: neurons, immune cells and glia." Nat Neurosci **10**(11): 1361-1368.

Schwarz, Q. and C. Ruhrberg (2010). "Neuropilin, you gotta let me know: should I stay or should I go?" Cell Adh Migr **4**(1): 61-66.

Sedlakova, R., R. R. Shivers and R. F. Del Maestro (1999). "Ultrastructure of the blood-brain barrier in the rabbit." J Submicrosc Cytol Pathol **31**(1): 149-161.

Segarra, M., M. R. Aburto, J. Hefendehl and A. Acker-Palmer (2019). "Neurovascular Interactions in the Nervous System." Annu Rev Cell Dev Biol **35**: 615-635.

Sharp, C. D., I. Hines, J. Houghton, A. Warren, T. H. t. Jackson, A. Jawahar, A. Nanda, J. W. Elrod, A. Long, A. Chi, A. Minagar and J. S. Alexander (2003). "Glutamate causes a loss in human cerebral endothelial barrier integrity through activation of NMDA receptor." Am J Physiol Heart Circ Physiol **285**(6): H2592-2598.

Shen, J., R. Samul, J. Zimmer, H. Liu, X. Liang, S. Hackett and P. A. Campochiaro (2004). "Deficiency of neuropilin 2 suppresses VEGF-induced retinal neovascularization." Mol Med **10**(1-6): 12-18.

Shi, Y. N., N. Zhu, C. Liu, H. T. Wu, Y. Gui, D. F. Liao and L. Qin (2017). "Wnt5a and its signaling pathway in angiogenesis." Clin Chim Acta **471**: 263-269.

Shirai, R., F. Hirano, N. Ohkura, K. Ikeda and S. Inoue (2009). "Up-regulation of the expression of leucine-rich alpha(2)-glycoprotein in hepatocytes by the mediators of acute-phase response." Biochem Biophys Res Commun **382**(4): 776-779.

Simonetti, M., A. M. Hagenston, D. Vardeh, H. E. Freitag, D. Mauceri, J. Lu, V. P. Satagopam, R. Schneider, M. Costigan, H. Bading and R. Kuner (2013). "Nuclear calcium signaling in spinal neurons drives a genomic program required for persistent inflammatory pain." Neuron **77**(1): 43-57.

Siqueira, M., D. Francis, D. Gisbert, F. C. A. Gomes and J. Stipursky (2018). "Radial Glia Cells Control Angiogenesis in the Developing Cerebral Cortex Through TGF-beta1 Signaling." Mol Neurobiol **55**(5): 3660-3675.

Soler-Botija, C., I. Ferrer, I. Gich, M. Baiget and E. F. Tizzano (2002). "Neuronal death is enhanced and begins during foetal development in type I spinal muscular atrophy spinal cord." Brain **125**(Pt 7): 1624-1634.

Solnica-Krezel, L. and D. S. Sepich (2012). "Gastrulation: making and shaping germ layers." Annu Rev Cell Dev Biol **28**: 687-717.

Stemple, D. L. (2005). "Structure and function of the notochord: an essential organ for chordate development." Development **132**(11): 2503-2512.

Stenman, J. M., J. Rajagopal, T. J. Carroll, M. Ishibashi, J. McMahon and A. P. McMahon (2008). "Canonical Wnt signaling regulates organ-specific assembly and differentiation of CNS vasculature." Science **322**(5905): 1247-1250.

Stevens, B., N. J. Allen, L. E. Vazquez, G. R. Howell, K. S. Christopherson, N. Nouri, K. D. Micheva, A. K. Mehalow, A. D. Huberman, B. Stafford, A. Sher, A. M. Litke, J. D. Lambris, S. J. Smith, S. W. John and B. A. Barres (2007). "The classical complement cascade mediates CNS synapse elimination." Cell **131**(6): 1164-1178.

Stifani, N. (2014). "Motor neurons and the generation of spinal motor neuron diversity." Front Cell Neurosci **8**: 293.

Stosser, S., N. Agarwal, A. Tappe-Theodor, M. Yanagisawa and R. Kuner (2010). "Dissecting the functional significance of endothelin A receptors in peripheral nociceptors in vivo via conditional gene deletion." Pain **148**(2): 206-214.

Stratman, A. N. and G. E. Davis (2012). "Endothelial cell-pericyte interactions stimulate basement membrane matrix assembly: influence on vascular tube remodeling, maturation, and stabilization." Microsc Microanal **18**(1): 68-80.

Sun, S., H. Cao, M. Han, T. T. Li, H. L. Pan, Z. Q. Zhao and Y. Q. Zhang (2007). "New evidence for the involvement of spinal fractalkine receptor in pain facilitation and spinal glial activation in rat model of monoarthritis." Pain **129**(1-2): 64-75.

Suter, T. and A. Jaworski (2019). "Cell migration and axon guidance at the border between central and peripheral nervous system." Science **365**(6456).

Takahashi, T., Y. Takase, T. Yoshino, D. Saito, R. Tadokoro and Y. Takahashi (2015). "Angiogenesis in the developing spinal cord: blood vessel exclusion from neural progenitor region is mediated by VEGF and its antagonists." PLoS One **10**(1): e0116119.

Takashima, S., M. Kitakaze, M. Asakura, H. Asanuma, S. Sanada, F. Tashiro, H. Niwa, J. Miyazaki Ji, S. Hirota, Y. Kitamura, T. Kitsukawa, H. Fujisawa, M. Klagsbrun and M. Hori (2002). "Targeting of both mouse neuropilin-1 and neuropilin-2 genes severely impairs developmental yolk sac and embryonic angiogenesis." Proc Natl Acad Sci U S A **99**(6): 3657-3662.

Tamagnone, L. and P. M. Comoglio (2000). "Signalling by semaphorin receptors: cell guidance and beyond." Trends Cell Biol **10**(9): 377-383.

Tanabe, Y., C. William and T. M. Jessell (1998). "Specification of motor neuron identity by the MNR2 homeodomain protein." Cell **95**(1): 67-80.

Tanga, F. Y., N. Nutile-McMenemy and J. A. DeLeo (2005). "The CNS role of Toll-like receptor 4 in innate neuroimmunity and painful neuropathy." Proc Natl Acad Sci U S A **102**(16): 5856-5861.

Tao-Cheng, J. H., Z. Nagy and M. W. Brightman (1987). "Tight junctions of brain endothelium in vitro are enhanced by astroglia." J Neurosci **7**(10): 3293-3299.

Tata, M., C. Ruhrberg and A. Fantin (2015). "Vascularisation of the central nervous system." Mech Dev **138 Pt 1**: 26-36.

Teoh, H. L., K. Carey, H. Sampaio, D. Mowat, T. Roscioli and M. Farrar (2017). "Inherited Paediatric Motor Neuron Disorders: Beyond Spinal Muscular Atrophy." Neural Plast **2017**: 6509493.

Thacker, M. A., A. K. Clark, T. Bishop, J. Grist, P. K. Yip, L. D. Moon, S. W. Thompson, F. Marchand and S. B. McMahon (2009). "CCL2 is a key mediator of microglia activation in neuropathic pain states." Eur J Pain **13**(3): 263-272.

Thaler, J., K. Harrison, K. Sharma, K. Lettieri, J. Kehrl and S. L. Pfaff (1999). "Active suppression of interneuron programs within developing motor neurons revealed by analysis of homeodomain factor HB9." Neuron **23**(4): 675-687.

Torres-Vazquez, J., A. D. Gitler, S. D. Fraser, J. D. Berk, N. P. Van, M. C. Fishman, S. Childs, J. A. Epstein and B. M. Weinstein (2004). "Semaphorin-plexin signaling guides patterning of the developing vasculature." Dev Cell **7**(1): 117-123.

Tozaki-Saitoh, H., H. Takeda and K. Inoue (2022). "The Role of Microglial Purinergic Receptors in Pain Signaling." Molecules **27**(6).

Trang, T., S. Beggs and M. W. Salter (2012). "ATP receptors gate microglia signaling in neuropathic pain." Exp Neurol **234**(2): 354-361.

Tsuchida, T., M. Ensini, S. B. Morton, M. Baldassare, T. Edlund, T. M. Jessell and S. L. Pfaff (1994). "Topographic organization of embryonic motor neurons defined by expression of LIM homeobox genes." Cell **79**(6): 957-970.

Tsuda, M., Y. Kohro, T. Yano, T. Tsujikawa, J. Kitano, H. Tozaki-Saitoh, S. Koyanagi, S. Ohdo, R. R. Ji, M. W. Salter and K. Inoue (2011). "JAK-STAT3 pathway regulates spinal astrocyte proliferation and neuropathic pain maintenance in rats." Brain **134**(Pt 4): 1127-1139.

Tsuda, M., T. Masuda, J. Kitano, H. Shimoyama, H. Tozaki-Saitoh and K. Inoue (2009). "IFN-gamma receptor signaling mediates spinal microglia activation driving neuropathic pain." Proc Natl Acad Sci U S A **106**(19): 8032-8037.

Ueno, M., Y. Fujita, T. Tanaka, Y. Nakamura, J. Kikuta, M. Ishii and T. Yamashita (2013). "Layer V cortical neurons require microglial support for survival during postnatal development." Nat Neurosci **16**(5): 543-551.

Urban, L., S. W. Thompson, A. J. Fox, S. Jeftinija and A. Dray (1995). "Peptidergic afferents: physiological aspects." Prog Brain Res **104**: 255-269.

van der Zwaag, B., A. J. Hellemons, W. P. Leenders, J. P. Burbach, H. G. Brunner, G. W. Padberg and H. Van Bokhoven (2002). "PLEXIN-D1, a novel plexin family member, is expressed in vascular endothelium and the central nervous system during mouse embryogenesis." Dev Dyn **225**(3): 336-343.

Verge, G. M., E. D. Milligan, S. F. Maier, L. R. Watkins, G. S. Naeve and A. C. Foster (2004). "Fractalkine (CX3CL1) and fractalkine receptor (CX3CR1) distribution in spinal cord and dorsal root ganglia under basal and neuropathic pain conditions." Eur J Neurosci **20**(5): 1150-1160.

Vieira, J. R., B. Shah, S. Dupraz, I. Paredes, P. Himmels, G. Schermann, H. Adler, A. Motta, L. Gartner, A. Navarro-Aragall, E. Ioannou, E. Dyukova, R. Bonnavion, A. Fischer, D. Bonanomi, F. Bradke, C. Ruhrberg and C. Ruiz de Almodovar (2022). "Endothelial PlexinD1 signaling instructs spinal cord vascularization and motor neuron development." Neuron **110**(24): 4074-4089 e4076.

Vieira, J. R., B. Shah and C. Ruiz de Almodovar (2020). "Cellular and Molecular Mechanisms of Spinal Cord Vascularization." Front Physiol **11**: 599897.

Vuopala, K., J. Ignatius and R. Herva (1995). "Lethal arthrogryposis with anterior horn cell disease." Hum Pathol **26**(1): 12-19.

Walchli, T., V. Pernet, O. Weinmann, J. Y. Shiu, A. Guzik-Kornacka, G. Decrey, D. Yuksel, H. Schneider, J. Vogel, D. E. Ingber, V. Vogel, K. Frei and M. E. Schwab (2013). "Nogo-A is a negative regulator of CNS angiogenesis." Proc Natl Acad Sci U S A **110**(21): E1943-1952.

Walchli, T., A. Ulmann-Schuler, C. Hintermuller, E. Meyer, M. Stampanoni, P. Carmeliet, M. Y. Emmert, O. Bozinov, L. Regli, M. E. Schwab, J. Vogel and S. P. Hoerstrup (2017). "Nogo-A regulates vascular network architecture in the postnatal brain." J Cereb Blood Flow Metab **37**(2): 614-631.

Wallez, Y., I. Vilgrain and P. Huber (2006). "Angiogenesis: the VE-cadherin switch." Trends Cardiovasc Med **16**(2): 55-59.

Wang, X., S. Abraham, J. A. G. McKenzie, N. Jeffs, M. Swire, V. B. Tripathi, U. F. O. Luhmann, C. A. K. Lange, Z. Zhai, H. M. Arthur, J. Bainbridge, S. E. Moss and J. Greenwood (2013). "LRG1 promotes angiogenesis by modulating endothelial TGF-beta signalling." Nature **499**(7458): 306-311.

Wang, Y., M. Nakayama, M. E. Pitulescu, T. S. Schmidt, M. L. Bochenek, A. Sakakibara, S. Adams, A. Davy, U. Deutsch, U. Luthi, A. Barberis, L. E. Benjamin, T. Makinen, C. D. Nobes and R. H. Adams (2010). "Ephrin-B2 controls VEGF-induced angiogenesis and lymphangiogenesis." Nature **465**(7297): 483-486.

Wild, R., A. Klems, M. Takamiya, Y. Hayashi, U. Strahle, K. Ando, N. Mochizuki, A. van Impel, S. Schulte-Merker, J. Krueger, L. Preau and F. le Noble (2017). "Neuronal sFlt1 and Vegfaa determine venous sprouting and spinal cord vascularization." Nat Commun **8**: 13991.

Wilhelm, I. and I. A. Krizbai (2014). "In vitro models of the blood-brain barrier for the study of drug delivery to the brain." Mol Pharm **11**(7): 1949-1963.

Willis, C. L., T. A. Brooks and T. P. Davis (2008). "Chronic inflammatory pain and the neurovascular unit: a central role for glia in maintaining BBB integrity?" Curr Pharm Des **14**(16): 1625-1643.

Willis, W. D. (2004). Sensory mechanisms of the spinal cord. New York, Kluwer Academic/Plenum Publishers.

Willis, W. D. and K. N. Westlund (1997). "Neuroanatomy of the pain system and of the pathways that modulate pain." J Clin Neurophysiol **14**(1): 2-31.

Wolburg, H. and A. Lippoldt (2002). "Tight junctions of the blood-brain barrier: development, composition and regulation." Vascul Pharmacol **38**(6): 323-337.

Wolpowitz, D., T. B. Mason, P. Dietrich, M. Mendelsohn, D. A. Talmage and L. W. Role (2000). "Cysteine-rich domain isoforms of the neuregulin-1 gene are required for maintenance of peripheral synapses." Neuron **25**(1): 79-91.

Wong, V. and B. M. Gumbiner (1997). "A synthetic peptide corresponding to the extracellular domain of occludin perturbs the tight junction permeability barrier." J Cell Biol **136**(2): 399-409.

Woolf, C. J. and Q. Ma (2007). "Nociceptors--noxious stimulus detectors." Neuron **55**(3): 353-364.

Wu, H., W. C. Xiong and L. Mei (2010). "To build a synapse: signaling pathways in neuromuscular junction assembly." Development **137**(7): 1017-1033.

Wu, S., Y. Wu and M. R. Capecchi (2006). "Motoneurons and oligodendrocytes are sequentially generated from neural stem cells but do not appear to share common lineage-restricted progenitors in vivo." Development **133**(4): 581-590.

Xanthos, D. N., I. Pungel, G. Wunderbaldinger and J. Sandkuhler (2012). "Effects of peripheral inflammation on the blood-spinal cord barrier." Mol Pain **8**: 44.

Xu, J., P. Li, F. Lu, Y. Chen, Q. Guo and Y. Yang (2023). "Domino reaction of neurovascular unit in neuropathic pain after spinal cord injury." Exp Neurol **359**: 114273.

Xu, Y., Y. Jiang, L. Wang, J. Huang, J. Wen, H. Lv, X. Wu, C. Wan, C. Yu, W. Zhang, J. Zhao, Y. Zhou and Y. Chen (2019). "Thymosin Alpha-1 Inhibits Complete Freund's Adjuvant-Induced Pain and Production of Microglia-Mediated Pro-inflammatory Cytokines in Spinal Cord." Neurosci Bull **35**(4): 637-648.

Yang, W. J., J. Hu, A. Uemura, F. Tetzlaff, H. G. Augustin and A. Fischer (2015). "Semaphorin-3C signals through Neuropilin-1 and PlexinD1 receptors to inhibit pathological angiogenesis." EMBO Mol Med **7**(10): 1267-1284.

Yuan, H., M. W. Gaber, T. McColgan, M. D. Naimark, M. F. Kiani and T. E. Merchant (2003). "Radiation-induced permeability and leukocyte adhesion in the rat blood-brain barrier: modulation with anti-ICAM-1 antibodies." Brain Res **969**(1-2): 59-69.

Yuan, L., D. Moyon, L. Pardanaud, C. Breant, M. J. Karkkainen, K. Alitalo and A. Eichmann (2002). "Abnormal lymphatic vessel development in neuropilin 2 mutant mice." Development **129**(20): 4797-4806.

Zhang, J. and Y. De Koninck (2006). "Spatial and temporal relationship between monocyte chemoattractant protein-1 expression and spinal glial activation following peripheral nerve injury." J Neurochem **97**(3): 772-783.

Zhang, J., X. Q. Shi, S. Echeverry, J. S. Mogil, Y. De Koninck and S. Rivest (2007). "Expression of CCR2 in both resident and bone marrow-derived microglia plays a critical role in neuropathic pain." J Neurosci **27**(45): 12396-12406.

Zhang, L., T. Berta, Z. Z. Xu, T. Liu, J. Y. Park and R. R. Ji (2011). "TNF-alpha contributes to spinal cord synaptic plasticity and inflammatory pain: distinct role of TNF receptor subtypes 1 and 2." Pain **152**(2): 419-427.

Zhang, Y., M. K. Singh, K. R. Degenhardt, M. M. Lu, J. Bennett, Y. Yoshida and J. A. Epstein (2009). "Tie2Cre-mediated inactivation of plexinD1 results in congenital heart, vascular and skeletal defects." Dev Biol **325**(1): 82-93.

Zhou, Q. and D. J. Anderson (2002). "The bHLH transcription factors OLIG2 and OLIG1 couple neuronal and glial subtype specification." Cell **109**(1): 61-73.

Zhou, Y., R. A. Gunput and R. J. Pasterkamp (2008). "Semaphorin signaling: progress made and promises ahead." Trends Biochem Sci **33**(4): 161-170.

Zhou, Y. Q., Z. Liu, Z. H. Liu, S. P. Chen, M. Li, A. Shahveranov, D. W. Ye and Y. K. Tian (2016). "Interleukin-6: an emerging regulator of pathological pain." J Neuroinflammation **13**(1): 141.

Zhuang, Z. Y., P. Gerner, C. J. Woolf and R. R. Ji (2005). "ERK is sequentially activated in neurons, microglia, and astrocytes by spinal nerve ligation and contributes to mechanical allodynia in this neuropathic pain model." Pain **114**(1-2): 149-159.

Zhuang, Z. Y., Y. Kawasaki, P. H. Tan, Y. R. Wen, J. Huang and R. R. Ji (2007). "Role of the CX3CR1/p38 MAPK pathway in spinal microglia for the development of neuropathic pain following nerve injury-induced cleavage of fractalkine." Brain Behav Immun **21**(5): 642-651.

Zhuang, Z. Y., Y. R. Wen, D. R. Zhang, T. Borsello, C. Bonny, G. R. Strichartz, I. Decosterd and R. R. Ji (2006). "A peptide c-Jun N-terminal kinase (JNK) inhibitor blocks mechanical allodynia after spinal nerve ligation: respective roles of JNK activation in primary sensory neurons and spinal astrocytes for neuropathic pain development and maintenance." J Neurosci **26**(13): 3551-3560.

Zudaire, E., L. Gambardella, C. Kurcz and S. Vermeren (2011). "A computational tool for quantitative analysis of vascular networks." PLoS One **6**(11): e27385.

Zygmunt, T., C. M. Gay, J. Blondelle, M. K. Singh, K. M. Flaherty, P. C. Means, L. Herwig, A. Krudewig, H. G. Belting, M. Affolter, J. A. Epstein and J. Torres-Vazquez (2011). "Semaphorin-PlexinD1 signaling limits angiogenic potential via the VEGF decoy receptor sFlt1." Dev Cell **21**(2): 301-314.

8. APPENDIX

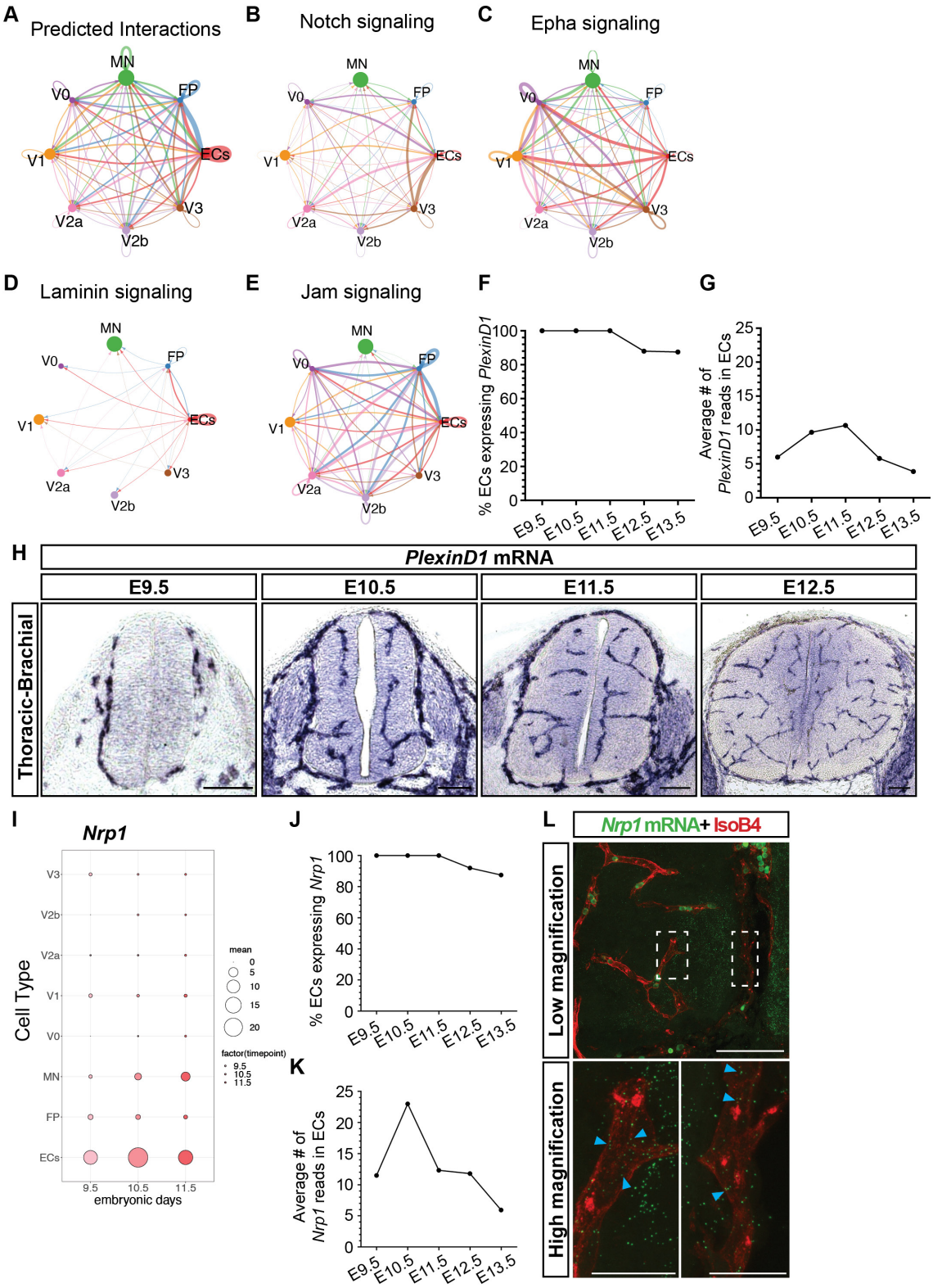

Appendix Fig. 1. Top predicted interactions between ventral spinal cord cells, and *PlexinD1* and *Nrp1* expression. (A) Graph showing the predicted interactions between the different cell types. (B-E) Graphs showing the predicted interactions between cell types using (B) Notch signaling, (C) Epha signaling, (D) Laminin signaling, and (E) Jam signaling. (F-G) Temporal plot of the percentage of ECs expressing *PlexinD1* (F) and

the average number of *PlexinD1* reads in ECs (G) between E9.5 to E13.5, using previously published single-cell RNAseq data (Delile, Rayon et al. 2019). (H) Representative images for *PlexinD1* ISH between E9.5 and E12.5. *PlexinD1* mRNA is expressed only in ECs at all the spinal cord levels. Scale bars 100 μm. (I) Predicted expression of *Nrp1* in the different cell types between E9.5 to E11.5, using previously published single-cell RNAseq data (Delile, Rayon et al. 2019). (J-K) Temporal plot of the percentage of ECs expressing *Nrp1* (J) and the average number of *Nrp1* reads in ECs (K) between E9.5 to E13.5, using previously published single-cell RNAseq data (Delile, Rayon et al. 2019). (L) Representative images of RNAscope Multiplex Fluorescent Assay using *Nrp1* probe combined with staining for ECs ($IsoB4^+$). Inset shows higher magnification of vessels surrounding the MN column. Blue arrowheads point at *Nrp1* dots within ECs. Scale bar 100 μm for low magnification and 25 μm for higher

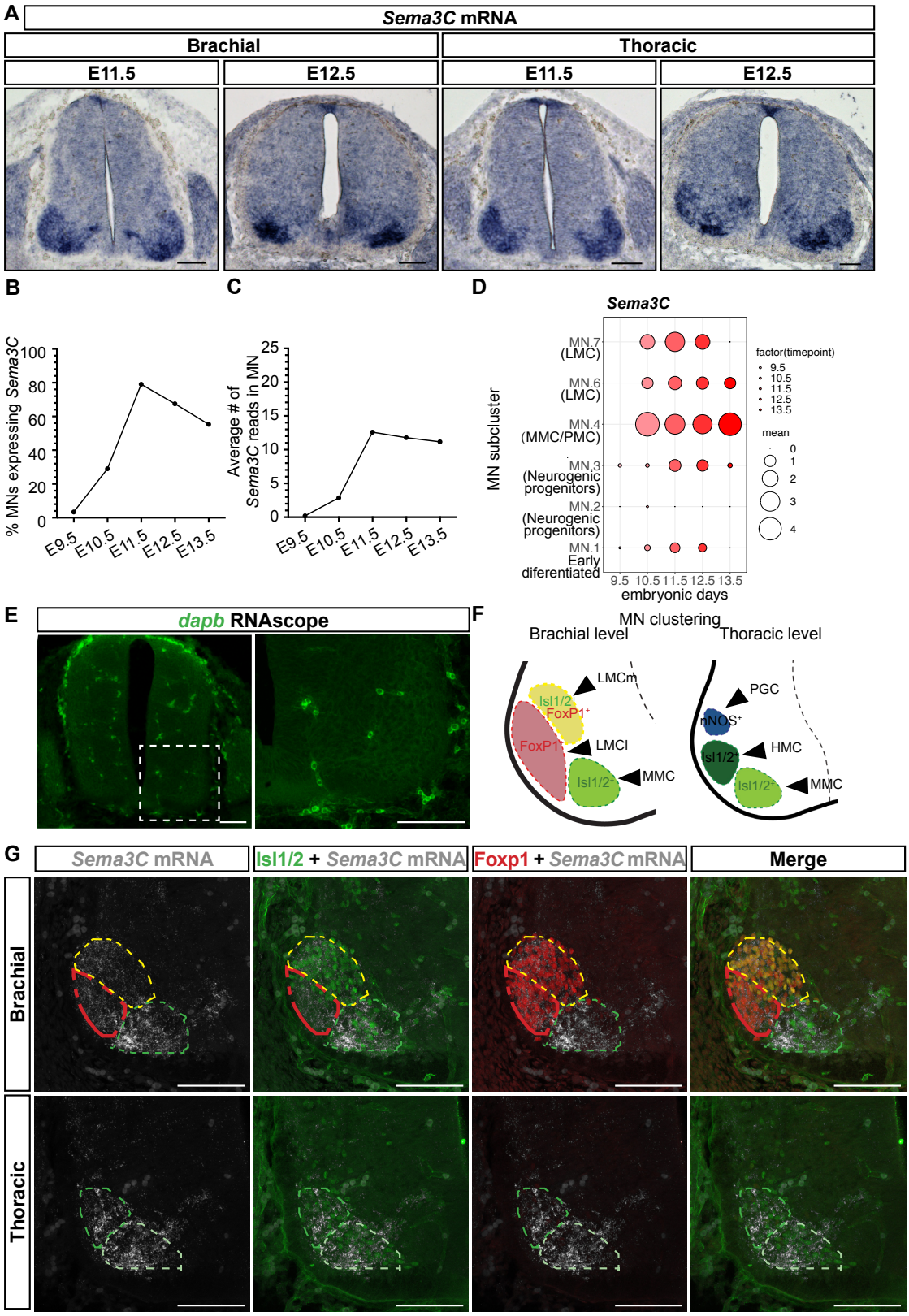

Appendix Fig. 2. *Sema3C* is expressed in MNs during spinal cord development. (A) Representative images of *Sema3C in situ* hybridization (ISH) at brachial and thoracic level between E11.5 and E12.5. (B-C) Percentage of MNs expressing *Sema3C* (B) and the average number of (C) *Sema3C* reads in MNs over the indicated developmental times, using previously published single- cell RNAseq data (Delile, Rayon et al. 2019). (D) Predicted expression of *Sema3C* in the different MN columns

using previously published single-cell RNAseq data (Delile, Rayon et al. 2019). (E) Representative RNAscope assay for the negative control *Dapb,* showing background staining prevenient from erythrocytes. The inset shows a higher magnification of MN column. (F) Schematic representation of MN clustering and positioning at brachial and thoracic levels of the spinal cord at E11.5. (G) Representative images of RNAscope assay using *Sema3C* probe combined with staining for MN columns (LMCl - red circle, Isl1/2^{-}Foxp1^{+}; LMCm - yellow circle, Foxp1^{+}Isl1/2^{+}; MMC – green circle, Foxp1^{-}Isl1/2^{+}). All scale bars 100 μm.

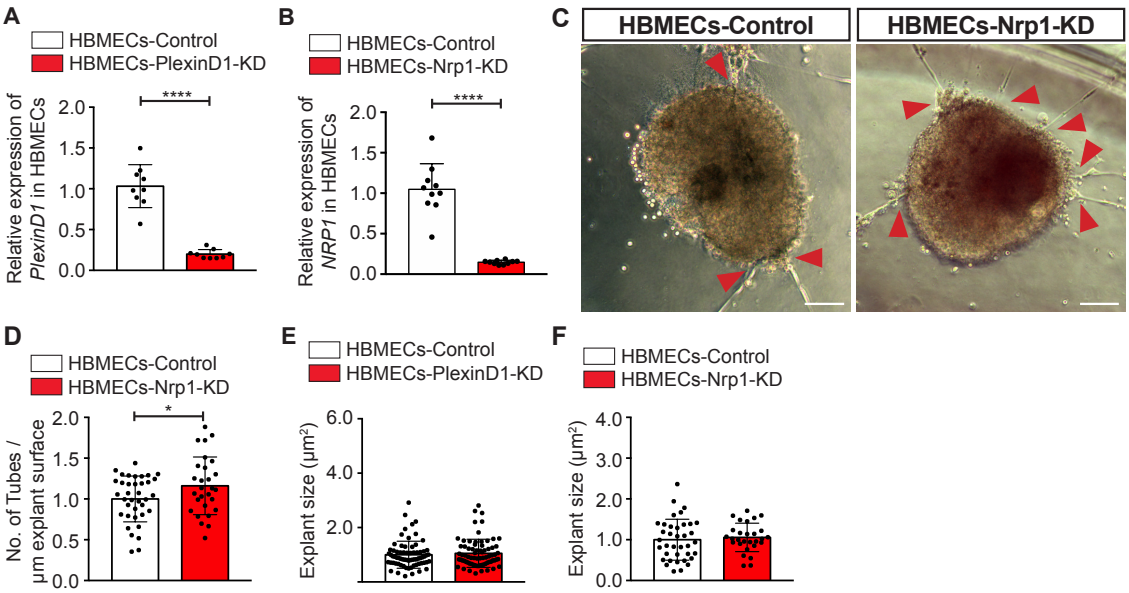

Appendix Fig. 3. Knockdown of *PlexinD1* and *Nrp1* in ECs results in increased HBMECs tubes contacting MN explants. (A) Relative *PlexinD1* mRNA expression in HBMECs upon transfection with siRNA PlexinD1 (HBMECs-PlexinD1-KD), normalized to siRNA Ctrl (HBMECs-Control) (n=9 siRNA Ctrl, n=9 siRNA PlexinD1, from two independent experiments). (B) Relative *Nrp1* mRNA expression in HBMECs upon transfection with siRNA Nrp1 (HBMECs-Nrp1-KD), normalized to siRNA Ctrl (HBMECs-Control) (n=10 siRNA Ctrl, n=10 siRNA Nrp1, from two independent experiments). (C) Representative images of the tube "touching" assay showing HBMEC-Control and HBMECs-Nrp1-KD tubes touching MN explants. Red arrowheads indicate contacts between HBMEC tubes and explants. Scale bars 1000 μm. (D) Quantification of the number of either HBMECs-Control or HBMECs-Nrp1-KD tubes touching MN explants, normalized to the explant perimeter (n=37 explants siRNA Ctrl, n=28 explants siRNA Nrp1, from 2 independent litters). (E) Quantification of MN explant size from BL6 WT embryos used for the tube touching assay (data are normalized to Control; n=72 explants cultured with HBMECs-Control, n=77 explants cultured with HBMECs-PlexinD1-KD, from two independent litters). (F) Quantification of the number of either HBMECs-Control or HBMECs-Nrp1-KD tubes touching MN explants, normalized to the explant perimeter (n=37 explants siRNA Ctrl, n=28 explants siRNA Nrp1, from 2 independent litter). All statistical analyses done using parametric distribution, two tailed unpaired Student's t-test. All data shown as mean ± SD.

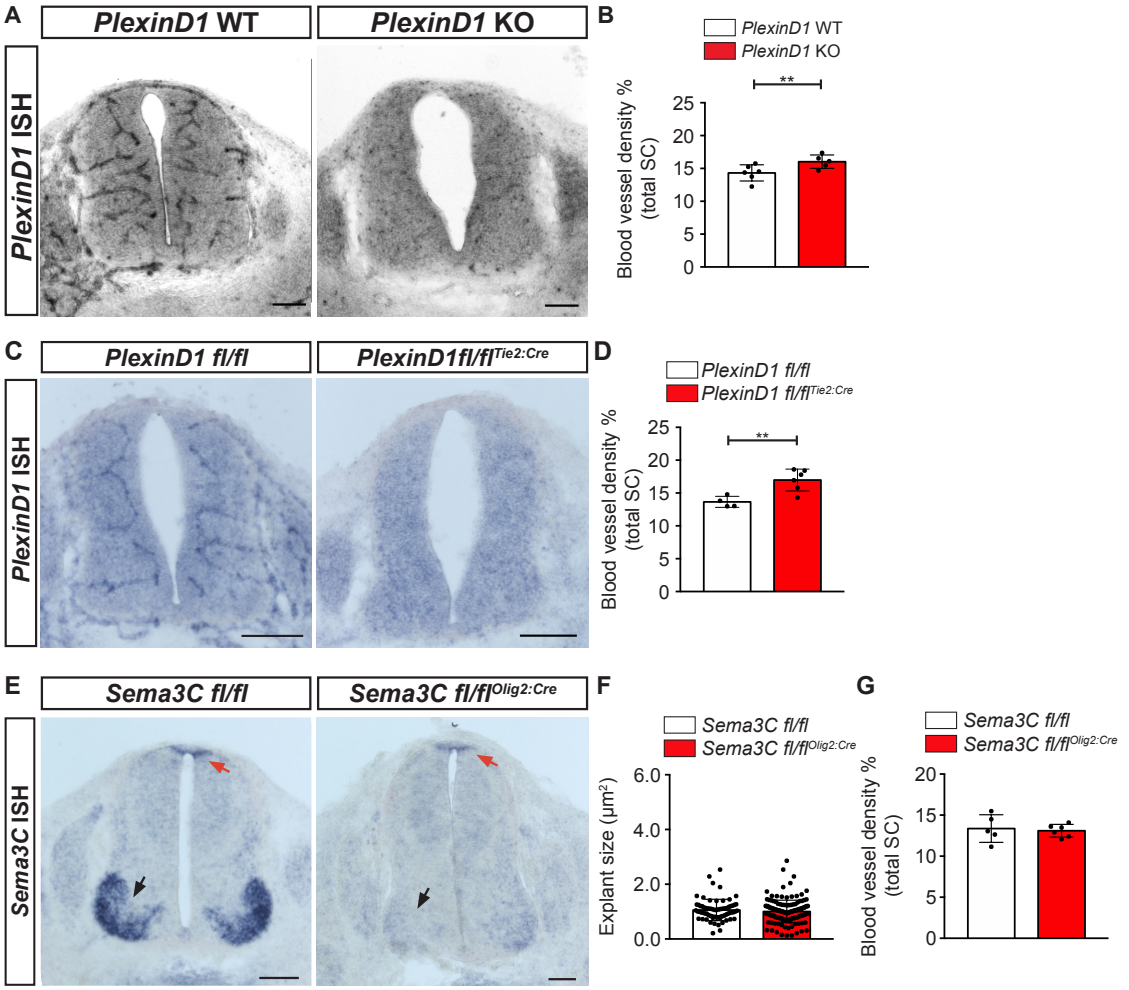

Appendix Fig. 4. PlexinD1 KO and *PlexinD1 fl/fl*$^{Tie2:Cre}$, but not *Sema3C fl/fl*$^{Olig2:Cre}$, show increased total spinal cord vascularization. (A) Representative images at brachial level of *PlexinD1* ISH in *PlexinD1* WT and KO embryos at E11.5 to confirm successful global *PlexinD1* deficiency. (B) Quantification of vessel density in the total spinal cord of *PlexinD1* WT and KO embryos at E11.5. n=6 PlexinD1 WT, n=5 PlexinD1 KO, from two independent litters. (C) Representative images at thoracic level of ISH for *PlexinD1* in *PlexinD1 fl/fl* and *PlexinD1 fl/fl*$^{Tie2:Cre}$ embryos at E11.5 to confirm successful *PlexinD1* knockdown in ECs. (D) Quantification of vessel density in the total spinal cord of *PlexinD1 fl/fl* and *PlexinD1 fl/fl*$^{Tie2:Cre}$ embryos at E11.5. n=4 *PlexinD1 fl/fl*, n=6 *PlexinD1 fl/fl*$^{Tie2:Cre}$, from two independent litters. (E) Representative image at thoracic level of ISH for *Sema3C* in *Sema3C fl/fl* and *Sema3C fl/fl*$^{Olig2:Cre}$ embryos at E11.5 to confirm successful and specific removal of *Sema3C* in MNs (black arrows) but not roof plate (red arrow). (F) Quantification of the explant sizes used from *Sema3C fl/fl* and *Sema3C fl/fl*$^{Olig2:Cre}$ E11.5 embryos (normalized to control littermates), n=40 explants *Sema3C fl/fl*, n=125 explants *Sema3C fl/fl*$^{Olig2:Cre}$, from two independent litters. (G) Quantification of vessel density in the total spinal cord of *Sema3C fl/fl* and *Sema3C fl/fl*$^{Olig2:Cre}$ embryos at E11.5. n=5 *PlexinD1 fl/fl*, n=6 *PlexinD1 fl/fl*$^{Tie2:Cre}$, from two independent litters. All statistical analyses done using parametric distribution, two tailed unpaired Student's t-test. All data shown as mean ± SD. All scale bars 100 µm.

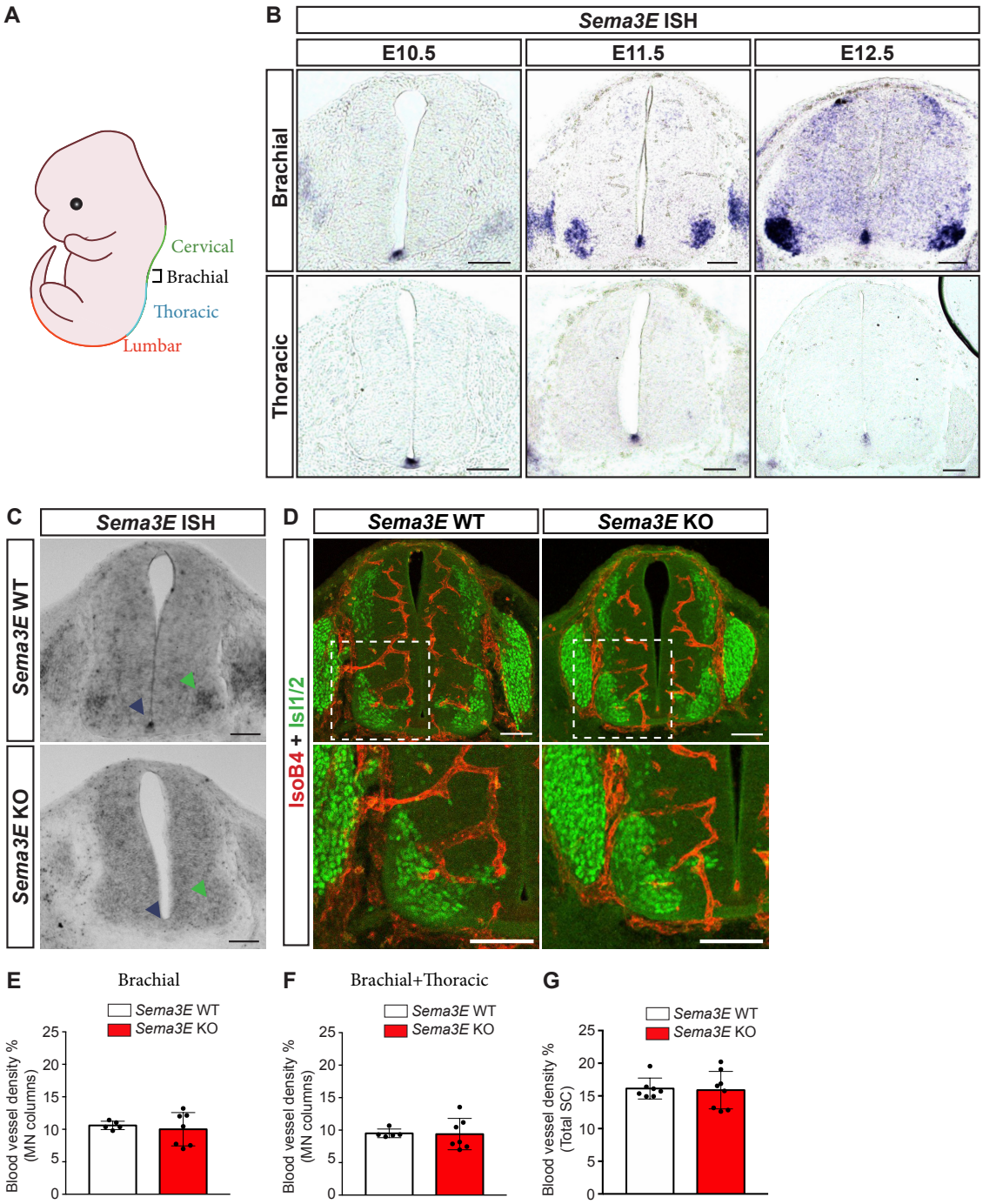

Appendix Fig. 5. *Sema3E* KO embryos do not show MN column vascularization defects. (A) Scheme of the different spinal cord levels in a rostral to caudal axis. (B) ISH for *Sema3E* in the developing spinal cord of WT embryos from E10.5 to E12.5 and at brachial and thoracic levels. (C) Representative image at brachial level of ISH for *Sema3E* in *Sema3E* WT and KO embryos at E11.5 to confirm successful global deletion of *Sema3E* (green arrowheads - MNs, blue arrowheads - FP). (D) Representative images of spinal cord sections stained for vessels (IsoB4^{+}) and MNs (Isl1/2^{+}) in *Sema3E* WT and KO embryos at E11.5. Insets show higher magnifications of MN columns. (E-G) Quantification of vessel density in MNs at brachial level (E), at brachial and thoracic levels together (F), and vessel density in the total spinal cord (G) of *Sema3E* WT and KO embryos at E11.5. n=5 *Sema3E* WT, n=7 *Sema3E* KO, from two independent litters. All statistical analyses done using parametric distribution, two tailed unpaired Student's t-test. All data shown as mean ± SD. All scale bars 100 µm.

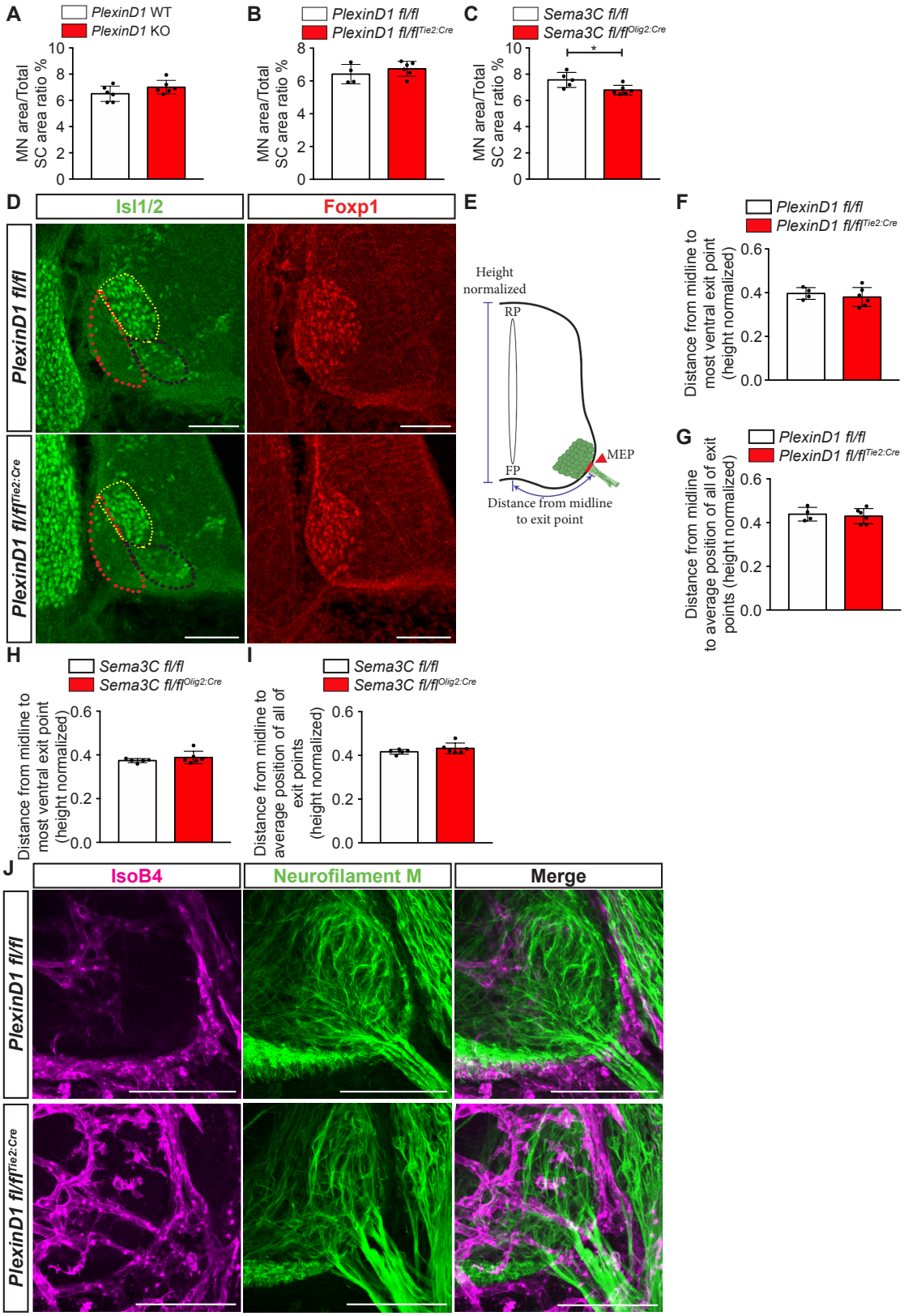

Appendix Fig. 6. Premature MN vascularization does not lead to defects in MN area and MN clustering, nor to defects in the position of the MEP. (A-C) Quantification of the ratio between MN area and total spinal cord area in *PlexinD1* WT and KO embryos (A), *PlexinD1 fl/fl* and *PlexinD1 fl/fl*$^{Tie2:Cre}$ embryos (B), and *Sema3C fl/fl* and *Sema3C fl/fl*$^{Olig2:Cre}$ embryos (C) at E11.5. n=6 *PlexinD1 WT*, n=6 *PlexinD1 KO*; n=4 *PlexinD1 fl/fl*, n=6 *PlexinD1 fl/fl*$^{Tie2:Cre}$; n=5 *Sema3C fl/fl*, n=6 *Sema3C fl/fl*$^{Olig2:Cre}$,

from two independent litters. (D) Immunostaining shows the localization of the different MN clusters at brachial level in *PlexinD1 fl/fl* and *PlexinD1 fl/fl*$^{Tie2:Cre}$ embryos. MN clustering into the medial division of the lateral motor column (LMCm, Isl1/2+ and FoxP1+, yellow dotted outline), lateral division of lateral motor column (LMCl, FoxP1+, red dotted outline), and medial motor column (MMC, Isl1/2+, black dotted outline) is not affected in *PlexinD1 fl/fl*$^{Tie2:Cre}$ embryos. (E) Scheme representation to illustrate how the distance from the midline to the most ventral exit point is calculated. (F-G) Quantification of the distance from the midline to the most ventral exit point (F), and the distance from the midline to the average position of the exiting motor axon bundles (G) in *PlexinD1 fl/fl* and *PlexinD1 fl/fl*$^{Tie2:Cre}$ embryos. n=4 *PlexinD1 fl/fl*, n=6 *PlexinD1 fl/fl*$^{Tie2:Cre}$, from two independent litters. (H-I) Quantification of the distance from the midline to the most ventral exit point (H) and the distance from the midline to the average position of the exiting motor axon bundles (I) in *Sema3C fl/fl* and *Sema3C fl/fl*$^{Olig2:Cre}$ embryos at E11.5. n=5 *Sema3C fl/fl*, n=6 *Sema3C fl/fl*$^{Olig2:Cre}$, from two independent litters. (J) Representative images of 300 µm thick sections at thoracic level co-labeled for blood vessels (IsoB4^{+}) and MN axons (neurofilament M) exiting the spinal cord in *PlexinD1 fl/fl* and *PlexinD1 fl/fl*$^{Tie2:Cre}$ embryos at E11.5. All statistical analyses done using parametric distribution, two tailed unpaired Student's t-test. All data shown as mean ± SD. All scale bars 100 µm.

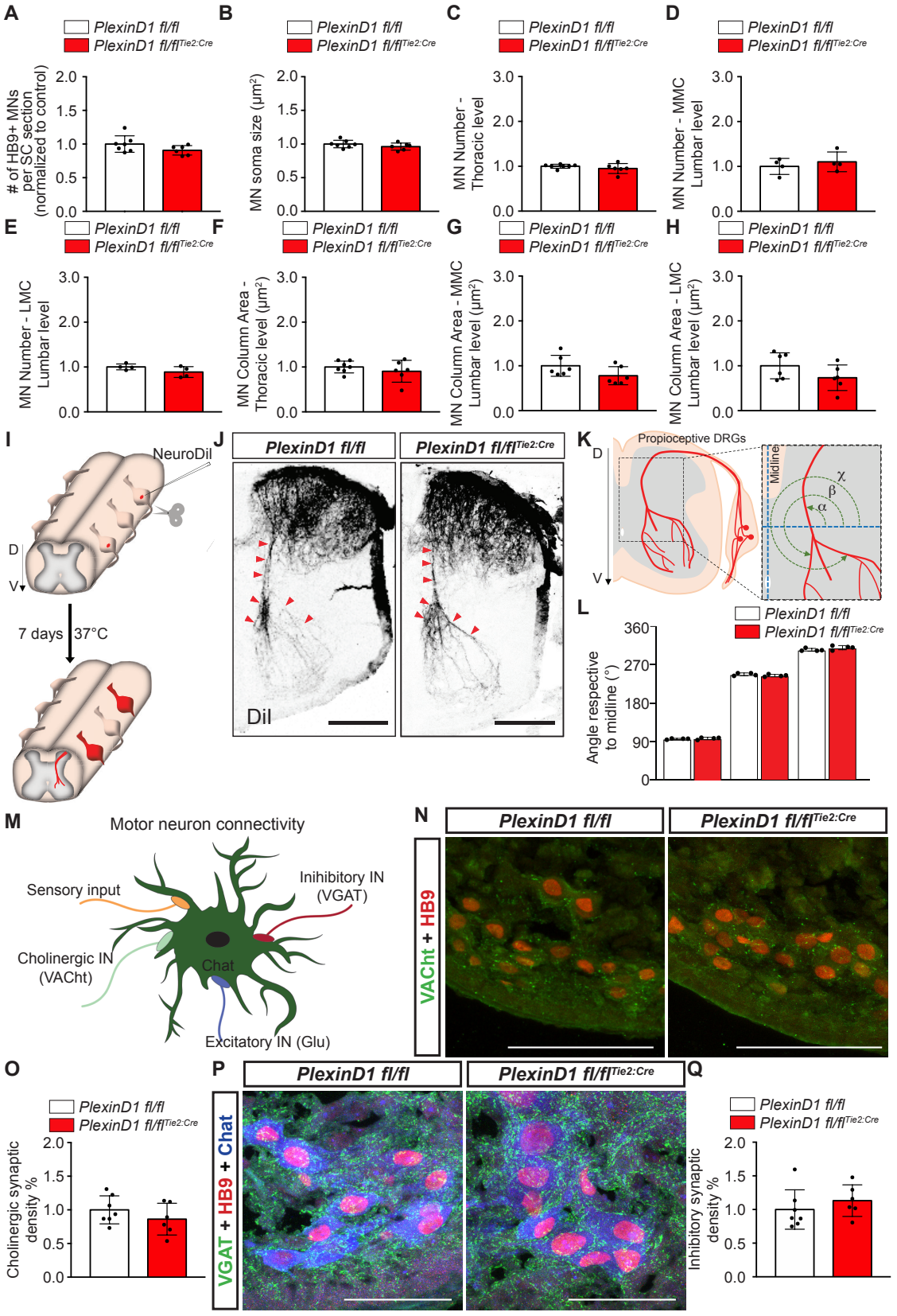

Appendix Fig. 7. Afferent inputs to MNs are not affected in *PlexinD1 fl/fl*$^{Tie2:Cre}$ embryos. (A) Quantification of the number of MNs (HB9^{+}) per spinal cord section at E18.5 in *PlexinD1 fl/fl* and *PlexinD1 fl/fl*$^{Tie2:Cre}$ embryos, normalized to control littermates. n=7 *PlexinD1 fl/fl*, n=6 *PlexinD1 fl/fl*$^{Tie2:Cre}$, from two independent litters. (B) Quantification of the MN soma size at E18.5 in *PlexinD1 fl/fl* and *PlexinD1 fl/fl*$^{Tie2:Cre}$ embryos,

normalized to control littermates. n=7 *PlexinD1 fl/fl*, n=6 *PlexinD1 fl/fl*$^{Tie2:Cre}$, from two independent litters. (C) Quantification of the number of MNs (HB9^{+}) at thoracic levels at E18.5 in *PlexinD1 fl/fl* and *PlexinD1 fl/fl*$^{Tie2:Cre}$ embryos, normalized to control littermates. n=7 *PlexinD1 fl/fl*, n=6 *PlexinD1 fl/fl*$^{Tie2:Cre}$, from two independent litters. (D-E) Quantification of the number of MNs (HB9^{+}) at lumbar levels at E18.5 in the MMC (D) and LMC (E) columns in *PlexinD1 fl/fl* and *PlexinD1 fl/fl*$^{Tie2:Cre}$ embryos, normalized to control littermates. n=4 *PlexinD1 fl/fl*, n=4 *PlexinD1 fl/fl*$^{Tie2:Cre}$, from two independent litters. (F) Quantification of the MN column area at thoracic levels at E18.5 in *PlexinD1 fl/fl* and *PlexinD1 fl/fl*$^{Tie2:Cre}$ embryos, normalized to control littermates. n=7 *PlexinD1 fl/fl*, n=6 *PlexinD1 fl/fl*$^{Tie2:Cre}$, from two independent litters. (G-H) Quantification of the MMC (G) and LMC (H) column areas at lumbar levels at E18.5 in *PlexinD1 fl/fl* and *PlexinD1 fl/fl*$^{Tie2:Cre}$ embryos, normalized to control littermates. n=6 *PlexinD1 fl/fl*, n=6 *PlexinD1 fl/fl*$^{Tie2:Cre}$, from two independent litters. (I) Schematic representation of the procedure for dorsal root tracing with NeuroDiI. (J) Representative images of coronal sections from E18.5 thoracic level spinal cords from *PlexinD1 fl/fl* and *PlexinD1 fl/fl*$^{Tie2:Cre}$ traced with NeuroDiI. Red arrowheads indicate the major proprioceptive descending bundle as well as its two main secondary branches. Scale bar 200 µm. (K) Scheme illustrating the procedure to obtain the angles for the major proprioceptive descending bundle (α) and its main secondary branches (β and χ) as shown in (J). (L) Quantification of (J). Experiment presented in (J-L) was performed by Dr. Sebástian Dupraz. Average angle for (α, β and χ). n=20 *PlexinD1 fl/fl* and n=27 *PlexinD1 fl/fl*$^{Tie2:Cre}$ spinal cord sections were analyzed from three independent experiments; Comparison in ordinary 1-way ANOVA. (M) Schematic representation of MN connectivity. MNs receive signal inputs from sensory neurons, cholinergic, inhibitory, and excitatory interneurons (IN). (N) Images of ventral spinal cords immunostained for MNs (HB9^{+}) and cholinergic inputs (VAChT^{+}) in *PlexinD1 fl/fl* and *PlexinD1 fl/fl*$^{Tie2:Cre}$ embryos at E18.5. Scale bars 100 µm. (O) Quantification of the cholinergic synaptic density contacting MNs in *PlexinD1 fl/fl* and *PlexinD1 fl/fl*$^{Tie2:Cre}$ embryos at E18.5. Data normalized to the control. n=7 PlexinD1 fl/fl, n=6 PlexinD1 fl/fl$^{Tie2:Cre}$, from two independent litters. (P) Images of ventral spinal cord immunostained for MNs (HB9^{+}), MN soma (HB9+ and Chat+), and inhibitory inputs (VGAT^{+}) in *PlexinD1 fl/fl* and *PlexinD1 fl/fl*$^{Tie2:Cre}$ embryos at E18.5. Scale bars 100 µm. (Q) Quantification of inhibitory synaptic density connecting to MNs in *PlexinD1 fl/fl* and *PlexinD1 fl/fl*$^{Tie2:Cre}$ embryos at E18.5, normalized to control littermates. n=7 PlexinD1 fl/fl, n=6 PlexinD1 fl/fl$^{Tie2:Cre}$, from two independent litters. All statistical analyses done using parametric distribution, two tailed unpaired Student's t-test, unless mentioned. All data shown as mean ± SD.

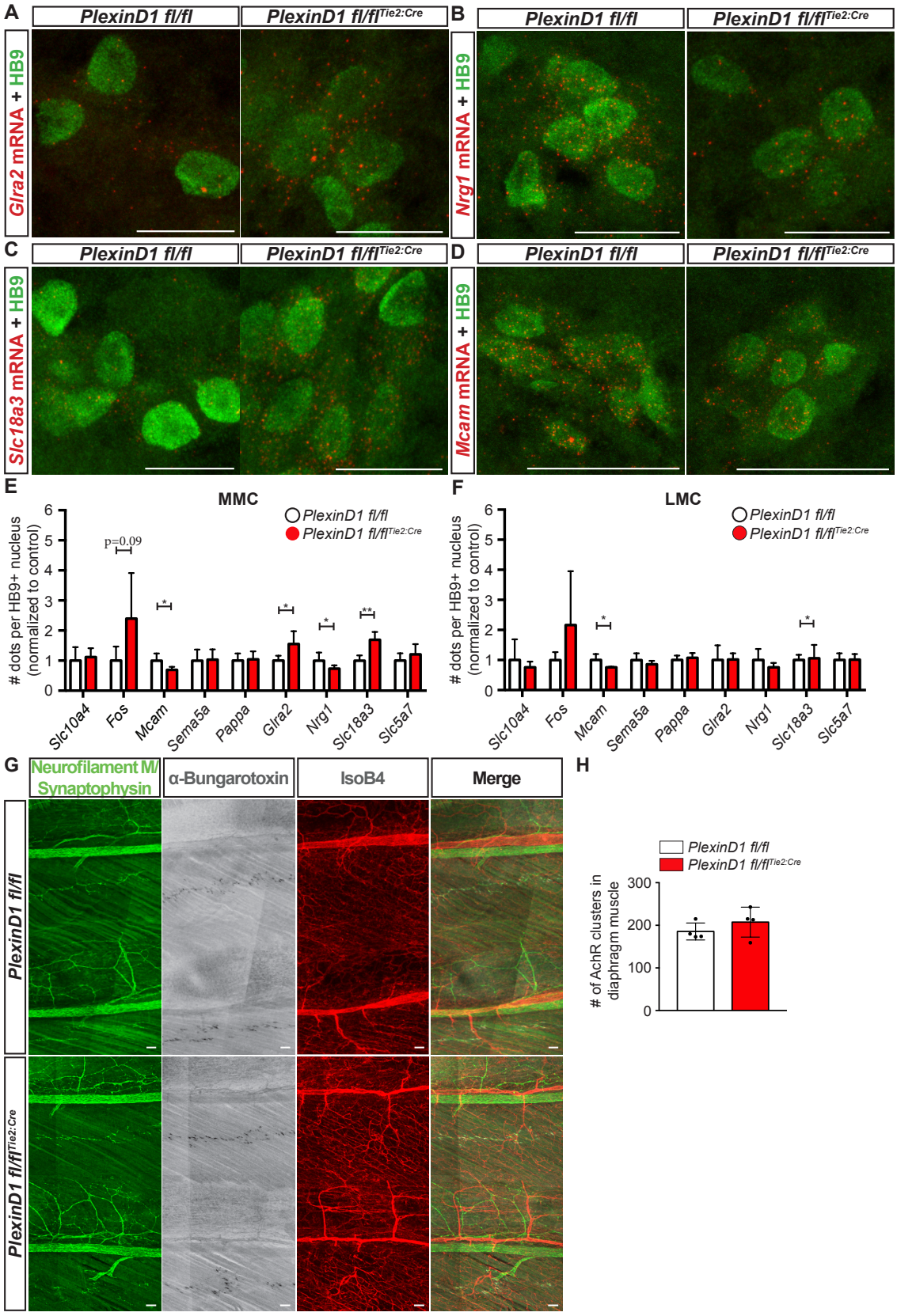

Appendix Fig. 8. Altered transcription of MN terminal differentiation markers and functional genes in *PlexinD1 fl/fl*$^{Tie2:Cre}$ embryos at E18.5. (A-D) Representative images of RNAscope for *Glra2 (A), Nrg1 (B), Slc18a3 (C), and Mcam (D)* co-stained with HB9 in *PlexinD1 fl/fl* and *PlexinD1 fl/fl*$^{Tie2:Cre}$ embryos. Scale bar 25 µm. (E-F) Quantification of the number of RNAscope dots for the different genes per HB9^{+} nucleus

in the MMC (E) and LMC (F) columns. Data normalized to control littermates. n=5 *PlexinD1 fl/fl*, n=4 *PlexinD1 fl/fl*$^{Tie2:Cre}$, from two independent litters; multiple Student's t-test. (G) Representative images of the intercostal muscles at E18.5 stained to show intercostal innervation (Neurofilament M + Synaptophysin), AchR^{+} clusters (α-bungaratoxin), and vessels (IsoB4) in *PlexinD1 fl/fl* and *PlexinD1 fl/fl*$^{Tie2:Cre}$ embryos. Scale bars 100 μm. (H) Quantification of the branching density of phrenic nerve at E18.5 in *PlexinD1 fl/fl* and *PlexinD1 fl/fl*$^{Tie2:Cre}$ embryos. n=4 *PlexinD1 fl/fl*, n=4 *PlexinD1 fl/fl*$^{Tie2:Cre}$, from two independent litters; parametric distribution, two tailed unpaired Student's t-test. All data shown as mean ± SD.

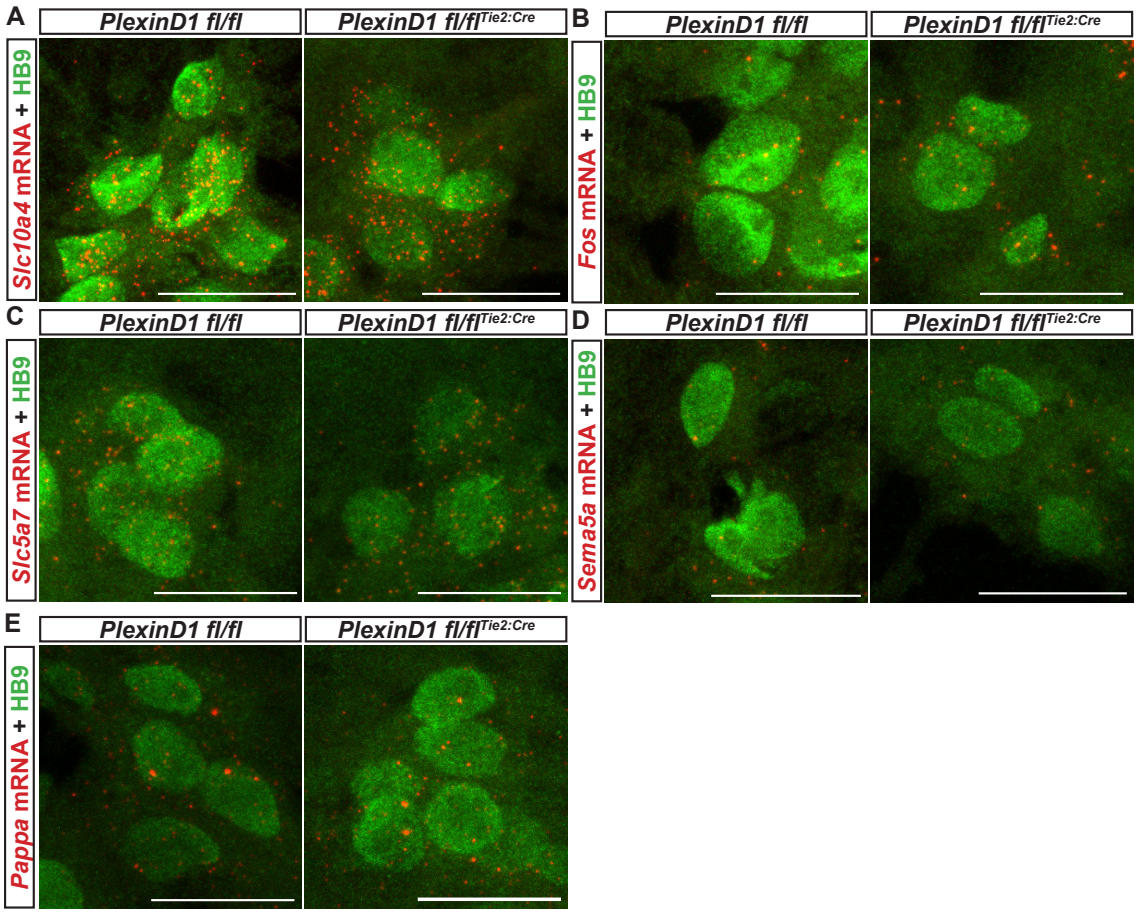

Appendix Fig. 9. Gene expression analysis via RNAscope in MNs of *PlexinD1 fl/fl* and *PlexinD1 fl/fl*^{Tie2}-*Cre* E18.5 embryos. (A-E) Representative images of RNAscope for *Slc10a4 (A), Fos (B), Slc5a7 (C), Sema5a* (D) and *Pappa* (E) co-stained with HB9 in *PlexinD1 fl/fl* and *PlexinD1 fl/fl*$^{Tie2:Cre}$ embryos. Scale bar 25 μm.

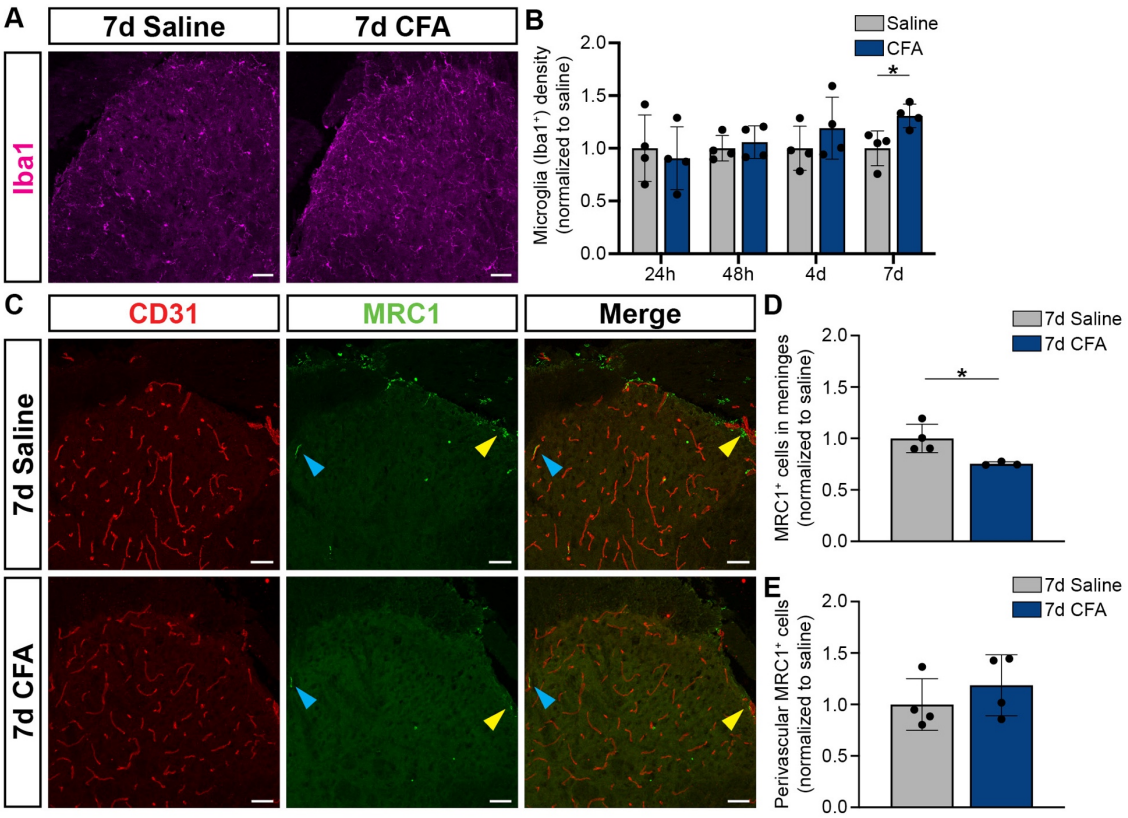

Appendix Fig. 10. Pro-inflammatory environment in the spinal cord following CFA injection. (A) Representative images of spinal cord sections stained for microglia (Iba1$^+$) 7 days after saline or CFA injection. (B) Quantification of microglia density after 24h, 48h, 4 days and 7 days following saline or CFA intraplantar injection. Data normalized to the control. n=4 saline, n=4 CFA. (C) Representative images of immunostaining for M2-macrophages (MRC1$^+$) together with vessels (CD31$^+$). Blue arrowheads indicate perivascular macrophages and yellow arrowheads meningeal macrophages. (D-E) Quantification of the number of MRC1$^+$ cells in meninges (D) and close to vessels (E) 7 days after saline or CFA injection. Data normalized to control. n=3 saline, n=4 CFA for (D) and n=4 saline, n=4 CFA for (E). The results presented in (C-E) were done together with Janina Hattemer, who did a lab rotation under my supervision. All scale bars 50 μm.

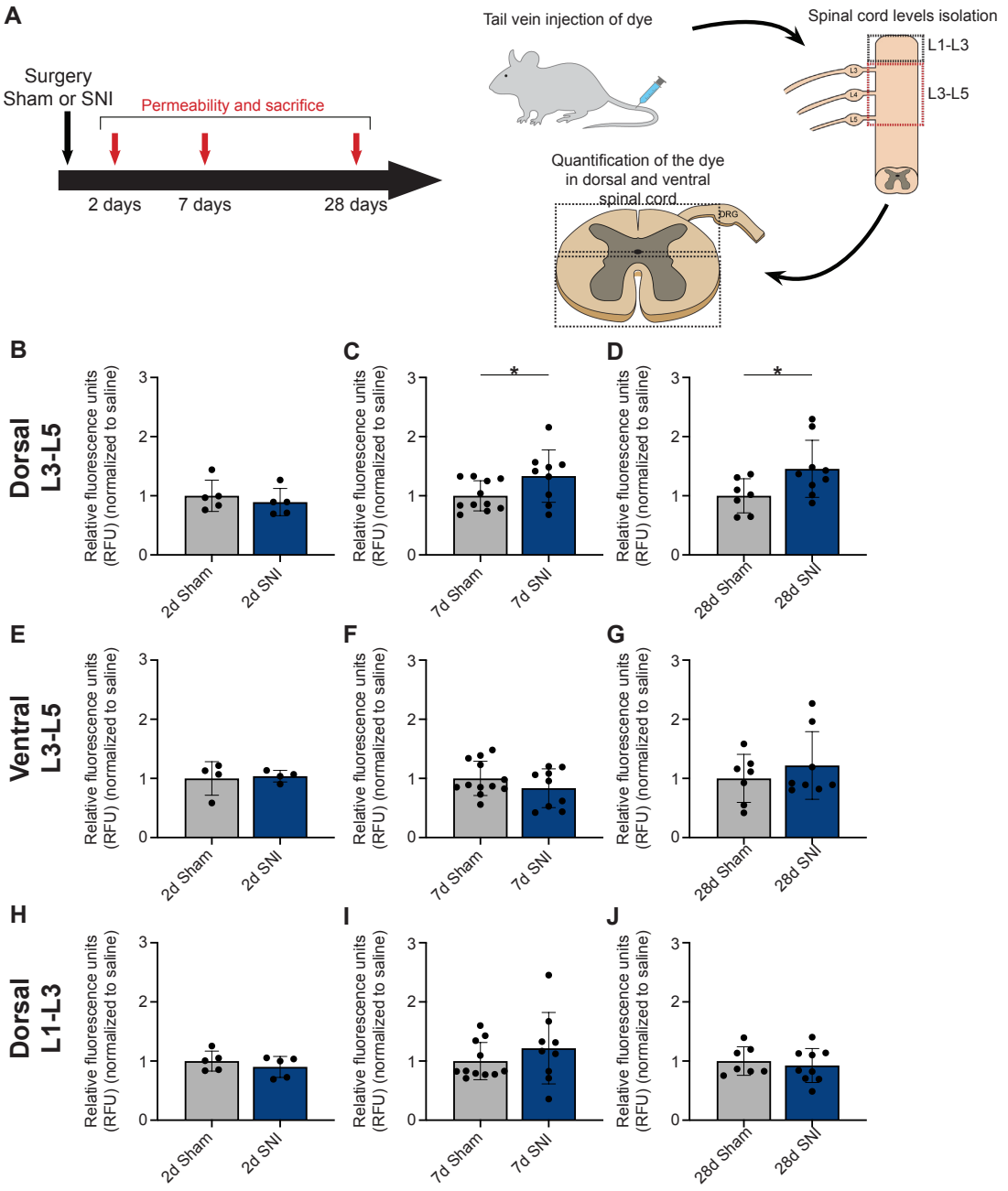

Appendix Fig. 11. BSCB permeability is increased in SNI neuropathic pain model. (A) Schematic illustration of the experimental protocol. Mice were submitted to sham or SNI and, at the respective timepoint, injected with sodium fluorescein (NaFlu), which was allowed to circulate for 30 min. Afterwards, mice were perfused with PBS, the spinal cord levels and regions dissected, and the extravasation of NaFlu into parenchyma was quantified. (B-D) Quantification of tracer extravasation into the dorsal region of L3-L5 spinal cord levels upon sham or SNI surgeries at the respective timepoints. Data normalized to the control. N=5 sham and n=5 SNI for 2 d; N=11 sham and n=9 SNI for 7 d ; N=7 sham and n=9 SNI for 28 d. (E-G) Quantification of tracer extravasation into the ventral region of L3-L5 spinal cord levels upon sham or SNI surgeries at the respective timepoints. Data normalized to the control. N=4 sham and n=4 SNI for 2 d; N=12 sham and n=9 SNI for 7 d ; N=7 sham and n=8 SNI for 28 d. (H-J) Quantification of tracer

extravasation into the dorsal region of L1-L3 spinal cord levels upon sham or SNI surgeries at the respective timepoints. Data normalized to the control. N=5 sham and n=5 SNI for 2 d; N=11 sham and n=9 SNI for 7 d ; N=7 sham and n=9 SNI for 28 d. All statistical analyses were done using parametric distribution, two tailed unpaired Student's t-test.

9. PUBLICATIONS

Vieira JR, Shah B, et al., (2022) “Endothelial PlexinD1 signaling instructs spinal cord vascularization and motor neuron development”. Neuron 110(24): 4074-4089e4076.
DOI: https://doi.org/10.1016/j.neuron.2022.12.005

Gião T, Saavedra J, **Vieira JR**, et al., Neuroprotection in early stages of Alzheimer's disease is promoted by transthyretin angiogenic properties. Alzheimers Res Ther. 2021;13(1):143. Published 2021 Aug 24. doi:10.1186/s13195-021-00883-8.
DOI: https://doi.org/10.1186/s13195-021-00883-8

Alemi M, Oliveira A, Tavares SC, **Vieira JR**, et al., Exploring the Physiological Role of Transthyretin in Glucose Metabolism in the Liver. Int J Mol Sci. 2021;22(11).
DOI: https://doi.org/10.3390/ijms22116073

Paredes I, **Vieira JR**, Shah B, et al., Oligodendrocyte precursor cell specification is regulated by bidirectional neural progenitor-endothelial cell crosstalk. Nat Neurosci. 2021;24(4):478-88.
DOI: https://doi.org/10.1038/s41593-020-00788-z

Vieira JR, Shah B, Ruiz de Almodovar C. Cellular and Molecular Mechanisms of Spinal Cord Vascularization. Front Physiol. 2020;11:599897.
DOI: https://doi.org/10.3389/fphys.2020.599897

10. ACKNOWLEDGMENTS

Although this section is not directly related with the scientific work presented in this thesis, and perhaps has no meaning for people other than me, it is one of the most important parts of this work. Throughout the academic journey, there are several “pillars” that make everything seem easier, on whom we know we can count, and who are by our side to support us, unconditionally. Without them, this PhD certainly would not have been as easy, enriching, and remarkable. I feel that I learned a lot and, mainly, that I grew both as a scientist and as a person. To these “pillars”, my enormous thanks.

First, a special thanks to my PhD supervisor, Prof. Dr. Carmen Ruiz de Almodóvar, who first gave me the opportunity to embrace the PhD journey under her supervision and supported me through these last five years. I am grateful for all your mentorship, guidance, encouragement and for making me grow as a scientist. It was a pleasure working with you and hopefully our paths will cross again in the future (hopefully I did not give much work during this time).

I thank my thesis advisory committee, Prof. Dr. Jochen Wittbrodt and Jun-Prof. Dr. Lázaro Centanin, for our fruitful discussions, their interest and input to my work during these last years. I would also like to thank Prof. Dr. Michael Brunner and Prof. Dr. Daniela Mauceri for being part of my thesis and defense examination committee.

A big thanks to all the Ruiz lab members during these long (but short-felt) years, for all the discussions, for the amazing scientific and personal environment constructed, for the help, support, and encouragement. Definitely you made these years funnier, scientific richer and easier. I will leave my PhD full of good experiences and happy memories. Aida, Robert, Nathalie, Andromachi, Isidora, Bhavin, Heike, Xiaohong, Geza, Emilia, and Carlita. Martina thank you for your kindness and having the patience to answer all my questions/doubts (since I got the acceptance!) and being always available to help. You took a lot of possible worries from my shoulders!

Huge thanks to Prof. Dr. Daniela Mauceri for hosting me and giving the chance to continue my work in her lab. From the first moment you always kept the door open for me to finish my work and PhD in your lab, which facilitated a lot my life and I appreciate it enormously. I really enjoyed my time here and I am grateful that I had the chance to collaborate and work closely with you!

I would also like to thank the members of the Mauceri's lab, Bahar, Javi and Anki, for the warm welcome and making this last PhD year, which should be the worst, super enjoyable. While we were not lab colleagues, it was also a pleasure working with you Christian, doing those long (and tiring) permeability experiments.

To the entire Department of Neurobiology for their sympathy, for integrating me so easily. It is amazing how such a great atmosphere goes in this department.

To my great friends who have been with me for a long time, my big thanks for all the support and encouragement. A particular thanks to my friends in Heidelberg/Mannheim who made the experience of living abroad for the first time easier and enjoyable. Chiara, Mario, Ale, Kaye, Rodrigo, Sherif, Sven, Marek, Giorgos, Lisa, Manlio (…).

Finally, and most importantly, to my family: to my brother, sister-in-law, mother, and father for all the unconditional support given in all my decisions, encouraging me to follow what I believe in, without ever questioning and doubting me. Thank you for being part of me and always being there. And also part of my family, my amazing girlfriend Federica for being always there for me throughout my PhD. Your unconditional support and encouragement eases my problems and I know you are always there for me. Thank you for everything and for being you.

Obrigado por tudo! Until next time!